THE UNIVERSITY of ADELAIDE

The Effects of Tubercles on Swept Wing Performance at Pre-Stall Angles of Attack

By

Michael Bolzon

A thesis submitted for the degree of Doctor of Philosophy at the

The School of Mechanical Engineering

The University of Adelaide

Australia

Abstract

Engineers are constantly seeking improvements in wing efficiency, as improved efficiency can translate into improved wing performance and reduced operating costs. A wing's efficiency can be improved by either increasing its lift production or reducing its drag. Tubercles are protuberances on a wing's leading edge that can improve an unswept wing's efficiency at stall and post-stall angles of attack, AOAs. However, many wings typically operate at pre-stall AOAs, and the effects of tubercles on wing performance at these AOAs are largely unknown. In addition, incorporating wing sweep has become an increasingly popular choice during wing design. Therefore, this thesis describes an investigation into the effects of tubercles on swept wing performance at pre-stall AOAs. Particular attention was given to their effects on the components of drag, and on the effects that various tubercle geometric parameters have on wing performance.

It was found that tubercles can increase a swept wing's performance through increasing its lift-to-drag ratio and reducing its drag coefficient at pre-stall AOAs. This conclusion was found from force measurements taken on a NACA 0021 wing swept with a quarter-chord sweep angle of 35°. For this particular wing, below 8° AOA, tubercles were found to reduce the lift and drag coefficients by 4-6% and 7-9.5%, respectively, and as a result, the wing's lift-to-drag ratio increased by 2-6%. Above 8° AOA, premature flow separation behind the tubercle troughs resulted in the tubercles reducing the lift coefficient, while dramatically increasing the drag coefficient. As a result, the lift-to-drag ratio was reduced. In addition, a Laminar Separation Bubble, LSB, formed over the smooth wing, which resulted in an increased lift-curve slope. Force measurements, flow visualisation, and a numerical model demonstrated that the tubercled wing affected the LSB formation and, as a result, reduced the augmented lift-curve slope. Wake surveys showed that the majority of the tubercled wing's drag coefficient reduction below 8° AOA was due to a reduced profile drag coefficient. Below 8° AOA, the tubercles had little effect on the induced drag coefficient. Above 8° AOA, the premature flow

separation over the tubercled wing resulted in an increased profile drag coefficient and a reduced induced drag coefficient. Furthermore, it was found that the tubercles modulate the profile and induced drag coefficients along the span of the wing, with local minima occurring behind the peaks and troughs, respectively. Conversely, local maxima in the profile and induced drag coefficients arise behind the troughs and peaks, respectively. The induced drag coefficient increases behind the peaks as the augmented circulation further tilts the augmented lift vector into the freestream velocity direction. Conversely, behind the troughs, the reduced circulation tilts the lift vector into the freestream velocity direction to a lesser extent, thereby reducing the induced drag coefficient. From the results presented in this thesis, it is apparent that the reasons for the modulation of the profile drag coefficient are extremely complex, involving boundary layer formation, LSB formation, and other observed flow patterns. Therefore, it is concluded that further investigation is required in order to fully understand the effects of tubercles on the profile drag coefficient. While an unswept tubercled wing produces pairs of equally strong, and oppositely signed, vortices, sweeping a tubercled wing results in the outboard vortex of each tubercle becoming stronger than its paired inboard vortex.

A new geometric parameter, the phase, has been introduced in this thesis to describe the point along a tubercle at which a wing terminates. A parametric analysis investigating the effects of the tubercle amplitude, wavelength, and phase on the wing's lift coefficient, induced drag coefficient, and lift-to-induced-drag ratio at pre-stall AOAs showed that the phase typically has the greatest effect on these wing performance parameters, while the wavelength has the least. The phase also polarises the effects of tubercles on these performance parameters, whereby termination on a trough results in reduced lift and induced drag coefficients, and an increased lift-to-induced-drag ratio. Conversely, termination on a peak results in increased lift and induced drag coefficients, and a reduced lift-to-induced-drag ratio. A genetic algorithm was developed to optimise the tubercle's amplitude, wavelength, phase, location, and number to achieve the greatest lift-to-induced-drag ratio; the result being a single trough located at the wingtip, which increased the lift-to-induced-drag

ratio by up to 4.3%. A final experimental campaign showed that a single tubercle terminating at a wingtip typically yields smaller performance benefits than tubercles along an entire leading edge.

As a result of this research, a framework now exists to design a tubercle's geometry to maximise a wing's lift coefficient, lift-to-drag ratio, or lift-to-induced-drag ratio, or to minimise its induced drag coefficient or total drag coefficient at pre-stall AOAs, given the operating conditions.

Declaration

I certify that this work contains no material which has been accepted for the award of any other degree or diploma in my name in any university or other tertiary institution and, to the best of my knowledge and belief, contains no material previously published or written by another person, except where due reference has been made in the text. In addition, I certify that no part of this work will, in the future, be used in a submission in my name for any other degree or diploma in any university or other tertiary institution without the prior approval of the University of Adelaide and where applicable, any partner institution responsible for the joint award of this degree.

I give consent to this copy of my thesis when deposited in the University Library, being made available for loan and photocopying, subject to the provisions of the Copyright Act 1968.

The author acknowledges that copyright of published works contained within this thesis resides with the copyright holder(s) of those works.

I also give permission for the digital version of my thesis to be made available on the web, via the University's digital research repository, the Library Search and also through web search engines, unless permission has been granted by the University to restrict access for a period of time.

Michael Bolzon Date

Acknowledgements

I thank all who have helped me during my Ph.D. candidature. I thank my supervisors, A/Profs Richard Kelso and Maziar Arjomandi, for their insights throughout. I also thank A/Prof Anthony Zander and Prof Ben Cazzolato for their guidance. To A/Prof Con Doolan, I am grateful for your assistance with my project.

To the mechanical and electronic workshops staff, I am very grateful for all of your help, and for all that I have learnt from you.

I thank Miss Alison-Jane Hunter for her help in editing the final parts of this thesis.

To the Sir Ross and Sir Keith Smith Fund, I appreciate all of the financial support you have given me throughout my Ph.D. candidature.

To my friends, looking back…it's just been one funny moment after another. Thank you.

To my family, especially Mum and Dad, thank you for all that you have done for me. Love Mike.

Nomenclature and Abbreviations

A	=	Tubercle amplitude
A/MAC	=	Tubercle-amplitude-to-mean-aerodynamic-chord ratio
AOA	=	Angle of attack
C_{Df}	=	Skin friction drag coefficient
C_f	=	Skin friction coefficient
CFD	=	Computational Fluid Dynamics
DBD	=	Dielectric barrier discharge
D_I	=	Induced drag
GA	=	Genetic Algorithm
h_{eff}	=	Tubercle effective height
L	=	Lift
LLT	=	Prandtl's lifting-line theory
MAC	=	Mean aerodynamic chord
q, q_∞	=	Freestream dynamic pressure
Re_c	=	Reynolds number at location "c"
s	=	Downstream, cross-sectional plane perpendicular to the freestream velocity
UAV	=	Unmanned aerial vehicle
U_∞	=	Streamwise velocity
v	=	Velocity in spanwise direction
V	=	Freestream velocity
w	=	Downwash velocity
y	=	Wall-normal direction
z	=	Direction normal to the freestream velocity and wall-normal directions
ZNMF	=	Zero net mass flux
α	=	Geometric angle of attack

α_w	=	Downwash angle of attack
Γ	=	Circulation
λ	=	Tubercle wavelength
λ_g	=	Gust longitudinal wavelength
λ/MAC	=	Tubercle-wavelength-to-mean-aerodynamic-chord ratio
μ	=	Kinematic viscosity
τ_w	=	Wall shear stress
ρ, ρ_∞	=	Density
σ	=	Cross-flow source
ω	=	Vorticity

Table of Contents

Table of Contents

Chapter 1

Introduction

1.1 Overview

The drag force that a fluid imparts on an object plays a key role in determining the object's aerodynamic performance. For a machine, such as a drag-based wind turbine, an increase in drag is beneficial, as it results in an increase in power production. However, for many applications, an increase in drag is detrimental to an object's performance. Such applications include: airplanes, compressors, and lift-based wind turbines, where an increase in drag will result in an increase in fuel consumption, a reduction in the pressure ratio, or a reduction in power production, respectively. Therefore, reducing drag in such instances is of great importance for an engineer and for industry.

The total drag of an object can typically be decomposed into components, and the weighting of each component on the total drag varies from application to application. For example, for a wing, the total drag can divided into the skin friction, pressure, and induced drags; the skin friction and pressure drags are often grouped to constitute the "profile", or "form", drag. However, if the wing does not produce lift, then the induced drag becomes negligible. Even an object operating under slightly different conditions can have other components of drag: for example, if the wing were to approach sonic speeds, a new component of drag, known as wave drag, would manifest. This wave drag could be so large that it dominates the total drag production. Therefore, reducing the total drag of an object is not a simple task, and this task becomes further complicated when considering the interaction between the different components of drag and their overall effects on the total drag. For example, a wing may be experiencing a high pressure drag that is caused by flow separation. Therefore, a potential method to reduce the pressure drag could be to maintain an attached flow over the entire wing surface. However, an attached flow will tend to increase the skin friction drag. Therefore, while one component of drag decreases, another component increases, and only by considering all the components of drag may a conclusion as to the effect on the total drag be drawn.

1.2 The Components of Drag

1.2.1 Skin Friction Drag

The skin friction of an object originates from the shear stress of a fluid moving over the surface. If a fluid flows over a non-slip surface, such as in fig. 1, a boundary layer will form and the shear stress at the wall, which is also known as the local skin friction, can be defined by eq. 1. The local skin friction coefficient can then be calculated from eq. 2 (Anderson, 2011), where $\frac{dU_\infty}{dy}\Big|_{y=0}$ is the spatial derivative of the streamwise velocity in the wall-normal direction at the wall. Assuming a Blasius boundary layer model for a laminar boundary layer and a power law profile for a turbulent boundary layer, the skin friction drag coefficient for laminar and turbulent boundary layers can be estimated using eqs. 3 and 4, respectively (Anderson, 1989; Anderson, 2011).

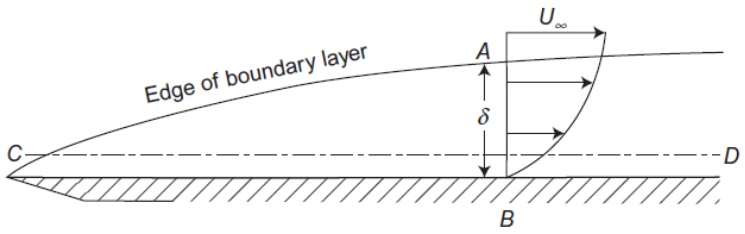

Figure 1: Boundary layer formation over a non-slip surface (Houghton *et al.*, 2013).

$$\tau_w = \mu \frac{dU_\infty}{dy}\Big|_{y=0} \quad \textbf{(1)}$$

$$C_f = \frac{\tau_w}{q_\infty} \quad \textbf{(2)}$$

$$C_{D_f} = \frac{1.328}{\sqrt{Re_c}} \quad \textbf{(3)}$$

$$C_{D_f} = \frac{0.074}{Re_c^{1/5}} \quad \textbf{(4)}$$

Therefore, from eqs. 1, 2, and 4**,** the state of the boundary layer will affect the shear stress a fluid imparts on a body directly, where a turbulent flow will tend to produce a greater shear stress, and hence a greater skin friction drag coefficient.

1.2.2 Pressure Drag

The pressure drag is the integral of the pressure over the surface area of an object, acting in the streamwise direction (Hoerner, 1965). A greater flow separation results in a larger wake, and a greater pressure drag. Figure 2 qualitatively shows the size of the wake; a more streamlined body, such as a wing, will incur a lower pressure drag penalty.

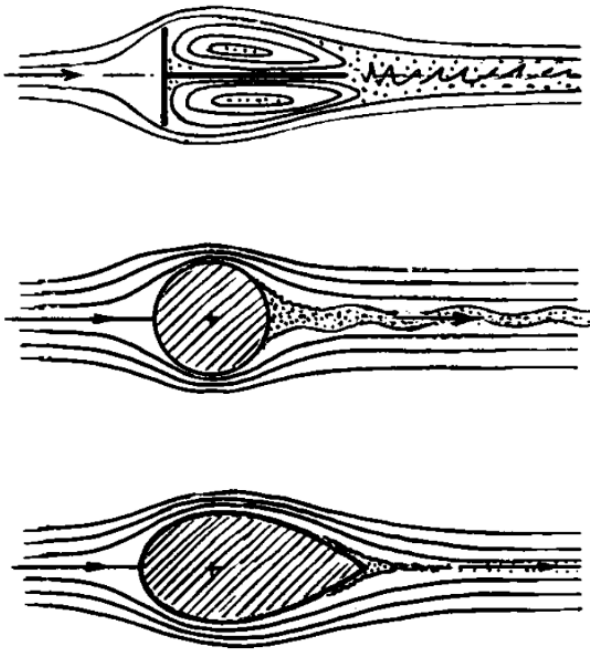

Figure 2: The effect of an object's shape on the wake size, hence pressure drag (Hoerner, 1965).

1.2.3 Induced Drag

Induced drag is only present on a body producing lift. It should be noted that for the remainder of this thesis a "wing" refers to a three-dimensional streamlined, lifting surface, whereas a "foil" refers to a two-dimensional streamlined, lifting surface. When a wing produces lift, it also produces downwash, as shown by the "w" vector in fig. 3, and this downwash tilts the lift vector away from perpendicular to the freestream velocity, which can be seen by the "ρqΓ" vector in fig. 3. This effectively results in the lift contributing slightly to the resistive force in the freestream velocity direction (Anderson, 2011). A greater lift production results in a greater induced drag. It should be noted that in fig**.** 3 the vector "L" is the component of the normal force perpendicular to the freestream velocity.

Perhaps, the most widely accepted method of calculating the induced drag is to use what is known as the "Oswald efficiency factor", or an equivalent non-dimensional parameter, which essentially normalises the induced drag of a given wing planform to the theoretical minimum of a planar wing (Roskam, 2005; Houghton and Brock, 1970). While this approach offers a reasonable approximation of induced drag with minimal calculations, it is not sufficiently accurate for research purposes. An alternative method to calculate the induced drag of a wing in an incompressible flow is to apply eqs. 5 to 9 to the near-field cross-sectional plane perpendicular to the freestream velocity downstream of the wing (Brune, 1994; Birch *et al.*, 2004; Gerontakos and Lee, 2006).

$$D_I \approx \frac{1}{2}\rho_\infty \int\int_S (\psi\omega - \phi\sigma)dydz \tag{5}$$

where

$$\sigma = \frac{\partial v}{\partial y} + \frac{\partial w}{\partial z} \tag{6}$$

$$\omega = \left(\frac{\partial w}{\partial y} - \frac{\partial v}{\partial z}\right) \tag{7}$$

$$\frac{\partial^2 \phi}{\partial y^2} + \frac{\partial^2 \phi}{\partial z^2} = \sigma \tag{8}$$

and

$$\frac{\partial^2 \psi}{\partial y^2} + \frac{\partial^2 \psi}{\partial z^2} = -\omega \tag{9}$$

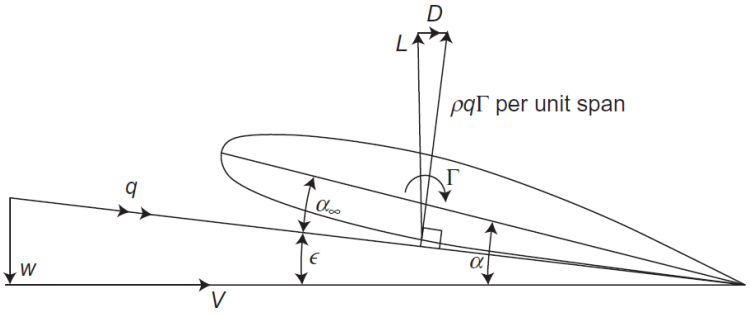

Figure 3: Downwash vector, "w", tilting the lift vector (Houghton *et al.*, 2013).

1.3 Drag Reduction Techniques

While the drag of a wing is a key parameter in its performance, it should also be noted that the lift production is also of key importance, as this ultimately determines the size of the wing required for flight. However, to deem one of these parameters more important than the other is inappropriate, as it is both of these parameters, as well as their effects on each other, that typically define a wing's efficiency. While this body of work is largely focussed on the drag of a wing, where appropriate, the lift of a wing will also be discussed. To that end, this section is aimed at discussing techniques of reducing the drag of a wing, and the effects of any given control technique on the lift of a wing will be discussed, when significant.

The techniques used to reduce the drag of a wing can be divided into two groups. The first group focusses on optimising the general wing profile and planform, while the second is to implement "flow control devices" to manipulate the flow over the wing. Typically, the wing profile and planform are optimised before flow control devices are implemented. These two categories of drag reduction methods will be discussed separately.

1.3.1 Wing Profile Optimisation

To optimise a wing profile to reduce drag, the angle of attack, AOA, and Reynolds number operating ranges must be considered, as these parameters will profoundly impact the design phase. For example, if a wing is prone to stalling under certain conditions, then it may be prudent to accelerate the onset of boundary layer turbulence, which, while the skin friction drag will increase, will result in a more attached flow and thereby reduce the pressure drag, and possibly reduce the total drag. Conversely, if the flow remains well attached over a wing, it may be beneficial to keep the flow as laminar as possible, which would reduce the skin friction drag.

Flow separation over a wing can be devastating to its performance, and can easily produce a pressure drag sufficiently great to dominate the total drag and severely reduce lift. Therefore, the following section discusses techniques to keep the flow attached.

A. Laminar Flows

For laminar flows, which for the remainder of this thesis refers to chord Reynolds numbers below approximately 70,000, the type of airfoil or wing that would produce the highest lift-to-drag ratio, a measure of the wing's efficiency, is one with a rough surface, such as a Dragonfly's wing (McMasters and Henderson, 1980). This is primarily because the flow is highly prone to separating at such a low

Reynolds number, and a rough surface increases the turbulence of the flow over the wing, which increases the flow's tendency to overcome the adverse pressure gradient, thereby preventing separation (Lissaman, 1983).

B. Transitional Flows

During the transitional regime, a chord Reynolds number of approximately 70,000 to 500,000, a smooth airfoil begins to produce a higher lift-to-drag ratio than a rough wing, as the flow becomes sufficiently turbulent to overcome the adverse pressure gradient and delay separation; the rough wing, while still able to keep the flow attached, introduces an unnecessarily high skin friction drag. This transition was explained by Lissaman (1983) to originate from the formation of a Laminar Separation Bubble, LSB.

C. Fully Turbulent Flows

For Reynolds numbers above approximately 10,000,000 (Hoerner, 1965), termed fully turbulent flow, the flow over a wing is usually less prone to separation. Transition to turbulence typically begins near the minimum pressure over the wing, which also corresponds to the beginning of the adverse pressure gradient and is highly beneficial as it promotes boundary layer attachment. Lissaman (1983) points out, however, that this transition is no guarantee of boundary layer attachment, as, if the adverse pressure gradient is sufficiently strong, the boundary layer may separate while still transitioning from laminar to turbulent. This risk can be minimised by altering the wing profile shape around the minimum pressure point to reduce the adverse pressure gradient. When the flow is fully turbulent, attempts at preventing separation are not nearly as common or necessary as at lower Reynolds numbers, due to the inherent ability of a turbulent flow to stay

attached, hence a profile that maximises the extent of laminar flow can be sought. Some common wing profiles that have been developed to such ends include the NACA 6 and 7-series.

1.3.2 Wing Planform Optimisation

A. Planar and Non-Planar Wing Planforms

A wing's planform has a large impact on its performance. For example, a wing with a high aspect ratio tends to have a relatively low induced drag but suffers from poor manoeuvrability. Munk (1923) showed that the minimum induced drag of a planar wing is achieved when the wake-induced downwash distribution is constant, which occurs when the lift distribution over a wing is elliptical. While an elliptical wing will produce a near-elliptical lift distribution, due to manufacturing difficulties and costs, they may not be feasible practically. Instead, by incorporating wing twist, which is much easier to manufacture, planforms can be designed to achieve a near-elliptical lift distribution, thereby reducing the induced drag (Kroo, 2001). A simple method to reduce the induced drag of a planform is to increase its aspect ratio, as sailplanes do. However, as suggested earlier, there are trade-offs with this approach, such as poor manoeuvrability and increased bending moments due to greater structural loading. Another approach to reduce the lift production near the wingtip of a planform is to taper the wing, which results in the wing's lift distribution approaching an elliptical distribution. This approach is common on modern passenger airliners. While an elliptical lift distribution over a planar wing results in a "minimum" induced drag for a given aspect ratio, extending the wing planform design to non-planar wings can result in an even lower induced drag. Figure 4 shows the potential span efficiency factors of various non-planar wings; while a wing with elliptical lift distribution will achieve the maximum theoretical planar span efficiency of 1, the planforms in fig. 4 achieve span efficiency factors of up to 1.46.

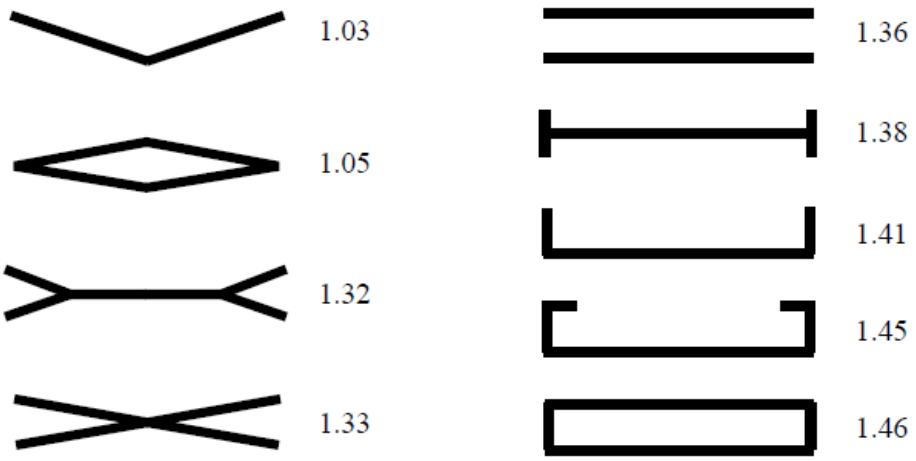

Figure 4: The span efficiency factor of various non-planar wings, with an aspect ratio of 5 (Kroo, 2001).

1.3.3 Flow Control Devices

The purpose of this section is to outline some common flow control devices designed to reduce the drag of a wing. Some of these flow control devices are not designed primarily to reduce the drag of a wing, but rather to increase the lift production; however, they often lead to a reduced drag. The flow control devices discussed will be separated into two groups; active and passive. Active flow control devices require control input, which can result in operation under a greater range of conditions, and greater drag reductions than passive flow control devices. Furthermore, if active flow control devices are detrimental to wing performance under certain conditions, they can be simply switched off. Some disadvantages of active flow control devices include that they are complicated to design and require a greater level of maintenance than passive flow control devices to continue performing effectively. Alternatively, a passive flow control device is one that, by virtue of its geometry, alters the flow physics without input.

A. Active Flow Control Devices

Vortex Generators

The vortex generator is one of the most diverse flow control devices, with designs ranging from active to passive, and designs that utilise multiple media. Active vortex generators include the Dielectric-Barrier-Discharge Plasma, DBD, vortex generator and the Zero-Net-Mass-Flux, ZNMF, vortex generator. The effects of vortex generators are varied and can delay flow separation, delay transition, or accelerate the onset of transition. A vortex generator delays separation by producing vortices that entrain higher momentum fluid into the boundary layer, thereby increasing the diminishing momentum of the boundary layer, whilst reducing its tendency to separate (Miklosovic *et al*., 2004).

Alternatively, a vortex generator can be used to influence the transition point of a boundary layer by either destructively or constructively interfering with its flow instabilities (Grundmann and Tropea, 2007; Grundmann and Tropea, 2008).

The vortex generator can also create either counter-rotating, or co-rotating, vortices, and these vortices can be oriented in a multitude of ways.

Plasma Vortex Generator

A DBD plasma vortex generator consists of two electrodes on either side of a dielectric material. By applying a sufficiently high voltage across the electrodes, the surrounding gas ionises and produces plasma (Corke *et al.*, 2010; Jukes and Choi, 2013). This plasma produces an electrohydrodynamic body force that imparts momentum to the adjacent air, which in turn produces vortices (Corke *et al.*, 2010; Jukes and Choi, 2013). For wings, a DBD plasma vortex generator is typically oriented to the oncoming flow, such that streamwise vortices are produced.

Zero Net Mass Flux Jets

ZNMF jets are cavities with membranes at the bottom. The membranes oscillate, drawing fluid into the cavity before expelling it, as shown in fig. 5. The expulsion of fluid results in the flow separating at the edge of the cavity, which produces a vortex that moves away from the wall (Glezer and Amitay, 2002).

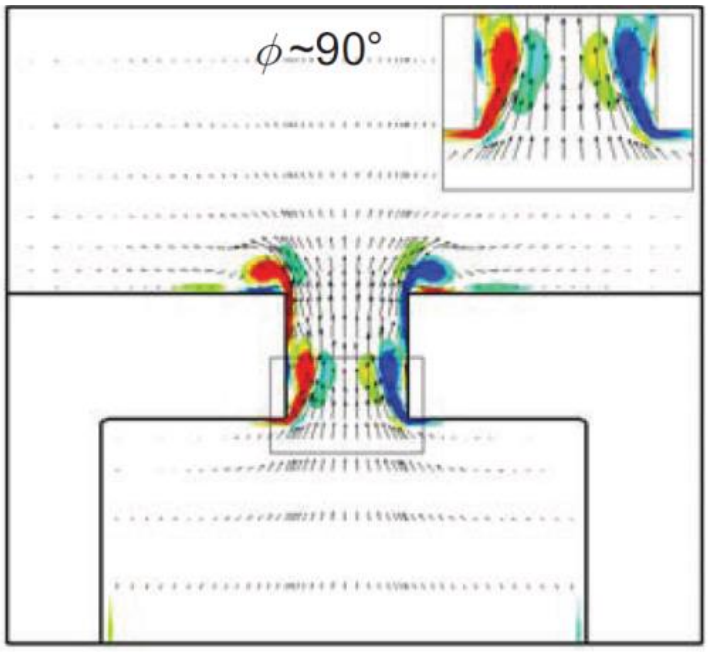

Figure 5: Zero Net Mass Flux jet forcing fluid out of the cavity and producing two vortices of opposite sign (Raju *et al*, 2009).

Circulation Augmentation

Circulation augmentation is where the exhaust of a jet is directed over the surface of a wing. This jet is attracted to the curved surface of the wing, which keeps the flow attached at higher AOAs (Houghton *et al.,* 2013). This effect is known as the Coandă effect, and the primary purpose of this flow control device is to allow lift generation at higher AOAs. An inherent drag reduction ensues from a reduced pressure drag. As a side note, the circulation around a wing can be augmented if the amount of air blown over the surface of the wing is greater than the amount required to keep the

flow attached (McCormick, 1999). This circulation augmentation then results in an increased lift production.

B. Passive Flow Control

Winglet

The winglet, as shown in fig. 6, is primarily used to reduce the induced drag of a wing producing lift. Reductions up to 15% have been observed (Yates and Donald, 1986). Winglets reduce the induced drag by reducing the strength of the wingtip trailing vortex and, in so doing, reduce the amount of momentum imparted to the wake.

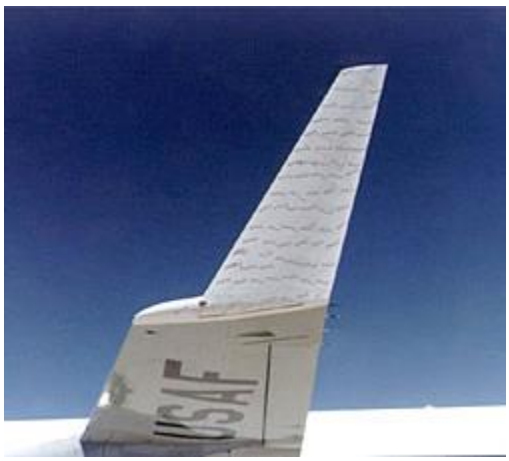

Figure 6: An airplane wing featuring a winglet (NASA, 2015).

Vortex Generators

Passive vortex generators aim to achieve a similar result to active vortex generators; to delay flow separation. Passive vortex generators are typically physical objects with a height similar to that of the boundary layer thickness. These objects then create vortices that interact with the boundary layer and the freestream flow, as shown in fig. 7. While this size of vortex generator is effective in delaying stall, there is often a profile drag penalty at low AOAs, where flow separation is not an issue (Lin, 2002). To overcome this disadvantage, vortex generators with heights ranging from 0.3 to 0.5 of

the boundary layer thickness can delay stall similarly, while incurring a minimal drag penalty at low AOAs (Lin, 2002).

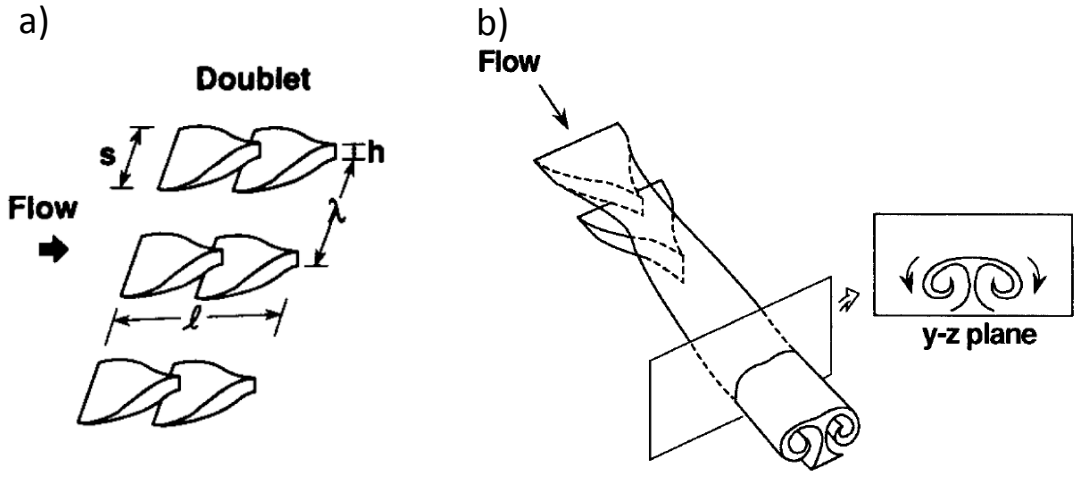

Figure 7: A) **a** typical passive vortex generator geometry and, b), vortex production (Lin *et al*, 1991).

Vortex generators can produce counter-rotating or co-rotating streamwise vortices with similar general effects on a wing's performance (Seshagiri, Cooper, and Traub, 2009). However, there are nuanced differences, such as the co-rotating vortex configuration delaying separation to a greater extent for three-dimensional separation, such as on swept wings, whereas counter-rotating vortex generators are slightly more effective at preventing two-dimensional separation (Lin, 2002).

Turbulators

A turbulator is a device that trips a laminar boundary layer to become a turbulent boundary layer. They are typically spanwise strips, as depicted in fig. 8, of sufficient height or roughness, or both, to cause transition without significantly increasing the pressure drag (Traub, 2011). Accelerating the onset of transition is beneficial at high AOAs, as it facilitates a greater mixing of momentum with the freestream, which delays separation (Simons, 1999). This ultimately results in the wing producing more lift and less drag.

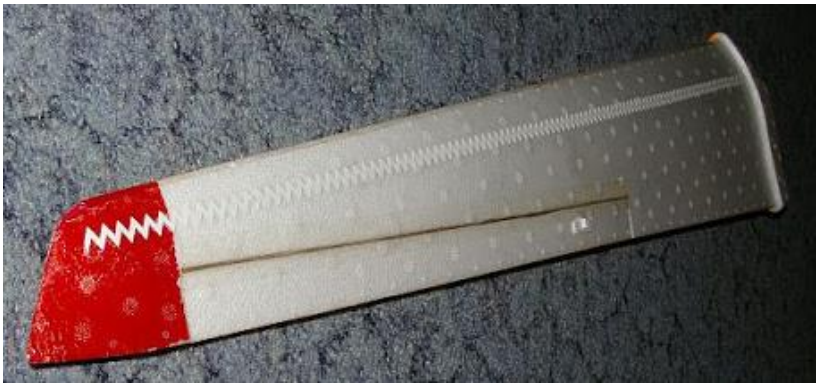

Figure 8: Wing with a turbulator along the entire span at approximately 25% of the wing chord (RC Groups, http://www.rcgroups.com/forums/showthread.php?t=740034&page=127, accessed 25th September 2015).

Wing Fences

Swept airfoils are subjected, due to their geometry, to spanwise flow. Spanwise flow increases the wing loading towards the wingtips (Harper and Maki, 1964), and subsequently increases the induced drag. Spanwise flow also results in a thicker boundary layer in the wingtip region, which causes the wingtips to stall at lower AOAs, reducing the wing's stability (Kocivar, 1980). Wing fences are surface-normal plates that run in the chordwise direction and act as physical barriers to hinder spanwise flow, shifting the lift distribution towards the wing root, which consequently decreases drag and increases stability (Berg and Hill, 1955). However, due to the additional surface area that the wing fences introduce, a friction drag penalty is incurred.

1.4 Tubercles

During the last decade, there has been increasing interest in a new, passive flow-control device known as tubercles. Tubercles are protuberances on the leading edge of a wing, and their origins lie with the Humpback whale. This type of flow control device is the focus of this thesis and will be discussed at length in the next chapter.

1.5 Gaps in the Knowledge of Tubercles and Motivation

From the literature review presented in Chapter 2, there are several effects of tubercles on wing performance that are unknown. These include:

1) How tubercles affect a swept wing's performance at pre-stall angles of attack.
2) How tubercles affect the components of drag of a wing.
3) How a tubercle's geometry affects a wing's performance.

It should be noted that a wing's performance refers to at least one of the following; the wing's lift coefficient, drag coefficient, or lift-to-drag ratio. By understanding these three gaps in the knowledge of tubercles, a more accurate assessment of potential tubercle applications can be made.

The first gap in the knowledge is important for a wide range of applications involving swept wings and rotating blades, such as the aforementioned passenger airliners, UAVs, turbomachinery, and wind turbines, as all of these applications will at some point in their operation function at pre-stall AOAs. The second gap in the knowledge of tubercles is also important, as by understanding the effects of tubercles on the components of a wing's drag, tubercles can be optimised to suit a given application. The third gap in the knowledge is relevant to every application of tubercles, as by understanding how the geometry of a tubercle affects a wing's performance, tubercles can be designed to maximise benefits. While some studies have considered a tubercle's amplitude and wavelength (Johari *et al.*, 2007; Hansen *et al.*, 2011), little is known about the effect of the "phase" of the tubercles on a wing's performance. The term, phase, is introduced in this thesis to describe the point along a tubercle at which a wing terminates. Therefore, the effect of the tubercle phase on the wing's performance will also be investigated. In accordance with the first gap, this investigation will be limited to swept wings at pre-stall AOAs. In addition to investigating the phase of the tubercles, the effects of the number of tubercles on the wing's performance will also be investigated. If a wing can be manufactured with one or two strategically placed tubercles, while still

delivering similar performance benefits, then the manufacturing costs are likely to be reduced. Furthermore, if tubercles can be used on less of a wing's leading edge, then a greater number of applications will be able to utilise tubercles. One example is the passenger airliner, which uses a range of leading-edge flow control devices, such as wing flaps and de-icing devices. Implementing tubercles in the areas where these flow control devices are used may not be feasible in significant numbers. Therefore, being able to use fewer tubercles in conjunction with other flow control devices will positively impact the applicability of tubercles.

1.6 Aims of the Thesis

From these gaps in the knowledge of tubercles, the aims of this thesis follow directly. These are:

1) To determine the effects of tubercles on swept wing performance at pre-stall angles of attack.
2) To determine the effects of tubercles on the components of drag at pre-stall angles of attack, and why they affect the components of drag at pre-stall angles of attack.
3) To determine the effects of a tubercle's geometry on wing performance at pre-stall angles of attack.

1.7 Approach

This thesis consists of six journal articles that are either published or submitted to high impact-factor international journals. This thesis consists of seven chapters; the first chapter being an introduction to this field. The second chapter details a comprehensive and current literature review of the field of tubercles. This literature review is a published journal article, and is used to develop the aims of this thesis. The third chapter consists of two journal articles that detail an investigation on two swept

wings, one without tubercles and one with tubercles along the entire leading edge. Through force measurements and wake surveys, the effects of tubercles on swept wing performance at pre-stall AOAs are determined, which allows a more accurate assessment of the effects of tubercles for a given application. It was found that tubercles reduced the lift coefficient by 4% to 6% and the drag coefficient by 7% to 9.5% in this range of AOAs. As a result, tubercles increased the lift-to-drag ratio by 2% to 6%. The reduced drag coefficient arose primarily from a reduced profile drag coefficient, with the tubercles having minimal effect on the induced drag coefficient. In addition, it was found that tubercles modulate both the profile and induced drag coefficients to form local maxima behind the troughs and peaks, respectively. Conversely, local minima in the profile and induced drag coefficients occurred behind the peaks and troughs, respectively. Additionally, the circulations of the tubercle vortices produced were calculated from the wake survey measurements, and it was found that sweeping a tubercled wing results in one vortex being stronger than the other; in this particular case, the outboard vortex of each tubercle was at least 5 times the strength of the inboard vortex.

The fourth chapter consists of one journal article that describes an oil-film flow visualisation investigation of the wings detailed in chapter three, and a computational fluid dynamics, CFD, model of the tubercled wing. This chapter elucidates the flow physics over the wings. It was found that, among other things, while the flow over the smooth wing began to separate from the trailing edge towards the leading edge in a uniform spanwise fashion, the flow over the tubercled wing began to separate behind the troughs first, due to a greater adverse pressure gradient than behind the peaks. The sweep resulted in the flow separating asymmetrically behind the troughs. To the author's knowledge, the first experimental evidence of the flow mechanism "Compartmentalization" was observed during the oil-film flow visualisation, whereby flow separation was confined to behind a single trough.

The fifth chapter consists of one journal article that details a numerically-conducted parametric analysis designed to investigate the effects of the tubercle amplitude, wavelength, and phase on a

wing's lift coefficient, induced drag coefficient, and lift-to-induced-drag ratio at low AOAs. In addition, this article details a Genetic Algorithm, GA, that optimises the tubercle amplitude, wavelength, phase, tubercle amount, and location in order to produce a wing with the greatest lift-to-induced-drag ratio. The benefit arising from this chapter is the ability to design tubercles to meet specific wing performance requirements. Before this parametric study was conducted, the framework for designing tubercles only covered the effects of the amplitude and wavelength on a wing's performance at stall and post-stall AOAs. The results of this article greatly extend this framework. This chapter shows that the phase of the tubercles has the greatest effect on the wing lift coefficient, induced drag coefficient, and lift-to-induced-drag ratio, whereas the wavelength has the least. As the amplitude and wavelength increase, the effects of tubercles on these performance parameters increase. The phase polarises the effects of tubercles, where in one phase range the tubercles reduce the lift and induced drag coefficients, while in another phase range the opposite occurs. It was found that if tubercles reduce the lift coefficient, then they typically reduce the induced drag coefficient as well, however, to a greater extent. This results in an increased lift-to-induced-drag ratio. The opposite trend, when tubercles increase the lift coefficient, was also found to be true.

The sixth chapter consists of one journal article that details the effects of a single tubercle on swept wing performance at pre-stall AOAs. This investigation compliments the investigation detailed in Chapter 5 as both chapters focus on the effects of the tubercle's geometry on wing performance. Chapter 6 focuses on three new wings, one with a smooth leading edge, and two tubercled leading edges that were manufactured and experimentally investigated. The basic planform was a swept wing with an interchangeable leading edge. A smooth leading edge, and two leading edges with single tubercles near the wingtips were tested. One of the tubercled leading edges ended on a certain phase while the other ended on the opposite phase. The three wings were investigated with the same experimental techniques as the first two wings. The results were that neither tubercle configuration significantly altered the lift coefficient, drag coefficient, or lift-to-drag ratio of the

smooth wing. At AOAs nearing stall, both tubercle configurations had increased effects on the profile and induced drag coefficients, with changes of 5% and 2%, respectively, seen. As a result, it was concluded that a single tubercle of conventional sizing terminating at the wingtip is not as effectual on the wing performance parameters as tubercles along a wing's entire leading edge.

The final chapter draws conclusions from the previous chapters and details general relationships between various tubercle geometric parameters and wing performance parameters. These relationships act as a framework for designing tubercles. In addition, potential directions for future investigations are presented and the significance of the detailed directions are discussed.

1.8 Publications

This thesis consists of several peer-reviewed publications and submitted journal articles in accordance with The University of Adelaide's Academic Program Rules 2016.

Journal articles included in this thesis are:

1. Bolzon, M.D., Kelso, R.M., Arjomandi, M., "Tubercles and Their Applications", *The Journal of Aerospace Engineering*, 2015. doi: 10.1061/(ASCE)AS.1943-5525.0000491.

2. Bolzon, M.D., Kelso, R.M., Arjomandi, M., "Force Measurements and Wake Surveys of a Swept Tubercled Wing", accepted for publication by *The Journal of Aerospace Engineering*, 2016.

3. Bolzon, M.D., Kelso, R.M., Arjomandi, M., "Formation of Vortices on a Tubercled Wing, and Their Effects on Drag", *Aerospace Science and Technology*, 2016. doi: 10.1016/j.ast.2016.06.025.

4. Bolzon, M.D., Kelso, R.M., Arjomandi, M., "Tubercles: A Flow Visualization Study", *submitted to Experimental Thermal and Fluid Science*, 2016.

5. Bolzon, M.D., Kelso, R.M., Arjomandi, M., "Leading Edge Tubercles: A Parametric and Optimization Study", *submitted to Journal of Aerospace Information and Systems*, 2016.

6. Bolzon, M.D., Kelso, R.M., Arjomandi, M., "Effects of a Single Tubercle Terminating at a Swept Wing's Tip on Wing Performance", *submitted to Experimental Thermal and Fluid Science*, 2016.

References

Anderson, J.D., "Introduction to Flight", McGraw-Hill, 3rd Edition, 1989.

Anderson, J.D., "Fundamentals of Aerodynamics", McGraw-Hill, 5th Edition, 2011.

Berg, M.W. and Hill, D., "Spanwise Flow Control of Fluid Swept Lifting Surfaces", U.S. Patent, Patent Number 2,709,052, 24th May 1955.

Birch, D., Lee, T., Mokhtarian, F., and Kafyeke, F., "Structure and Induced Drag of a Tip Vortex", *Journal of Aircraft*, Vol. 41, No. 5, 2004.

Brune, G.W., "Quantitative Low-Speed Wake Surveys", *Journal of Aircraft*, Vol. 31, No. 2, 1994.

Corke, T.C., Enloe, C.L., and Wilkinson, S.P, "Dielectric Barrier Discharge Plasma Actuators for Flow Control", *Annual Reviewof Fluid Mechanics*", Vol. 42, pp. 505-529, 2010. doi: 10.1146/annurev-fluid-121108-145550.

Gerontakos, P. and Lee, T., "Near-Field Tip Vortex Behind a Swept Wing Model", *Experiments in Fluids*, Vol. 40, pp. 141-155, 2006.

Glezer, A. and Amitay, M., "Synthetic Jets", *Annual Review of Fluid Mechanics*, Vol. 34, pp. 503-529, 2002.

Grundmann, S. and Tropea, C., "Experimental Transition Delay Using Glow-Discharge Plasma Actuators", *Experiments in Fluids*, Vol. 42, pp. 653-657, 2007. doi: 10.1007/s00348-007-0256-8.

Grundmann, S. and Tropea, C., "Active Cancellation of Artifically Introduced Tollmien-Schlichting Waves Using Plasma Actuators", *Experiments in Fluids*, Vol. 44, pp. 795-806, 2008. doi: 10.1007/s003-48-007-0436-6.

Hansen, K.L., Kelso, R.M. and Dally, B.B., "Performance Variations of Leading-Edge Tubercles for Distinct Airfoil Profiles", *American Institute of Aeronautics and Astronautics* (AIAA) Journal, Vol. 49, No. 1, Jan. 2011, pp.185-194. doi: 10.2514/1.J050631.

Harper, C.W. and Maki, R.L., "A Review of the Stall Characteristics of Swept Wings", *NASA Technical Note* D-2373, Calif., 1964.

Hoerner, S.F., "Fluid- Dynamic Drag", Hoerner Fluid Dynamics, Bakersfield, 1965.

Houghton, E.L. and Brock, A.E., "Aerodynamics for Engineering Students", Butler and Tanner Ltd., London, 2nd ed., 1970.

Houghton, E.L., Carpenter, P.W., Collicott, S.H. and Valentine, D.T., "Aerodynamics for Engineering Students, Butler and Tanner Ltd., London, 6th Edition., 2013.

Johari, H., Henoch, C., Custodio, D., and Levshin, A., "Effects of Leading-Edge Protuberances on Airfoil Performance", *AIAA Journal*, Vol. 49, No. 1, pp. 185-194, 2007. doi: 10.2514/1.J050631.

Jukes, T.N. and Choi, K.S., "On the Formation of Streamwise Vortices by Plasma Vortex Generators", *Journal of Fluid Mechanics*, Vol. 733, pp. 370-393, 2013.

Kocivar, B., "Wrong-Way Wings Aid Maneuverability of Supersonic Planes", *Popular Science*, April, 1980.

Kroo, I., "Drag Due to Lift: Concepts for Prediction and Reduction", *Annual Review of Fluid Mechanics*, Vol. 33, pp. 587-617, 2001.

Lin, J., Selby, G.V., and Howard, F.G., "Exploratory Study of Vortex-Generating Devices for Turbulent Flow Separation Control", *AIAA, 29th Aerospace Sciences Meeting*, Jan, 1991, Reno, Nevada.

Lin, J.C., "Review of Research on Low-Profile Vortex Generators to Control Boundary-Layer Separation", *Progress in Aerospace Sciences*, Vol. 38, pp. 389-420, 2002.

Lissaman, P.B., "Low-Reynolds-Number Airfoils", *Annual Review of Fluid Mechanics*, Vol.15, pp. 223-239, 1983.

McCormick, B.W., "Aerodynamics, Aeronautics, and Flight Mechanics", John Wiley & Sons, Inc., 2nd Edition.

McCormick, B.W., "Aerodynamics of V\STOL Flight", Dover Publications, New York, pp. 8.

McMasters, J.H. and Henderson, M.L, "Low Speed Single Element Airfoil Synthesis", *Tech. Soaring*, Vol. 6, No. 4, 1981.

Miklosovic, D.S., Murray, M.M., Howle, L.E., and Fish, F.E., "Leading-Edge Tubercles Delay Stall on Humpback Whale (Megaptera Novaeangliae) Flippers", *Physics of Fluids*, Vol. 16, L39, 2004. doi: 10.1063/1.1688341.

Munk, M., "The Minimum Induced Drag of Aerofoils", *Report No. 121, National Advisory Committee for Aeronautics*, 1923.

NASA, "Wake Vortex Study at Wallops Island", 4th May 1990. Photo ID: EL-1996-00130.

NASA, "Winglets". Accessed 10th September 2015, http://www.nasa.gov/centers/dryden/about/Organizations/Technology/Facts/TF-2004-15-DFRC.html.

Raju, R., Aram, E., Mittal, R., and Cattafesta, L., "Simple Models of Zero-Net Mass-Flux Jets for Flow Control Simulations", *International Journal of Flow Control*, Vol. 1, No. 3, 2009.

Roskam, J., "Airplane Design Part I: Preliminary Sizing of Airplanes", Design, Analysis and Research Corporation, Kansas, 4th ed., 2005.

Seshagiri, A., Cooper, E., and Traub, L.W., "Effects of Vortex Generators on an Airfoil at Low Reynolds Numbers", *Journal of Aircraft*, Vol. 46, No. 1, 2009. Doi:

Simons, M., "Model Aircraft Aerodynamics", Hempel Hempstead, United Kingdom, 2002.

Traub, L.W., "Experimental Investigation of the Effect of Trip Strips at Low Reynolds Number", *Journal of Aircraft*, Vol. 48, No. 5, 2011. doi: 10.2514/1.c031375.

Yates, J.E. and Donald, C.D., "Fundamental Study of Drag and an Assessment of Conventional Drag-Due-to-Lift Reduction Devices", NASA Contract Rep 4004, 1986.

Chapter 2

Literature Review

This chapter includes the following journal article:

Bolzon, M.D., Kelso, R.M., Arjomandi, M., "Tubercles and Their Applications", *The Journal of Aerospace Engineering*, 2015. doi: 10.1061/(ASCE)AS.1943-5525.0000491.

This chapter consists of a thorough literature review of tubercles and their applications. This covers the key findings of tubercles to date. From this literature review, the gaps in the knowledge of tubercles, motivation, aims, and approach to the thesis, as detailed in chapter 1. As such, this chapter provides the basis for this thesis, as it provides the direction for investigation, and presents the significance of this thesis. The literature review detailed in this chapter is divided into two sections. The first section is a review article that has been published in The Journal of Aerospace Engineering, which covers the literature pertaining to tubercles from the beginning of their fluid mechanics studies to the end of 2014, when the review article was accepted for publication. The second section is an addendum to the first section, and covers the literature pertaining to tubercles from the start of 2015 to the time of this thesis submission.

2.1 Literature Review Article

Statement of Authorship

Title of Paper	Tubercles and Their Applications
Publication Status	☑ Published ☐ Accepted for Publication ☐ Submitted for Publication ☐ Unpublished and Unsubmitted w ork w ritten in manuscript style
Publication Details	Bolzon, M.D., Kelso, R.M., Arjomandi, M., "Tubercles and Their Applications", *The Journal of Aerospace Engineering*, 2015. doi: 10.1061/(ASCE)AS.1943-5525.0000491.

Principal Author

Name of Principal Author (Candidate)	Michael Bolzon		
Contribution to the Paper	Researched literature, interpreted information, wrote manuscript, and acted as corresponding author.		
Overall percentage (%)			
Certification:	This paper reports on original research I conducted during the period of my Higher Degree by Research candidature and is not subject to any obligations or contractual agreements with a third party that would constrain its inclusion in this thesis. I am the primary author of this paper.		
Signature		Date	

Co-Author Contributions

By signing the Statement of Authorship, each author certifies that:

i. the candidate's stated contribution to the publication is accurate (as detailed above);

ii. permission is granted for the candidate in include the publication in the thesis; and

iii. the sum of all co-author contributions is equal to 100% less the candidate's stated contribution.

Name of Co-Author	Richard Kelso		
Contribution to the Paper	Supervised research, aided interpretations, and reviewed manuscript.		
Signature		Date	

Name of Co-Author	Maziar Arjomandi		
Contribution to the Paper	Supervised research, aided interpretations, and reviewed manuscript		
Signature		Date	

Tubercles and Their Applications

Michael. D. Bolzon[1]; Richard M. Kelso[2]; and Maziar Arjomandi[3]

Abstract: The implementation of tubercles on foils has demonstrated significant benefits, with the most evident occurring during post-stall. However, the flow mechanism(s) responsible for these benefits is currently unknown, and several possibilities have been proposed. These include compartmentalization, vortex lift, varying effective angle of attack, and boundary layer momentum exchange. Currently, it is only known that tubercles create pairs of streamwise, counter-rotating vortices. By determining how tubercles work, the effects of their addition to untested foils in untested conditions can be hypothesized. This paper reviews the current status of the field of tubercles, comparing hypotheses with published results. The effects of tubercles on the principal components of drag are conjectured from consideration of similar flow control devices. Current applications of tubercles are detailed, and potential applications are suggested. **DOI: 10.1061/(ASCE)AS.1943-5525.0000491.**

Author keywords: Aerodynamics; Aerospace engineering; Control; Flow; Vortices; Mechanics.

Introduction to Tubercles

Flow control devices are commonly used on airfoils, hydrofoils, and wings to enhance their performance. These devices, whether passive or active, are designed to increase foil efficiency, stability, and/or reduce operational cost. There are many different types of devices aimed at achieving these goals, and some perform better than others. Recently, there has been a growing interest in a new type of flow control device, one which can be found in the natural world; tubercles. Tubercles are protuberances found on the leading edge of a Humpback whale pectoral flipper as shown in Fig. 1. They can be ideally characterized by two parameters, amplitude (A) and wavelength (λ), as shown in Fig. 2. Jurasz and Jurasz (1979) noted that for their size, the Humpback whale is incredibly agile, capable of underwater acrobatics. Fish and Battle (1995) suggested that the tubercles on the leading edge of the Humpback whale may be responsible for the whale's agility.

It is now well documented that when tubercles are placed on the leading edge of a foil or wing, the stall becomes more gradual and is typically delayed (Stein and Murray 2005; Miklosovic et al. 2004). The most evident effects of tubercles occur at high angles of attack, and currently, little is known about their effects at other angles of attack. It should be noted that from here on a foil will mean a two-dimensional lifting surface, whereas a wing will mean a finite or semifinite lifting surface. In the paper, the tubercle geometry nomenclature first proposed by Hansen (2012) is adopted. The amplitude, A, and wavelength, λ, are used in a condensed form, for example $A4\lambda10$ indicates tubercles with amplitudes of 4 mm and wavelengths of 10 mm.

[1]Ph.D. Candidate, Dept. of Mechanical Engineering, Univ. of Adelaide, Adelaide, SA 5005, Australia (corresponding author). E-mail: michael.bolzon@adelaide.edu.au

[2]Associate Professor, Dept. of Mechanical Engineering, Univ. of Adelaide, Adelaide, SA 5005, Australia.

[3]Senior Lecturer, Dept. of Mechanical Engineering, Univ. of Adelaide, Adelaide, SA 5005, Australia.

Note. This manuscript was submitted on April 28, 2014; approved on January 12, 2015; published online on April 14, 2015. Discussion period open until September 14, 2015; separate discussions must be submitted for individual papers. This paper is part of the ***Journal of Aerospace Engineering***, © ASCE, ISSN 0893-1321/04015013(10)/$25.00.

Tubercle Designs and Tests

Tubercular Geometry

There are several tubercle geometric parameters that affect their performance, with the most researched being amplitude, A, and wavelength, λ. In addition to these two parameters, the A/λ ratio has also been investigated by Hansen (2012), where it was hypothesized that there existed an optimal ratio.

While these parameters can describe a tubercle geometry, there is one more key property that determines their shape, and that is whether they are merely additions to the leading edge, so the foil has a constantly changing thickness-to-chord ratio, such as that found in Johari et al. (2007), or whether the thickness-to-chord ratio remains constant, such as that found in Hansen (2012). The former option results in the foil geometry after the leading edge to remain largely unchanged, whereas the latter option results in the entire foil being altered, and ridges and valleys forming along the entire chord of the foil. Currently, these methods of manufacturing tubercles have not been widely discussed, and the term *tubercle* typically refers to both possibilities. For the commonly tested tubercule amplitudes and wavelengths, typically in the order of 2–10 mm and 8–50 mm, respectively, this factor does not appear to alter the performance, as both types produce similar effects on lift and drag. However, if the wavelengths of the tubercles were much smaller, and the tubercled foil was designed to preserve a constant thickness-to-chord ratio, then tubercles would start to approximate longitudinal striations. This could then alter their effects on foil performance.

Conditions and Types of Foils and Wings Tested

The highest Reynolds number wind tunnel test conducted to date reached 6.31×10^5 (Miklosovic et al. 2007), which, depending on the tunnel turbulence intensity and flow conditioning, could still be considered transitional. Low Reynolds numbers are found in many applications, such as micro-aerial vehicles (Kunz 2003), and such experiments allow a direct assessment of their viability to such applications. However, large-scale applications, such as modern passenger aircraft, operate at Reynolds numbers two orders of magnitude higher than this, and are well into the fully turbulent region. Although the highest Reynolds number wind tunnel test may be

Fig. 1. Humpback whale showing tubercles on pectoral flippers (image by Wilfried Niedermayr, with permission)

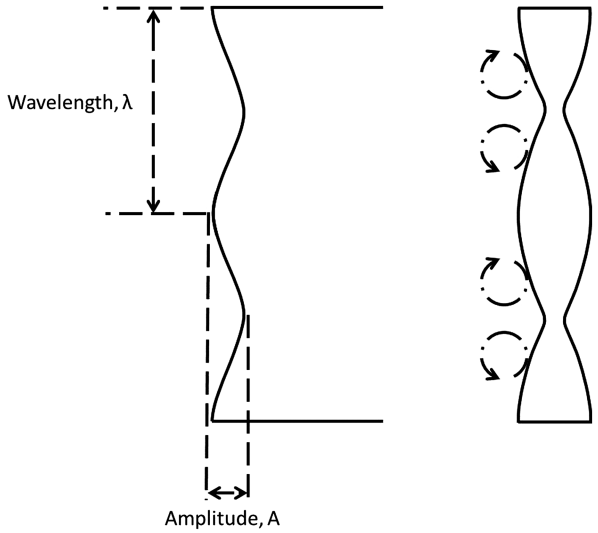

Fig. 2. Sketch of tubercles on the leading edge of a foil. Left indicates tubercle geometric parameters; right is a cross section of a tubercled foil sketch, showing the streamwise, counter-rotating vortices produced by the tubercles; notation is adapted from Hansen et al. (2009)

considered fully turbulent, albeit marginally, further insight into tubercles at higher Reynolds numbers can be found by considering a water tunnel test by Weber et al. (2010), which consider Reynolds numbers up to 8.6×10^5.

Weber et al. (2010) tested three rudders, one smooth and two tubercled, each with a NACA 0016 profile. The tubercled rudders had the same amplitudes, but different wavelengths. They found that at low Reynolds numbers, the stall was more progressive, which resulted in a reduced lift near the stall angle of attack, but a higher lift post-stall. As the Reynolds number increased, the stall was still more progressive for the tubercled rudders; however, the lift at the stall angle of attack increased. This indicates that tubercles may have greater benefits for wings at higher Reynolds numbers; however, further testing is required.

Hansen (2012) largely considered the effects of tubercles on thick foils at a Reynolds number of 120,000. She found that, like other experiments, tubercles produce a more gradual stalling foil. She also found that due to the Reynolds number, laminar separation bubbles were forming on the suction sides of the foils. She also tested the effects of a boundary layer trip to simulate higher Reynolds number flow, and found that except for the presence and effects of laminar separation bubbles, the tripped tubercled foils had the same stall characteristics as the untripped tubercled foils. This suggests that the general effects of tubercles on foil performance are Reynolds number independent.

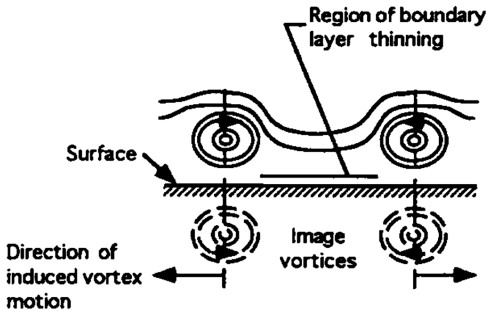

Fig. 3. Boundary layer thinning, (reprinted from Jacobi and Shah 1995, with permission from Elsevier)

Currently, the majority of tests have only considered thick, symmetric foils and wings as they approximate Humpback whale flippers (Fish and Battle 1995). However, Deutsches Zentrum für Luft- und Raumfahrt (DLR) is investigating the effects of tubercles on helicopter blades (Coxworth 2012). While no quantitative information has been released, qualitative media releases suggest that tubercles do have similar effects for thinner foils and wings, namely, reducing the severity of and delaying stall.

Tubercle Mechanisms

It is known that tubercles produce pairs of streamwise, counter-rotating vortices (Pedro and Kobayashi 2008; Stanway 2008; Kerschgens 2008; Hansen 2012) as shown in Fig. 2, but the way in which these vortices interact with the flow over a foil or wing is unknown. There have been many attempts to explain how tubercles affect the flow over a foil or wing; however, none has been conclusive. The more widely accepted theories will be discussed below. It should be pointed out that by applying the method of images to these vortices, it can be seen that vortices with a common downwash will move down and away from each other, as shown in Fig. 3. The opposite will occur for vortices with a common upwash. Therefore, the net effect of vortices in the regions of downwash will be greater than the net effect of vortices upwashing, as seen in Pauley and Eaton (1987). This is important, as many theories explaining how tubercles work suggest that the vortices have one effect in the common downwash regions, while having the opposite effect in the common upwash regions.

Vortex Generators

One of the stronger theories was proposed by Miklosovic et al. (2004), who suggested that the stall benefits of tubercles arise as they act in a similar way to vortex generators. Vortex generators are often used on conventional aircraft, and their purpose is to increase the momentum of the boundary layer through mixing with the freestream, which will result in a delayed stall (Slangen 2009). It is notable that the height of a vortex generator is typically in the same order of magnitude as the boundary layer thickness (Lin 2002), whereas the amplitude and wavelength of a tubercle is typically larger than the boundary layer thickness. Hence, it was proposed that tubercles could not act in a similar fashion to vortex

generators (Van Nierop 2009). Hansen (2012) proposed that the effective height of a tubercles is calculated as $h_{\text{eff}} = A \sin \alpha$, where A is the tubercle amplitude and α is the angle of attack. Using this parameter, the effective-height-to-boundary-layer-thickness ratio is typically less than 1 (Zhang et al. 2013), which is similar to with typical vortex generators. Moreover, Zhang et al. (2014) determined that the effective-height-to-boundary-layer-thickness ratio of a tubercle is typically 0.1–0.5, which is more similar to micro-vortex generators.

To investigate whether tubercles do act like vortex generators, Stein and Murray (2005) conducted tests comparing tubercles and vane vortex generators on NACA 0020 foils. The tubercles had an amplitude of 7.1 mm and a wavelength of 36.5 mm (or $A7.1\lambda36.5$ according to the nomenclature of Hansen 2012), while the vortex generator shape, location, and size were optimized through the guidelines of Taylor (1950). They found that when compared with the smooth foil, the vortex generator foil produced similar pre-stall lift, while producing slightly more post-stall lift. In comparison, the tubercled foil only produced the same lift from 0 to 3 degrees as the smooth airfoil, and from then on its lift was significantly reduced. From this major difference, this study might suggest that tubercles do not act like vortex generators; however, the vortex generators used were optimized, whereas the tubercles were not. There are other vane vortex generator geometries that yield similar lift characteristics to the tested tubercled foil (Seshagiri et al. 2009), and furthermore, other tubercle geometries tested by Hansen (2012) and Johari et al. (2007) are capable of producing similar lift characteristics to the vortex generator foil tested by Stein and Murray (2005). While this study is important in showing the potential differences between tubercles and vortex generators, the results obtained are not sufficiently extensive to conclude that tubercles do not act in a similar fashion to vortex generators.

Induced Flow and Vortex Lift

The second and third theories, termed here *induced flow* and *vortex lift*, respectively, are seemingly different; however, one is potentially just an extreme case of the other, as will be discussed. As outlined in Fig. 2, tubercles produce pairs of streamwise, counter-rotating vortices, and as such a region of common downwash occurs over each peak, while a region of common upwash occurs over each trough. Where downwash occurs, it is suggested that the effective angle of attack is reduced, resulting in an increased stall angle, whereas the opposite will occur where there is upwash (Van Nierop et al. 2008). This spatially periodic change in stall angle will then result in a more gradual stall process, where it is stretched out over a greater range of geometric angles of attack. In addition to this effect, the downwash will thin the boundary layer over the peaks, and vice versa over the troughs, resulting in a further delayed onset of stall over the peaks and a further aided onset of stall over the troughs. This theory can then be further extended to another theory, vortex lift.

Vortex lift is a way of producing lift that is less susceptible to stalling. By creating strong vortices over the suction side of a foil or wing, the downwash of the vortices causes the flow to remain attached over the surface, thereby delaying flow separation. An example of this type of lift can be found on a delta wing, whereby the leading edges are sharp and highly swept, which aids the formation of these vortices. It has been proposed that the streamwise, counter-rotating vortices created by tubercles could manipulate the flow in a similar fashion to delta wings (Custodio 2007). However, there are at least two major differences between a tubercled wing and a delta wing. The first major difference is that while a delta wing creates a single pair of streamwise counter-rotating vortices, only the common downwash section occurs over the wing surface, while the upwash areas are located away from the wing surface. Therefore, while a tubercle may produce vortex lift in regions of common downwash, regions of common upwash will cause the flow to separate sooner. From this difference, it is proposed that the two theories outlined in this section could be just one single theory, where neither explanation is complete. To further elucidate, the induced flow theory does not consider the possibility of vortex lift, whereas the theory of vortex lift proposed by Custodio (2007) does not consider the regions of upwash occurring over a wing surface.

The second major difference between a tubercled wing and a delta wing is that a tubercle is much smaller, only making up a small portion of the wing area. Therefore, the strength of the vortices created by the tubercles cannot be expected to rival those created by the much larger leading edge of a delta wing. Therefore, a question arises as to how much vortex lift a small tubercle can actually produce.

It is expected that if tubercles produce significant amounts of vortex lift, the pitching moment will change, as the lift distribution will change. Results from Miklosovic et al. (2007) showed that for both foils and wings, tubercles do not alter the pitching moment during pre-stall or post-stall, but during stall, from 10 to 17° and 16 to 18° for foils and wings, respectively, tubercles clearly alter the pitching moment. As the pitching moment only changes during stall, the amount of vortex lift seems to be minimal, as if a significant amount of vortex lift were produced, the pitching moment should be affected not only during stall, but post-stall as well. This is because tubercles typically increase the amount of post-stall lift, indicating that if vortex lift is the driving mechanism then it should be present post-stall as well. To further support this point, as the angle of attack increases more vortex lift should be produced, thereby potentially increasing the effect of tubercles on pitching moment. As almost no effect on pitching moment is seen post-stall, the idea that vortex lift is the driving mechanism does not seem consistent with what is expected.

The magnitude of the vortex lift created by a wing is dependent on the sweep angle (Luckring 2004). Currently, two tubercle geometry sensitivity analyses have been performed (Johari et al. 2007; Hansen et al. 2011). The more extensive considered the following three tubercle geometries: $A2\lambda7.5$, $A4\lambda15$, and $A8\lambda30$ (Hansen et al. 2011). This is important as all three of these geometries have the same local sweep angle, but each successive one is double the previous one's physical dimensions. Fig. 4 shows the lift and drag of each tubercled foil along with the smooth counterpart. It shows that as the tubercles increase in size, the lift near stall drops, and stall starts to occur at a lower angle of attack. If tubercles were to produce significant amounts of vortex lift, it would be expected that stall should be somewhat delayed. Instead, the opposite is seen. Furthermore, unlike delta wings, where the total lift is typically equal to, or greater than what is predicted by potential flow theory for all angles of attack (Polhamus 1966, 1971; Hemsch and Luckring 1990), the addition of tubercles results in lower lift for angles of attack just prior to stall. Additionally, the amount of lift produced post-stall does not significantly exceed what is experienced pre-stall. These differences between what is expected and what occurs, suggest that the amount of vortex lift created by tubercles is, at best, very small, and therefore is most likely not the driving mechanism of tubercles, at least for this range of angles of attack.

Wing Fences

The next theory attempting to explain how tubercles work is *compartmentalization*. This theory was proposed by Watts and Fish (2001), who conducted one of the first fluid mechanics studies of tubercles. This study consisted of an inviscid panel method

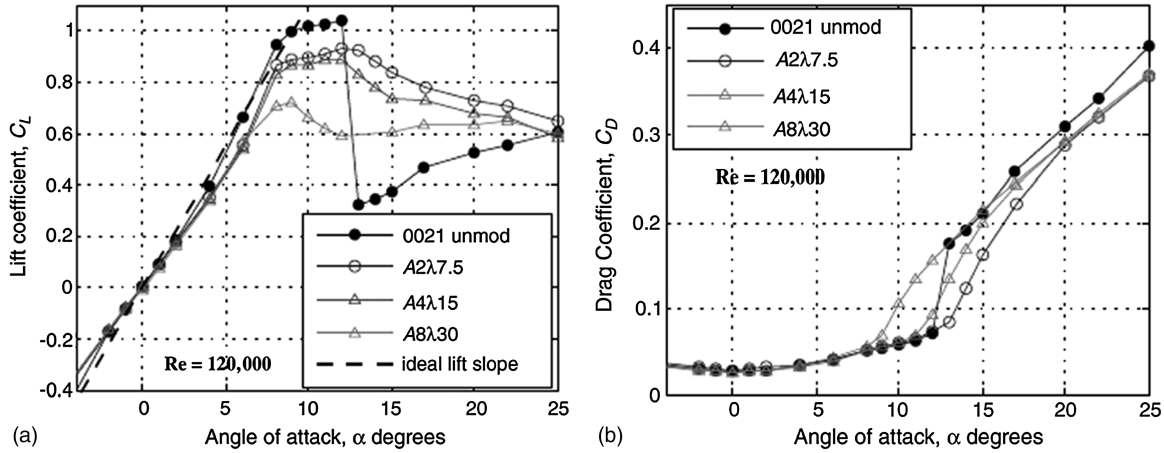

Fig. 4. Constant amplitude-to-wavelength (A/λ) (reprinted from Hansen et al. 2011, with permission): (a) lift; (b) drag

simulation, of a wing with and without tubercles. At a 10° angle of attack, a 4.8% increase in lift and a 10.9% reduction in drag were found. Due to the model being inviscid, it was concluded that the drag reduction must have been a reduction in induced drag. From this simulation, it was proposed that tubercles act in a similar fashion to wing fences, whereby the flow is prevented from traveling spanwise. Unlike wing fences, which are physical barriers, tubercles would create virtual barriers through the streamwise, counter-rotating vortices. This theory can be extended to explain the gradual stall of a tubercled foil or wing.

When a section of a foil or wing starts to stall, the stall cell then starts to spread to the rest of the wing. By compartmentalizing the flow into pockets, if one pocket stalls, other pockets will not be affected. Hence stall cells become confined and more of the foil will continue to produce lift [T. Wang, "Aircraft wing stall control device and method," U.S. Patent No. 4,702,441 (1987)]. In addition, compartmentalization could have further stall benefits for swept-back wings, as the boundary layer becomes thicker near the wingtip trailing edge and is much more prone to separation.

The numerical simulation by Pedro and Kobayashi (2008) also demonstrated similarities between tubercles and wing fences, providing further evidence for this mechanism. However, there is a significant discrepancy between common results and this proposed mechanism. Compartmentalization could produce the observed gradual stall phenomenon by reducing the ability for stall to progress, but it would not give rise to a delayed initial stall angle for an unswept wing, as the angle of attack when stall first occurs would not be affected. Therefore, if this mechanism is present, then there must be at least one other mechanism that is responsible for the delayed initial stall angle.

Greater Distance for Pressure Recovery

Early studies of tubercles treated them as leading edge extensions, essentially attachments that did not alter the thickness of the foil. This led to a hypothesis that the addition of tubercles periodically increased the chord along the span, resulting in a lower thickness-to-chord ratio. The section that had reductions in thickness-to-chord ratios, behind the peaks, would then result in a lower pressure gradient and would stall at a higher angle of attack (Van Nierop et al. 2008). However, later, Hansen et al. (2011) utilized a design that preserved the thickness-to-chord ratio along each tubercular wavelength. It was found that these specimens were still able to soften stall. Therefore, it is unlikely that this mechanism is the responsible for the effects tubercles.

One extension of this theory suggests that as the pressure over the peaks is observed to be greater than in the troughs (Hansen 2012; Watts and Fish 2001), the pressure gradient in the troughs must then be higher than over the peaks. This could result in the troughs separating prematurely. However, the flow structure may be more complex than this simple description, as the troughs, which are at a lower pressure, may relieve the higher pressure over the peaks, causing lateral flow and thereby reducing the pressure gradient in the troughs and increasing it over the peaks. Whether this potential phenomenon exists, and to what extent, is unclear.

Mechanism Present

From the above discussions of each potential tubercle mechanism, it appears unlikely that there is just one mechanism present, but multiple with each having some effect. However, from what is currently known about tubercles, the driving mechanism appears to be that tubercles act like vortex generators. Experimental results (Zhang et al. 2013, 2014) and numerical simulation (Rostamzadeh et al. 2014) suggest that the vortices created by tubercles can alter the boundary layer velocity profile and the direction of flow within the boundary layer. Therefore, it is highly likely that these vortices can mix higher momentum fluid into the near wall flow, which would delay stall in a similar fashion to vortex generators.

Effect of Tubercles on Foil and Wing Performance

The effects of tubercles on foil and wing performance can be separated into three main groups: pre-stall, stall, and post-stall. The most obvious effects occur during stall and in the post-stall regimes. Furthermore, tubercles have slightly different effects on foils to wings, and these will also be discussed.

Pre-Stall

Currently, the vast majority of tubercle studies have been performed in laminar or transitional flows, and the effects of tubercles on foil and wing performance have been very small, where the most noticeable effect occurs when a laminar separation bubble is present. For wings and foils alike, the presence of a laminar separation bubble (LSB) can be beneficial under the right circumstances. Data from Hansen (2012) showed that an LSB can increase the lift of a wing or foil, while having very little effect on drag. However, for a tubercled wing or foil, the LSB still increases lift, but less

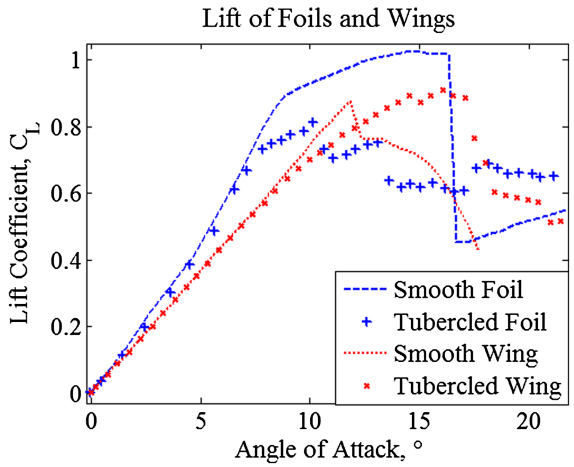

Fig. 5. Lift slope comparison between foils and wings, with and without tubercles (data from Miklosovic et al. 2007)

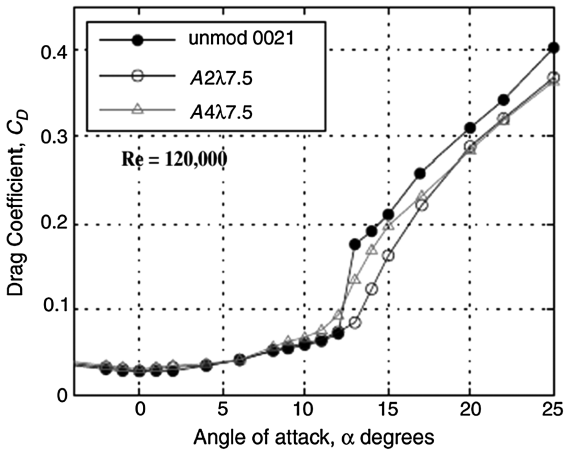

Fig. 7. Effect of tubercles amplitude (A) on drag of a foil (reprinted from Hansen et al. 2011, with permission); unmod 0021 refers to a smooth NACA 0021 foil

than for the smooth foil or wing. In addition, the presence of an LSB can severely increase drag, as can be seen in Fig. 4 for a tubercle geometry of $A8\lambda30$.

Stall

Fig. 5 shows that tubercles make the stall more gradual, not only on foils, but on wings as well. However, unlike for foils, tubercles can also delay wing stall, which also results in a reduction in drag, and potentially increase the maximum lift. The reason why tubercles affect wings more than foils is currently unknown; however, it does provide a clue as to which one of the aforementioned potential mechanisms could be occurring.

As tubercles significantly delay stall for a wing, but not for foils, it is evident that the three-dimensional effects of a wing influence the effects of tubercles. From the previously presented theories, only one is mainly dependent on three-dimensional effects, and that is compartmentalization. It could be that the tubercles are restricting the spanwise flow over a wing, thereby delaying the stall in some regions.

Sensitivity studies have shown that, for both wing and foils, increasing the tubercle amplitude results in a more progressive stall, and lower maximum lift (Johari et al. 2007; Hansen et al. 2011), as shown in Fig. 6. As the stall becomes more gradual, the lift prematurely decreases, while the drag prematurely increases. The effect of the tubercle wavelength is not as clear, with one sensitivity study suggesting that an increase in wavelength results in a more sudden stall (Hansen 2012), whereas another study shows that changing the tubercle wavelength results in little change to the lift (Johari et al. 2007).

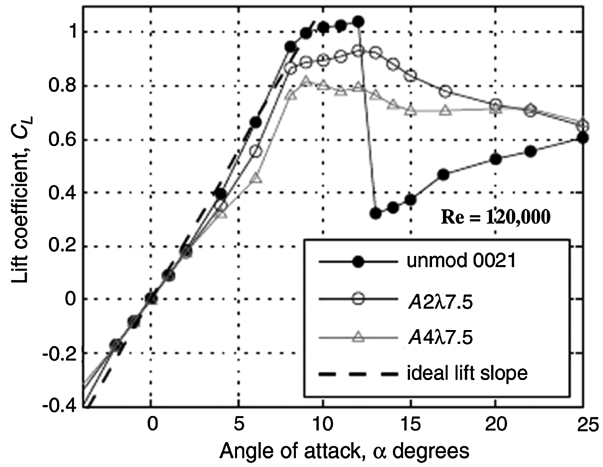

Fig. 6. Effect of tubercles amplitude (A) on lift of a foil (reprinted from Hansen et al. 2011, with permission); unmod 0021 refers to a smooth NACA 0021 foil

Post-Stall

As tubercles tend to reduce the severity of the stall of foils and wings, post-stall lift is subsequently increased. In addition to this benefit, tubercles can also reduce foil and wing post-stall drag, as shown in Fig. 7. One major advantage that tubercles give wings during post-stall is an increased stability. As tubercles typically increase the stall angle for wings, the moment coefficient is usually more constant than a smooth wing (Miklosovic et al. 2007). This effect is not seen on tubercled foils, as the stall angle is not affected by tubercles.

Noise Reduction

It has been suggested that tubercles may alter the noise production of foils and wings [S. W. Dewar et al., "Turbine and compressor employing tubercle leading edge rotor design," U.S. Patent No. 8535008 B2 (2013); Hansen et al. 2012]. The first suggestion was based on the idea that tubercles could prevent spanwise flow, through compartmentalization, and thereby decrease wing tip turbulence, and subsequently noise. This was one of the claims made in the patent by Dewar et al. ["Turbine and compressor employing tubercle leading edge rotor design," U.S. Patent No. 8535008 B2 (2013)] for the application of tubercles on turbomachinery.

The second theory that tubercles could reduce foil noise was proposed because of two reasons. The first is that, much of a foil's noise is produced by coherent vortex shedding on the trailing edge (Nash et al. 1999). The second, that tubercles vary the separation line long the span of a foil (Pedro and Kobayashi 2008). From these reasons, Hansen (2012) reasoned that, as the coherency of the vortex shedding of a tubercled foil's trailing edge reduced, the noise associated would also reduce. This hypothesis was also supported by Lau and Kim's (2013) findings, whereby tubercles were found to reduce coherence during gusts.

The data reported in Hansen (2012), and briefly displayed in Hansen et al. (2012), consisted of two different baseline models, a NACA 0021 and NACA 65-021, with several different tubercle geometries. For the NACA 0021 foil, a general trend emerged suggesting that tubercles suppress the tonal noise at the frequency found on smooth foils, but create a tonal noise, of a lower sound pressure level, at a higher frequency. It was also found that the most ineffective tubercles for this foil were those with the highest amplitude-to-wavelength ratio (Hansen 2012). For the NACA 65-021, the implementation of tubercles completely removed tonal noise at the angles of attack tested. In addition to affecting tonal noise, for both types of foils, tubercles also showed a slight suppression of broadband noise for frequencies near the tonal frequency.

During flight, aircraft often encounter gusts of wind which can, among other effects, cause noise. Two main parameters characterize the tubercular geometry to the gust, and the ensuing noise effects. The first parameter, which is the most significant, is the ratio of the tubercle amplitude to the gust longitudinal wavelength (A/λ_g), and the second ratio is, the tubercle wavelength to the gust longitudinal wavelength (λ/λ_g) (Lau and Kim 2013). It has been found that the noise decreases with an increasing A/λ_g, with a limiting value of 1, and where above 0.3 a noise reduction of 80% is produced (Lau and Kim 2013). Although the λ/λ_g ratio was found to have a much smaller effect on the noise production when compared to A/λ_g, significant noise reductions were also seen for ratios between 1 and 1.5 (Lau and Kim 2013).

Effect of Tubercles on the Components of Drag

The drag experienced by a foil can be divided into the following components: pressure, skin friction, and wave drag (compressible flow only, and will not be discussed). In addition to these components of drag, wings also have induced drag due to the presence of three-dimensional flow. The effects of tubercles on these components have not been explicitly tested, with the majority of research only concerning the total drag. Therefore, this section will suggest potential effects based on what is known about tubercles, and what is known about similar flow control devices.

Effect of Tubercles on Pressure Drag

The pressure drag of a foil or wing pre-stall is typically very small compared to the other components of drag. Therefore, any potential benefit that tubercles may have for pressure drag during this regime cannot greatly affect the total drag. In contrast, the pressure drag of a foil or wing during stall and post-stall contributes greatly to the total drag, and the effect of tubercles on pressure drag during this region is substantially significant.

As shown in Figs. 4–6, tubercles are capable of reducing the severity of the stall of a foil or wing, thereby increasing the angle of attack at which stall is complete, as well as increasing lift post-stall. This will result in a reduced pressure drag, as the flow remains more attached. In addition, tubercles can also delay stall for wings, and this also will result in a reduced pressure drag.

Effect of Tubercles on Skin Friction Drag

The effects of tubercles on skin friction drag is possibly the most complex area of interest of this flow control device. There are numerous possible ways for a laminar boundary layer to transition to turbulent, but one common way is the introduction, growth, and breakdown of a Tollmien-Schlichting wave (T-S wave).

It was previously mentioned that, due to the movement of the streamwise, counter-rotating vortices, the effects on common downwash regions will outweigh the effects of common upwash regions. It is logical that streamwise, counter-rotating vortices will thin the boundary layer in common downwash areas, and thicken the boundary layer in common upwash areas, as partly suggested by the aforementioned possible tubercle mechanism *induced flow*. Thinning a boundary layer has two potential effects on the shear stress. The first is that it suppresses T-S wave growth, and subsequently delays a transition to turbulence. The second is that it increases the near-wall velocity gradient, thereby increasing the shear stress. The first effect only occurs during transition; hence, if the boundary layer is completely laminar, or completely turbulent, then this will not have any effect on friction drag. The second effect is always present, regardless of the state of the boundary layer; hence, it will always increase the friction drag.

There is, potentially, one more effect of tubercles on wing friction drag, and it is mainly applicable to aircraft. Swept-back wings can experience attachment line instability. This is where a disturbance from the wing root and fuselage junction travels down the wing leading edge, causing a premature transition outboard. The greater the sweep of the wing, the further down this disturbance will travel, and more of the wing will be exposed to turbulent flow. One of the first flow control devices designed to eradicate this problem is a *bump* near the root of the wing, which runs along the chord of the wing (Gaster 1965), much like a tubercle would. It was designed to cause a flow bifurcation and confine the disturbance to between the wing root and fuselage junction and the inside of the bump (Gaster 1965), somewhat akin to wing fences. In so doing, the rest of the wing's boundary layer would not be affected. As this bump is similar in design to a tubercle, then it could be possible that tubercles would yield similar benefits for a swept wing, and reduce the amount of turbulent flow over the outboard section of a wing.

Effect of Tubercles on Induced Drag

From their simulation of a straight NACA 0021 wing, Watts and Fish (2001) concluded that at an angle of attack of 10°, tubercles offer a 10.9% reduction in induced drag. The reason for this reduction was not stated; however, through considering Prandtl's lifting line theory, some insight may be found.

From Prandtl's theory the induced drag of a wing is related to the lift distribution, and the circulation gradient, where the lowest induced drag of a planar wing is obtained by an elliptical lift distribution. For rectangular wings, the lift distribution and circulation gradient are altered, resulting in more lift production at the wingtips, and a greater induced drag. The addition of tubercles to a rectangular wing further alters the lift distribution (Rostamzadeh et al. 2013). It is proposed then, that tubercles on the outboard section of the wing reduced the lift production near the wingtips in Watts and Fish's (2001) simulation, thereby reducing the circulation gradient, and subsequently reducing the induced drag of the wing. It should be pointed out that as two-dimensional lifting surfaces do not incur an induced drag, this potential benefit is not expected to occur for tubercled foils.

Potential Heat Transfer Benefits

It is well known that tubercles produce pairs of streamwise, counter-rotating vortices (Pedro and Kobayashi 2008; Stanway 2008; Kerschgens 2008; Hansen 2012), and the vast majority of studies to date have focused on the effects of these vortices on foil and wing performance. However, these vortices may offer benefits for heat transfer. There have been numerous devices designed to increase the heat transfer to and from a surface, and many of these

utilize streamwise, counter-rotating vortices (Jacobi and Shah 1995). As previously discussed these vortices thin and thicken the boundary layer through common downwash and upwash, respectively, as shown in Fig. 3. Boundary layer thinning, through streamwise vortices, has shown to facilitate up to a 25% increase in heat transfer, whereas boundary layer thickening results in a decrease of 15% (Eibeck and Eaton 1987), resulting in a net increase in heat transfer. Hence, there may be potential for tubercles to increase heat transfer rates in a similar way.

Current Applications of Tubercles

Currently, the major implementation of tubercles has been on rotary wings, such as those found on helicopters (DLR 2013), and wind turbines (Wind Energy Institute of Canada 2008; Ontario Power Authority 2010). Additionally, tubercles have also seen implementation on rudders with varied success (Weber et al. 2010; Johari 2011).

The DLR has focused on using tubercles to overcome the stall characteristics associated with the dynamic stall on the rotor blades. For a rotating wing, the retreating phase of operation often results in the angle of attack exceeding the steady-state stall angle of attack. Once the retreating blade surpasses the steady stall angle of attack, a vortex develops and grows in strength, then sheds as the blade angle of attack decreases (Carr et al. 1977; Sahin et al. 2003). This process results in a constantly changing lift, which introduces vibrations, and subsequently causes blade fatigue. By incorporating tubercle-like control devices, the goal is to reduce the lift decrease during stall, thereby reducing the cyclical loading (Coxworth 2012). Quantitative data is not currently available; however, qualitative flight testing has indicated an improvement in performance (Coxworth 2012).

Tubercles have also been implemented on wind turbines. This has largely been done for similar reasons as outlined by DLR, namely, to reduce fatigue and increase performance, as will be discussed (WhalePower 2010). The angle of attack of a wind turbine blade is dependent of the wind speed and direction. Therefore, during excessively high wind speeds the blades can stall, rendering the wind turbines ineffective (Danish Wind Industry Association 2013). During this stalling region, severe loading is placed on the generator and blades, leading to increased wear and fatigue, respectively (Shipley et al. 1995; WhalePower 2010). To overcome the severe loading placed on the turbine during high wind speeds, stronger generators and blades could be used. However, this results in reduced performance during lower wind speeds (WhalePower 2010). This could be overcome by pitching the blades at a higher angle of attack during low wind speeds, but would result in stall for conventional turbine blades, and potentially damage the turbine. By implementing tubercles, the blades have a much larger range of angles of attack to operate over, which allows power generation at a greater range of wind speeds. In addition, as tubercles typically reduce the severity of stall, cyclic loading on the turbine as the blades go through stall decreases (WhalePower 2010).

In addition to increasing power production of wind turbines, tubercles may also reduce turbine noise. The noise generation associated with wind turbines is a significant obstacle in wind farming, as it can lead to health problems (Harrison 2011). As outlined earlier, wings typically produce noise through vortex shedding (Nash et al. 1999), and wingtip turbulence [S. W. Dewar et al., "Turbine and compressor employing tubercle leading edge rotor design," U.S. Patent No. 8535008 B2 (2013)]. The implementation of tubercles has demonstrated the ability to reduce tonal noise, and broadband noise near the tonal noise frequency (Hansen 2012). By implementing tubercles, WhalePower (2010) aimed at overcoming some of these problems and have reported that, in the six-month test, they were successful at reducing noise associated with tip stall and general operation. However, once again, no quantitative evidence has been published.

In addition to wind turbines, the effects of tubercles on turbomachinery, such as turbines and compressors, have been considered [S. W. Dewar et al., "Turbine and compressor employing tubercle leading edge rotor design," U.S. Patent No. 8535008 B2 (2013)]. This is partly due to the aforementioned advantageous stalling characteristics, which lead to greater power production, but also due to benefits from the possible compartmentalization that tubercles produce. For rotary wings, spanwise flow can significantly diminish aerodynamic performance; however, the presence of tubercles may hinder or even prevent spanwise flow thereby increasing efficiency [S. W. Dewar et al., "Turbine and compressor employing tubercle leading edge rotor design," U.S. Patent No. 8535008 B2 (2013)]. Currently, there have been no studies confirming the claims from the patent by Dewar et al. ["Turbine and compressor employing tubercle leading edge rotor design," U.S. Patent No. 8535008 B2 (2013)].

Envira North Systems Ltd. (2014) manufacture ceiling fans with tubercles on the leading edges of the blades. They claim that these tubercles make the fan more efficient by reducing spanwise pumping. Spanwise pumping is a phenomenon whereby fluid flowing over a rotating wing migrates outwards towards the wingtip. This reduces the rotating wing efficiency and produces noise. Envira North Systems Ltd. also claims that these tubercles reduce the fan's operational noise.

Tubercles have also been implemented on rudders (Weber et al. 2010) and surfboard fins (Wooden Surfboards 2010). The main for implementing them on rudders was to delay the onset of cavitation, as cavitation generally decreases lift and increases drag, thereby decreasing the performance of the rudder (Weber et al. 2010). Additionally, noise (Weber et al. 2010) and rudder erosion (Shen et al. 1997) occur when these air pockets collapse. Investigation by Weber et al. (2010) suggested that tubercles were mostly detrimental to rudder performance, as they "accelerated the onset of cavitation" and decreased lift and increased drag for moderate angles of attack and low Reynolds numbers. However, at high angles of attack and the same Reynolds numbers, tubercles displayed higher lift than the smooth rudder equivalent.

Tubercles have recently been implemented on the leading edge of the *top flap* of Formula One cars. They have also been implemented, unexpectedly, on the trailing edge of the *main plane* (Madier 2014). The top flap is a wing located above and behind the main plane, and its angle of attack can be adjustable throughout the race to provide either more downforce during cornering or less drag through the straights. Therefore, this wing is required to operate at a range of angles of attack; however, a conventional wing typically can only be optimized to give the greatest efficiency for a narrow range of angles of attack, which results in diminished performance at other angles of attack. Hence, the role of the tubercles on the top flap is to create a wing that is more efficient at a greater range of angles of attack, so that at any required angle of attack, the wing performance is augmented (Madier 2014). The reason why tubercles have been implemented on the trailing edge of the main plane currently is not publically available; however, speculation from the technical file reporting this modification suggests that the tubercles reduce the velocity deficit associated with the wake of the main plane, making the top flap, which is located aft of the main plane, more effective at producing the required downforce.

Zibkoff ["Spoked bicycle wheel," U.S. Patent Application No. US20090236902 (2009)] was granted a patent application outlining

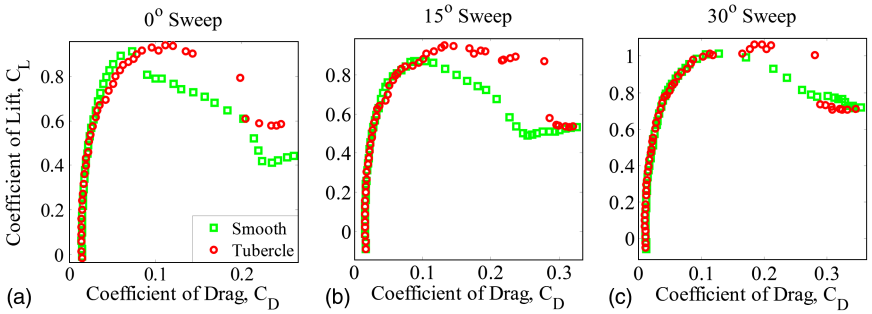

Fig. 8. Comparison of smooth and tubercled drag polars for swept foils (data from Murray et al. 2005): (a) 0° sweep; (b) 15° sweep; (c) 30° sweep

the usage of tubercles on the leading edge of bicycle wheel spokes. It is claimed that tubercles can reduce the tendency of airflow to travel width-wise along the spoke, thereby decreasing drag and reducing noise of the spokes and wheel. To the best of the authors' knowledge there is no published data indicating the effectiveness of this design.

Potential Applications of Tubercles

The most promising applications appear to be where foils or wings are pitched at high angles of attack, such as in wind turbines. As previously mentioned, there is a great interest into the effects of tubercles on axial turbomachinery; however, there may also be significant benefits for centrifugal compressors, as they are subject to similar flow phenomena that can be controlled by the implementation of tubercles.

Micro aerial vehicles (MAV) and small unmanned aerial vehicles (UAV) typically operate at low Reynolds numbers. This results in severe stall at low angles of attack. Tubercles have consistently demonstrated the ability to delay and decrease the severity of stall. Implementing tubercles on the leading edges of MAVs and UAVs could make these aircraft more stable over a greater range of angles of attack. In addition, due to the severe stall characteristics of MAVs and UAVs, they are affected by atmospheric turbulence, which could cause premature separation. Tubercles could reduce the sensitivity of these vehicles to turbulence, thereby making them more stable.

There is potential for tubercles to be utilized for transonic flight, as they may offer a reduction in wave drag. From simulations by Watts and Fish (2001) and Skillen et al. (2013), the pressure over the surface of a tubercled wing fluctuates with a spatial periodicity, and some regions have a lower pressure than a smooth wing counterpart, and other have a higher pressure. The pressure is related to the critical Mach number, meaning that the lower pressure regions will have a lower critical Mach number, and vice versa for the higher pressure regions. This has important ramifications, as the critical Mach number indicates when the flow will become sonic, and hence when drag will start to rapidly increase. Due to the periodic fluctuation of pressure over a tubercled wing, the Mach number at which sonic flow will occur over each section will be different, essentially stretching out the range of the first appearance of sonic flow, to when the entire wing experiences sonic flow. This means that while a tubercled wing may first reach the critical Mach number, the drag divergence may not be as great as a smooth wing; therefore, at higher Mach numbers the drag of the smooth wing may be greater than the tubercled wing.

This possible reduction in wave drag may also benefit supersonic applications, due to its potential compression wave pattern and a renewed interest in supersonic transport aircraft (SST). A major restriction of past SST aircraft is the constraint on supersonic flight over land. This limitation has resulted from the sonic boom that propagates to the surface, even from cruise heights (Hatanaka and Saito 2007). One of the current theories to reduce the sonic boom strength suggests decreasing the ability for the compression waves to coalesce into a stronger wave (Howe 2005). For a wing, the leading edge is usually a source of one of these compression waves; however, introducing tubercles may result in many smaller waves being produced, and if these waves are sufficiently weak, they will not coalesce, thereby reducing the wave drag and its associated noise.

There may also be applications for tubercles on swept wings, where further benefits have already been seen with increasing sweep (Murray et al. 2005). Fig. 8 shows the drag polars, adapted from Murray et al. (2005). This shows that for low angles of attack, the lift-to-drag ratio (L/D) is approximately the same for the unswept smooth and tubercled wings. However, as the angle of attack increase, L/D of the tubercled wing decreases, and finally after stall the tubercled wing has a higher L/D. As the sweep angle increases, a general trend appears which shows that the deficiency of the tubercled wing near stall decreases. At a sweep angle of 30° this deficiency has reduced so much, that it is no longer apparent. This may occur as tubercles may be compartmentalizing the flow, thereby hindering the spanwise flow along the leading edge of the foil. Therefore, the typical thick boundary layer that develops near the wingtip, which is responsible for premature stall on a smooth swept foil, is no longer present, and a thinner boundary layer occurs instead. Hence, the flow over the wingtip may stay attached to a higher angle of attack, causing an increase in lift and decrease in drag. Therefore, using tubercles for sufficiently swept foils may not be detrimental for any phase of operation, while offering slight benefits post-stall.

For aircraft applications, the area of interest is low angles of attack. Looking in this region for swept foils, there may be slight increases in L/D; however, due to errors associated with reading the published data, and to a lesser extent the experiment, comparisons at these low angles of attack are not possible. However, even a small increase in efficiency could translate into significant savings, as a 1% decrease in drag would result in a saving of approximately $100,000 per passenger aircraft per year in fuel, along with further savings in maintenance (Brown 1997; Bradley 2009).

Conclusion

Tubercles have demonstrated several effects on the performance of foils and wings. The most prominent effects are the more gradual stall, and for wings, an increase in the angle of stall. They have also been shown to increase the maximum lift, decrease the lift gradient near stall and decrease drag in the post-stall region, as well as reduce tonal and gust induced noise. Research into the effects of

tubercles on the components of drag is very limited; however, work by Watts and Fish (2001) showed a 10.9% decrease in induced drag. Post-stall there is an obvious reduction in drag, which is most likely due to a reduction in pressure drag.

The flow mechanism(s) responsible for these effects has not been fully understood, and an array of theories exists. All of these theories utilize the presence of the streamwise, counter-rotating vortices found in experiments and numerical simulations. Sensitivity analyses concerning the effects of tubercular geometries on the foil's performance have revealed a strong correlation between the tubercular amplitude and stall severity, and a general correlation between wavelength and the lift gradient near stall. In addition to the tubercular amplitude and wavelength, one analysis in particular suggested that the ratio of the amplitude-to-wavelength is also an important factor as this could influence the strength of the vortices produced.

Currently, the main applications for tubercles have concerned rotary wings, in particular helicopter blades, and turbine and compressor blades. They have been used on these rotary devices because of the favorable stall characteristics tubercles introduce. For helicopters, these favorable stall characteristics may reduce blade vibration and produce more consistent lift. For wind turbines and compressor blades, the addition of tubercles is claimed to increase operating range and decrease noise. In addition to rotary wings, tubercles have also been implemented on boat and surfboard rudders with varied effects. The quantitative data from the boat rudder testing suggests that tubercles are detrimental to hydrodynamic performance at low angles of attack, while offering benefits at higher angles of attack. In addition, qualitative results from surfboard rudders suggest that the addition of tubercles increase hydrodynamic performance.

Despite the uncertainty in the flow mechanism(s) of tubercles, numerous potential applications can still be found from what is already known. Numerical simulations have demonstrated that tubercles alter the pressure distribution on the wing surface by dividing the low-pressure region into several smaller low-pressure regions. This may initially result in a greater amount of flow becoming supersonic, as the speed of sound is approached, but increasing the flow speed further may result in less of the tubercled wing surface reaching the critical Mach number. If the drag of the tubercled wing has not diverged greatly, the smooth wing drag may exceed the tubercled wing drag, resulting in a better wing design for transonic speeds. The effects of tubercles on supersonic flow may also have benefits for the renewed interest in quiet supersonic transport aircraft, as the many weak waves produced by the tubercles could remain separate, and thereby reduce noise.

Acknowledgments

This work has been supported by The Sir Ross & Sir Keith Smith Fund.

References

Bradley, G. (2009). "Shark fin wings give airline chiefs something to smile about." The New Zealand Herald, Auckland, New Zealand.

Brown, F. (1997). "Test could cut aircraft fuel costs." *Aerosp. Technol. Innovation*, 5(4).

Carr, L. W., McAlister, K. W., and McCroskey, W. J. (1977). "Analysis of the development of dynamic stall based on oscillating airfoil measurements." *NASA Technical Note D-8382*, Moffett Field California, CA.

Coxworth, B. (2012). "Humpback whales inspire better helicopter rotor blades." ⟨http://www.gizmag.com/humpback-whales-rotor-blades/21332/⟩ (Aug. 30, 2013).

Custodio, D. (2007). "The effect of humpback whale-like leading edge protuberances of hydrofoil performance." M.S. thesis Worcester Polytechnic Institute, Worchester, MA.

Danish Wind Industry Association. (2013). "Power control." ⟨http://wiki.windpower.org/index.php/Power_control⟩ (Jun. 20, 2013).

DLR (Deutsches Zentrum für Luft- und Raumfahrt). (2013). "Was haben Buckelwale mit hubschraubern zu tun?" ⟨http://www.dlr.de/next/desktopdefault.aspx/tabid-7773/13263_read-33745/⟩ (Jun. 19, 2013).

Eibeck, P. A., and Eaton, J. K. (1987). "Heat transfer effects of a longitudinal vortex embedded in a turbulent boundary layer." *J. Heat Transfer*, 109(1), 16–24.

Envira North Systems Ltd. (2014). "Altra-air fans with WhalePower technology." ⟨http://www.enviranorth.com/altra-air.html⟩ (Aug. 26, 2014).

Fish, F. M., and Battle, J. M. (1995). "Hydrodynamic design of the humpback whale flipper." *J. Morphol.*, 225(1), 51–60.

Gaster, M. (1965). *On the flow along swept leading edges*, The College of Aeronautics, Cranfield, U.K.

Hansen, K., Kelso, R., and Doolan, C. (2012). "Reduction of flow induced airfoil tonal noise using leading edge sinusoidal modifications." *Acoust. Aust.*, 40(3), 172–177.

Hansen, K. L. (2012). "Effect of leading edge tubercles on airfoil performance." Ph.D. thesis Univ. of Adelaide, Adelaide, Australia.

Hansen, K. L., Kelso, R. M., and Dally, B. B. (2009). "The effect of leading edge tubercle geometry on the performance of different airfoils." *Proc., 7th World Conf. on Experimental Heat Transfer, Fluid Mechanics and Thermodynamics*, Elsevier.

Hansen, K. L., Kelso, R. M., and Dally, B. B. (2011). "Performance variations of leading-edge tubercles for distinct airfoil profiles." *AIAA J.*, 49(1), 185–194.

Harrison, J. P. (2011). "Wind turbine noise." *Bull. Sci. Technol. Soc.*, 31(4), 256–261.

Hatanaka, K., and Saito, T. (2007). "Numerical analysis of weak shock attenuation resulting from molecular vibrational relaxation." *Shock Waves*, 21(2), 121–129.

Hemsch, M. J., and Luckring, J. M. (1990). "Connection between leading-edge sweep, vortex lift, and vortex strength for delta wings." *J. Aircr.*, 27(5), 473–475.

Howe, D. C. (2005). "Improved sonic boom minimization with extendable nose spike." *Proc., AIAA Aerospace Sciences Meeting and Exhibit*, AIAA, Reston, VA.

Jacobi, A. M., and Shah, R. K. (1995). "Heat transfer surface enhancement through the use of longitudinal vortices: A review of recent progress." *Exp. Therm. Fluid Sci.*, 11(3), 295–309.

Johari, H. (2011). "Applications of hydrofoils with leading edge protuberances." *Final Technical Rep.*, Office of Naval Research, Arlington, VA.

Johari, H., Henoch, C., Custodio, D., and Levshin, A. (2007). "Effects of leading-edge protuberances on airfoil performance." *AIAA J.*, 45(11), 2634–2642.

Jurasz, C. M., and Jurasz, V. P. (1979). "Feeding modes of the Humpback whale, Megaptera novaeangliae, in Southeast Alaska." *Sci. Rep. Whales Res. Inst.*, 31, 69–83.

Kerschgens, B. (2008). "Ähnlichkeitstheoretische adaption eines Buckelwalflossenprofils für den einsatz in kompressiblen medien und anschließende untersuchung der resultierenden geometrie mittels CFD." Institut für Strahlantriebe und Turboarbeitsmaschinen, Aachen, Germany.

Kunz, P. J. (2003). "Aerodynamics and design for ultra-low Reynolds number flight." Ph.D. dissertation Stanford Univ., Stanford, CA .

Lau, A. S., and Kim, J. W. (2013). "The effect of wavy leading edges on aerofoil-gust interaction noise." Univ. of Southhampton, Southhampton, U.K.

Lin, J. C. (2002). "Review of research on low-profile vortex generators to control boundary-layer separation." *Prog. Aerosp. Sci.*, 38(4–5). 389–420.

Luckring, J. M. (2004). "Compressibility and leading-edge bluntness effects for a 65° delta wing." *Proc., AIAA Aerospace Sciences Meeting and Exhibit*, AIAA, Reston, VA.

Madier, D. (2014). "Aerodynamic & mechanical updates 2014 volume II." Formula One Technical Files, ⟨http//www.f1-forecast.com/index.php?

option=com_content&view=article&id=84&Itemid=502&lang=en⟩ (Nov. 23, 2014).
Miklosovic, D. S., Murray, M. M., and Howle, L. E. (2007). "Experimental evaluation of sinusoidal leading edges." *J. Aircr.*, 44(4), 1404–1407.
Miklosovic, D. S., Murray, M. M., Howle, L. E., and Fish, F. E. (2004). "Leading-edge tubercles delay stall on Humpback whale (Megaptera novaeangliae) flippers." *Phys. Fluids*, 16(5), L39–L42.
Murray, M. M., Miklosovic, D. S., Fish, F., and Howle, L. (2005). "Effects of leading edge tubercles on a representative whale flipper model at various sweep angles." *Proc., Unmanned Untethered Submersible Technology*, Autonomous Undersea Systems Institute, NH.
Nash, E. C., Lowson, M. V., and McApline, A. (1999). "Boundary-layer instability noise on aerofoils." *J. Fluid Mech.*, 382, 27–61.
Ontario Power Authority. (2010). "Energy-efficient fans blow cool for dairy farming." *Electr. Conserv. Ontario Farms*, 4(2), 1–4.
Pauley, W. R., and Eaton, J. K. (1987). "Experimental study of the development of longitudinal vortex pairs embedded in a turbulent boundary layer." *AIAA J.*, 26(7), 816–823.
Pedro, H. T., and Kobayashi, M. H. (2008). "Numerical study of stall delay on humpback whale flippers." *Proc., AIAA Aerospace Sciences Meeting and Exhibit*, AIAA, Reston, VA.
Polhamus, E. C. (1966). "A concept of the vortex lift of sharp-edge delta wings based on a leading-edge-suction analogy." *NASA Technical Note D-3767*, Langley Research Center, Hampton, VA.
Polhamus, E. C. (1971). "Predictions of vortex-lift characteristics by a leading-edge suction analogy." *J. Aircr.*, 8(4), 193–199.
Rostamzadeh, N., Hansen, K. L., Kelso, R. M., and Dally, B. B. (2014). "The formation mechanism and impact of streamwise vortices on NACA 0021 airfoil's performance with undulating leading edge modification." *Phys. Fluids*, 26(10), 107101.
Rostamzadeh, N., Kelso, R. M., Dally, B. B., and Hansen, K. L. (2013). "The effect of undulating leading-edge modifications on NACA 0021 airfoil characteristics." *J. Phys. Fluids*, 25(11), 117101.
Sahin, M., Sankar, L. N., Chandrasekhara, M. S., and Tung, C. (2003). "Dynamic stall alleviation using a deformable leading edge concept: A numerical study." *J. Aircr.*, 40(1), 77–85.
Seshagiri, A., Cooper, E., and Traub, L. W. (2009). "Effects of vortex generators on an airfoil at low Reynolds numbers." *J. Aircr.*, 46(1), 116–122.
Shen, Y. T., Jiang, C. W., and Remmers, K. D. (1997). "A twisted rudder for reduced cavitation." *J. Ship Res.*, 41(4), 260–272.
Shipley, D. E., Miller, M. S., and Robinson, M. C. (1995). "Dynamic stall occurrence on a horizontal axis wind turbine blade." U.S. Dept. of Energy, Houston.
Skillen, A., Revell, A., Favier, J., Pinelli, A., and Piomelli, U. (2013). "Investigation of wing stall delay effect due to an undulating leading edge: An LES study." *Proc., Int. Symp. on Turbulence and Shear Flow Phenomena*, Univ. of Manchester, U.K.
Slangen, R. A. (2009). "Experimental investigation of artificial boundary layer transition: A comparison of different tripping devices." M.S. thesis, Delft Univ. of Technology, Delft, Netherlands.
Stanway, M. J. (2008). "Hydrodynamic effects of leading-edge tubercles on control surfaces and in flapping foil propulsion." M.S. thesis, Massachusetts Institute of Technology, Cambridge, MA.
Stein, B., and Murray, M. M. (2005). "Stall mechanism analysis of Humpback whale flipper models." Unmanned Untethered Submerisible Technology (UUST), Autonomous Undersea Systems Inst., Lee, NH.
Taylor, H. D. (1950). "Summary report on vortex generators." United Aircraft Research Dept., *Rep. R-05280-9*, United Aircraft Corporation, East Hartford, CT.
Van Nierop, E. A. (2009). "Flow in films and over flippers." Ph.D. dissertation, Harvard Univ., Cambridge, MA.
Van Nierop, E. A., Alben, S., and Brenner, M. P. (2008). "How bumps on whale flippers delay stall: An aerodynamic model." *Phys. Rev. Lett.*, 100(5), 054502.
Watts, P., and Fish, F. E. (2001). "The influence of passive, leading edge tubercles on wing performance." Unmanned Untethered Submersible Technology (UUST), Autonomous Undersea Systems Inst., Lee, NH.
Weber, P. W., Howle, L. E., and Murray, M. M. (2010). "Lift, drag and cavitation onset on rudders with leading edge tubercles." *Mar. Technol.*, 47(1), 27–36.
WhalePower. (2010). "Fans." ⟨http://www.whalepower.com/drupal/?q=node/2⟩ (Jun. 19, 2013).
Wind Energy Institute of Canada. (2008). "WhalePower tubercle blade power performance test report." Wind Energy Institute of Canada, North Cape Prince Edward Island, Canada.
Wooden Surfboards. (2010). "Whale inspired fins." ⟨http://woodensurfboards.blogspot.com.au/2010/08/whale-inspired-fins.html⟩.
Zhang, M. M, Wang, G. F., and Xu, J. Z. (2014). "Experimental study of flow separation control on a low-Re airfoil using leading-edge protuberance method." *Exp. Fluids*, 55, 1710.
Zhang, M. M., Wang, G. F., and Xu, J. Z. (2013). "Aerodynamic control of low-Reynolds-number airfoil with leading-edge protuberances." *AIAA J.*, 51(8), 1960–1971.

2.2 Literature Review Addendum

2.2.1 Tubercle Flow Physics

Over the last two years, significant advancements in the understanding of the flow physics over a tubercled wing have occurred. One of the greatest advancements in this understanding is that the vortices created by tubercles originate at the wing surface and lift off (Hansen *et al*., 2016). In so doing, they interact with the boundary layer (Wei, 2015; Hansen *et al.*, 2016), which overcomes the major criticism of the tubercle flow mechanism "vortex generators". Therefore, these results prove that tubercles do act in a similar fashion to vortex generators. In addition to this finding, it has also been found that the strengths of the tubercle vortices increase, approximately linearly from the wing's leading edge to its trailing edge through the continued entrainment of boundary layer vorticity (Hansen *et al.*, 2016), thereby showing the continued interaction of the vortices with the boundary layer along the wing's chord. The vorticity forms from the difference in pressure gradients behind the peaks and troughs. Additionally, a pressure difference occurs between the peaks and the troughs, which results in the flow being directed towards the troughs (Rostamzadeh *et al*., 2016).

Also, further evidence that the adverse pressure gradient is stronger behind the troughs than the peaks (van Nierop *et al*., 2009) has been found (Ibrahim *et al.*, 2015; Hansen *et al.*, 2016), which leads to the flow separating behind the troughs at a lower AOA than the peaks, as was also found by other researchers (Johari *et al.*, 2007; Pedro and Kobayashi, 2008). In addition, the peaks produce a greater lift per unit span than the troughs (Hansen *et al*., 2016).

Several researchers have documented that as the AOA increases, the flow and its separation become increasingly unsteady (Wei *et al.*, 2015; Hansen *et al.*, 2016; de Paula *et al.*, 2016), which is thought to be due to vortex wandering (Wei *et al.*, 2015) and unsteady vorticity production (Hansen *et al.*, 2016).

The presence of streamwise vortices can also lead to increased surface shear stresses, which result in an increased drag coefficient (Hansen *et al.*, 2016).

2.2.2 Reynolds Number Effects

Since the review article was written, several research groups have focussed on the effects of the Reynolds number on tubercled wing performance (Custodio *et al.*, 2015; de Paula *et al.*, 2016; Moore *et al.*, 2016; Rostamzadeh *et al.*, 2016).

To the author's knowledge, Rostamzadeh *et al.* (2016) has studied the effects of tubercles in the greatest Reynolds number range; 120,000 (transitional) to 1,500,000 (near-turbulent). The underlying flow mechanism, which involves the transverse and streamwise vorticity productions, was common in this range.

As explained above, tubercles are renowned for delaying and softening stall on foils and wings. However, as the Reynolds number increases, the stall AOA of a smooth wing typically increases. As a result, the beneficial effects of tubercles in the stall and post-stall regimes are usually reduced (Custodio *et al.*, 2015; de Paula *et al.*, 2016; Moore *et al.*, 2016; Rostamzadeh *et al.*, 2016).

Rostamzadeh *et al.* (2016) noted an interesting change in the effects of tubercles on the drag coefficient between a transitional flow and a near-turbulent one in the post-stall regime; in the transitional flow regime, the tubercles that were investigated reduced the drag coefficient, however, in a near-turbulent flow regime, the dimensionally-scaled equivalent tubercles increased the drag coefficient. It is unclear if this difference was caused by different flow mechanisms at the two different Reynolds numbers, or if it was caused by the dimensional-scaling of the tubercle geometry.

2.2.3 The Effects of Tubercles on Swept Wing Performance

Since the review article above was written, to the author's knowledge, only one study has described the effects of tubercles on swept wing performance (Custodio *et al.*, 2015). The results of this study were that the implemented tubercles reduced the lift coefficient and lift-to-drag ratio, and increased the drag coefficient at pre-stall AOAs. At post-stall AOAs, the tubercles increased both the lift coefficient and lift-to-drag ratio, while having little effect on the drag coefficient. The reduced performance of the swept wing at pre-stall AOAs was not conclusive due to the relatively large error bars of the drag coefficient measurements, in the order of 10%.

In addition to this study, many studies have investigated the effects of tubercles on turbomachinery performance (Ibrahim *et al.*, 2015; Moore *et al.*, 2016; Bai *et al.*, 2016; Shi *et al.*, 2016 a; Shi *et al.*, 2016 b), with varied effects observed. Ibrahim *et al.* (2015) detailed the effects of tubercles on propellers and found up to 10% increases in thrusts and torques, but as much as 5% reductions in efficiency (Ibrahim *et al.*, 2016). Moore *et al.* (2016) showed that tubercles implemented on UAV propellers, in the order of 100mm in diameter and operating at Reynolds numbers from 29,000 to 53,000, typically reduced thrust and efficiency. When tubercles are implemented on turbines, they have been found to typically increase the power coefficient and reduce the turbine's "cut-in speed", thereby improving their "start-up" performance (Bai *et al.*, 2016; Shi *et al.*, 2016 b).

2.2.4 The Effects of an Airfoil's Profile on Tubercled Wing Performance

To the author's knowledge, only one investigation has addressed the effects of tubercles on different airfoil profiles since the end of 2014; de Paula *et al.* (2016). This investigation detailed the effects of tubercles on the lift and drag coefficients when implemented on NACA 0012 and NACA 0020 profiles. Tubercles softened the stall of both wings, however, they increased the post-stall lift

coefficient of the NACA 0012 profile to a greater extent than that of the NACA 0020 profile. The tubercles affected the drag coefficients of the two NACA profiles to similar extents.

Other studies have investigated the effects of tubercles on cambered and asymmetrical profiles (Wei *et al.*, 2015; Moore *et al.*, 2016; Bai *et al.*, 2016; Shi *et al.*, 2016 a), with similar effects on the wing performance observed to that typically found on symmetrical NACA profiles, e.g. NACA 0021.

2.2.5 The Effects of a Tubercle's Geometry on Wing Performance

Wei *et al.* (2015) recently clarified earlier observations that a larger A/λ ratio (Hansen *et al.*, 2011) further delays stall.

When tubercles are implemented on turbomachinery, at high AOAs, smaller tubercle wavelengths typically increase the power coefficient (Bai *et al.*, 2016). In addition, as the freestream velocity increases, larger tubercle amplitudes and wavelengths result in greater power coefficients (Bai *et al.*, 2016).

The effects of the tubercle location along a wing's span has received significant attention since the review article was written (Cai *et al.*, 2016; Shi *et al.*, 2016 a; Shi *et al.*, 2016 b). Cai *et al.* (2016) showed that a single tubercle, A10λ25, placed mid-span of a full-span NACA 63_4-021 foil, with a chord of 100mm and a span of 350mm, can still soften the foil's stall. Shi *et al.* (2016 a) detailed the effects of tubercles along portions of an S814 profile wind turbine blade leading edge in the transitional regime; Reynolds numbers ranging from 300,000 to 600,000. The investigation considered tubercles along 25%, 50%, 75%, and 100% of the wingspan from the wingtip. All tubercle configurations increased the lift coefficient during stall. Tubercles along 100% of the wingspan produced the greatest lift coefficient. Unlike the other tubercle configurations, the configuration with tubercles located along 25% of the wingspan typically reduced the drag coefficient at pre-stall AOAs, which resulted in lift-to-drag ratio increases from 5% to 25%. These increases in the lift-to-

drag ratio were of similar magnitudes to any increases caused by the other tubercle configurations, however, these increases were more consistently observed at pre-stall AOAs. Shi *et al.* (2016 b) detailed similar effects of tubercles along 25% of a wingspan to Shi *et al.* (2016 a).

2.2.6 The Effects of a Tubercle's Shape on Wing Performance

Since the review article was written, to the author's knowledge, only one investigation has detailed tubercles with geometries differing from the typical sinusoidal shape (Moore *et al.*, 2016). Moore *et al.* (2016) investigated UAV propellers with spherical tubercles on the leading edge. As described above, these tubercles reduced both the propeller's thrust and efficiency.

2.2.7 The Effects of Tubercles on Dynamic Wing Performance

Ng *et al.* (2016) demonstrated the effects of tubercles on the dynamic aeroelastic effects of a Goland wing. It was found that increasing the tubercle amplitude increases the flutter speed, with augmentations up to 7% observed. Conversely, reducing the tubercle wavelength increases the flutter speed, with augmentations up to 5.5% observed. In addition, as the sweep angle increases, the tubercles become less effective at increasing the flutter speed (Ng *et al.*, 2016).

References

Bai, C.J., Wang, W.C., and Chen, P.W., "The Effects of Sinusoidal Leading Edge of the Turbine Blade on the Power Coefficient of Horizontal-Axis Wind Turbine (HAWT)", *International journal of Green Energy*, 2016. doi: 10.1080/15435075.2016.1180624.

Cai, C., Zuo, Z., Liu, S., and Wu, Y., "Effect of a Single Leading-Edge Protuberance on NACA 63_4-021 Airfoil Performance", *Proceedings of the International Symposium on Transport Phenomena and Dynamics of Rotating Machinery*, Honolulu, 2016.

Custodio, D., Henoch, C.W., and Johari, H., "Aerodynamic Characteristics of Finite Span Wings with Leading-Edge Protuberances", *American Institute of Aeronautics and Astronautics* (AIAA) Journal, Vol. 53, No. 7, 2015. doi: 10.2514/.J053568.

de Paula, A.A., Padiha, B.R., Mattos, B.D., and Meneghini, J.R., "The Airfoil Thickness Effect on Wavy Leading Edge Performance", *AIAA SciTech*, 4th-8th January 2016, San Diego.

Hansen, K.L., Kelso, R.M. and Dally, B.B., "Performance Variations of Leading-Edge Tubercles for Distinct Airfoil Profiles", *American Institute of Aeronautics and Astronautics* (AIAA) Journal, Vol. 49, No. 1, Jan. 2011, pp.185-194. doi: 10.2514/1.J050631.

Hansen, K.L., Rostamzadeh, N., Kelso, R.M., and Dally, B.B., "Evolution of the Streamwise Vortices Generated Between Leading Edge Tubercles", *Journal of Fluid Mechanics*, Vol. 788, pp. 730-766, 2016. doi: 10.1017/jfm.2015.611.

Ibrahim, I.H. and New, T.H., "Flow Separation Control of Marine Propeller Blades through Tubercle Modifications", *Proceedings of the 10th Pacific Symposium on Flow Visualization and Image Processing*, Naples, 2015.

Johari, H., Henoch, C., Custodio, D. and Levshin, A., "Effects of Leading-Edge Protuberances on Airfoil Performance", *American Institute of Aeronautics and Astronautics* (AIAA) Journal, Vol. 45, No. 11, 2007. doi:10.2514/1.28497.

Moore, K.R. and Ning, A., "Aerodynamic Performance Characterization of Leading Edge Protrusions on Small Propellers", *AIAA SciTech*, 4th-8th January 2016, San Diego.

Ng, B.F., New, T.H. and Palacios, R., "Effects of Leading-Edge Tubercles on Wing Flutter Speeds", *Bioinspiration & Biomimetics*, Vol. 11, 2016. doi: 10.1088/1748-3190/11/3/036003.

Pedro, H.T. and Kobayashi, M.H., "Numerical Study of Stall Delay on Humpback Whale Flippers", AIAA *Aerospace Sciences Meeting and Exhibit*, 7th-11th January 2008, Reno.

Rostamzadeh, N., Kelso, R.M., and Dally, B.B., "A Numerical Investigation into the Effects of Reynolds Number on the Flow Mechanism Induced by a Tubercled Leading Edge", *Theoretical Computational Fluid Dynamics*, 2016. doi: 10.1007/s00162-016-0393-x.

Shi, W., Altar, M., Norman, R., Aktas, B., and Turkmen, S., "Numerical Optimization and Experimental Validation for a Tidal Turbine blade with Leading-Edge Tubercies", *Renewable Energy*, Vol. 96, pp. 42-55, 2016, a. doi: 10.1016/j.renene.2016.04.064 0960-1481.

Shi, W., Rosli, R., Atlar, M., Norman, R., Wang, D., and Yang, W., "Hydrodynamic Performance Evaluation of a Tidal Turbine with Leading-Edge Tubercles", *Ocean Engineering*, Vol. 117, pp. 246-253, 2016, b. doi: 10.1016/j.oceaneng.2016.03.044 0029-8018.

Van Nierop, E.A., Alben, S. and Brenner, M.P., "How Bumps on Whale Flippers Delay Stall: an Aerodynamic Model", *Physical Review Letters*, PRL 100, 054502, February 2009.

Wei, Z., New, T.H., and Cui, Y.D., "An Experimental Study on Flow Separation Control of Hydrofoils with Leading-Edge Tubercles at Low Reynolds Number", *Ocean Engineering*, Vol. 108, pp. 336-349, 2015. doi: 10.1016/j.oceaneng.2015.08.004 0028-8018.

Chapter 3

The Effects of Tubercles on a Swept Wing's Performance at Pre-Stall Angles of Attack

This chapter includes the following journal articles:

Bolzon, M.D., Kelso, R.M. and Arjomandi, M., "Force Measurements and Wake Surveys of a Swept Tubercled Wing", accepted for publication by *The Journal of Aerospace Engineering*, 2016.

Bolzon, M.D., Kelso, R.M. and Arjomandi, M., "Formation of Vortices on a Tubercled Wing, and Their Effects on Drag", *Aerospace Science and Technology*, 2016. doi: 10.1016/j.ast.2016.06.025.

The aim of this chapter is to determine the effects of tubercles on a swept wing's lift, total drag, profile drag, and induced drag coefficients at pre-stall AOAs, in accordance with the first two aims of this thesis. By understanding these effects of tubercles, it can be determined whether tubercles can be beneficial to wing performance at pre-stall AOAs, thereby increasing their range of potential applications. To achieve these aims, two wings were manufactured and tested; one without tubercles and one with tubercles along its entire leading edge. The lift and total drag were measured via a load cell, while the total drags, the drag components, the vorticity fields and circulations produced by each wing were determined from wake survey data. The first journal paper details the effects of tubercles on the lift and total drag coefficients of a swept wing. The total drag coefficient was decomposed to produce the spanwise drag coefficient distribution in the wake plane of each wing.

The second journal paper is an extension of the first journal paper. The total drag coefficients of both of the wings were decomposed into the profile and induced drag coefficients. The circulations of the vortices produced by the smooth and tubercle wings were calculated and analysed to determine the effect of tubercles on the wingtip vortex, as well as how the sweep affects the strength of the streamwise, counter-rotating vortex pairs produced by tubercles.

These experiments showed that at pre-stall AOAs, tubercles can reduce the lift and total drag coefficients of a swept wing, while increasing the lift-to-drag ratio. Reductions in the drag coefficient

at pre-stall AOAs were caused by reductions in the profile drag coefficient. These reductions occurred across the full span of the wing. Tubercles did not significantly affect the induced drag coefficient at pre-stall AOAs. It was also found that sweeping a tubercled wing results in one vortex in each counter-rotating, streamwise pair being stronger than the other.

Finally, this chapter shows that there are distinct ranges of pre-stall AOAs where the tubercles have particular effects on the wing performance. For example, below 8° AOA, tubercles typically reduce the profile drag coefficient, however, above 8° AOA, they typically increase it. To the author's knowledge, this is the first time that these distinct pre-stall AOA ranges, and the effects of tubercles on the above wing performance characteristics in these ranges, have been documented.

Statement of Authorship

Title of Paper	Force Measurements and Wake Surveys of a Swept Tubercled Wing
Publication Status	☐ Published ☑ Accepted for Publication ☐ Submitted for Publication ☐ Unpublished and Unsubmitted w ork w ritten in manuscript style
Publication Details	Bolzon, M.D., Kelso, R.M. and Arjomandi, M., "Force Measurements and Wake Surveys of a Swept Tubercled Wing", *accepted for publication by the Journal of Aerospace Engineering*, 2016.

Principal Author

Name of Principal Author (Candidate)	Michael Bolzon		
Contribution to the Paper	Designed and built wake survey rig, performed experiments, processed data, wrote manuscript, and acted as corresponding author.		
Overall percentage (%)			
Certification:	This paper reports on original research I conducted during the period of my Higher Degree by Research candidature and is not subject to any obligations or contractual agreements with a third party that would constrain its inclusion in this thesis. I am the primary author of this paper.		
Signature		Date	

Co-Author Contributions

By signing the Statement of Authorship, each author certifies that:

i. the candidate's stated contribution to the publication is accurate (as detailed above);

ii. permission is granted for the candidate in include the publication in the thesis; and

iii. the sum of all co-author contributions is equal to 100% less the candidate's stated contribution.

Name of Co-Author	Richard Kelso		
Contribution to the Paper	Supervised experimental development, aided interpretation of results, and reviewed manuscript.		
Signature		Date	

Name of Co-Author	Maziar Arjomandi		
Contribution to the Paper	Supervised experimental development, aided interpretation of results, and reviewed manuscript.		
Signature		Date	

Force Measurements and Wake Surveys of a Swept Tubercled Wing

Michael D. Bolzon[1], Richard M. Kelso[2], and Maziar Arjomandi[3]
The University of Adelaide, Adelaide, South Australia, 5005, Australia

Force measurements and wake surveys have been conducted on two swept NACA 0021 wings. One wing had a smooth leading edge, while the other wing had a tubercled leading edge. The force measurements and the wake survey results were in good agreement. Between 0° and 8° angles of attack, tubercles reduced the lift coefficient by 4 to 6%. For the same range of angles of attack, tubercles reduced the drag coefficient by 7 to 9.5%. Tubercles increased the lift-to-drag ratio of this wing by 2 to 6%, and increased the maximum lift-to-drag ratio by 3%. At angles of attack higher than 8° tubercles typically decreased the lift coefficient and the lift-to-drag ratio, while substantially increasing the drag coefficient. The wake surveys revealed that tubercles reduced the drag coefficient near the wingtip and that they also spatially modulated the drag coefficient into local maxima and minima in the spanwise direction. Typically, tubercles reduced the drag coefficient over the peaks where the tubercle vortices produced downwash. Conversely, tubercles increased the drag coefficient over the troughs, where upwash occurred. The majority of the drag coefficient reduction occurred over the tubercled wingspan.

Introduction

Despite their massive size, the Humpback whale is remarkably agile. They are capable of performing underwater acrobatics, including somersaults (Jurasz and Jurasz 1979). Furthermore, they are unique among Baleen whales as they have leading edge protuberances, termed tubercles, on their pectoral flippers. This unique geometry has been suggested to, in part, be responsible for the whale's agility (Fish and Battle 1995).

[1] Ph.D. Candidate, The School of Mechanical Engineering, The University of Adelaide, Australia, 5005, michael.bolzon@adelaide.edu.au.
[2] Associate Professor, The School of Mechanical Engineering, The University of Adelaide, Australia, 5005, richard.kelso@adelaide.edu.au.
[3] Associate Professor, The School of Mechanical Engineering, The University of Adelaide, Australia, 5005, maziar.arjomandi@adelaide.edu.au.

Recent studies into the effects of tubercles on foil and wing performance have revealed that each tubercle produces a pair of counter-rotating, streamwise vortices, which results in a common downwash over the peaks of the tubercles and a common upwash in the troughs. The main effects of tubercles are to soften and delay stall (Miklosovic *et* al. 2004; Stein and Murray 2005), however, little is known about the effects of tubercles at lower angles of attack, AOAs. It should be noted that herein low AOAs will refer to AOAs where the flow is still largely attached, moderate AOAs will refer to AOAs where the flow begins to separate through to complete stall, and high AOAs will refer to AOAs where the wing has completely stalled. There may be significant economic benefit for investigating the effects of tubercles at low AOAs as a 1% reduction in drag for a modern airliner could result in a $100,000 saving in fuel costs each year, along with further savings in maintenance costs (Brown 1997; Bradley 2009).

In addition, the vast majority of tubercle studies have only considered unswept foils or wings. One of the few studies that did consider the effects of tubercles on swept wing performance investigated the effects of tubercles on the lift and drag coefficients of a model Humpback whale flipper (Murray *et al.* 2005). For low AOAs the effects of tubercles on the lift-to-drag ratio, L/D, was indiscernible, and during post-stall tubercles increased the L/D (Murray *et al.* 2005; Bolzon *et al.* 2015). Interestingly, for an unswept wing at moderate AOAs tubercles reduced the L/D, but this reduction diminished as the flipper sweep angle increased. Therefore, tubercles may offer additional benefits for swept wings.

The aim of this study is to experimentally determine if tubercles can improve the performance of a swept wing at low, pre-stall, AOAs. To achieve this, two methods have been employed. The first method was a force measurement, which was used to determine the lift and drag coefficients of a smooth leading edge and a tubercled leading edge wing. Wake surveys were also conducted and the drag coefficients were calculated from this method. The results from these wake surveys can be compared to the force measurements as well as elucidate how tubercles are affecting the wing performance.

Methods and Uncertainties

Wing Models

To carry out these experiments, two wings were Computer Numerical Control-machined, CNC-machined, out of aluminium 6061, as shown in fig. 1. One had a smooth leading edge, fig. 1 a), while the other had a tubercled

leading edge, fig. 1 b). The tubercles have been constructed to preserve a constant thickness-to-chord ratio, and have a constant amplitude of 10.5mm and a constant wavelength of 60mm (A10.5λ60, Hansen 2011). Apart from this difference, the two wings were identical. Figure 1c shows the geometry of the tubercled wing to highlight that the tubercles create a "wavy" surface along the span of the wing, and this "waviness" washes out from the leading edge towards the trailing edge. The tubercles were created from a spline connecting wing profiles positioned every 10mm along the span. A NACA 0021 profile was chosen as it is thick and symmetrical, and conforms to previous studies of tubercles (Watts and Fish 2001; Miklosovic *et al.* 2007; Hansen *et al.* 2011). The wing profile and the tubercle geometry detailed were in the swept-flow direction. The wings had a span of 330mm and a Mean Aerodynamic Chord, MAC, of 130mm, a root chord of 175mm, and a wingtip chord of 70mm. They had a quarter-chord sweep angle of 35° and a taper ratio of 0.4. Taper was chosen as swept wings typically incorporate taper to reduce induced drag. At the wing root, the tubercles started midway between a tubercle trough and peak, and terminated at the wingtip midway between a tubercle peak and trough giving a phase of π (Bolzon *et al.* 2016). This resulted in 6 peaks and 5 troughs along the wingspan.

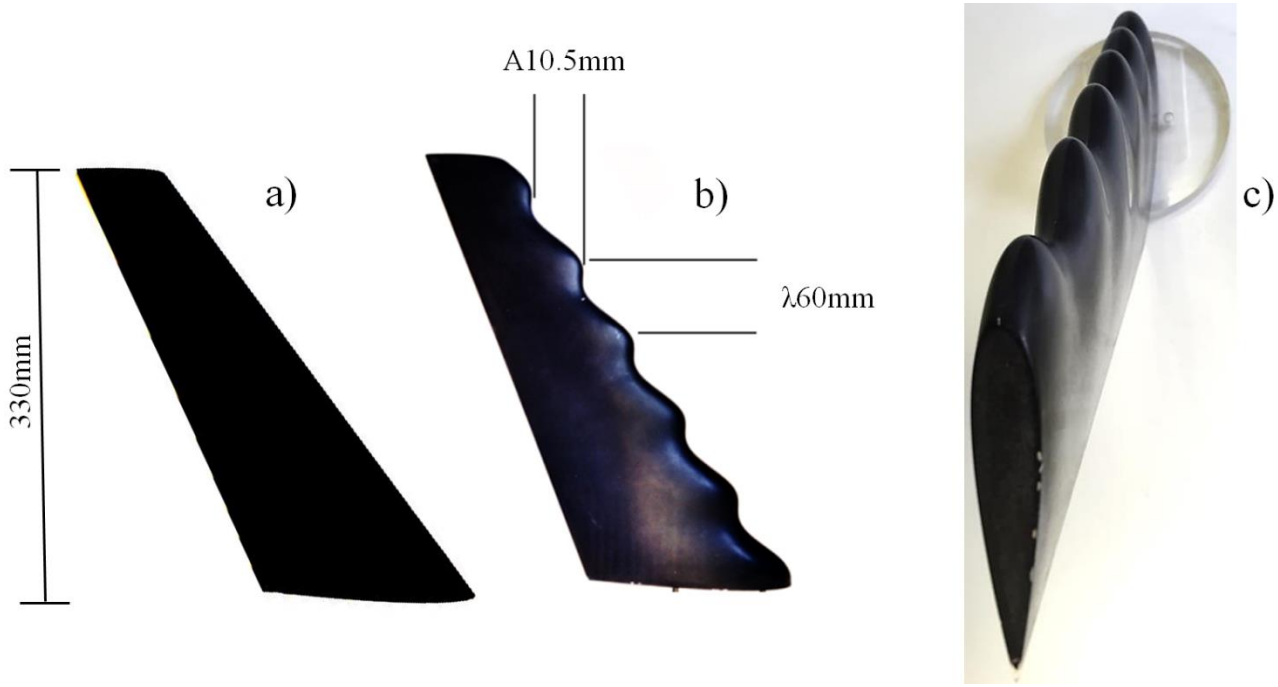

Fig. 1 Wings manufactured without tubercles, a, with tubercles, b, and tubercled wing along span highlighting tubercles washing out towards the trailing edge, c. Tubercles have a geometry of A10.5λ60.

Force Measurements

Force measurements were carried out in the "KC Wind Tunnel" at the University of Adelaide. This wind tunnel is typically open-jet, however, a duct was incorporated in the test section during the force measurements to make the wind tunnel closed in order to reduce disturbances, as shown in fig. 2. The working section of the closed-duct was 0.5 x 0.5 m, resulting in a 170mm clearance between the working section ceiling and the wingtip, and ample space for the wingtip vortex to form without significant wall interference (Barlow *et al.* 1999). In addition, the effects of the horizontal buoyancy on the flow physics over the wings were negligible (Barlow *et al.* 1999). The turbulence intensity of the tunnel in the open-jet configuration was 0.6~0.8% and the freestream velocity was 27.5 m/s, giving a MAC Reynolds number of 225,000.

Six experimental runs were performed for each wing, with the wings removed, reattached, and realigned after every three runs. The averages of these runs were then calculated. The wings were rotated from an AOA of -2° to 20° in 1° increments. As shown in fig. 2, the wings were attached to a six-component JR3 brand load cell, which was used to determine the orthogonal forces acting on the wings. The JR3 load cell had an internal factory calibration matrix used to decouple the force measurements during the experiment. The lift and drag were found through a co-ordinate transformation, as in eq. 1, where α is the AOA. The load cell was in turn mounted on a Vertex brand rotary table, which was used to change the AOA. Two uncertainties arose from this setup, the first being the uncertainty of the load cell force measurements, and the second being the uncertainty in the alignment of the wings.

$$\begin{bmatrix} L \\ D \end{bmatrix} = \begin{bmatrix} \cos\alpha & -sin\alpha \\ sin\alpha & cos\alpha \end{bmatrix} \begin{bmatrix} F_x \\ F_y \end{bmatrix} \quad (1)$$

where L is the lift, D is the drag, α is the AOA, and F_x and F_y are the forces in the x- and y-directions, respectively.

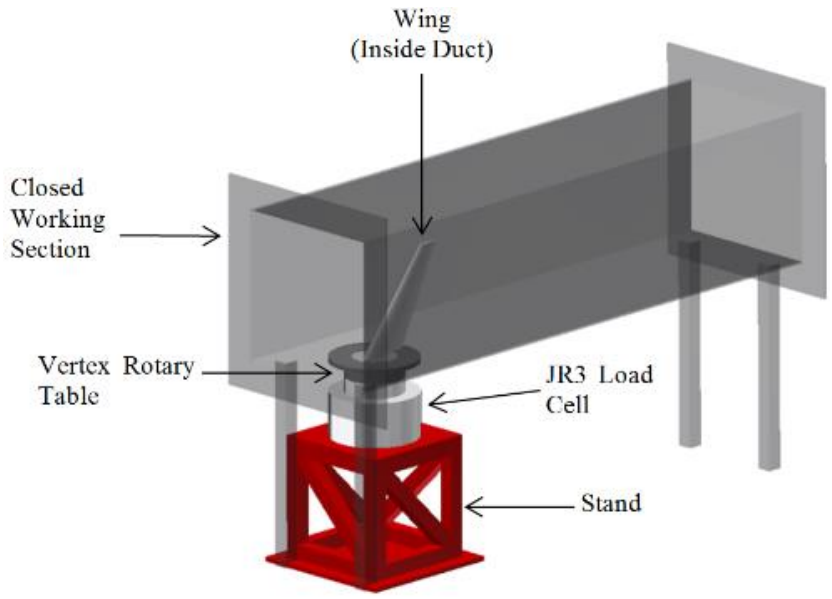

Fig. 2 Force measurement setup. Wing leading edge at the root located 450mm from duct beginning. Duct is 2200mm long.

The first uncertainty was accounted for by performing a load cell calibration for a number of forces spanning the expected range in each respective direction. For each load attached to the load cell, measurements were taken for at least 10 seconds at a sampling frequency of 100 Hz and the mean was then found. The distributions of the samples for each force fit a normal curve, therefore, the 95% confidence interval was calculated for each run. The load cell had a 95% confidence interval of $\pm$1.75% for a force of 0.5 N to $\pm$1% for a force of 2.2 N in the x-direction, and the y-direction corresponded to $\pm$1.76% for a force of 0.5 N to $\pm$1.5% for a force of 5.9 N. Linear interpolation was used to determine the uncertainty of force measurements between the calibration forces.

The wings were designed such that at a 0° AOA, the drag and lift forces would be aligned with the x and y-components of the load cell, respectively. As the wings were CNC-machined, the misalignment of the drag and lift with the x and y-components of the load cell were assumed to be small. Hence, as the wings were symmetrical, initially they were aligned such that the y-component of force, and therefore the lift, was zero. From this setup the drag was more sensitive to the angular misalignment than the lift. Therefore, during post-processing any residual misalignment was accounted for by offsetting the AOA such that the drag at -2° match as close to the drag at 2° AOA while still preserving zero-lift at 0° AOA. Zero-lift was defined as when the wing had a lift coefficient less than 0.001, which produced a maximum angular misalignment of approximately $\pm$0.02°. As such the angular

misalignment corrects were minimal. The uncertainty in the AOA arising from the rotary table was estimated to be $\pm 0.017°$.

The uncertainty in the load cell was processed by the method prescribed by Holman (1994) and Dieck (1992), which is also known as the "Jitter method". In addition, wake blockage, solid blockage, streamline curvature, and downwash corrections were applied as outlined by Barlow *et al.* (1999). The maximum correction factor applied was 0.92%.

Wake Survey

Following the force measurements, a wake surveying analysis was performed in the "KC wind tunnel" at The University of Adelaide. While the wings were positioned within a closed-duct for the force measurements, the wake survey rig was open, as shown in fig. 3, to reduce the experimental setup complexity and allow the traverse to move freely. In addition, using an open-jet for the wake surveys also reduced the wake blockage downstream of the wing by the wake surveying apparatus intruding into the flow. The wind tunnel area was vacated during the wake survey stage of experiments and observed remotely, which reduced possible disturbances to the flow. On the other hand, during the force measurements stage of experiments two operators were required in the vicinity of the wind tunnel to operate instruments. One of the operators was near the upstream flow and could unintentionally disturb the flow due to the required close proximity. The closed-duct removed this potential disturbance.

The following discusses the potential differences in the flow physics between the two different wind tunnel setups and their effects on the data measured. The solid and wake blockage corrections of the wings in the closed-duct were calculated to be 0.00068 and 0.0054 (Barlow *et al.* 1999), which were insignificant compared with measurement tolerances, therefore, the downstream pressure was expected to be the same as the open-jet. These values indicate that the flow separation and boundary layer development over the wings were very similar between the two wind tunnel configurations. The wings spanned 0.66 of the closed-duct, which was less than the maximum 0.7 required to neglect the wall effects (Barlow *et al.* 1999). Therefore, differences in the lift distribution and wake roll-ups of the wings between the two wind tunnel configurations were likely to be negligible. Finally, as stated previously, the necessary corrections to the lift and drag data were applied to the closed-duct results. Therefore the flow physics and data measured between the two wind tunnel configurations were comparable.

As presented in the results section, the absolute and relative changes in the drag coefficients as measured from the load cell and wake surveys were in very good agreement, indicating that comparing data from the closed-duct and the open-jet in these experiments was acceptable.

The wake surveys were also carried out at a freestream speed of 27.5 m/s, and at 0°, 3°, 6°, 9°, and 12° AOAs. 12° AOA was the highest as above this AOA the wings' wakes were too large to survey within the allotted timeframe. Three runs were conducted for each of the smooth and tubercles wings, and the averages have been reported.

As shown in fig. 3, the wings were again mounted on the JR3 load cell, which was used for alignment in the same manner described above, and this load cell was then mounted on the rotary table. The rotary table was, again, used to change the AOA about the axis depicted in fig. 3 b). A 2-axis traverse was used to move a Turbulent Flow Instrumentation, TFI, brand Cobra probe to the desired location in the y-z plane, also known as the "wake plane". The Cobra probe was located 3 MACs downstream of the wing trailing edge at the MAC spanwise location. The Cobra probe was a four-hole pressure probe with a triangular head measuring 3mm x 3mm (TFI 2011). A pressure port was located at each corner of the triangle and one in the middle as shown in fig. 4 (Shepherd 1981; TFI 2011). The Cobra probe used had a frequency response of 600 Hz, as indicated by TFI. From the four measured pressures the stagnation pressure and three orthogonal velocity components can be calculated from calibration curves supplied by TFI for a specific Cobra probe (TFI 2011). The method used to calibrate and calculate the stagnation pressure and three orthogonal velocity components can be found in Shepherd (1981).

The total drag of each wing was calculated through eq. 2 (Brune 1994). The integrals in this equation apply to the wake plane located downstream of the wing. In addition, the first integrands of eq. 2 have been computed to give the "discrete drag", which is the local pressure. This discrete drag coefficient has then been non-dimensionalized to give C_D''. The second integrands of eq. 2 have been computed in the Z-direction to give the "spanwise drag coefficient" and non-dimensionalized to the local chord to give C_D'. ω and σ have been computed via the forward-difference scheme. Equations 5 and 6 were solved via the Gauss-Siedel iterative method and these equations were considered solved once the root-mean-square of the difference between consecutive iterations was less than 10^{-7}. This threshold resulted in the drag value to converge for both wings at all AOAs. ψ was solved with the Dirichlet boundary condition of 0, and ϕ was solved with the Neumann boundary condition of $\partial\phi/\partial n$ equal to 0. Physically, these boundary conditions mean that the flow is parallel to the boundary and that no flow exits through the

boundary. This method of calculating the drag from the wake survey measurements is typically used in an enclosed test section (Brune 1994), hence its use in an open-jet configuration must be justified.

As discussed previously, the differences in the flow physics between the open-jet and closed-duct wind tunnel configurations were minimal. In addition, every term in eq. 2 except ψ and ϕ are only dependent on the viscous wake, and for these wake surveys the viscous wake did not extend to the open-jet shear layer, therefore, their use in the open-jet configuration is as valid as in the enclosed test section configuration. To calculate ψ and ϕ the whole wake must be used and the boundary must be chosen such that the aforementioned boundary conditions are satisfied (Brune 1994). The boundary was selected to be the interface between the potential core and the shear layer as at this point the flow is parallel to the boundary, and for these particular wings from 0° to 12° AOAs the flow only exited the wake plane and not through the shear layers, as checked prior to the surveys. Therefore, under the given conditions using eqs. 2 to 8 to calculate the drag of these two wings in an open-jet wind tunnel is justified.

$$D \approx \frac{1}{2}\rho_\infty \int\int_S (\psi\omega - \phi\sigma)dydz + \int\int_S \left[P_{T\infty} - P_T + \frac{\rho}{2}(U^* - u)(U^* + u - 2U_\infty)\right].dydz \tag{2}$$

where

$$\omega = \left(\frac{\partial w}{\partial y} - \frac{\partial v}{\partial z}\right) \tag{3}$$

$$\sigma = \frac{\partial v}{\partial y} + \frac{\partial w}{\partial z} \tag{4}$$

$$\frac{\partial^2 \psi}{\partial y^2} + \frac{\partial^2 \psi}{\partial z^2} = -\omega \tag{5}$$

$$\frac{\partial^2 \phi}{\partial y^2} + \frac{\partial^2 \phi}{\partial z^2} = \sigma \tag{6}$$

$$U^* = \sqrt{u^2 + \left(\frac{2}{\rho}\right)(P_{T\infty} - P_T)} \tag{7}$$

$$u' = U^* - U_\infty \tag{8}$$

The parameters required to calculate eq. 2 were obtained from the instruments as given in the flow chart in fig. 5 a). The Cobra probe was used to measure the downstream total pressure, P_t, and velocities, u, v, and w. The 95% confidence interval of the Cobra probe in the measurement range was found to be $\pm$0.45 m/s for the u velocity, and $\pm$0.31 m/s for the v and w velocities, which corresponded to approximately $\pm$1.6% of the freestream velocity of 27.5 m/s, and $\pm$10% for the typical v and w velocities. The Cobra probe's accuracy was contingent on the flow being within a 45° cone. A MKS brand Baratron connected to the Pitot hole of a Pitot-static probe was used to calculate the upstream total pressure, $P_{t\infty}$. The 95% confidence interval of the Baratron was found to be $\pm$0.5 pa, which corresponded to approximately $\pm$0.1% of the dynamic pressure at a freestream velocity of 27.5 m/s. A Scanivalve brand DSA3217 pressure scanner was connected to the static holes of the Pitot-static probe, which, in conjunction with the Baratron reading, would give the upstream dynamic pressure. The 95% confidence interval of the Scanivalve was found to be $\pm$3.0 pa, which corresponded to approximately $\pm$0.6% of the dynamic pressure at a freestream velocity of 27.5 m/s. These two instruments were used to minimize the total error of the drag.

To further reduce the uncertainty of the drag calculation, the density of air was also calculated, which required the temperature, barometric pressure, and humidity. The upstream and downstream densities, ρ_∞ and ρ, were assumed to be the same due to the flow being incompressible. The temperature was measured from a TSI brand IFA300 Constant Temperature Anemometer module, the barometric pressure was measured from a Bosch brand BMP085 pressure module, and the humidity was found from a DHT22 module. The IFA300 had a 95% confidence interval of $\pm$0.1° C. The BMP085 had a 95% confidence interval of $\pm$5 pa and DHT22 had a 95% confidence interval of $\pm$2% relative humidity. The BMP085 and DHT22 modules were connected to an Arduino Uno R3, which was connected serially to the data acquisition system.

Any potential drag arising from flow quality issues without a wing present was accounted for by subtracting this drag from the drag of the wings in the same wake plane (Brune 1994). The above uncertainties were processed as prescribed by Holman (1994) and Dieck (1992), which gave an average uncertainty of $\pm$2.0% of the overall drag coefficient.

The wake plane size increased with AOA, which resulted in a longer time to complete each survey. A longer experimental time was more impractical, and would also result in the instrument measurements drifting further away

from their calibrations, thereby reducing the accuracy of the entire experiment. Furthermore, only the viscous wake needed to be measured (Brune 1994). To reduce the experimental time, the area surveyed for each AOA differed but remained constant between wings.

A grid independence study was conducted on both the smooth and tubercled wings at 6° AOA for 3mm, 5mm, and 6mm node spacings. The wingtip region was surveyed as this experienced the highest $C_D{''}$ as well as the greatest spatial gradient in $C_D{''}$. Therefore, any change in the C_D found in this region is expected to be smaller if the entire wake were to be surveyed, as the absolute $C_D{''}$ and the $C_D{''}$ spatial gradient would be reduced. Furthermore, the spatial gradient in $C_D{''}$ for both wings is expected to be greatest at 6° AOA because at 9° AOA the flow in the wingtip region begins to separate, and at 3° AOA the $C_D{''}$ in the wingtip region is lower. Therefore, a suitable grid spacing for this region at 6° AOA would be sufficient for the rest of the wake and for all of the AOAs surveyed.

Figure 6 shows the change in the drag coefficients calculated from the 5mm and 6mm spacings relative to the 3mm spacing. The drag coefficients calculated for the smooth and tubercled wings at 6mm differed by 6.9% and 0.6% to the 3mm spacing drag coefficients, respectively. For the tubercled wing, the drag coefficient deviation for the 6mm grid spacing fell within the estimated uncertainty, whereas for the smooth wing, the drag coefficient did not. Overall, refining the grid spacing to 5mm did not yield an improvement in the drag coefficient measurements. Using a 3mm instead of a 6mm grid spacing would result in the experiments taking four times as long. The initial wake surveying drag measurements at a 6mm grid spacing agreed well with the drag measurements obtained from the load cell, therefore, a 6mm grid spacing was used for the rest of the wake surveys. In addition, the ratio of the tubercle wavelength to the Cobra probe head size was 10:1, which was reasonable as the downstream vortices scale with the tubercle wavelength.

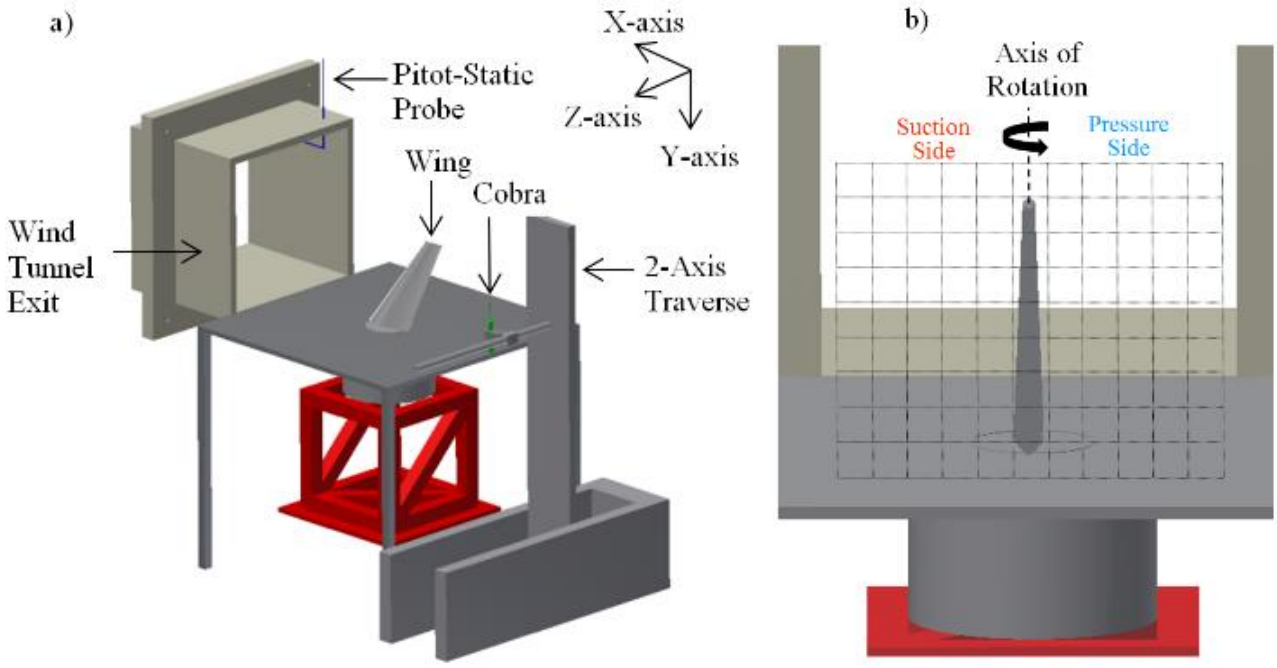

Fig. 3 a) wake surveying setup with the Cobra probe located 3 Mean Aerodynamic Chords downstream of wing trailing edge at Mean Aerodynamic Chord spanwise location. b) Rear view highlighting axis of rotation and wake survey mesh (mesh not to scale).

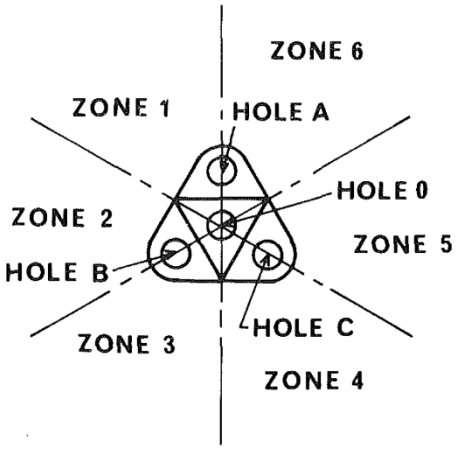

Fig. 4 Cobra probe schematic and location of holes (Shepherd 1981). Reprinted with permission from The American Society of Mechanical Engineers.

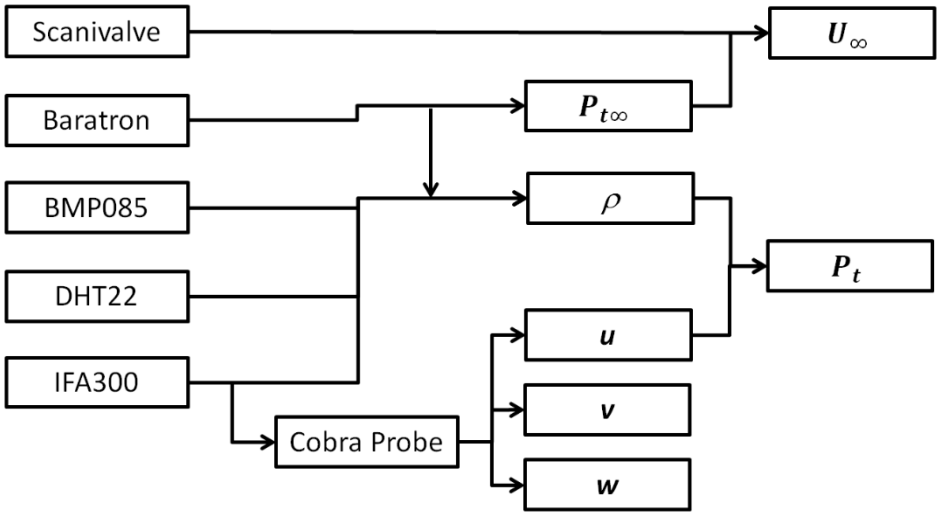

Fig. 5 Depicts a flow chart of how each parameter, in bold, is obtained from the given instruments.

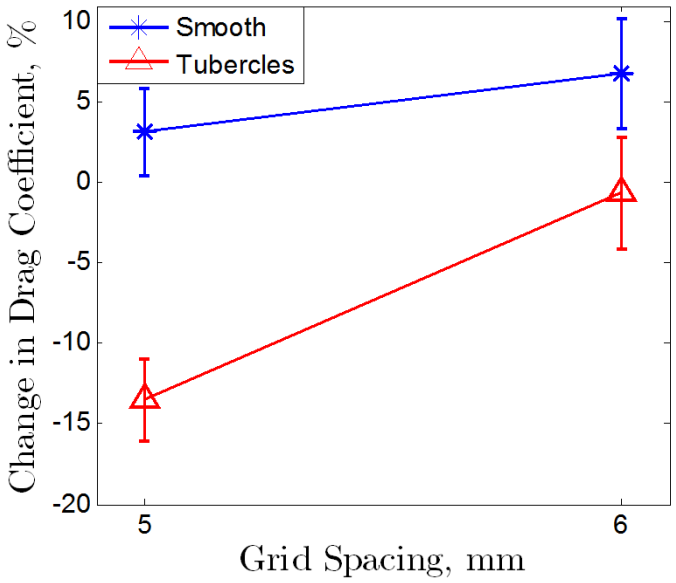

Fig. 6 The change in the drag coefficient at a given grid spacing with respect to 3mm grid spacing drag coefficient expressed as a percentage of the 3mm grid spacing drag coefficient. Normalized to the 3mm drag coefficient for each respective wing.

Results

Figure 7 show the lift and drag coefficients of the wings obtained through the load cell, respectively. It should be noted that the error bars, as seen in the respective figures, do not overlap.

For low-to-moderate AOAs, tubercles reduce the lift, as shown in fig. 7. This finding is consistent with other studies (Johari *et al.* 2007; Hansen 2012) where tubercles tend to reduce lift as the stall angle is approached. At high AOAs the tubercles tend to a produce higher lift coefficient (Johari *et al.* 2007; Hansen 2012), however, fig. 7 shows that the smooth wing continues to produce a higher lift coefficient than the tubercled wing. From approximately 6° AOA onwards, the lift-curve slopes of both of the wings increase. The slopes of the lift-curves have been calculated by the use of the central difference scheme and the results are plotted in fig. 8. There is a clear increase in the lift-curve slope from 6° AOA. Hansen (2012) suggested that an increase in the lift-curve slope, as is seen in these results, is due to the formation of a Laminar Separation Bubble, LSB, on the suction side of the wings. As the Reynolds number of this experiment is optimal for LSB formation, this explanation is the likely cause. It should be noted that while some tubercle related studies have documented the presence of an LSB (Hansen 2012; Rostamzadeh *et al.* 2014), other studies of similar airfoil profiles and test conditions have not (Miklosovic *et al.* 2004; Johari *et al.* 2007). While in this study the LSB appears to be affecting both wings, the lift-curve slope of the smooth wing increases at a greater rate than the tubercled wing, suggesting that the interaction between the LSB and the tubercles negatively impacts the augmented lift produced by the LSB. This may be caused by premature flow separation in the troughs of the tubercled wing (Rostamzadeh *et al*. 2014).

While the lift-curve slope increases from 6° AOA, fig. 8 shows that a reduction starts to occur at 8° and 7° AOAs for the smooth and tubercled wings, respectively. The lift-curve slopes of both wings decrease shortly after increasing, which is likely caused by flow separation. As these wings are relatively thick, the stall will start to occur at the trailing edge and progress towards the leading edge with increasing AOA. Coupling this with the LSB formation, the stall pattern of this wing will be type-III as outlined by Luckring (2010).

From 9° AOA onwards, the lift-curve slopes of the wings are very similar suggesting that these tubercles do not significantly soften the stall, unlike what is typically found (Johari *et al.*2007; Hansen 2012). This could be because the wings are swept, and as the stall behaviour is more gradual for a swept wing than an unswept wing, the addition of tubercles may not have any further obvious impact on the severity of the stall. This phenomenon was also seen in Murray *et al.* (2005), where for a whale flipper model tubercles had less of an impact on the stall severity with increasing sweep angle. Both of these swept wings have positive lift-curve slopes at 20° AOA, which is consistent with literature (Harper and Maki, 1964; Custodio *et al.*, 2015). Custodio *et al.* (2015) investigated a NACA 63_4-021 wing profile with a leading edge sweep of 26.1° and an aspect ratio of 4.0. They found that the smooth leading edge

wing had a lift coefficient of approximately 1.2 at an AOA of 23°. They also found that tubercles typically reduced the lift coefficient at pre-stall AOAs.

For AOAs up to 8° tubercles reduce the drag coefficient, as shown in fig. 7, whereas for AOAs greater than 8° and up to 18°, tubercles substantially increase the drag coefficient. This trend is also clearly seen in fig. 11, which shows the change in the drags obtained from the wake survey measurements and the force measurements, which will be further discussed below. As the reduction in the lift-curve slope occurs at approximately the same AOA as the sudden increase in the drag coefficient, it is expected that the same mechanism is responsible both of these phenomena. This trend in drag production was also seen in Hansen *et al.* (2011), who studied full-span NACA 0021 tubercled airfoils in the same facility as this study. They found that for some tubercle geometries, namely A4λ60 and A8λ30, below a certain AOA tubercles appear to slightly reduce the drag, while above this AOA a sudden increase in drag arises. The data presented in Hansen *et al.* (2011) also demonstrates that this transition AOA is dependent on the tubercle geometry.

There is considerable evidence that tubercles act like vortex generators (Pedro and Kobayashi 2008; Wei *et al.* 2015) and that tubercles can modulate an LSB formation (Rostamzadeh *et al.* 2014) in a similar manner to vortex generators (Seshagiri *et al.* 2009). Furthermore, Seshagiri *et al.* (2009) found that drag reductions can result from the LSB modulation by vortex generators. Therefore, the manner in which tubercles reduce drag may be the same as the manner in which vortex generators reduce drag.

As tubercles reduce the drag coefficient more than the lift coefficient, tubercles increase the L/D of this wing. It should be noted that due to the overlapping errorbars of the L/Ds of each wing up to 9° AOA, conclusions drawn are not final. Figure 9 shows that between 1° and 8° AOAs tubercles increase L/D by 2% to 6%, without accounting for errorbars. In addition, tubercles increase the maximum L/D by 3% without accounting for errorbars, which occurs at 6° AOA, making the wing more efficient. At an AOA above 8°, tubercles greatly reduce L/D. Custodio *et al.* (2015) found that tubercles typically reduced the lift coefficient and increased the drag coefficient of the swept wing they investigated. As a result, tubercles tended to reduce the L/D ratio.

To further highlight the relative changes in the lift, total drag and L/D, fig. 10 shows the effect of tubercles on these parameters as a percentage of the smooth wing counterpart. This highlights that tubercles reduce lift by 4% to 6% and reduce drag by 7% to 9.5% for AOAs between 0° and 8°. Above 8° AOA, the continued reduction in lift and

sudden increase in drag results in a large reduction in L/D which decreases to a reduction deficit of 1.9% at 20° AOA.

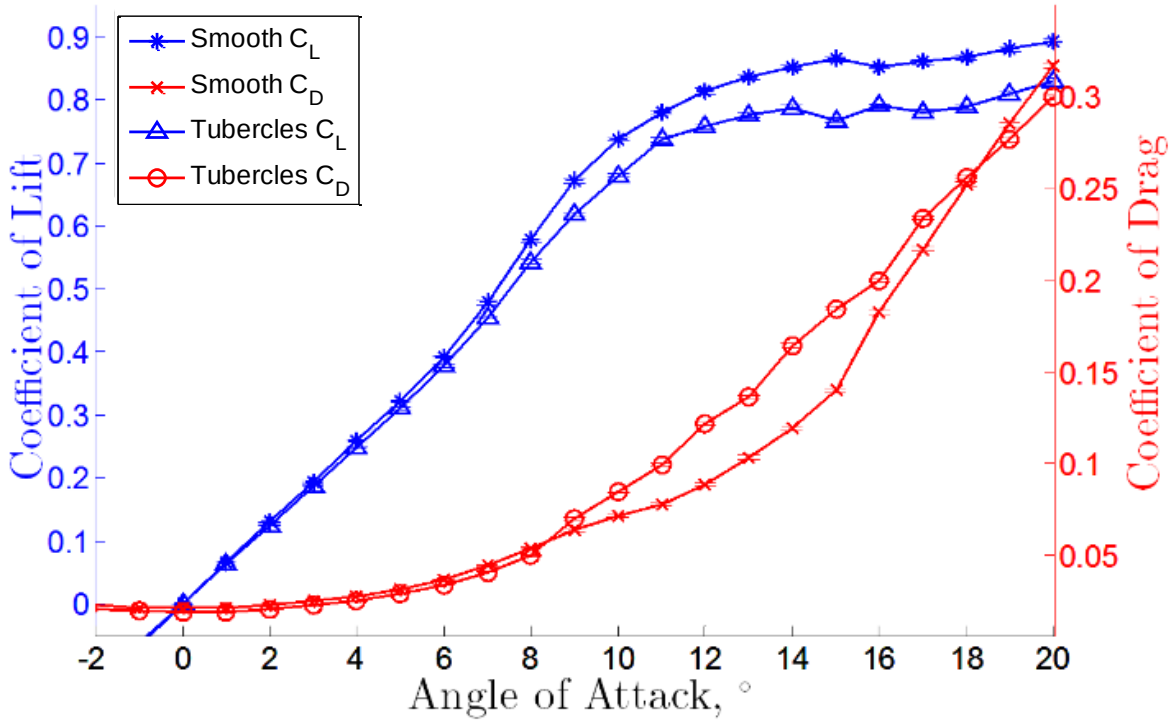

Fig. 7 Lift and drag coefficients of the smooth and tubercled wings, 35° quarter chord sweep angle at a 225,000 Mean Aerodynamic Chord Reynolds number.

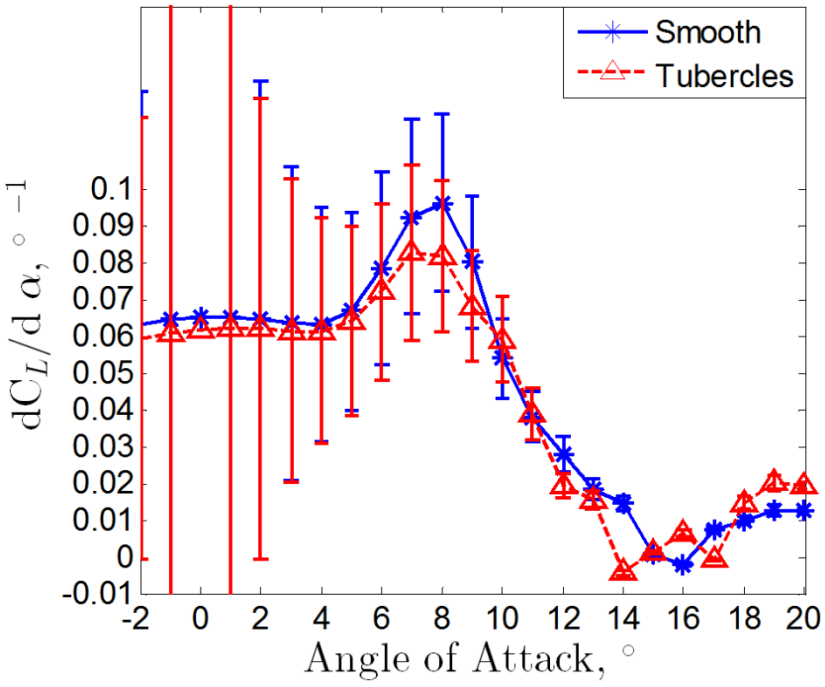

Fig. 8 Change in the lift-curve slope of the smooth and tubercled wings at a Mean Aerodynamic Chord Reynolds number of 225,000.

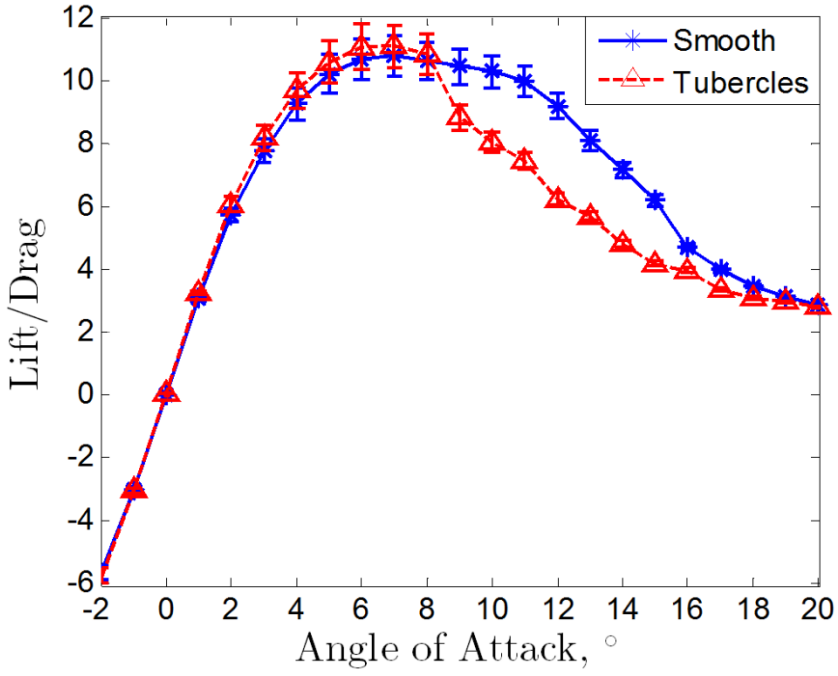

Fig. 9 Lift-to-drag ratio of the smooth and tubercled wings at a Mean Aerodynamic Chord Reynolds number of 225,000.

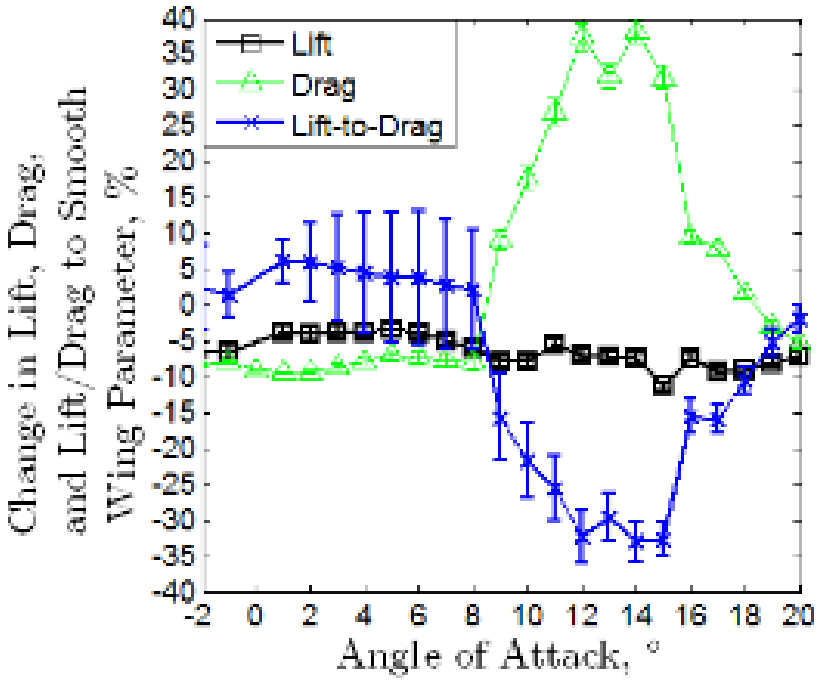

Fig. 10 The effects of tubercles on lift coefficient, drag coefficient, and the lift-to-drag ratio. The change is expressed as a percentage of the smooth wing's respective performance parameter, where positive indicates an increase. Mean aerodynamic chord Reynolds number is 225,000.

Figure 11 a) shows the drag coefficients of the smooth and tubercled wings as measured from the load cell and the wake surveys from 0° to 12° AOAs. Very good agreement between the load cell and wake survey results can be seen for 3° AOA and higher. Significant differences in the drag coefficients exist at 0° AOA. The drag coefficients of the smooth and tubercled wings in the open-jet configuration at 0° AOA have been calculated from the forces measured by the load cell during wing alignment. In the open-jet configuration, the smooth and tubercled wings have drag coefficients of 0.0206 and 0.01966, respectively, which are -2.4% and +2.1% different from the corresponding drag coefficients calculated from the load cell data taken in the closed-duct configuration. These differences are within the experimental uncertainties described above. Therefore, it is concluded that the differences in the drag coefficients at 0° AOA, presented in fig. 11 a), are not statistically significant and are unlikely to be due to the two different wind tunnel configurations used during this study. The load cell and wake survey measurements are in agreement with the transition AOA as well. Figure 11 b) shows that the relative change in the drag coefficients, as measured by the load cell and wake surveys, are in very good agreement between 3° and 12° AOAs.

This shows that the random errors have been adequately accounted in both techniques. Once again, a significant discrepancy occurs at 0° AOA. The good agreement in the load cell and wake survey results indicates that the wakes of both wings at all AOAs were adequately captured.

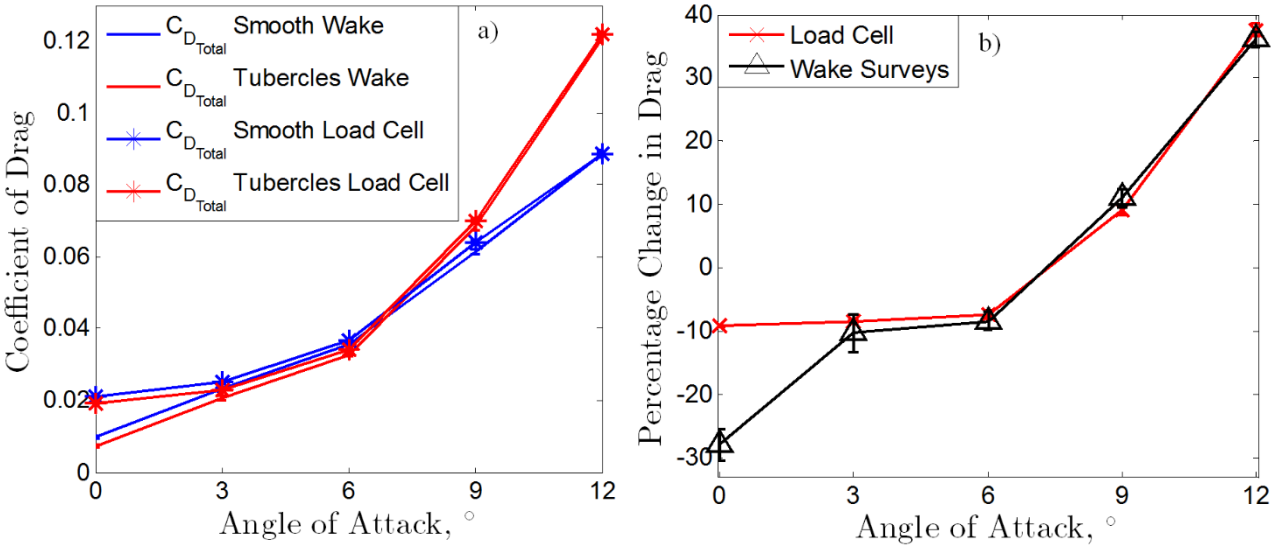

Fig. 11 Comparison between load cell and wake survey drag coefficients, a, and the relative change of the tubercled wing's drag coefficient with respect to the smooth wing as calculated from the load cell and wake survey measurements, b).

The $C_D{''}$ contours displayed in fig. 12 of the smooth, a), and tubercled, b), wings has been rotated clockwise 90° to what is shown in fig. 3 b) such that the pressure side located on the lower portion of the figures, denoted by negative vertical axis values, and the suction side on upper portion, denoted by positive vertical axis values. The horizontal axis is referenced and normalized to the wing half-span, where 0 is the wing root and 1 is the wingtip. The vertical axis is referenced to the chord-line of the wing at the given AOA. A dashed line running the entire horizontal axis at the vertical axis coordinate of 0 has been included to indicate the projection of the wing chord-line at a given AOA. Below approximately 24mm at the wing root, the drag has been removed as this largely corresponds to the boundary layer of the flat plate in fig. 3, a, and as such does not reflect the drag of the wing itself. Furthermore, the measurements from the load cell do not include this flat plate boundary layer but only the drag over the baseplate attaching the wing to the load cell. This baseplate was circular with a diameter of 140mm, whereas the approximate length and width of the table exposed to the flow during the wake survey measurements were 500mm x 900mm. Therefore, the amount of drag produced by this baseplate would be minimal compared to

the entire table. Furthermore, the baseplate was acrylic, and as such was smooth, hence it is expected to incur a minimal skin friction drag penalty.

The smooth wing produces a uniform C_D'' distribution along its entire span whereas tubercles modulate the C_D'' into local maxima along the entire leading edge, as shown in fig. 12 a) and b). The vorticity distributions of the smooth and tubercled wings at 0° AOA, as shown in fig. 12 c) and d), show that there are no discernible wingtip vortex, suggesting that the wings are well aligned, and that the alignment assumption is valid. The vorticity fields presented in figs. 12 and 13 agree with the findings of other studies on tubercles (Hansen 2012; Rostamzadeh *et al.* 2014; Hansen *et al.* 2016); each tubercle produces a pair of counter-rotating vortices. Therefore, the Cobra probe size of 3mm x 3mm and the 6mm grid spacing were sufficiently small to measure the vortices produced by the tubercles. At 0° AOA, these vortices are aligned such that the vortices are stacked vertically in each pair. At 6° AOA, the vorticity fields of the smooth and tubercled wings are typical of these wings at non-zero degree AOAs; both wings produce lift, which results in wingtip vortices to form at a spanwise location of 1.0. The smooth wing produces a relatively uniform vorticity field from the wing root to the wingtip, whereas the tubercled wing produces distinct vorticity cores from each tubercle. For the tubercled wing, sweeping the leading edge results in an asymmetry in the vorticity pairs from each tubercle.

Figure 12 a) shows a local maximum in the C_D'' at the wingtip, and since this symmetrical wing was well-aligned this maximum is not due to induced drag. Instead, it was due to flow separation at the junction of the wing leading edge and the wingtip, as found on finite cylinders (Rostamy *et al.* 2013; Porteous *et al.* 2014). The tubercled wing reduces this local maximum at 0° AOA. Comparing figs. 12 b) and 12 d), the local C_D'' maxima over the tubercled wing occur at spanwise locations where two vorticity cores of opposite sign appear. These cores form approximately midway between a tubercle trough and peak.

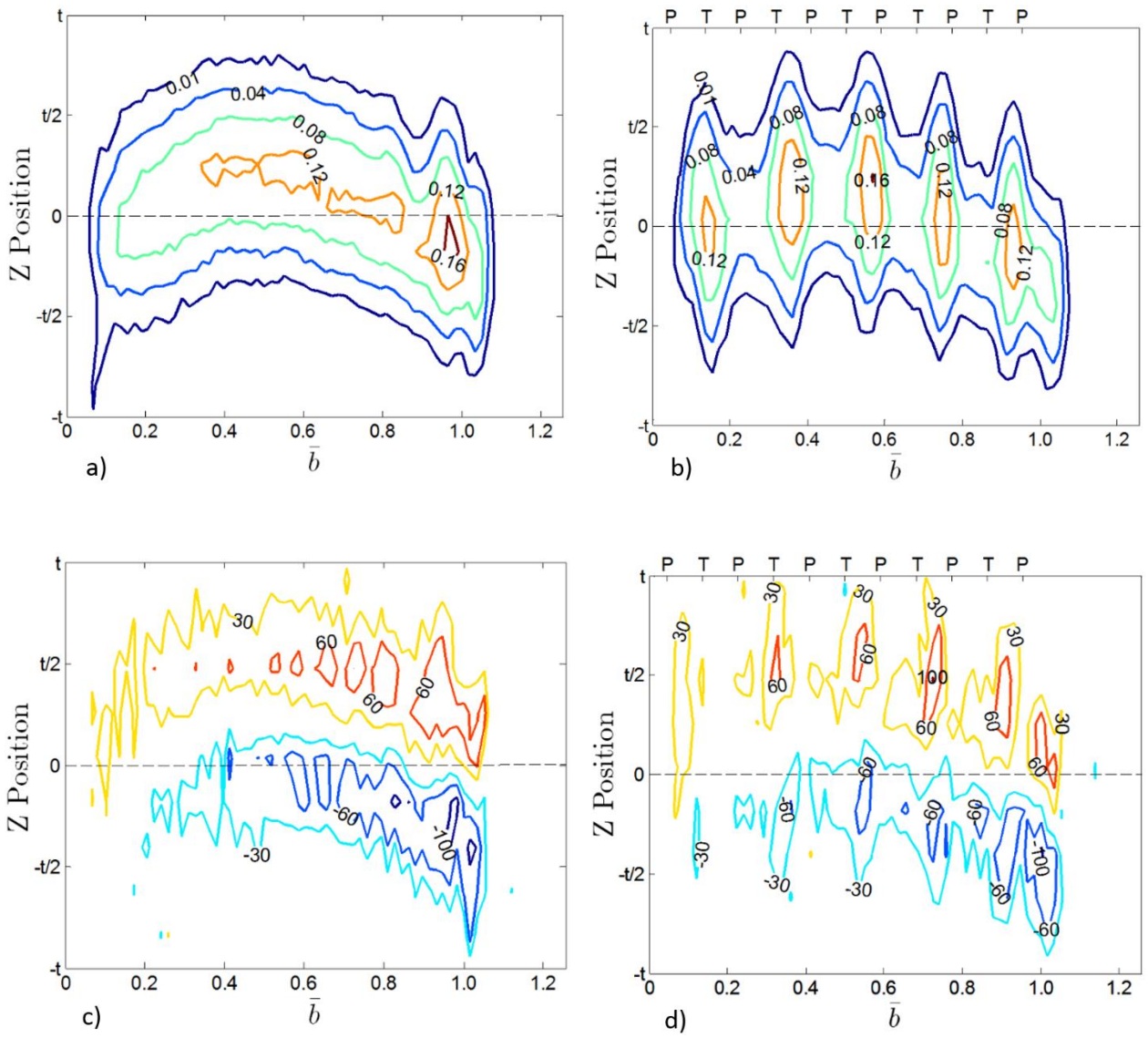

Fig. 12 Discrete drag coefficient contour plots of a), smooth wing, and b), tubercled wing at an angle of attack of 0°. Vorticity plot of smooth wing, c), and tubercled wing, d), at an angle of attack of 0°. The vorticity is positive for a counter-clockwise rotation. The horizontal axis is normalized to $\bar{b}$; the half-span. The vertical axis is normalized to the wing Mean Aerodynamic Chord thickness. The top horizontal axes of b) and d) indicate the locations of peaks, P, and troughs, T.

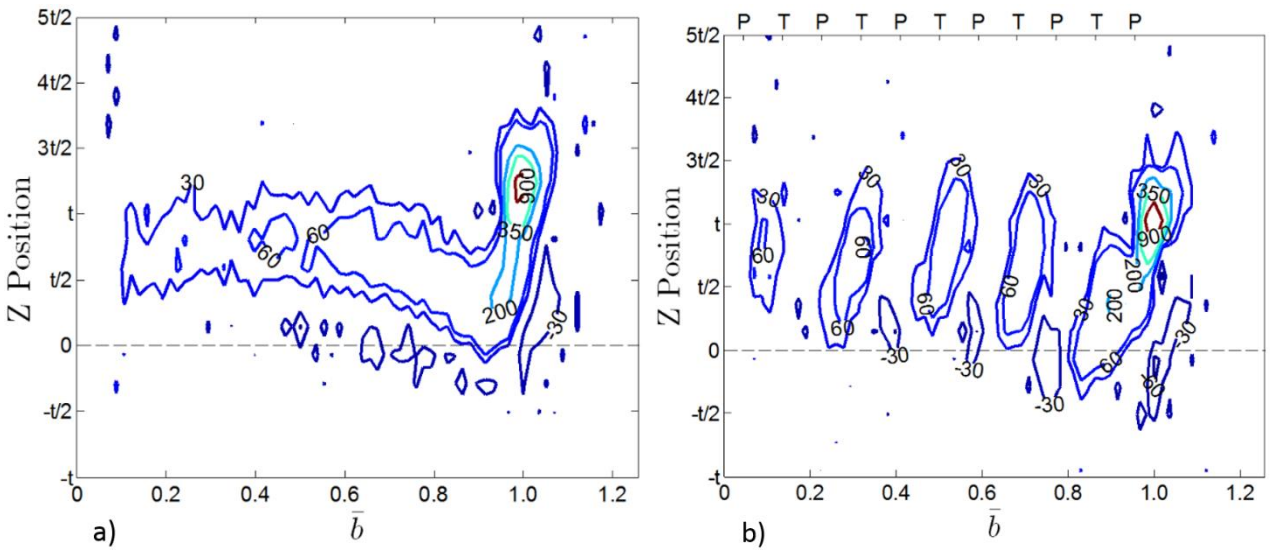

Fig. 13 Streamwise vorticity distributions downstream of the smooth wing, a), and tubercled wing, b), at an angle of attack of 6°. The vorticity is positive for a counter-clockwise rotation. The horizontal axis is normalized to $\bar{b}$; the half-span. The vertical axis is normalized to the wing Mean Aerodynamic Chord thickness. The top horizontal axis of b) indicates the locations of peaks, P, and troughs, T.

While the $C_D{}''$ distributions show how tubercles affect the local drag coefficient, it is difficult to determine the overall effects. Therefore, the $C_D{}'$ of both wings at 0°, 3°, 6°, 9°, and 12° AOAs are shown in figs. 14 to 18. At 0° AOA, the smooth wing produces a uniform $C_D{}'$ along the entire leading edge with a spike in $C_D{}'$ at the wingtip. This local maximum at the wingtip was also found in the $C_D{}''$ distribution in fig. 12 and is most likely caused by flow separation. The $C_D{}''$ modulation cause by tubercles is also shown in fig. 14 with local minima and maxima forming along the entire span. A local maximum in the $C_D{}'$ also occurs at the wingtip, however, it is significantly smaller and narrower than the smooth wing. Interestingly, at 0° AOA, the width of the local maxima in the $C_D{}'$ of the tubercled wing is narrower than the local minima, which suggests that overall more of the tubercled wing is experiencing a drag coefficient reduction. Near the wing root the local $C_D{}'$ maxima occur in tubercle troughs whereas the local minima occur over the tubercle peaks. Near the wingtip the local maxima and minima shift slightly towards the midway points between the peaks and troughs, which may be caused by the spanwise flow influencing the wake roll-up. This trend exists for all AOAs considered.

At 3° AOA, the tubercles do not produce a noticeable reduction in the wingtip $C_D{}'$. Despite this, the tubercled wing still reduces the drag coefficient at 3° AOA, which primarily occurs over the span; the $C_D{}'$ local minima are both wider and greater than the local maxima. A similar trend occurs at 6° AOA, as shown in fig. 16, where minimal

reduction in the drag coefficient occurs in the wingtip regions, but reductions continue over the entire span. Comparing figs. 13 b) and 16, which correspond to the vorticity field and the $C_D{}'$ distribution of the tubercled wing at 6° AOA, respectively, the $C_D{}'$ local maxima form in the common upwash regions, whereas the $C_D{}'$ local minima form in the common downwash regions. Therefore, the tubercle troughs increase the $C_D{}'$, while the tubercle peaks reduce the $C_D{}'$. Rostamzadeh *et al.* (2014) found that boundary layers in the tubercle troughs typically begin to separate at much lower AOAs than over the peaks. Therefore, we suggest that the $C_D{}'$ local maxima in the troughs are caused by premature flow separation. At 9° AOA, the local $C_D{}'$ maxima over the tubercled wing are now greater and cover more of the wingspan than the local minima, which is consistent with the increase in the drag coefficient seen in figs. 7 and 11. Furthermore, these local maxima are flatter when compared to the local maxima found at 0°, 3°, and 6° AOAs. We suggest that this flattening at 9° AOA is caused by the flow significantly separating in the troughs, which correlates with the lift-curve slope reduction found in fig. 8.

Note that at 3° and 6° AOAs there are small local maxima in the $C_D{}'$ just before the tubercled wingtip region, however, at 9° and 12° AOAs these local maxima are gone, which supports the argument that the flow has greatly separated at these higher AOAs.

At 12° AOA, the tubercled wing has significantly stalled in the wingtip region as evidenced by the large increase in $C_D{}'$. Furthermore, the tubercled wing is increasing $C_D{}'$ over almost the entire wingspan, suggesting widespread flow separation. The local $C_D{}'$ maxima and minima are no longer distinct and the tubercle peaks and troughs produce similar $C_D{}'$.The smooth wing has a greater and sharper $C_D{}'$ local maxima in the wingtip region, suggesting that the flow has separated more over the tubercled wing than the smooth wing.

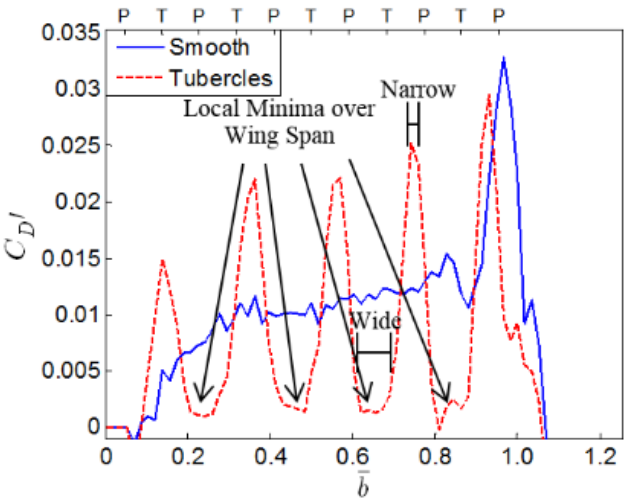

Fig. 14 Spanwise drag coefficient of smooth and tubercled wings at an angle of attack of 0°. The horizontal axis is normalized to $\bar{b}$; the half-span. The vertical axis is the spanwise drag coefficient. The top horizontal axis of b) indicates peak, P, or trough, T.

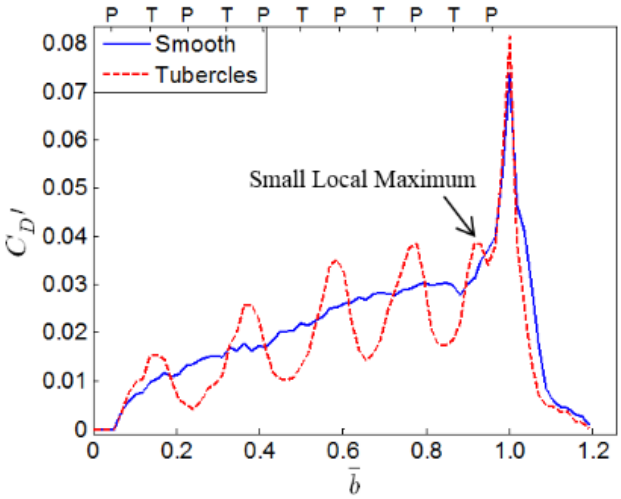

Fig. 15 Spanwise drag coefficient of smooth and tubercled wings at an angle of attack of 3°. The horizontal axis is normalized to $\bar{b}$; the half-span. The vertical axis is the spanwise drag coefficient. The top horizontal axis of b) indicates peak, P, or trough, T.

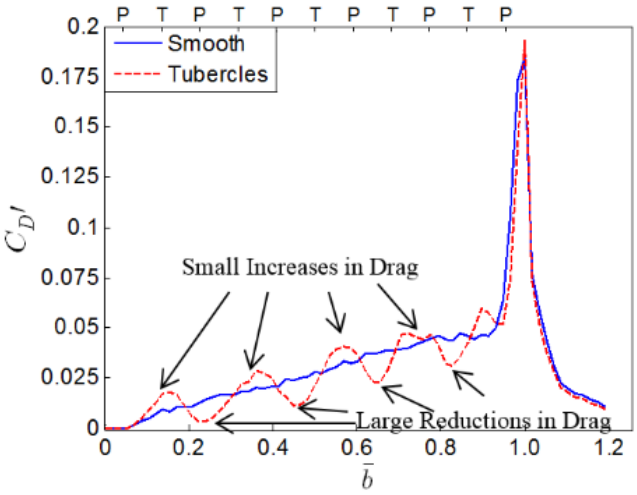

Fig. 16 Spanwise drag coefficient of smooth and tubercled wings at an angle of attack of 6°. The horizontal axis is normalized to $\bar{b}$; the half-span The vertical axis is the spanwise drag coefficient. The top horizontal axis of b) indicates peak, P, or trough, T.

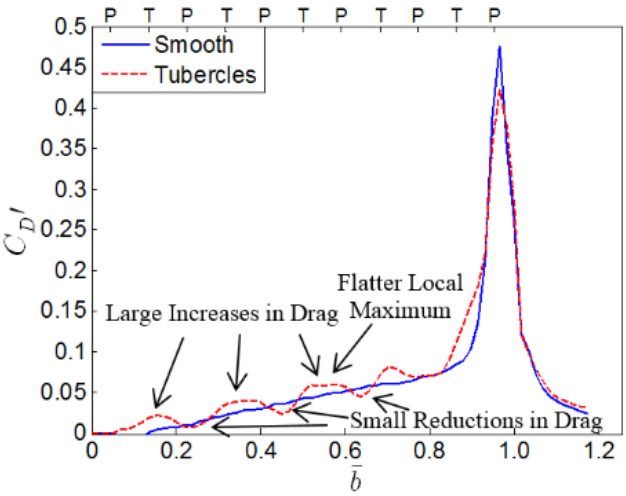

Fig. 17 Spanwise drag coefficient of smooth and tubercled wings at an angle of attack of 9°. The horizontal axis is normalized to $\bar{b}$; the half-span. The vertical axis is the spanwise drag coefficient. The top horizontal axis of b) indicates peak, P, or trough, T.

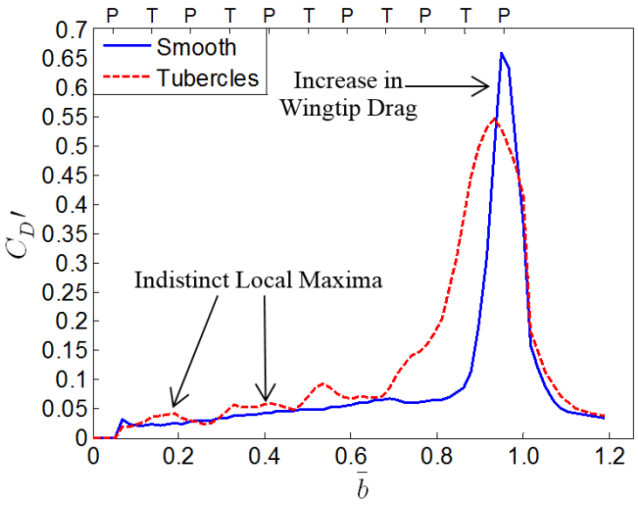

Fig. 18 Spanwise drag coefficient of smooth and tubercled wings at an angle of attack of 12°. The horizontal axis is normalized to $\bar{b}$; the half-span. The vertical axis is the spanwise drag coefficient. The top horizontal axis of b) indicates peak, P, or trough, T.

Conclusion

The lift and drag of two swept wings, one smooth and one tubercled, were measured by a load cell. It was found that for angles of attack ranging from 0° to 8° tubercles reduced the lift coefficient by 4 to 6%, and reduced the drag coefficient by 7 to 9.5%. This resulted in an increase in the lift-to-drag ratio of 2 to 6%. Tubercles also increased the maximum lift-to-drag ratio, which occurred at 6° angle of attack, by 3%. From an angle of attack of 8° onwards, tubercles reduced the lift coefficient and increased the drag coefficient, which resulted in a reduced lift-to-drag ratio. This sudden drop in performance of the tubercled wing has been attributed to the premature onset of flow separation. It was found that while tubercles typically soften the stall for unswept wings, they had little effect on the severity of the stall region for this swept wing.

Wake surveys were also conducted on these two wings, and the drag coefficients were calculated and compared to the force measurement results for the wings at 0°, 3°, 6°, 9° and 12° angles of attack. Very good agreement between the force measurements and the wake survey were found for the drag coefficient, and the angle of attack at which the tubercled wing transitioned from producing a lower drag coefficient to a higher one.

The wake surveys also showed that tubercles reduced the local drag coefficient in the wingtip region at 0° angle of attack, however, at non-zero, pre-stall angles of attack, there was little change. While for the smooth wing the spanwise drag coefficient was relatively consistent along the span, the tubercled wing spatially modulated the spanwise drag coefficient and formed local maxima and minima. From comparison to other works, the increases in the drag coefficient found in the troughs were reasoned to be caused by early onset of stall, while the reductions in the drag coefficient over the peaks were caused by the flow staying attached to a greater extent.

Acknowledgments

The authors appreciate the assistance of Sophie Dawson, Oliver Durance, Tony Huang, Simon McDonald, and Jeremy Yu.

The authors thank Assoc. Prof. Con Doolan and Dr. Zebb Prime for their contributions to this work.

Research undertaken for this report has been assisted with a grant from the Sir Ross and Sir Keith Smith Fund (Smith Fund) (www.smithfund.org.au). The support is acknowledged and greatly appreciated.

References

Barlow, J.B., Rae, W.H. Jr., and Pope, A. (1999). *Low-Speed Wind Tunnel Testing*, 3rd ed., Wiley, New York.

Bolzon, M.D., Kelso, R.M. and Arjomandi, M. (2015). "A Review of Tubercles and Their Applications", *The Journal of Aerospace Engineering*. doi: 10.1061/(ASCE)AS.1943-5525.

Bolzon, M.D., Kelso, R.M., and Arjomandi, M. (2015). "Parametric Study of the Effects of a Tubercle's Geometry on Wing Performance Through the Use of the Lifting-Line Theory", *Proceedings of 54th AIAA Aerospace Science Meeting*, San Diego, CA. doi: 10.2514/6.2016-0295.

Bradley, G. (2009). "Shark Fin Wings Give Airline Chiefs Something to Smile About." The New Zealand Herald, Auckland, New Zealand.

Brown, F. (1997). "Test Could Cut Aircraft Fuel Costs", *Aerospace Technology Innovation*, 5(4).

Brune, G.W. (1994). "Quantitative Low-Speed Wake Surveys", *Journal of Aircraft*, 31(2), 249-255. doi: 10.2514/3.46481.

Custodio, D., Henoch, W., and Johari, H. (2015). "Aerodynamic Characteristics of Finite Span Wings with Leading-Edge Protuberances", *AIAA Journal*, 53(7), 1878-1893. doi: 10.2514/1.J053568.

Dieck, R.H. (1992). *Measurement Uncertainty: Methods and Applications*, The Instrument Society of America, N.C..

Fish, F.M., and Battle, J.M. (1995). "Hydrodynamic Design of the Humpback Whale Flipper", *Journal of Morphology*, 255, 51-60. doi: 10.1002/jmor.1052250105.

Hansen, K.L. (2012). "Effect of Leading Edge Tubercles on Airfoil Performance", Ph.D. Dissertation The University of Adelaide, Adelaide, Australia.

Hansen, K.L., Kelso, R.M. and Dally, B.B. (2011). "Performance Variations of Leading-Edge Tubercles for Distinct Airfoil Profiles", *AIAA* Journal, 49(1), 185-194. doi: 10.2514/1.J050631.

Hansen, K.L., Rostamzadeh, N., Kelso, R.M., and Dally, B.B. (2016). "Evolution of the Streamwise Vortices Generated Between Leading Edge Tubercles", *Journal of Fluid Mechanics*, 788, 730-766. doi: 10.1017/jfm.2015.611.

Holman, J.P. (1994). *Experimental Methods for Engineers*, 6th ed., McGraw-Hill, New York.

Harper, C.W. and Maki, R.L. (1964). "A Review of the Stall Characteristics of Swept Wings", *NASA Technical Note*, NASA TN D-2373.

Johari, H., Henoch, C., Custodio, D., and Levshin, A. (2007). "Effects of Leading-Edge Protuberances on Airfoil Performance", *AIAA Journal*, 49(1), 185-194. doi: 10.2514/1.J050631.

Jurasz, C.M., and Jurasz, V.P. (1979). "Feeding Modes of the Humpback Whale, Megaptera Novaeangliae, in Southeast Alaska", *The Scientific Reports of the Whales Research Institute*, 31, 69-83.

Luckring, J.M. (2010). "A Survey of Factors Affecting Blunt Leading-Edge Separation for Swept and Semi-Slender Wings", *Proceedings of AIAA 28th Applied Aerodynamics Conference*, IL, U.S. doi: 10.2514/6.2010-4820.

Miklosovic, D.S., Murray, M.M., and Howle, L.E. (2007). "Experimental Evaluation of Sinusoidal Leading Edges", *Journal of Aircraft*, 44(4). doi: 10.2514/1.30303.

Miklosovic, D. S., Murray, M. M., Howle, L. E. and Fish, F. E. (2004). "Leading-edge Tubercles Delay Stall on Humpback Whale (Megaptera Novaeangliae) Flippers", *Physics of Fluids*, 16(5) L39-L42, doi:10.1063/1.1688341.

Murray, M.M, Miklosovic, D.S., Fish, F., and Howle, L. (2005). "Effects of Leading Edge Tubercles on a Representative Whale Flipper Model at Various Sweep Angles", *Proceedings of Unmanned Untethered Submersible Technology (UUST)*, NH, U.S.

Pedro, H.T., and Kobayashi, M.H. (2008). "Numerical Study of Stall Delay on Humpback Whale Flippers", *AIAA Aerospace Sciences Meeting and Exhibit*, Reno.

Porteous, R., Moreau D.J, and Doolan, C.J. (2014). "A Review of Flow-induced Noise from Finite Wall-mounted Cylinders", *Journal of Fluids and Structures*, 51, 240-254. doi: 10.1016/j.jfluidstructs.2014.08.012.

Rostamy, N., Sumner, D., Bergstrom, D.J., and Bugg, J.D. (2013). "Instantaneous Flow Field Above the Free End of Finite-Height Cylinders and Prisms", *International Journal of Heat and Fluid Flow*, 43, 120-128. doi: 10.1016/j.ijheatfluidflow.2013.04.005

Rostamzadeh, N, Hansen, K.L., Kelso, R.M. and Dally, B.B. (2014). "The Formation Mechanism and Impact of Streamwise Vortices on NACA 0021 Airfoil's Performance with Undulating Leading Edge Modification", *Physics of Fluids*, 26(10). doi:10.1063/1.4896748.

Seshagiri, A., Cooper, E., and Traub, L.W. (2009). "Effects of Vortex Generators on an Airfoil at Low Reynolds Numbers", *Journal of Aircraft*, 46(1). doi: 10.2514/1.36241.

Shepherd, I.C. (1981). "A Four Hole Pressure Probe for Fluid Flow Measurements in Three Dimensions", *Journal of Fluids Engineering*, 103, 590-594. doi: 10.1115/1.3241774.

Stein, B., and Murray, M.M. (2005). "Stall Mechanism Analysis of Humpback Whale Flipper Models", *Proceedings of Untethered Submersible Technology (UUST),*Autonomous Undersea Systems Inst., NH, U.S.

TFI (2011). "Getting Started Series 100 Cobra Probe", *Turbulent Flow Instrumentation Pty. Ltd*.

Watts, P., and Fish, F.E. (2001). "The Influence of Passive, Leading Edge Tubercles on Wing Performance", *Proceedings of Unmanned Untethered Submersible Technology (UUST)*, Autonomous Undersea Systems Inst., NH, U.S.

Wei, Z., New, T.H., and Cui, Y.D. (2015). "An Experimental Study on Flow Separation Control of Hydrofoils with Leading-Edge Tubercles at Low Reynolds Number", *Ocean Engineering*, 108, 336-349. doi:10.1016/j.oceaneng.2015.08.004.

Statement of Authorship

Title of Paper	Formation of Vortices on a Tubercled Wing, and Their Effects on Drag
Publication Status	☑ Published ☐ Accepted for Publication ☐ Submitted for Publication ☐ Unpublished and Unsubmitted w ork w ritten in manuscript style
Publication Details	Bolzon, M.D., Kelso, R.M. and Arjomandi, M., "Formation of Vortices on a Tubercled Wing, and Their Effects on Drag", *Aerospace Science and Technology*, 2016. doi: 10.1016/j.ast.2016.06.025

Principal Author

Name of Principal Author (Candidate)	Michael Bolzon		
Contribution to the Paper	Designed and built wake survey rig, performed experiments, processed data, wrote manuscript, and acted as corresponding author.		
Overall percentage (%)			
Certification:	This paper reports on original research I conducted during the period of my Higher Degree by Research candidature and is not subject to any obligations or contractual agreements with a third party that would constrain its inclusion in this thesis. I am the primary author of this paper.		
Signature		Date	

Co-Author Contributions

By signing the Statement of Authorship, each author certifies that:

i. the candidate's stated contribution to the publication is accurate (as detailed above);

ii. permission is granted for the candidate in include the publication in the thesis; and

iii. the sum of all co-author contributions is equal to 100% less the candidate's stated contribution.

Name of Co-Author	Richard Kelso		
Contribution to the Paper	Supervised experimental development, aided interpretation of results, and reviewed manuscript.		
Signature		Date	

Name of Co-Author	Maziar Arjomandi		
Contribution to the Paper	Supervised experimental development, aided interpretation of results, and reviewed manuscript.		
Signature		Date	

Aerospace Science and Technology 56 (2016) 46–55

Contents lists available at ScienceDirect

Aerospace Science and Technology

www.elsevier.com/locate/aescte

Formation of vortices on a tubercled wing, and their effects on drag

Michael D.P. Bolzon *, Richard M. Kelso, Maziar Arjomandi

The University of Adelaide, Adelaide, 5005, Australia

ARTICLE INFO

Article history:
Received 7 December 2015
Received in revised form 24 June 2016
Accepted 30 June 2016
Available online 9 July 2016

ABSTRACT

Wake surveys of 2 swept NACA 0021 wings were conducted at angles of attack of 0°, 3°, 6°, 9°, and 12°. One wing had a smooth leading edge and the other had a tubercled leading edge. Sweeping the tubercled wing resulted in one vortex in each vortex pair being at least 4 times stronger than the other. There was little difference between the strength of the wingtip vortices of either wing at 3°. From 6° onwards tubercles reduced the strength of the wingtip vortex. The tubercle troughs tended to produce local maxima and minima in the profile and induced drag coefficients, respectively. The converse was true over the peaks. The change in the profile, induced, and total drag coefficients primarily arose from over the wingspan; there was little contribution from the wingtip region.

1. Introduction

Humpback whales are enormous creatures, yet they remain remarkably agile. They can execute underwater somersaults and swim at high angles of attack during feeding [1], feats unique among Baleen whales. Their pectoral flippers are also unique, featuring bumps on the leading edges, termed tubercles, and it is now known that these tubercles are, in part, responsible for the Humpback whale's nimbleness [2].

Tubercles can be categorised by two main parameters, the amplitude, which refers to the distance between a tubercle peak and neighbouring trough, and the wavelength, which refers to the distance between two neighbouring tubercle troughs or peaks. Research has revealed that tubercles create pairs of counter-rotating, streamwise vortices [3–5] as shown in Fig. 1. It was proposed by Hansen et al. [6] that the strength of these vortices is directly related to the Amplitude-to-Wavelength ratio, where increasing this ratio would result in a greater local sweep of the leading edge and an increase in the vortices' strengths. To the authors' knowledge there have been no investigations into the effect of wing sweep on the relative strengths of the pairs of streamwise, counter-rotating vortices.

The main effects of tubercles are a softening and delaying of stall [2,7–9], however, they can also provide significant reductions in drag, as well as increases in the lift-to-drag ratio, for a swept wing at pre-stall angles of attack [10,11]. The aim of the present study is to further investigate the effects of tubercles on swept wing drag, and to determine how tubercles are able to reduce drag.

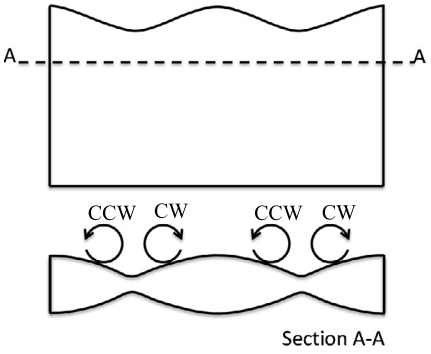

Fig. 1. Diagram of a wing with leading edge tubercles and the approximate location and sign of the vortices produced. CCW refers to a counter-clockwise rotation and CW refers to a clockwise rotation.

To investigate the counter-rotating, streamwise vortex pairs produced by the tubercles, a wake survey has been conducted on the same two wings used in Bolzon et al. [10]. From this wake survey the vorticity distributions and the profile and induced drag coefficients of these wings have been calculated and compared.

2. Methodology

2.1. Wing configurations

Two NACA 0021 wings, swept at a quarter-chord angle of 35°, were CNC machined from aluminium. One wing had a smooth leading edge, whereas the other wing had tubercles with an amplitude of 10.5 mm and a wavelength of 60 mm along its entire leading edge. The tubercles were machined to preserve a constant

* Corresponding author.
E-mail address: michael.bolzon@adelaide.edu.au (M.D.P. Bolzon).

http://dx.doi.org/10.1016/j.ast.2016.06.025
1270-9638/

Nomenclature

$\bar{b}$	Normalized span	U_∞	Upstream velocity in x-direction ..... m/s
C_{D_I}	Induced drag coefficient	u	Downstream velocity in x-direction ..... m/s
C_{D_P}	Profile drag coefficient	v	Downstream velocity in y-direction ..... m/s
$C_{D_{Total}}$	Total drag coefficient	w	Downstream velocity in z-direction ..... m/s
D_I	Induced drag ..... N	Γ_{vel}	Circulation calculated from velocity distribution. m^2/s
D_P	Profile drag ..... N	Γ_{vor}	Circulation calculated from vorticity distribution m^2/s
P_{D_∞}	Upstream dynamic pressure ..... Pa	ρ	Downstream density of air ..... kg/m^3
P_{S_∞}	Upstream static pressure ..... Pa	ρ_∞	Upstream density of air ..... kg/m^3
P_T	Downstream total pressure ..... Pa	σ	Cross-flow source 1/s
P_{T_∞}	Upstream total pressure ..... Pa	ω	Vorticity ..... s^{-1}
S	Downstream surface perpendicular to wake, also referred to as "wake plane"		

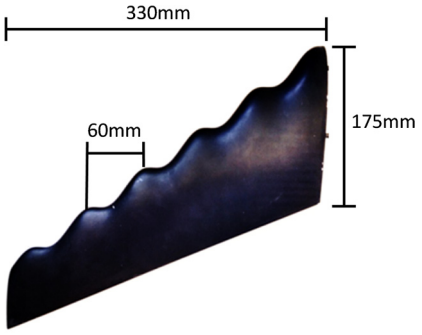

Fig. 2. Tubercled wing shown. Tubercles have an amplitude of 10.5 mm and a wavelength of 60 mm. Both wings are the same except for the addition of tubercles.

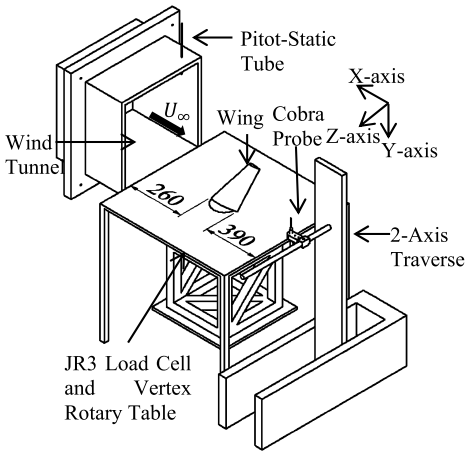

Fig. 3. Wake survey experimental setup in open-return wind tunnel. Cobra probe located at 390 mm downstream of the wing trailing edge.

thickness-to-chord ratio along the wing span, which resulted in a chordwise ridge to form over each tubercle peak and a valley to form in each tubercle trough. These ridges and valleys washed-out towards the trailing-edge. The tubercled wing can be seen in Fig. 2. The amplitude has not been dimensioned as the sweep visually affects the amplitude dimension. Apart from the tubercles, the wings were exactly the same and had the same reference area. The wings had a span of 330 mm, a Mean Aerodynamic Chord, MAC, of 130 mm, and a taper ratio of 0.4. A non-unity taper ratio was chosen as swept wings are typically tapered in an effort to reduce lift production at the wingtip and hence induced drag.

2.2. Wake survey

Wake surveys were conducted in the open-jet "KC wind tunnel" at The University of Adelaide. The wind tunnel had a turbulence intensity of $0.6 \sim 0.8\%$ and was operated at a freestream velocity of 27.5 m/s, which resulted in a MAC Reynolds number of 225,000. The experimental setup can be seen in Fig. 3.

The wings were mounted on a JR3 45E15A-163 load cell such that the lift at 0° corresponded solely to the z-axis direction of the load cell, and the drag to the x-axis. The wings were then deemed aligned to 0° when the z-axis load was zero. The misalignment error resulting from the CNC machined wings and the rotary table was estimated to be $\pm 0.05°$. The following five angles of attack were surveyed: 0°, 3°, 6°, 9° and 12°. Three runs were conducted for each wing and the averages were then calculated.

A multi-hole pressure probe was located 3 MACs downstream of the wing root trailing edge on a two-directional traverse. This traverse moved the probe to a predefined grid located in the y–z plane, as shown in Fig. 3, known as a wake plane. The size of this wake plane was dependent on the wing's angle of attack, whereby a higher angle of attack typically resulted in a greater wake size. A greater wake plane size resulted in a longer experimental time, which was not only more impractical, but also resulted in the instruments drifting further from their calibrations, thereby reducing the accuracy of the experiment. To reduce the experimental time the area surveyed was different for each angle of attack, but was kept constant between the two wings. The area surveyed was divided into nodes with a distance of 6 mm between each node. This spacing was chosen as a compromise between experimental time and accuracy.

An off-the-shelf Turbulent Flow Instrumentation brand multi-hole pressure probe, known as a Cobra Probe, was used for these experiments. The Cobra probe had a head size of 3 mm × 3 mm and a sampling frequency of 600 Hz [12]. This particular multi-hole probe measured 4 pressures from which the three orthogonal downstream velocities, u, v, and w were calculated from factory calibration curves [12], as found in Shepherd [13]. The measured mean velocity fields were then used to determine the vorticity in the y–z plane, as shown by Eq. (1). Note that a body-fixed reference frame was used. Any errors in the vorticity calculations arising from the flow quality were accounted for by subtracting the cross-flow velocities of the wake plane without a wing present from the cross-flow velocities with the wings present. A vortex's circulation can be calculated using either Eqs. (2) and (3), however, the circulation calculated from Eq. (2) is typically more accurate than the circulation calculated from Eq. (3) [13]. Therefore, Eq. (2) was used for the remainder of this study to calculate the circulation of any vortex. The region of integration, ROI, was determined in the same manner as in Hassan et al. [14], whereby the maximum vorticity in a given region was found, then each neighbouring point was included in the ROI if its vorticity was within a given threshold and the distance between this point and the point of

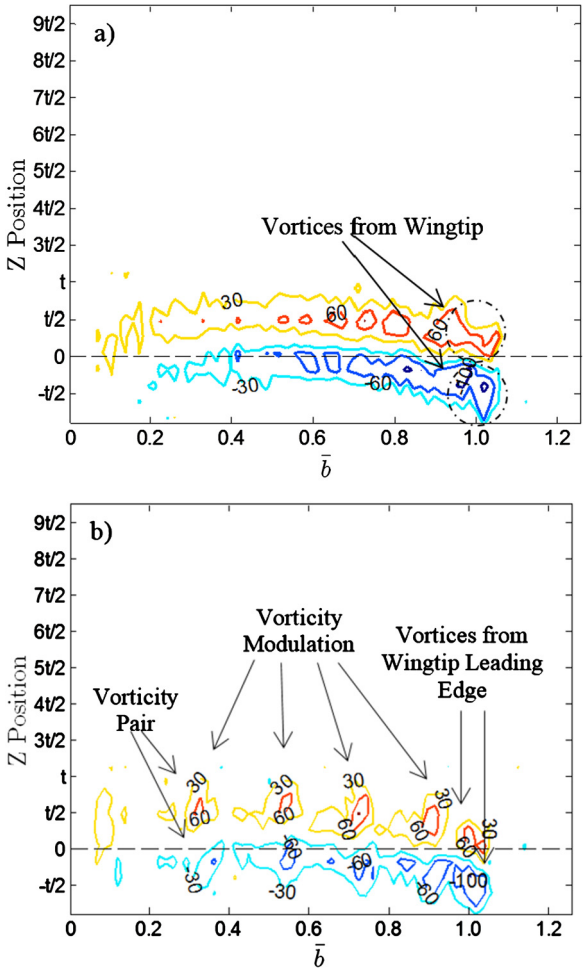

Fig. 4. Vorticity, 1/s, contour of a) smooth, and b) tubercled wings at 0°.

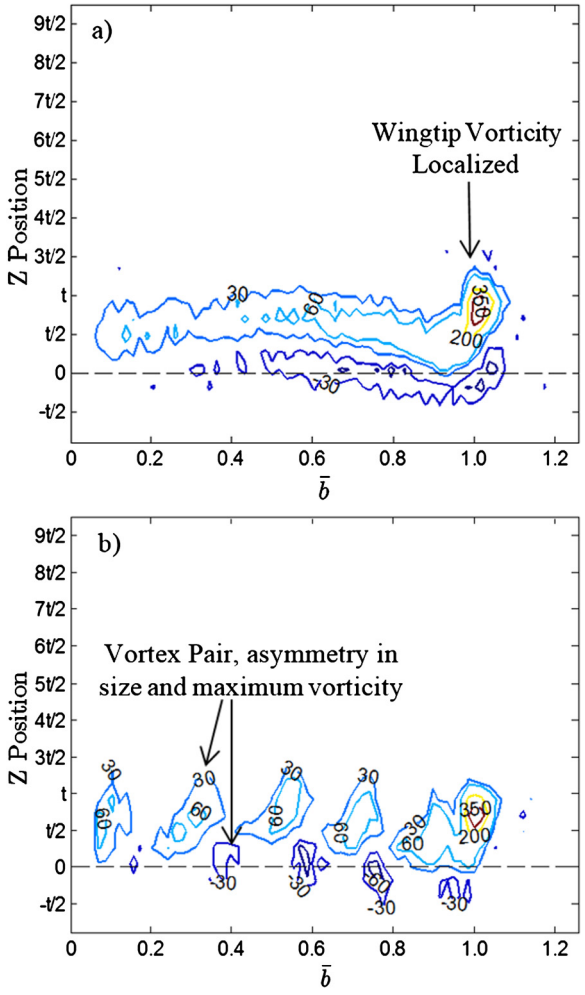

Fig. 5. Vorticity, 1/s, contour of a) smooth, and b) tubercled wings at 3°.

maximum vorticity was within a predefined limit. For all circulations calculated, the vorticity thresholds were −30 1/s and 30 1/s for negative and positive vortices, respectively, which from 3° to 12° typically resulted in the demarcation of the tubercle vortices from each other, and from the vortex sheet. When these thresholds did not differentiate a tubercle vortex, a tubercle vortex was defined as from its vortex core to the point of minimum vorticity between this vortex and any other vortex. The vorticity thresholds were sufficient to define the tubercled wing's tip vortex from the vortex sheet. To define the wingtip vortex from neighbouring tubercle vortices, the edge of the wingtip vortex was taken as the point of minimum vorticity between the wingtip vortex and any other vortex. The smooth wing's wingtip vortex was defined from the vortex sheet by implementing the same distance from the wingtip vortex core to the outer edges determined for the tubercled wing's tip vortex. Forward-difference, central-difference, and fourth-order polynomial schemes were considered for the vorticity, and it was found that the forward-difference scheme consistently gave the most accurate induced drags while the fourth-order polynomial consistently gave the least accurate induced drags. Therefore, the forward-difference scheme was used for the calculation of both the vorticity and the source terms.

The induced and profile drags were calculated from wake survey measurements from Eqs. (4) to (10) [15]. Equations (6) and (7) were solved via the Gauss–Siedel iterative method. The equations were deemed solved once the root-mean-square of the difference between sequential iterations was less than 10^{-7}, which resulted in the induced drags of both wings at all tested angles of attack to converge. The Dirichlet boundary condition of ψ is 0 and the Neumann boundary condition of $\partial\phi/\partial n$ is 0 at the shear layer were used [15]. Typically this method is used for closed-return wind tunnels [15,16]. However, this method can be used in an open-jet wind tunnel if the flow only enters through one plane upstream and leaves through the downstream plane that encompasses the wake plane, as this will approximate a closed-return wind tunnel configuration.

$$\omega = \left(\frac{\partial w}{\partial y} - \frac{\partial v}{\partial z}\right) \tag{1}$$

$$\Gamma_{vel} = \oint_c (v dy + w dz) \tag{2}$$

$$\Gamma_{vor} = \iint_s \omega . ds \tag{3}$$

Any errors in the drag calculations that were associated with the flow quality were accounted for by subtracting the induced, profile, and total drag coefficients of the wake plane without either wing present from the induced, profile, and total drag coefficients, respectively, of each wing [14]. The induced, profile, and total drag coefficients of the tubercled wing have been corrected from 0° to 9° to produce coefficients if the tubercled wing were to produce the same lift coefficient as the smooth wing. The 12° angle of attack was not corrected as the extrapolation of data in this region is not accurate due to unknown flow separation. The

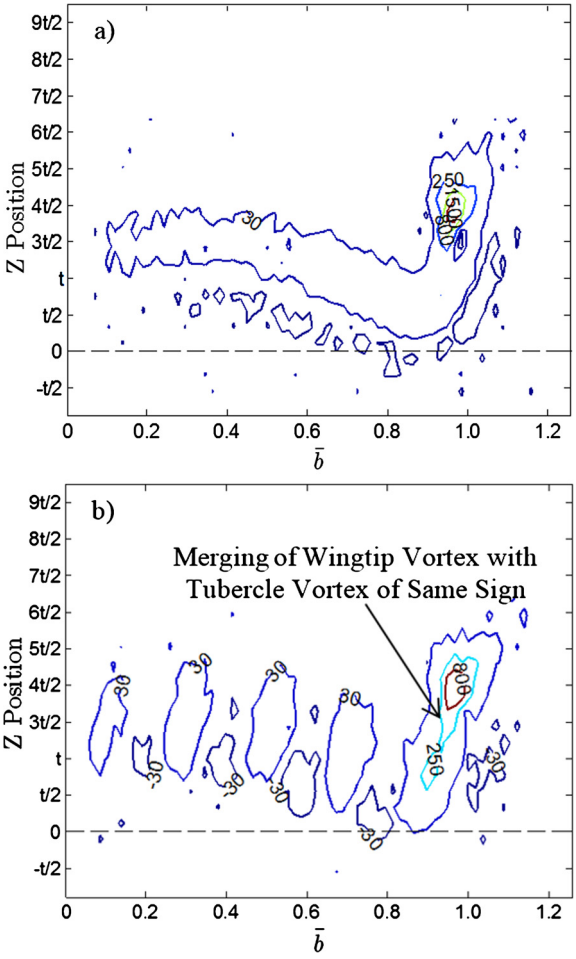

Fig. 6. Vorticity, 1/s, contour of a) smooth, and b) tubercled wings at 9°.

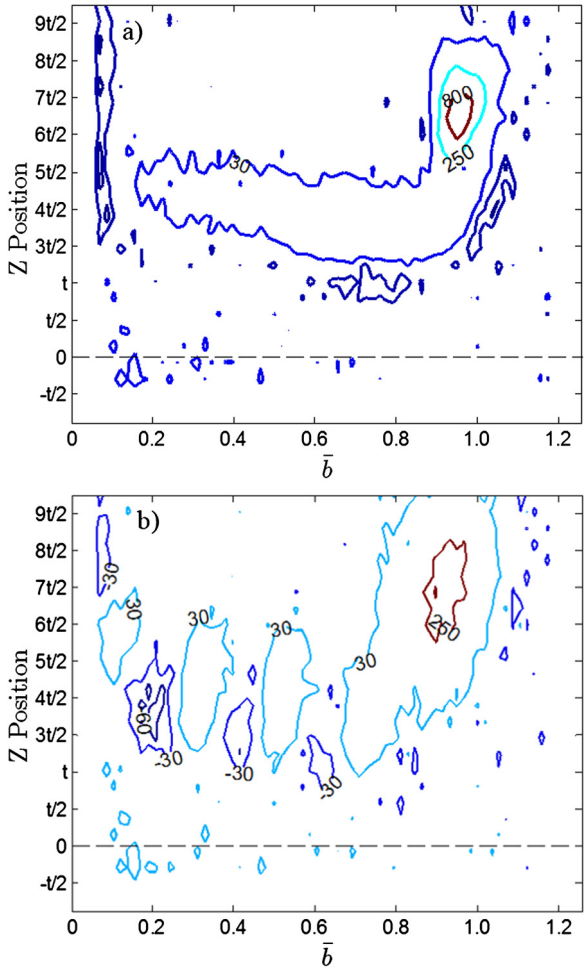

Fig. 7. Vorticity, 1/s, contour of a) smooth, and b) tubercled wings at 12°.

corrections were spline interpolations. Both the uncorrected and corrected values are presented in 3.2. In addition, the same method of correction has been applied to the wingtip vortex strength of the tubercled wing from 3° to 9°, and both the uncorrected and corrected values are presented in 3.1.

As the objects tested were streamline bodies, and there were no obvious defects, only in a high lift configuration would the wing sufficiently redirect flow such that flow would exit the control volume laterally. Preliminary experiments demonstrated that the wake of the wings from 0° to 9° stayed well within the survey area, and evidence can be seen from the vorticity distributions in Figs. 4 to 7. Therefore, for angles of attack within this range, the wake was sufficiently traversed. At an angle of attack of 12° most of the wake was still traversed, however, there were some small sections that were not, as can be seen on the outskirts of the vorticity distribution in Fig. 8. These regions were intentionally excluded from the traversed area to reduce the experimental time and potentially increase the accuracy of the experiments because the instruments would better approximate their initial calibrations. This did not result in an appreciable error in the induced drag calculation.

The variables that are measured for use in Eqs. (4) to (10) are $P_{T\infty}$, P_T, ρ_∞, ρ, u, v, w, and U_∞. The $P_{T\infty}$ was measured by an MKS brand Baratron that was connected to the Pitot port of an upstream Pitot-static probe. A Scanivalve brand DSA3217 pressure scanner was connected to the static port. The P_T was measured by the Cobra probe. The flow was considered incompressible, therefore, the ρ_∞ was assumed to be the same as the ρ. Both of the densities were calculated through the temperature, barometric pressure, and relative humidity. The temperature was measured from a TSI brand IFA300 constant temperature anemometer module, the barometric pressure was measured from a Bosh brand BMP085 module, and the humidity was measured from a DHT22 module. The BMP085 and DHT22 modules were connected to an Arduino Uno R3, which was connected serially to the data acquisition system. The u, v, and w velocities were measured by the Cobra probe. The U_∞ was calculated from the $P_{D\infty}$, which was calculated from the difference between the measurements of the Pitot and static ports of the Pitot-static probe, and the density.

$$D_I \approx \frac{1}{2}\rho_\infty \iint_S (\psi\omega - \phi\sigma)dydz \tag{4}$$

where

$$\sigma = \frac{\partial v}{\partial y} + \frac{\partial w}{\partial z} \tag{5}$$

and

$$\frac{\partial^2\psi}{\partial y^2} + \frac{\partial^2\psi}{\partial z^2} = -\omega \tag{6}$$

and

$$\frac{\partial^2\phi}{\partial y^2} + \frac{\partial^2\phi}{\partial z^2} = \sigma \tag{7}$$

$$D_P = \iint_S \left[P_{T\infty} - P_T + \frac{\rho}{2}(U^* - u)(U^* + u - 2U_\infty)\right]dydz \tag{8}$$

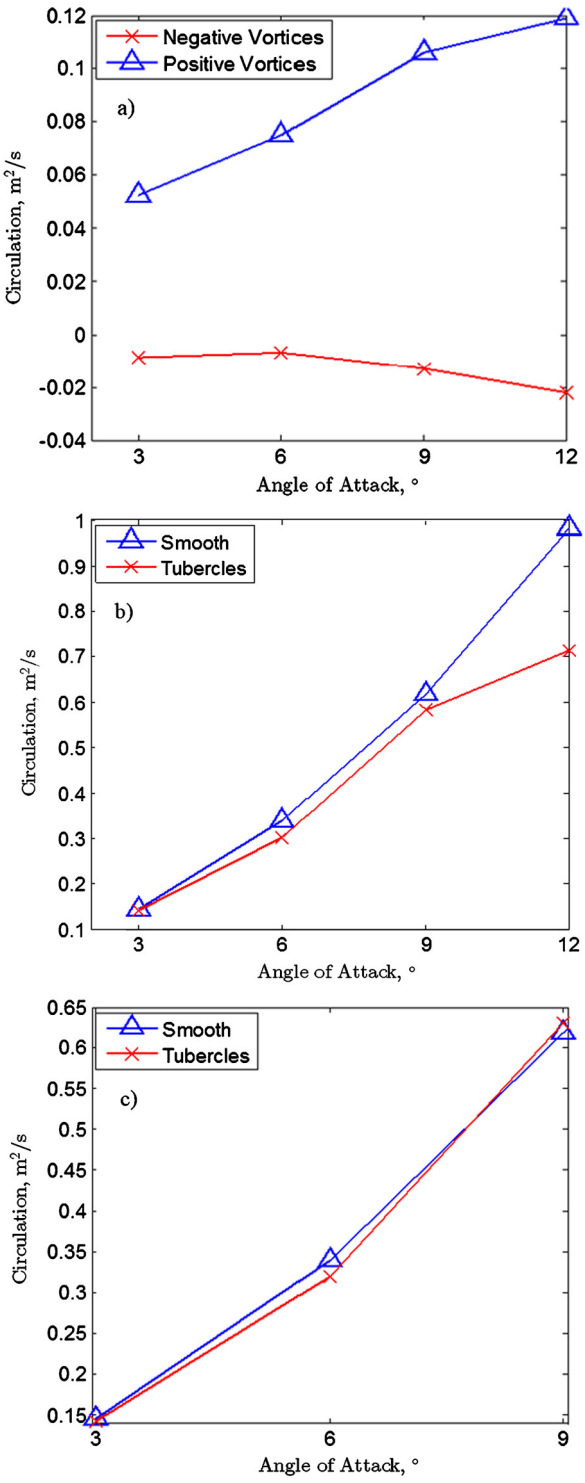

Fig. 8. Average circulation of negatively and positively signed vortices of the tubercled wing, a). Wingtip vortex strength of smooth and tubercled wings, b), at 3°, 6°, 9°, and 12°. Corrected wingtip vortex strength of smooth and tubercled wings, c), at 3°, 6°, and 9°.

where

$$U^* = \sqrt{u^2 + \left(\frac{2}{\rho}\right)(P_{T\infty} - P_T)} \tag{9}$$

and

$$u' = U^* - U_\infty \tag{10}$$

Table 1
The 95% confidence intervals of the measurements taken during the wake surveys, and the percentage uncertainty of the typical values measured.

Instrument	Variable measured	95% confidence interval (of typical value)
Baratron	P_{T_∞}, P_{D_∞}	±0.5 Pa (±0.1% of P_{D_∞})
Scanivalve	P_{S_∞}, P_{D_∞}	±3.0 Pa (±0.6% of P_{D_∞})
Cobra probe	u	±0.45 m/s (±1.75%)
	v	±0.31 m/s (±17%)
	w	±0.31 m/s (±29%)
IFA300	Temperature	±0.1 °C (±0.03%)
BMP085	Barometric pressure	±5 Pa (negligible)
DHT22	Relative humidity	±2%

2.3. Uncertainty analysis

The uncertainties in the drag, induced, and profile drag coefficients were calculated via the "Jitter Method" [17–19]. A 95% confidence interval was used for all measurements, and the uncertainties of the instruments for the typical measuring ranges during these experiments are presented in Table 1. Only the Scanivalve and the BMP085 module significantly drifted; 0.12 Pa/hr and 0.01 Pa/hr, respectively. Due to the method used to calculate the induced drag, and subsequently the induced drag coefficient, the uncertainty arising from linear effects of v and w velocities on the induced drag was used.

3. Results

3.1. Vorticity and circulation

Vorticity contours for both wings at 0°, 3°, 9°, and 12° are given in Figs. 4 to 9, 6° is omitted as no new trends appeared. While the wings were mounted vertically, as shown in Fig. 3, it should be noted that the contour maps have been rotated such that the wing span corresponds to the x-axis of each figure and the y-axis corresponds to the direction perpendicular to the wing surface. The x-axes of the contour maps have been normalized to the half-wingspan such that 0 corresponds to the wing root and 1 to the wingtip. The y-axes have been normalized to the MAC thickness of the wing. The origins of the y-axes correspond to the projection of the wing chord-line at a given angle of attack. Dashed lines have been included, spanning the entire window along the y-axes coordinates of 0. Positive vorticity is counter-clockwise rotation. For all angles of attack there are uniform regions of vorticity extending over most of the wingspan, however, tubercles modulate the vorticity into regions of high and lower vorticity, as shown in Fig. 4a) and b). These regions of vorticity are produced by the tubercles [3,4]. The wings were well aligned, as shown by the similarity in the vorticity in the wingtip regions in Fig. 4a) and b). At non-zero angles of attack, the sizes of the vorticity regions produced by a pair of streamwise, counter-rotating vortices are asymmetrical with one vorticity region consistently being larger and having a greater absolute maximum vorticity, as labelled in Fig. 5b). The average circulations of the negatively signed and positively signed vortices for the tubercled wing at 3°, 6°, 9°, and 12° are given in Fig. 8a); for all angles of attack considered, the positively signed vortices are on average 6 times stronger than the negatively signed vortices. Therefore, by sweeping the tubercled wing one vortex in each pair becomes stronger than the other instead of being equal in strength, as is the case for an unswept wing [20]. Increasing the sweep of a wing should logically result in an increased disparity between the strength of the tubercle vortices. Lin [21] suggested that generally, counter-rotating vortices are more effective at controlling two-dimensional flow separation, whereas co-rotating vortices are more effective for three-dimensional flow

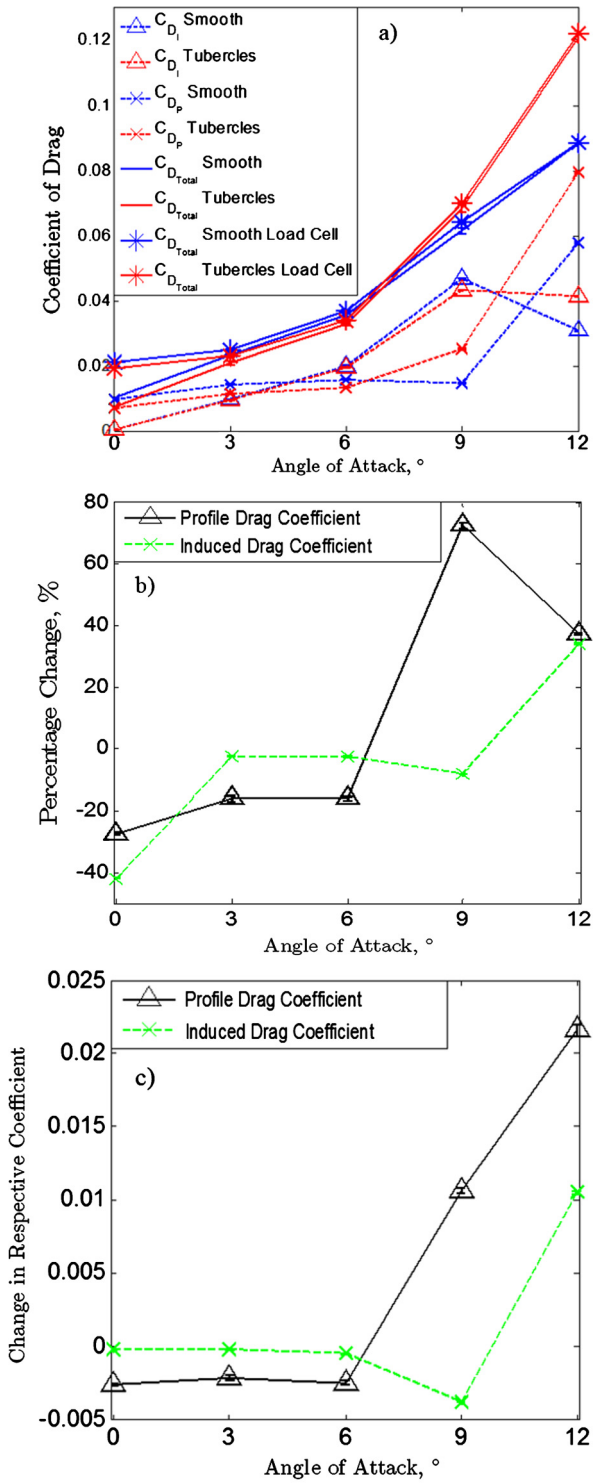

Fig. 9. Total drag and its components breakdown, a), the relative effect of tubercles on the profile and induced drag, b), the absolute effect of tubercles on the profile and induced drag, c). Note: for b) and c), negative means a reduction.

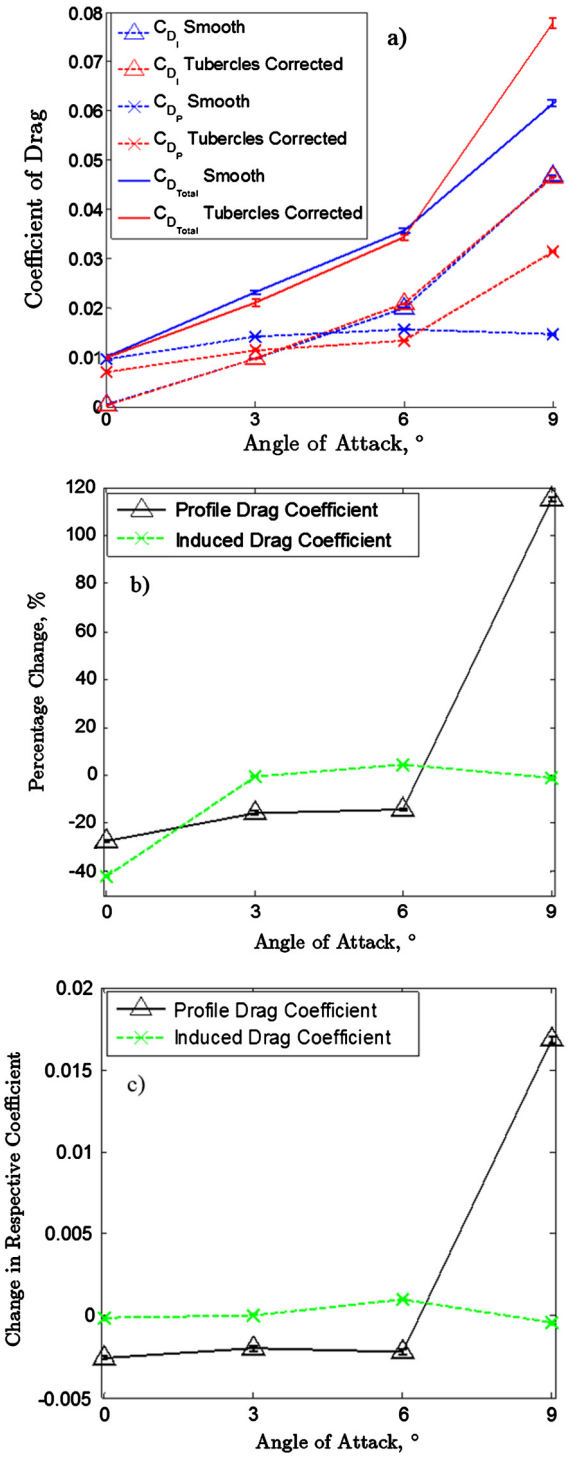

Fig. 10. Corrected total drag and its components breakdown, a), the relative effect of tubercles on the corrected profile and induced drag, b), the absolute effect of tubercles on the corrected profile and induced drag, c). Note: for b) and c), negative means a reduction.

separation, such as on a swept wing. Therefore, as tubercles act like vortex generators [3] this disparity in the vortices' strengths may be beneficial in keeping the flow attached over the swept wing.

As the angle of attack increases the strength of the vortices produced by the tubercles increases, which would result in a greater boundary layer momentum exchange [7], and thereby result in the flow staying attached to a higher angle of attack.

At 3°, 6°, and 9° the vorticity in the wingtip region, ostensibly due to the wingtip vortex is localized to a small area for both the smooth and tubercled wings, as labelled in Fig. 4a) as an example. However, at 12° the wingtip vorticity of the tubercled wing suddenly expands and occupies a much larger region than at the lower angles of attack, which suggests that the flow over the wingtip is largely separating. The uncorrected circulations of the wingtip vortices of both wings at 3°, 6°, 9°, and 12° are given in Fig. 8b); there is little difference in the wingtip strength of either

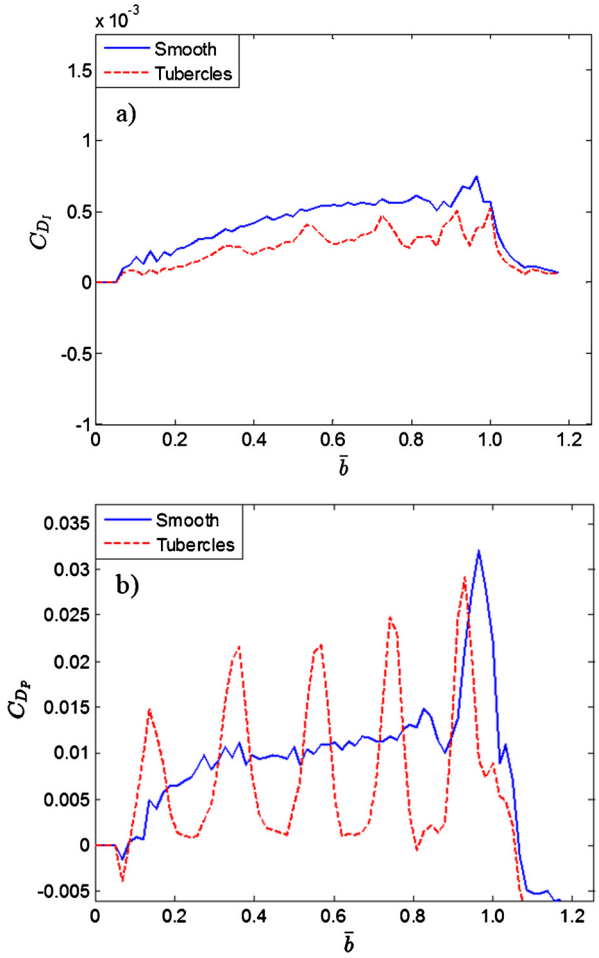

Fig. 11. Spanwise induced, a), and profile, b), drag coefficient distributions for smooth and tubercled wings at 0°.

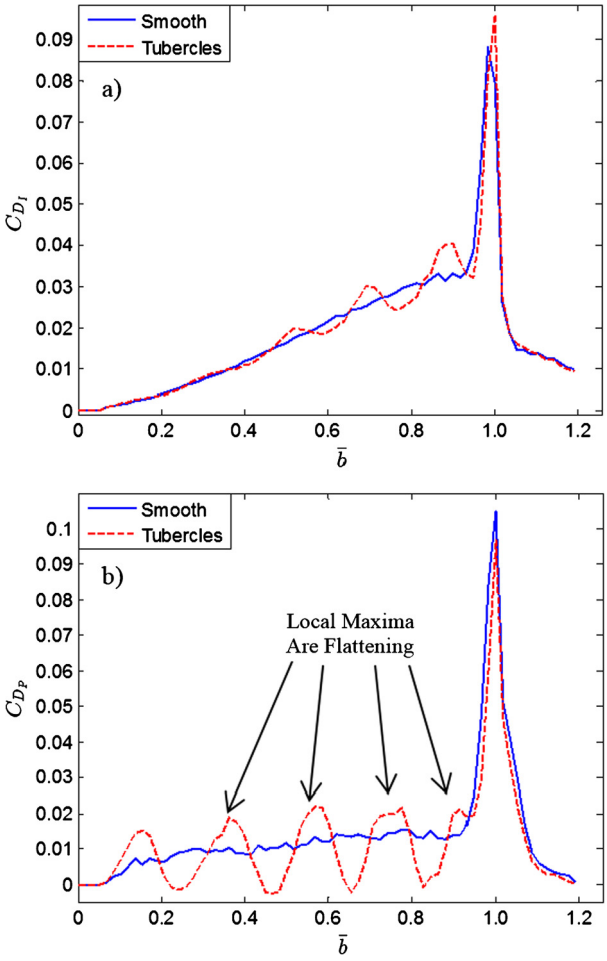

Fig. 12. Spanwise induced, a), and profile, b), drag coefficient distributions for smooth and tubercled wings at 6°.

wing at 3°, however, from 6° to 9° the smooth wingtip vortex is stronger than the tubercled wingtip vortex by approximately 8.5%. At 12°, tubercles reduce the wingtip vortex strength by 27.2%. The reduced wingtip vortex strength may be beneficial for some applications as it may lead to a shorter breakdown length-scale. Fig. 8c) shows that if the tubercled wing were to produce the same lift coefficient as the smooth wing, tubercles would have little effect on the wingtip vortex strength from 3° to 9°.

As expected, for non-zero degree angles of attack the tubercled wing's wingtip vortex tends to merge with tubercle vortices of the same sign, as labelled on Fig. 6b).

3.2. Drag breakdown

The total drag coefficients for both wings at all angles of attack considered have been calculated and compared to the force measurements of these exact wings found in Bolzon et al. [9,10]. Note that a full comparison can be found in [9]. Fig. 9a) shows that there is good agreement between the wake survey total drag coefficients and the load cell total drag coefficients for 3° to 12°. Furthermore, the relative effects of tubercles on the total drag coefficients for these angles of attack are within 2%. There is a significant difference between the wake survey and the load cell total drag coefficients for both wings at 0°, which is due to a severe underestimation of the profile drag coefficients. The reason for this underestimation is unknown. As expected, the induced drag coefficients of both the smooth and tubercled wings at 0° are negligible.

From Fig. 9a) and b) tubercles reduce the profile drag coefficient by approximately 20% from 0° to 6° while increasing it by approximately 50% at 9° and 12°. The reason for the sudden increases at 9° and 12° will be elucidated from the spanwise drag coefficient distributions presented in 3.3. From 0° to 6° tubercles do not significantly affect the induced drag coefficient as shown by Figs. 9b) and c). At 9° tubercles reduce the induced drag coefficient by 8% before increasing it by 34% at 12°. Fig. 10 shows the corrected induced, profile, and total drag coefficients of the tubercled wing compared to the smooth wing. The drag coefficients presented in this figure are for when both wings produce the same lift coefficients. As found in the uncorrected case, from 0° to 6°, tubercles reduce the profile drag coefficient by approximately 20%. At 9°, tubercles also increase the profile drag coefficient, however, by a significantly greater amount, 115%, which the authors attribute to greater flow separation over the tubercled wing than the smooth wing. Fig. 10 indicates that if the tubercled wing produces the same lift coefficient as the smooth wing from 0° to 9°, tubercles would have negligible effects on the induced drag coefficient. From 0° to 6°, when the tubercled wing produces the same lift coefficient as the smooth wing, tubercles would still reduce the total drag coefficient. In addition, at 9°, tubercles would still increase the total drag coefficient.

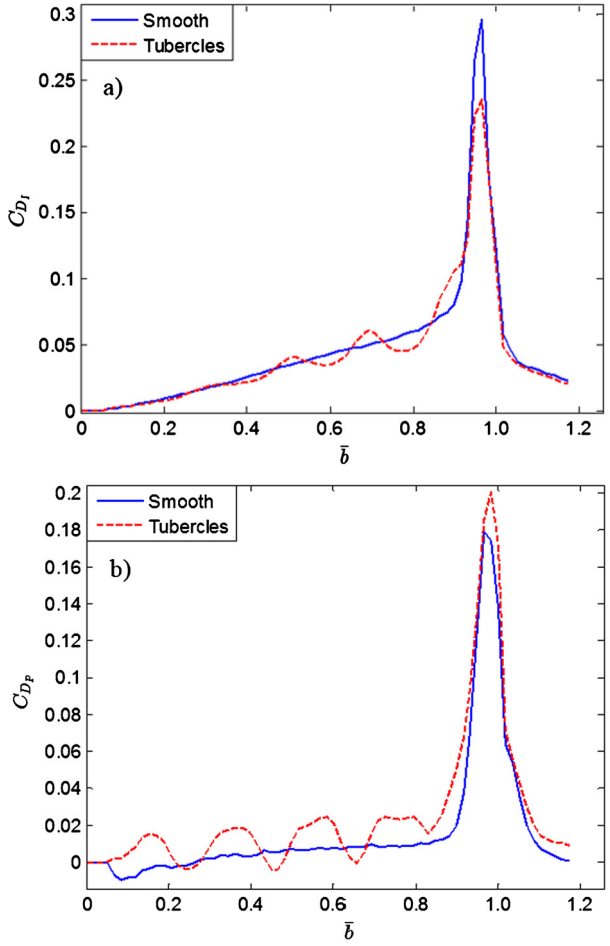

Fig. 13. Spanwise induced, a), and profile, b), drag coefficient distributions for smooth and tubercled wings at 9°.

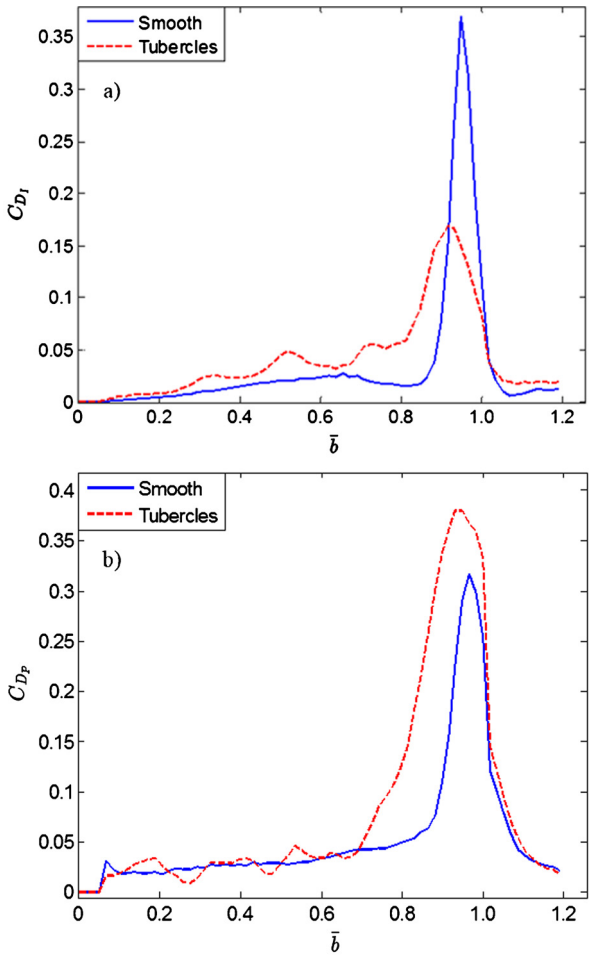

Fig. 14. Spanwise induced, a), and profile, b), drag coefficient distributions for smooth and tubercled wings at 12°.

3.3. Spanwise drag coefficient distributions

The first integrands of Eqs. (4) and (8) have been integrated in the wing thickness direction to produce spanwise drag coefficient distributions, which are given in Figs. 11 to 14.

Note that the spanwise drags were non-dimensionalised to the local chord. There was an average spanwise velocity of approximately 0.4 m/s for all wings towards the wingtip, as given by the Cobra probe readings. Therefore, while the wings have a span of 330 mm, the "virtual" wingtip was taken as the position of the peak in the profile drags, which resulted in 348 mm. The local chords were then computed by a simple translation of 348/330 down the wingspan. The spanwise drag coefficient distributions of the wings at 3° have not been included as no new trends appeared. At 0° the induced drag coefficient is negligible, therefore, the spanwise induced drag coefficient distributions are approximately 0. For all non-zero degree angles of attack tubercles modulate the spanwise induced drag coefficient into local minima and maxima.

They become more pronounced towards the wingtip. Similarly, for all angles of attack, tubercles modulate the spanwise profile drag coefficient, however, the modulation is relatively constant along the span. The locations of these local minima and maxima have been determined by tracing through the vorticity distribution in Fig. 15. The local maxima and minima in the spanwise profile drag coefficient tend to occur in regions of common Upwash and downwash, respectively, which correspond to the troughs and peaks, respectively. Conversely, the local maxima and minima of the spanwise induced drag coefficient tend to occur in the regions of common downwash and upwash, respectively. At 0° there is a reduction in the profile drag coefficient in the wingtip region, however at 3° and 6° there is little difference in the profile drag coefficient distributions between the wings in the wingtip region, therefore, the reductions in the profile drag coefficient in Fig. 9 must largely result from reductions over the wingspan.

At 9°, while the vorticity contour plots in Fig. 6 do not indicate obvious flow separation in the wingtip region of the tubercled wing, the sudden increase in the tubercled wing's spanwise profile drag coefficient compared to the smooth wing indicates flow separation in this region. Furthermore, in the wingtip region, the tubercled wing increases the profile drag coefficient, but reduces the induced drag coefficient, therefore, flow separation is likely occurring in this region. This flow separation explains the sudden increase in the profile drag coefficient at 9° as presented in Fig. 9. At 12° the tubercled wing has largely stalled in the wingtip region as the profile drag coefficient has greatly increased and the induced drag coefficient has greatly reduced in Fig. 14. The earlier flow separation on a tubercled wing has also been noted in other works such as Johari et al. [22] and Murray et al. [23]. Interestingly, at 0° and 3° the local maxima in the profile drag coefficient distributions are sharp, however, from 6° onwards, these local maxima become flatter, as labelled on Fig. 12b), suggesting that flow is separating in the troughs.

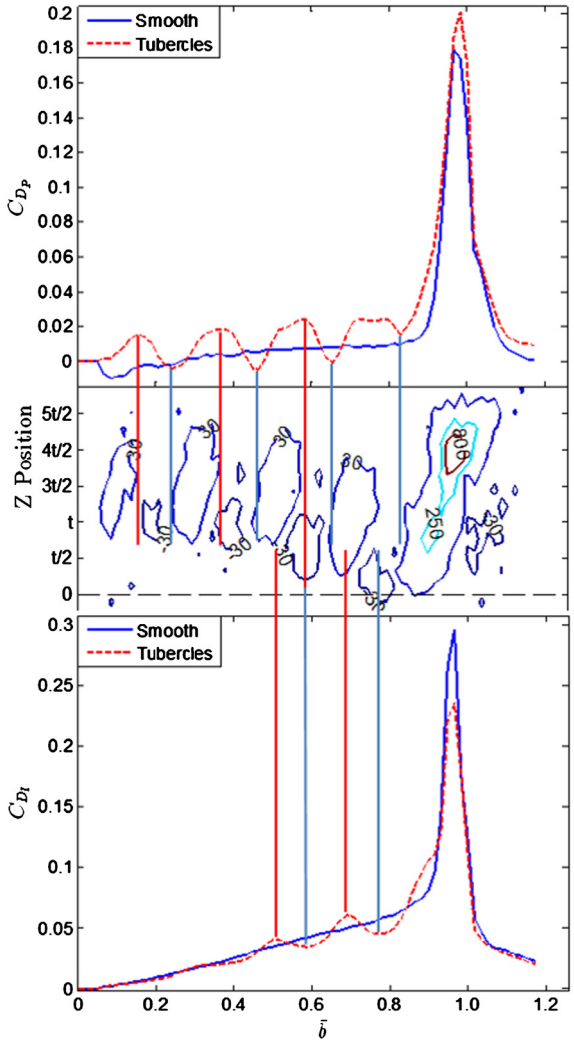

Fig. 15. Locating the local minima and maxima in the induced and profile spanwise drag distributions with the vorticity contour plot; 9°.

3.4. Location of drag changes

Fig. 16 shows the relative change in the profile, induced, and total drag coefficients over the wingspan, from 0 to 1, and the wingtip, from 1 onwards. For all angles of attack, the majority of the change in the profile drag coefficient occurs over the wingspan, with the wingtip region only accounting for approximately 20% of the change. For 0°, 6°, 9°, and 12° the vast majority of the change in the induced drag occurs over the wingspan, with minimal change occurring in the wingtip region. However, at 3° the converse is true. For all angles of attack, the majority of the change in the total drag coefficient arises from over the wingspan. These trends suggest that to achieve the greatest change in the drag and its components, and hence the greatest potential reductions, tubercles should be implemented along the entire leading edge.

4. Conclusion

Wake surveys were conducted at 0°, 3°, 6°, 9°, and 12° on two swept wings, one with a smooth leading edge and one with a tubercled leading edge. Sweeping a tubercled wing resulted in an asymmetry in the strengths of the vortices produced by a single tubercle. Additionally, the strengths of the tubercle vortices increased with angle of attack. Below 3° there was little difference between the strength of the wingtip vortices of either wing, while

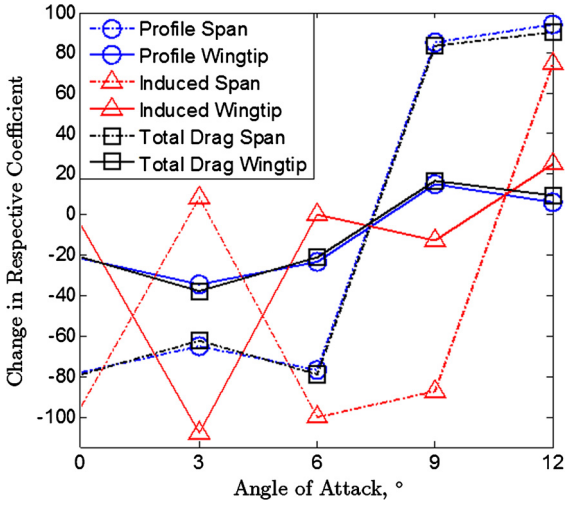

Fig. 16. Relative changes in the profile, induced, and total drag coefficients over span and wingtip. Note: negative percentage means reduction.

above 6° the smooth wing produced a stronger wingtip vortex. For angles of attack 6° and below the tubercled wing reduced the profile drag coefficient, but had little effect on the induced drag coefficient. From 9° onwards the tubercled wing increased the profile drag coefficient and reduced the induced drag coefficient, ostensibly because of flow separation near the wingtip region. Corrected drag coefficients of the tubercled wing when producing the same lift coefficient as the smooth wing were calculated at 0°, 3°, 6°, and 9°. The same trends were found as in the uncorrected case, except at 9° where tubercles did not significantly affect the induced drag coefficient.

The smooth wing produced relatively uniform profile and induced drag coefficient distributions along its entire span with peaks at the wingtip. Conversely, tubercles modulated the profile and induced drag coefficients along the entire span, with local maxima and minima in the profile drag coefficients forming in the troughs and over the peaks, respectively. Typically, tubercles produced local maxima and minima in the induced drag coefficients over the peaks and in the troughs, respectively. The majority of change in either the profile or induced drag coefficients occurred over the wingspan, but small changes were also observed in the wingtip region.

Conflict of interest statement

There is no conflict of interest.

Acknowledgements

Funding: This work was supported by The Sir Ross and Sir Keith Smith Fund (Smith Fund) (www.smithfund.org.au). The authors thank Eyad Hassan and Peter Lanspeary at The University of Adelaide for their assistance in calculating the vortices' circulations.

References

[1] C.M. Jurasz, V.P. Jurasz, Feeding modes of the Humpback Whale, Megaptera Novaeangliae, in Southeast Alaska, Sci. Rep. Whales Res. Inst. 31 (1979) 69–83.
[2] F.E. Fish, P.W. Weber, M.M. Murray, L.E. Howle, The tubercles on Humpback Whales' Flippers: application of bio-inspired technology, Integr. Comp. Biol. 51 (1) (2011) 203–213.
[3] H.T. Pedro, M.H. Kobayashi, Numerical study of stall delay on Humpback Whale Flippers, in: AIAA Aerospace Sciences Meeting and Exhibit, Reno, 2008.
[4] M.J. Stanway, Hydrodynamic effects of leading-edge tubercles on control surfaces and in flapping foil propulsion, M.S. Thesis, Massachusetts Institute of

Technology, MA, February 2008.
[5] T. Swanson, K.M. Isaac, Biologically inspired wing leading edge for enhanced wind turbine and aircraft performance, in: AIAA Theoretical Fluid Mechanics Conference, Honolulu, 2011.
[6] K.L. Hansen, R.M. Kelso, B.B. Dally, Performance variations of leading-edge tubercles for distinct airfoil profiles, AIAA J. 49 (1) (2011) 185–194, http://dx.doi.org/10.2514/1.J050631.
[7] B. Stein, M.M. Murray, Stall mechanism analysis of Humpback Whale Flipper models, in: Unmanned Untethered Submersible Technology (UUST), Autonomous Undersea Systems Inst., Lee, NH, 2005.
[8] M.D. Bolzon, R.M. Kelso, M. Arjomandi, Tubercles and their applications, J. Aerosp. Eng. 29 (1) (2016), http://dx.doi.org/10.1061/(ASCE)AS.1943-552511.0000491.
[9] D.S. Miklosovic, M.M. Murray, L.E. Howle, F.E. Fish, Leading-edge tubercles delay stall on Humpback Whale (Megaptera Novaeangliae) flippers, Phys. Fluids 16 (5) (2004) L39–L42, http://dx.doi.org/10.1063/1.1688341.
[10] M.D. Bolzon, R.M. Kelso, M.A. Arjomandi, Force measurements and wake surveys of a swept tubercled wing, J. Aerosp. Eng. (2016), accepted for publication, http://dx.doi.org/10.1061/(ASCE)AS.1943-5525.0000683.
[11] M.D. Bolzon, R.M. Kelso, M. Arjomandi, The effects of tubercles on swept wing performance at low angles of attack, in: Australasian Fluid Mechanics Conference, RMIT, Melbourne, 2014.
[12] TFI, Getting Started Series 100 Cobra Probe, Turbulent Flow Instrumentation Pty. Ltd., 2011.
[13] I.C. Shepherd, A four hole pressure probe for fluid flow measurements in three dimensions, J. Fluids Eng. 103 (1981) 590–594.
[14] E.R. Hassan, T.C. Lau, R.M. Kelso, Accuracy of circulation estimation schemes applied to discretised velocity field data, in: Australasian Fluid Mechanics Conference, Gold Coast, 2007.
[15] G.W. Brune, Quantitative low-speed wake surveys, J. Aircr. 31 (2) (1994) 249–255, http://dx.doi.org/10.2514/3.46481.
[16] K. Kusunose, J.P. Crowder, Extension of wake-survey analysis method to cover compressible flows, J. Aircr. 39 (6) (2002) 954–963, http://dx.doi.org/10.2514/2.3048.
[17] R.J. Moffat, Contributions to the theory of single-sample uncertainty analysis, J. Fluids Eng. 104 (June 1982) 250–258.
[18] J.P. Holman, Experimental Methods for Engineers, 6th ed., McGraw–Hill, New York, 1994, pp. 48–51.
[19] R.H. Dieck, Measurement Uncertainty: Methods and Applications, The Instrument Society of America, North Carolina, 1992.
[20] K.L. Hansen, Effect of leading edge tubercles on airfoil performance, Ph.D. Dissertation, The School of Mechanical Engineering, The University of Adelaide, South Australia, 2012.
[21] J.C. Lin, Review of research on low-profile vortex generators to control boundary-layer separation, Prog. Aerosp. Sci. 31 (2002) 389–420, http://dx.doi.org/10.1016/S0376-0421(02)00010-6.
[22] H. Johari, C. Henoch, D. Custodio, A. Levshin, Effects of leading-edge protuberances on airfoil performance, AIAA J. 45 (11) (2007) 2634–2642, http://dx.doi.org/10.2514/1.28497.
[23] M.M. Murray, D.S. Miklosovic, F. Fish, L. Howle, Effects of leading edge tubercles on a representative whale flipper model at various sweep angles, in: Proceedings of Unmanned Untethered Submersible Technology, UUST, NH, US, 2005.

Chapter 4

Flow Physics Over a Swept Tubercled Wing

This chapter includes the following journal article:

Bolzon, M.D., Kelso, R.M. and Arjomandi, M., "Tubercles: A Flow Visualisation Study", *submitted to Experimental Thermal and Fluid Science*, 2016.

In the preceding chapters, the effects of tubercles on swept wing performance at pre-stall AOAs have been found. This chapter investigates the flow physics over the wings presented in Chapter 3 in order to elucidate why the effects detailed above occur. This improved understanding will aid the development of a framework to design tubercles that achieve a desired wing performance. Oil-film flow visualisation was conducted on the smooth and tubercled wings. In addition, a computational fluid dynamics, CFD, model of the tubercled wing was developed in order to further elucidate the flow physics observed in the oil-film flow visualisation. The oil-film flow visualisation and CFD model were conducted at 0°, 3°, 6°, 9°, and 12° AOAs, at the same freestream velocity detailed in Chapter 3; 27.5 m/s.

The oil-film flow visualisation showed that at all AOAs considered, a uniformly-sized laminar separation bubble, LSB, extended over the span of the smooth wing's suction surface, from the root to the wingtip. Tubercles modulated this LSB such that it formed closer to the wing's leading edge behind the troughs and further from the leading edge behind the peaks, which was also seen in the CFD model results. The boundary layer transition line mimicked these trends. Flow began to separate behind the troughs at a lower AOA than behind the peaks, and also compared with the smooth wing. The flow behind the peaks typically remained attached to higher AOAs than the flow over the smooth wing. The CFD results showed that greater adverse pressure gradients occurred behind the troughs that the peaks, which is the expected cause of the tubercled wing's separation trend. Furthermore, for the first time to the author's knowledge, **experimental** results have been obtained showing that tubercles "compartmentalize" the flow, resulting in isolation of the flow

separation regions from the regions of attached flow. Similar trends were observed in the CFD model. From the oil-film flow visualisation and the CFD model, the flow topology over the tubercled wing was interpreted and reported. This study showed that sweeping a tubercled wing results in an asymmetry in the topology about the trough centreline. The vortex detachment points were observed behind each tubercle trough, and as a result of the wing's sweep, one detachment point was larger than the other. Furthermore, a bifurcation line formed behind each peak, however, this line formed closer to the smaller detachment point, and expectedly weaker vortex.

Finally, the oil-film flow visualisation and CFD results confirmed a hypothesis presented in Chapter 3; the flow over the junction of the wing leading edge and wingtip separates before reattaching downstream. This separation zone is the probable cause of the increased profile drag coefficient in the wingtip region that was identified in Chapter 3.

From the results detailed in this chapter, the findings pertaining to the first and second aims of this thesis are further understood. Furthermore, it is now understood how tubercles affect the flow, and conjectures can be made as to their effects under different conditions and with different geometries.

Statement of Authorship

Title of Paper	Tubercles: A Flow Visualisation Study
Publication Status	☐ Published ☐ Accepted for Publication ☑ Submitted for Publication ☐ Unpublished and Unsubmitted w ork w ritten in manuscript style
Publication Details	Bolzon, M.D., Kelso, R.M. and Arjomandi, M., "Tubercles: A Flow Visualisation Study", *submitted to Experimental Thermal and Fluid Science*, 2016.

Principal Author

Name of Principal Author (Candidate)	Michael Bolzon		
Contribution to the Paper	Performed experiments, developed numerical model, processed data, wrote manuscript, and acted as corresponding author.		
Overall percentage (%)			
Certification:	This paper reports on original research I conducted during the period of my Higher Degree by Research candidature and is not subject to any obligations or contractual agreements with a third party that would constrain its inclusion in this thesis. I am the primary author of this paper.		
Signature		Date	

Co-Author Contributions

By signing the Statement of Authorship, each author certifies that:

i. the candidate's stated contribution to the publication is accurate (as detailed above);

ii. permission is granted for the candidate in include the publication in the thesis; and

iii. the sum of all co-author contributions is equal to 100% less the candidate's stated contribution.

Name of Co-Author	Richard Kelso		
Contribution to the Paper	Supervised experimental and numerical development, aided interpretation of results, and reviewed manuscript.		
Signature		Date	

Name of Co-Author	Maziar Arjomandi		
Contribution to the Paper	Supervised experimental and numerical development, aided interpretation of results, and reviewed manuscript.		
Signature		Date	

Tubercles: A Flow Visualization Study

Abstract:

An oil film flow visualization study was conducted on two swept and tapered wings of NACA 0021 profile and at a Reynolds number of 225,000. One wing had a smooth leading edge while the other had leading edge protuberances, termed tubercles. A computational fluid dynamics (CFD) model of the tubercled wing was developed and validated against the experimental results and literature. Whilst a uniformly-sized laminar separation bubble formed on the suction side of the smooth wing, the tubercles spatially modulated this bubble and, as a result, the laminar separation bubble formed closer to the leading edge behind the troughs than the peaks. It was found that, unlike the smooth wing, the flow separated over the tubercled wing in a non-uniform fashion, with the flow behind the troughs separating at lower angles of attack than behind the peaks. The flow visualization and CFD model depicted tubercles "compartmentalizing" the flow, thereby isolating regions of separated flow from the rest of the wing. The laminar separation bubble formation and the flow separation regions were asymmetrical about the trough centreline, due to the sweep. An interpreted flow topology over the tubercled wing has been included, and shows the primary and secondary vortex formations.

Introduction:

Despite their massive size, Humpback whales are renowned for their agility and nimbleness. Their agility is, in part, owed to their unique pectoral flipper geometry as they have bumps, known as tubercles, on the leading edge. Tubercles are typically characterized by two parameters, the amplitude, A, which is the distance between a tubercle trough and peak, and the wavelength, λ (Hansen *et al.*, 2011), which is the distance between two adjacent tubercles. It is known that tubercles produce pairs of counter-rotating, streamwise vortices, which induce a common downwash behind the peaks and a common upwash behind the troughs (Pedro and Kobayashi, 2008; Stanway, 2008; Kerschgens, 2008; Hansen, 2012). Two of the most promising theories describing the flow mechanism that tubercles introduce are, that tubercles act to "compartmentalize" the flow (Watts and Fish, 2001), and that they act in a similar fashion to vortex generators, mixing higher momentum fluid into the boundary layer (Miklosovic *et al.*, 2004).

The most obvious effects of tubercles on foil and wing performance are delayed and softened stall (Miklosovic *et al.*, 2004; Stein and Murray, 2005; Bolzon *et al.*, 2015). Tubercles can also reduce drag and increase the lift-to-drag ratio at pre-stall angles of attack (AOAs) (Bolzon *et al.*, 2016, a).

The presence of a Laminar Separation Bubble (LSB) on a smooth airfoil or wing can produce significant increases in lift at AOAs below the stall angle (Hansen *et al.*, 2014; Bolzon *et al.*, 2016, a). This is due to the LSB increasing the effective camber of the airfoil or wing, thereby resulting in an increased lift-curve slope (Hansen *et al.*, 2014). Numerical simulations by Rostamzadeh *et al.* (2014) showed that while an LSB over a smooth airfoil forms as a long region spanning much of its chord, the addition of tubercles results in the LSB becoming shorter in chordwise extent behind the troughs, which in an extreme case can result in the elimination of the LSB in these regions.

In addition, investigating the shape, size, and location of an LSB provides insight into the state of the boundary layer and surface shear stresses; when a sufficiently strong adverse pressure gradient acts

on a laminar boundary layer, separation will occur. Transition to turbulence will typically occur within this separation zone, and if this flow reattaches, an LSB will form (Alam and Sandham, 2000).

The progression of stall over an airfoil or wing, herein termed the stall pattern, is also important as it qualitatively indicates the amount of lift generated, the stability of the airfoil or wing, as well as the pressure drag. Johari *et al.* (2007) and Rostamzadeh *et al.* (2014) demonstrated that for an unswept tubercled airfoil, or wing, the flow first separates behind the troughs, and symmetrically about the trough's centerline. This flow separation symmetry is expected, as the vortices produced by a tubercle on an unswept airfoil, or wing, are equal and opposite in strength (Hansen, 2012; Hansen *et al.*, 2016). However, a tubercle on a swept wing results in one vortex being stronger than the other (Bolzon *et al.*, 2016, b). Therefore, it is an aim of this study to determine how this asymmetry in the vortex pair strengths affects the stall pattern of the tubercled wing, as well as the general flow physics.

To investigate the effects of tubercles on the flow field, LSB formation, and stall characteristics over a swept wing, an oil film flow visualization experiment has been conducted. An oil film approach was chosen as it provides a comprehensive visualization of the flow streaklines and can highlight flow features such as LSBs and separation lines (Merzkirch, 1987). In addition, a Reynolds-Averaged Navier-Stokes (RANS) computational fluid dynamics (CFD) model of the tubercled wing has been developed to elucidate the flow features and physics.

Methodology:

Wings:

Two NACA 0021 wings were studied in this work (fig. 1). One wing had a smooth leading edge, while the other had a tubercled leading edge. The tubercled wing was designed to preserve a constant thickness-to-chord ratio along the span, which resulted in "bumps" and "valleys" forming in the chordwise direction that washed out towards the wing's trailing edge. Both of the wings had quarter-chord sweep angles of 35°. The wings had spans of 330mm, mean aerodynamic chords (MACs) of 130mm, and taper ratios of 0.4. Taper was incorporated as swept wings are usually tapered in order to reduce induced drag. The tubercles had an amplitude of 10.5mm and a wavelength of 60mm (A10.5λ60 according to the nomenclature of Hansen *et al.*, 2011). The wings were machined from aluminium.

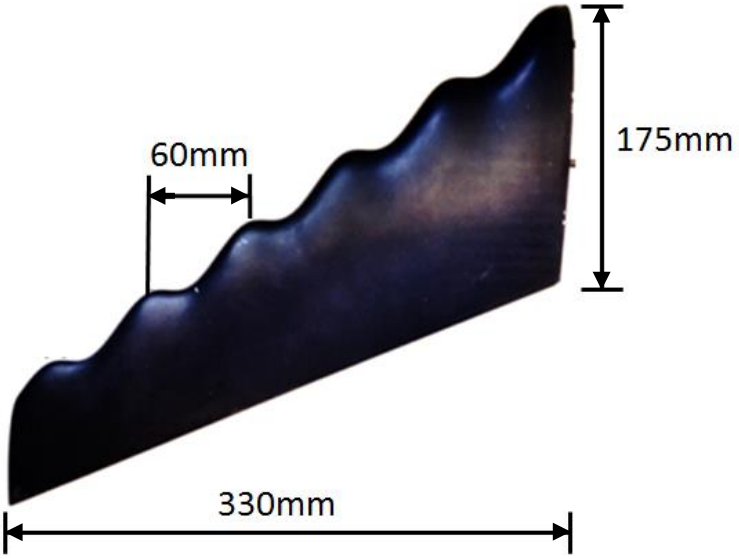

Figure 1: Picture of the tubercled NACA 0021 wing. The tubercles have a geometry of A10.5λ60.

Oil Film Flow Visualization:

The oil film flow visualization experiments were conducted in The University of Adelaide's "KC Wind Tunnel" in an open-loop configuration. This tunnel was operated at a freestream velocity of 27.5 m/s, which resulted in a MAC Reynolds number of 225,000. The turbulence intensity of this wind tunnel was 0.6% ~ 0.8%. The wings were mounted vertically on a JR3 45E15 six-component load cell, and the load cell was mounted on a Vertex HV-6 rotary table. The load cell was used for the initial angular alignment of the wings, and the rotary table was used to change the wings' AOAs. The co-ordinate system adopted can be seen in fig. 2. It was assumed that at an AOA of 0°, the measurement from the Y-axis component of the load cell corresponded solely to the lift. Therefore, a reading of zero in the Y-axis direction indicated the 0° AOA of each wing. The maximum misalignment error due to this assumption was in the order of $\pm$0.05° (Bolzon *et al.*, 2016, b).

Flow visualization experiments were conducted on both wings at 0°, 3°, 6°, 9°, and 12° AOAs. The flow visualization was conducted on the suction side of the wing and not the pressure surface, as the flow features of interest, namely the LSB formation and flow separation patterns, typically occur on the suction side of this particular airfoil profile (Hansen *et al.*, 2014). Furthermore, the tubercle vortex formations are visible on the suction side (Rostamzadeh *et al.*, 2014). In addition, flow visualization was conducted on the wing's tip to investigate possible flow separation and wingtip vortex rollup patterns in order to investigate effects that tubercles have on the profile and induced drag coefficients of these wings, respectively (Bolzon *et al.*, 2016, b). Two oil film mixtures were used to visualize the flow patterns, as each mixture better identified certain flow structures. The first mixture consisted, by weight, of 5 parts kerosene, 2 parts linseed oil, and 1 part talcum powder. This mixture, designated as the kerosene mix, was useful in determining the streaklines on the wings' surfaces as it did not readily dry. The second mixture consisted, by weight, of 5 parts ethanol and 2 parts talcum powder. This mixture, designated as the ethanol mix, dried quickly and as such was ideal for visualizing the surface shear stress patterns on the wings and the vortices produced by the tubercles. As a general rule, the kerosene mix was applied as sparingly as possible to the wing surfaces, as the mix would pool in *foci* and a more generous application would result in the detail of

the flow patterns being lost. Conversely, due to the fast drying time of the ethanol mix, a more generous application would better highlight the flow structures. The mixtures were applied to the wings' surfaces with a paintbrush to produce a uniform coverage.

A Nikon D200 DSLR camera was used to photograph the flow visualization results, and the pictures were converted to grayscale and processed using Matlab. Pictures of both the wing suction side and the wingtip were taken.

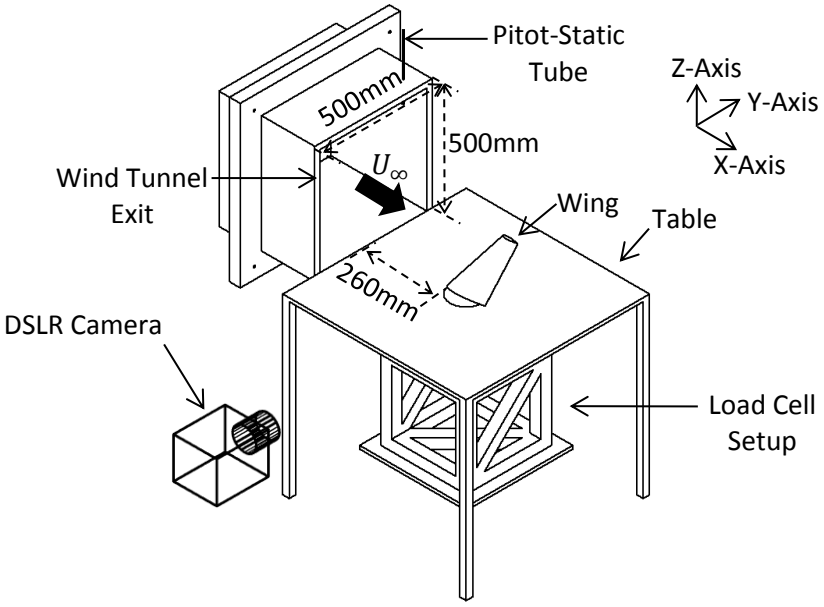

Figure 2: Oil film flow visualization setup.

Computation Fluid Dynamics Model:

ANSYS-CFX 14.5 was used to model the flow over the half-span tubercled wing at 0°, 3°, 6°, 9°, and 12° AOAs. The freestream velocity was 27.5 m/s. The shear stress transport $\gamma - Re_\theta$ model was used to solve the transient RANS equations, as it can adequately capture the flow features in a transitional flow regime, such as LSBs (Counsil and Boulama, 2012; Rostamzadeh *et al.*, 2014). Here the term γ is the intermittency and Re_θ is the momentum thickness Reynolds Number. Detailed explanations of this model can be found in Menter (1994) and Counsil and Boulama (2012).

The computational domain was created in a C-grid shape, as shown in fig. 3, and the domain size and the boundary conditions were chosen in order to produce flow conditions similar to these of the experiment. The inlet was located 6 MACs from the wing-root trailing edge, the outlet was located 15 MACs downstream of the wing-root trailing edge, the top and bottom planes were located 6 MACs from the wing mean-thickness line, and the left plane was located 10 MACs from the wing root. The wing's AOA was determined from the flow direction through the inlet. The outlet, top, bottom, and left planes had relative pressures of 0 Pascals. The symmetry plane was a free slip wall.

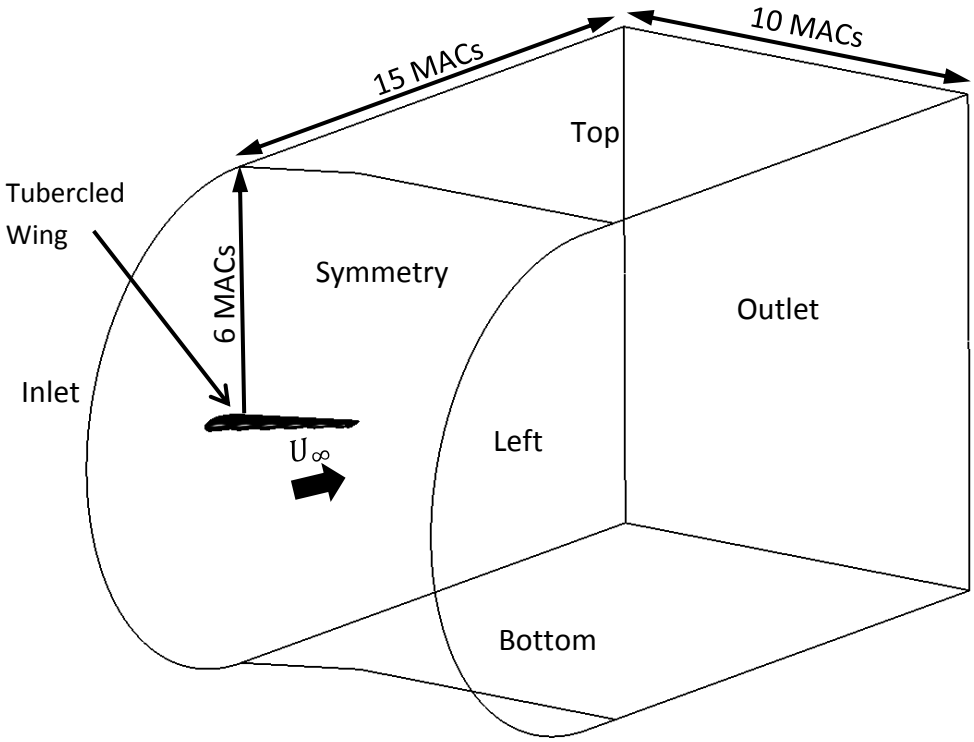

Figure 3: The computational domain of the tubercled wing.

A high-resolution scheme was used for spatial discretization, and a second-order backward Euler scheme was used for the transient computations.

For a given AOA, the model was deemed solved once the lift and drag coefficients varied less than 1% of their respective magnitudes over one hundred timesteps. Figure 4 shows the convergence history of the lift and drag coefficients of the tubercled wing at 9° AOA, which represents a typical convergence history of the tubercled wing's lift and drag coefficients at all AOAs.

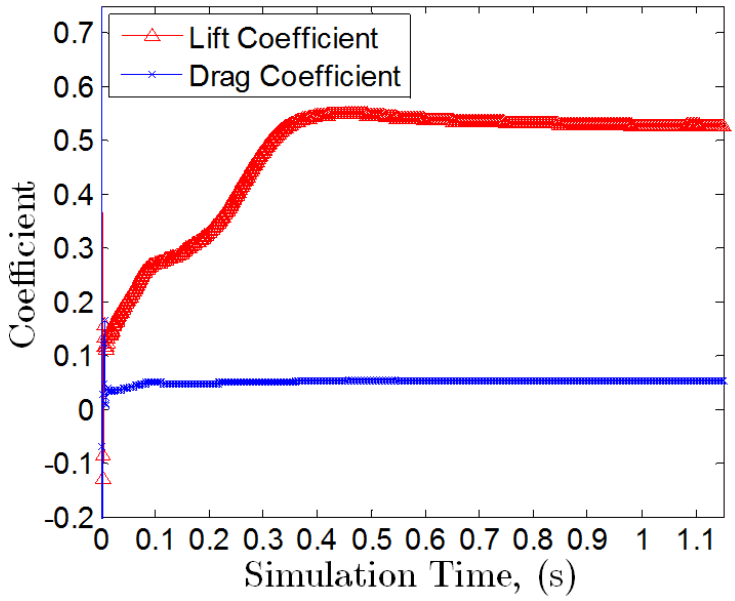

Figure 4: Convergence history of the lift and drag coefficients of the tubercled wing at 9° AOA.

The mesh was constructed with an inflation layer such that the y-plus value was below 1.0 at all AOAs over the tubercled wing's surface, as required by the $\gamma - Re_\theta$ model. To produce mesh-independent lift and drag coefficients, two meshes were constructed. The finer mesh was produced by refining the coarser mesh by a factor of approximately $\sqrt{2}$ in all directions, as this factor is suitable for a mesh-independency study using the $\gamma - Re_\theta$ model in the transitional Reynolds number regime (Counsil and Boulama, 2012; Rostamzadeh *et al.*, 2014). This mesh independency study was conducted at 0° and 9° AOAs, and the results can be seen in table 1. These two AOAs were chosen for the independency study as they represent two different performance regimes of the tubercled wing; below 9°, the tubercled wing has a lower drag coefficient than the smooth wing, but at 9°, the tubercled wing's drag coefficient begins to increase dramatically (Bolzon *et al.*, 2016 a, b). The coarser mesh was used for the remainder of this study as the benefits of the slight refinements in the lift and drag coefficients did not outweigh the costs of added computational time. In addition, the coarser mesh was satisfactorily validated from 0° to 6° AOAs, as discussed below, and the refined mesh did not improve the validity of the model at 9° and 12° AOAs significantly.

Table 1: The results of the mesh-independency study of the tubercled wing at a Reynolds number of 225,000.

Angle of Attack, °	Number of Elements	Lift Coefficient	Drag Coefficient
0	3,202,778	0.000	0.0185
0	4,522,824	0.000	0.0177
9	3,202,778	0.526	0.0543
9	4,522,824	0.518	0.0566

The turbulence intensity affects the boundary layer physics over a tubercled wing (Rostamzadeh *et al.*, 2014), therefore, a turbulence intensity study was conducted at 0° and 9° AOAs. The effects of 1% and 5% turbulence intensities, as prescribed at the inlet, on the lift and drag coefficients were investigated, as these parameters are highly sensitive to the boundary layer state. The results are presented in table 2. Typically, reducing the turbulence intensity reduced the lift coefficient and increased the drag coefficient. The lift and drag coefficients obtained from the CFD model were validated with the lift and drag coefficients of the same tubercled wing that was experimentally investigated by Bolzon *et al.* (2016, a). The lower turbulence intensity produced lift and drag coefficients more similar to the coefficients in Bolzon *et al.* (2016, a), which indicate a more similar boundary layer development to that in the experiments (Bolzon *et al.*, 2016, a). In addition, the experiments detailed in Bolzon *et al.* (2016, a) were carried out in the same wind tunnel as the oil film flow visualization. The lowest turbulence intensity option in the CFD package was 1%, which was also the closest available option to wind tunnel's turbulence intensity. Therefore, a freestream turbulence intensity of 1% was used for the remainder of the CFD investigation.

Table 2: The effects of the turbulence intensity on the lift and drag coefficients of the tubercled wing at a Reynolds number of 225,000.

Angle of Attack, °	Turbulence Intensity, %	Lift Coefficient	Drag Coefficient
0	1	0.000	0.0185
0	5	0.000	0.0174
9	1	0.526	0.0543
9	5	0.541	0.0507

A timestep independency analysis was performed with timesteps of 1×10^{-4} and 5×10^{-5} seconds at 0° and 9° AOAs. The differences in the lift and drag coefficients between these timesteps were typically 2%, and the flow features were almost identical. Therefore, a timestep of 1×10^{-4} was used for the remainder of the study.

In figs. 5 and 6, respectively, the lift and drag coefficients calculated from the CFD model from 0° to 12° AOAs have been plotted against the experimentally-determined lift and drag coefficients of this tubercled wing, as reported in Bolzon *et al.* (2016, a). These figures show that from 0° to 6° AOAs, the lift and drag coefficients obtained from the CFD model are very similar to the experimental results reported in Bolzon *et al.* (2016, a), therefore, it can be concluded that the CFD model is validated at these AOAs. At 9° and 12° AOAs, both the lift and drag coefficients obtained from the CFD model begin to diverge from the experimental results. The lift-curve slope of the tubercled wing from Bolzon *et al.* (2016, a) is presented in fig. 7, and at 6° AOA, the lift-curve slope of the tubercled wing increases. It was deduced that this increase was caused by an LSB on the tubercled wing's suction side (Bolzon *et al.*, 2016, a). However, in fig. 5 the lift-curve slope of the CFD results does not increase to the same extent as that presented in Bolzon *et al.* (2016, a). This indicates that the CFD model is not producing the same LSB-related effects on the wing performance, as found in the experimental data. This is probably due to the slightly greater turbulence intensity prescribed in the

CFD model to the turbulence intensity occurring in the wind tunnel. In the transitional Reynolds number regime, the turbulence intensity impacts the LSB's formation (Roberts, 1980), where a larger turbulence intensity could even cause the boundary layer to transition without an LSB forming. A lower turbulence intensity at 9° and 12° AOAs is expected to produce lift and drag coefficients that are more similar to the experimental results, however, the lowest turbulence intensity available in the CFD package was 1%, which was employed. The lift-to-drag ratio of the tubercled wing determined from the CFD model at all AOAs was compared with the experimentally-determined lift-to-drag ratio in fig. 8. From 0° to 6° AOAs, the CFD results are in very good agreement with the experimental results. At 9° and 12° AOAs, the deviations of the CFD results from the experimental results are less than those seen in the lift and drag coefficient comparisons, which suggests that at these AOAs, the CFD model is generally under-predicting the lift and drag coefficients to similar extents.

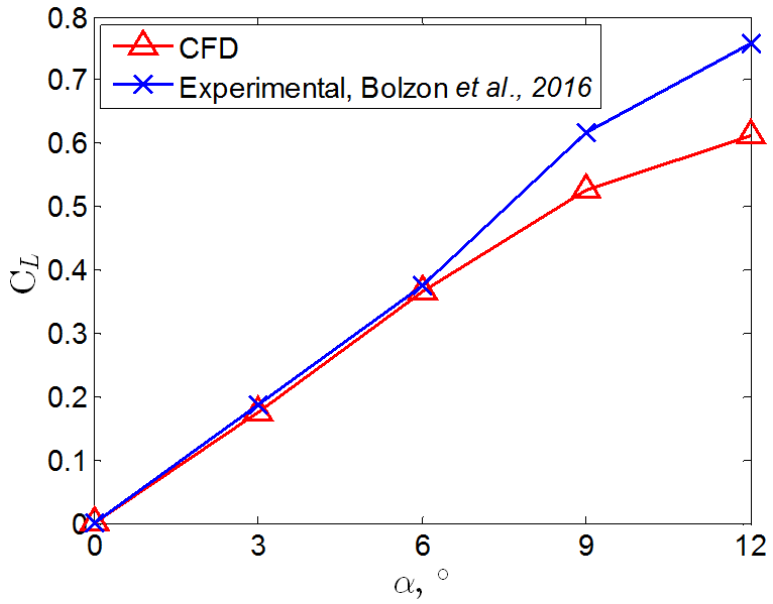

Figure 5: Comparison of the lift coefficient obtained from the CFD models and from the experiment in Bolzon *et al.* (2016, a) for the tubercled wing.

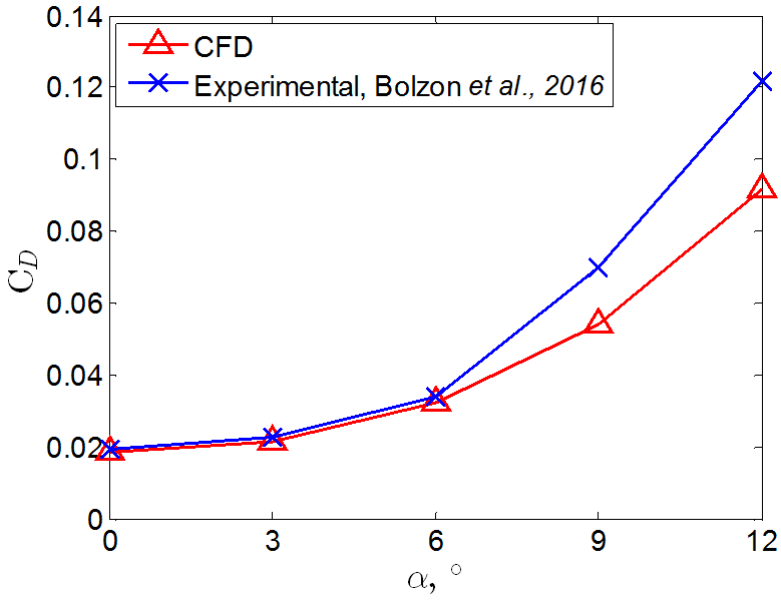

Figure 6: Comparison of the drag coefficient obtained from the CFD models and from the experiment in Bolzon *et al.* (2016, a) for the tubercled wing.

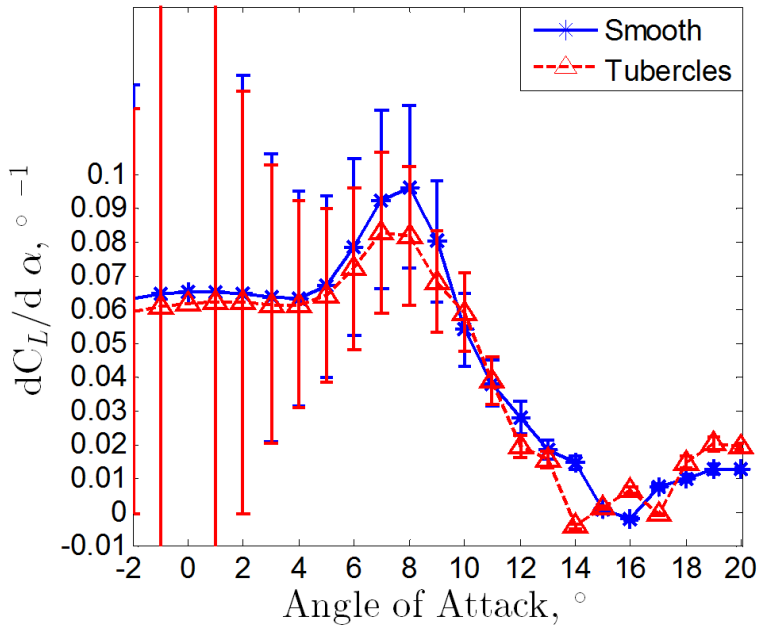

Figure 7: The lift-curve slope of the smooth and tubercled wings (Bolzon *et al.*, 2016, a).

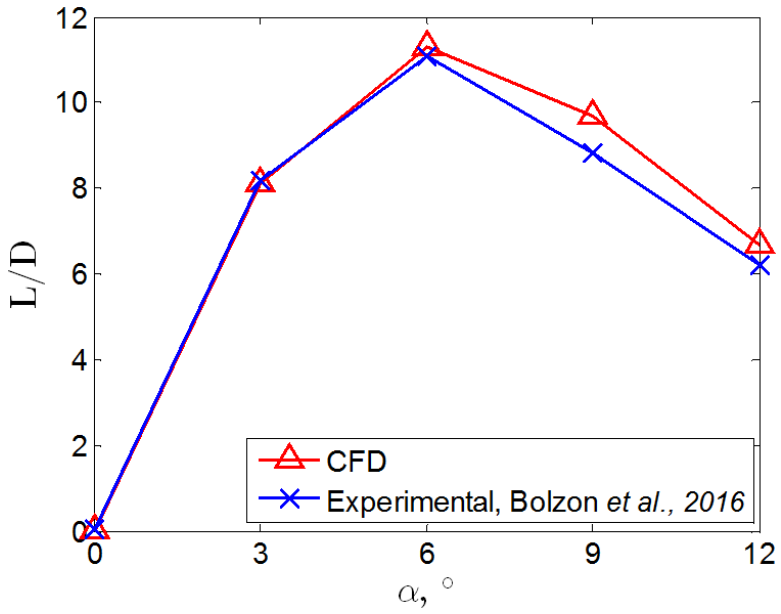

Figure 8: Comparison of the lift-to-drag ratios obtained from the CFD models and from the experiment in Bolzon *et al.* (2016, a) for the tubercled wing.

Results:

The Effects of Tubercles on Laminar Separation Bubble Formation:

Figures 9 to 14 present the kerosene mix oil film flow visualization of the smooth wing. At all AOAs, a large LSB forms over the suction side of the smooth wing, which can be seen from the large regions of white, bounded by two distinct white lines running almost the entire span of the wing. The LSB has been outlined for clarity in fig. 9. The spanwise line closest to the leading edge indicates the start of the LSB and the spanwise line furthest from the leading edge shows the end of the LSB (Nakayama *et al.*, 1988). The front white spanwise line forms at the convergence of the forward and reverse flows at the separation line. The rear white spanwise line forms at the reattachment line, where the mixture downstream of the line moves towards the trailing edge, revealing the black surface of the wing. Further evidence of the LSB's presence at all AOAs is that behind the rear white spanwise line, the flow is more erratic, as seen by the increased "waviness" of the streaklines. This indicates that the flow is now turbulent. The start and end locations of the LSB over the smooth wing have been measured at the spanwise location of the MAC, and expressed as a percentage of the MAC in table 3.

At 0° AOA, the LSB extends approximately one third of the MAC of the smooth wing, and starts from approximately one third of the wing MAC from the leading edge, as detailed in table 3. As the AOA increases, the LSB decreases in chordwise extent and moves towards the leading edge, which is likely to result in the flow transitioning to turbulence further upstream.

Figure 14 shows a close-up of the Kerosene mix flow visualization of the smooth wing at 6° AOA. As the flow approaches the front of the LSB, it starts to flow slightly laterally towards the wingtip. After

the flow reattaches, it also starts to curve slightly towards the wingtip. These small curvatures have also been observed in another oil film study of a swept wing (Nakayama *et al.*, 1988), and are likely caused by the adverse pressure gradient that decelerates the streamwise component of flow, thereby making the spanwise flow comparatively larger.

The oil film flow visualization images of the tubercled wing at various AOAs, using the kerosene mix, are presented in figs. 15 to 19. In addition, companion images from the CFD model depicting regions of negative streamwise wall shear, which indicate the LSBs and the extents of flow separation, are presented in these figures. The LSBs observed during the oil film flow visualization are visible in figs. 15 to 19; behind the peaks, they appear as matt white regions with very few streaklines, which is due to the low near-wall shear stresses. For clarity, the LSB over the tubercled wing at 0° AOA has been outlined in fig. 15 a). Unlike the smooth wing, which exhibits a uniformly-sized LSB along the wing span, the tubercled wing has a long LSB but it is modulated, forming closer to the leading edge of the wing behind the troughs, and further away behind the peaks. The LSB shape and location can also be determined using the ethanol mix, as the near-wall shear stresses inside the LSB are comparatively low and the drying time of the ethanol mix is inversely proportional to the shear stress. A slower drying time indicates the presence of the LSB. Figure 15 c) shows the results of the ethanol mix applied to the wing, and the LSB is very clear, appearing as the darker region. The shape of this darker region is consistent with the shape of the LSB observed with the kerosene mix and from the CFD model. It should be noted that while the drying of the ethanol mix is useful in determining the shape of the LSB, it is not accurate in determining its size because the amount of dried ethanol mix is a function of the experimental time and the uniformity of the application of the mix. The LSB shape and size visualized with the kerosene mix remains relatively constant with time. Therefore, the kerosene mix will be used for the remainder of this section to determine the LSB shape and size.

At 0° AOA, the LSB's shape and size over the tubercled suction side, as found in the CFD model, is very similar to that observed during the flow visualization experiments. As the tubercled wing's AOA increases, the LSB's shape and size observed in the CFD model near the inboard sections continue to resemble the LSB's shape and size observed during the flow visualization, however, near the wingtip region, the CFD model shows large-scale flow separation. This flow separation is most obvious at 12° AOA, where the CFD model shows that the outboard half of the tubercled wing has undergone complete stall.

The modulation of the LSB's shape by the tubercles, shown in figs. 15 to 19, was also observed by Rostamzadeh *et al.* (2014). In spite of the differences in sweep, these numerical simulations and this present study indicate that the LSB occurs in a spanwise-periodic pattern with separation occurring principally downstream of the tubercle troughs. The asymmetry in the LSB's shape about the trough centreline found in the experiment and the CFD model is likely caused by the asymmetry in the vortex pair strengths resulting from the sweep of this tubercled wing (Bolzon *et al.*, 2016, b).

The chordwise locations of the LSB over the tubercled wing behind the third trough, and the average behind the third and fourth peak have been measured from the experimental results, and expressed as a percentage of the local chord in table 3**.** The LSB behind the trough typically starts and ends closer to the leading edge than behind the peak. As a result, it is expected that the transition to turbulence occurs further upstream behind the trough than behind the peak. Vortex generators

have exhibited similar effects on LSB formations (Kerho *et al.*, 1993; Seshagiri *et al.*, 2009). From the CFD model, the adverse pressure gradient is typically higher behind a tubercle trough than a peak, as shown in fig. 20, which is consistent with literature (van Nierop *et al.*, 2008; Hansen, 2012; Rostamzadeh *et al.*, 2014). Therefore, the LSB is expected to form closer to the leading edge behind a trough than behind a peak (Gaster, 1969). Figures 15 to 19 and table 3 show that, similar to the smooth wing, as the AOA increases, the LSB behind the troughs of the tubercled wing moves towards the leading edge and reduces in chordwise length. However, while the separation line of the LSB behind the peaks also moves upstream with increasing AOA, its reattachment line remains at a relatively fixed chordwise-location. This trend is generally consistent with the CFD results. Therefore, we conclude that the LSB behind the peaks increases in chordwise extent with increasing AOA. These effects of tubercles on the LSB formations are the expected causes of the reduced lift-curve slope of the tubercled wing between 5° and 9° AOAs, compared to the smooth wing, as observed by Bolzon *et al.* (2016, a) in fig. 7.

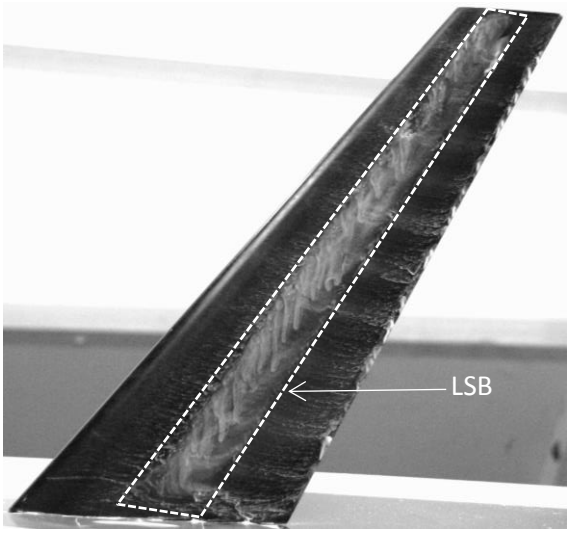

Figure 9: Kerosene mix flow visualization of suction side, smooth wing at 0° AOA.

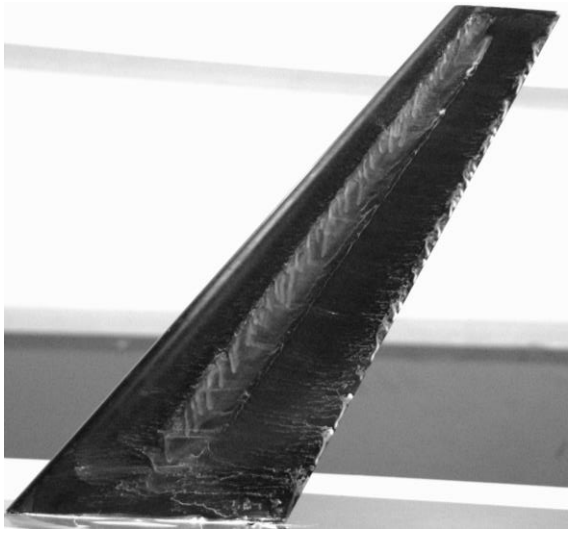

Figure 10: Kerosene mix flow visualization of suction side, smooth wing at 3° AOA.

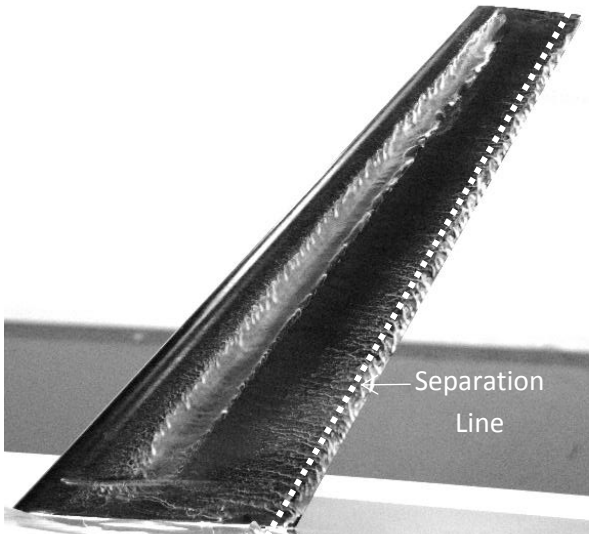

Figure 11: Kerosene mix flow visualization of suction side, smooth wing at 6° AOA.

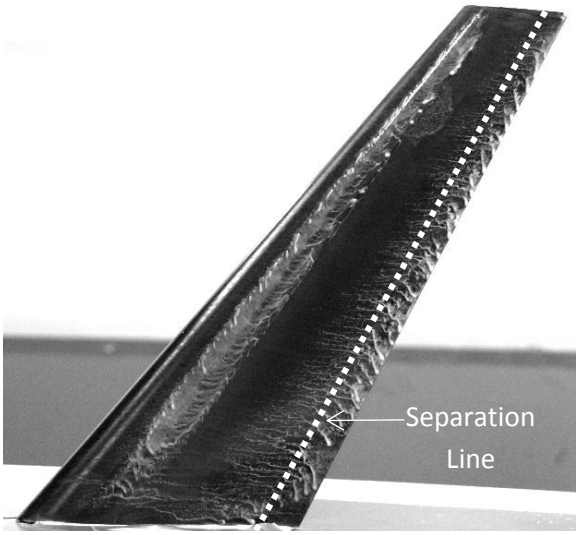

Figure 12: Kerosene mix flow visualization of suction side, smooth wing at 9° AOA.

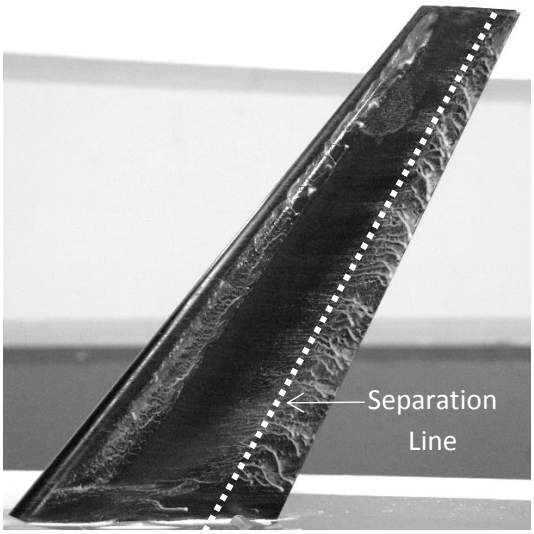

Figure 13: Kerosene mix flow visualization of suction side, smooth wing at 12° AOA.

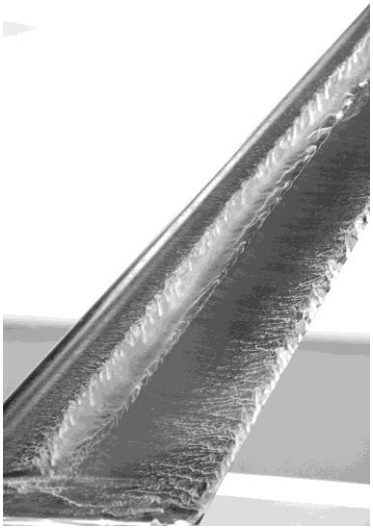

Figure 14: Kerosene mix flow visualization of suction side, smooth wing at 6° AOA close-up.

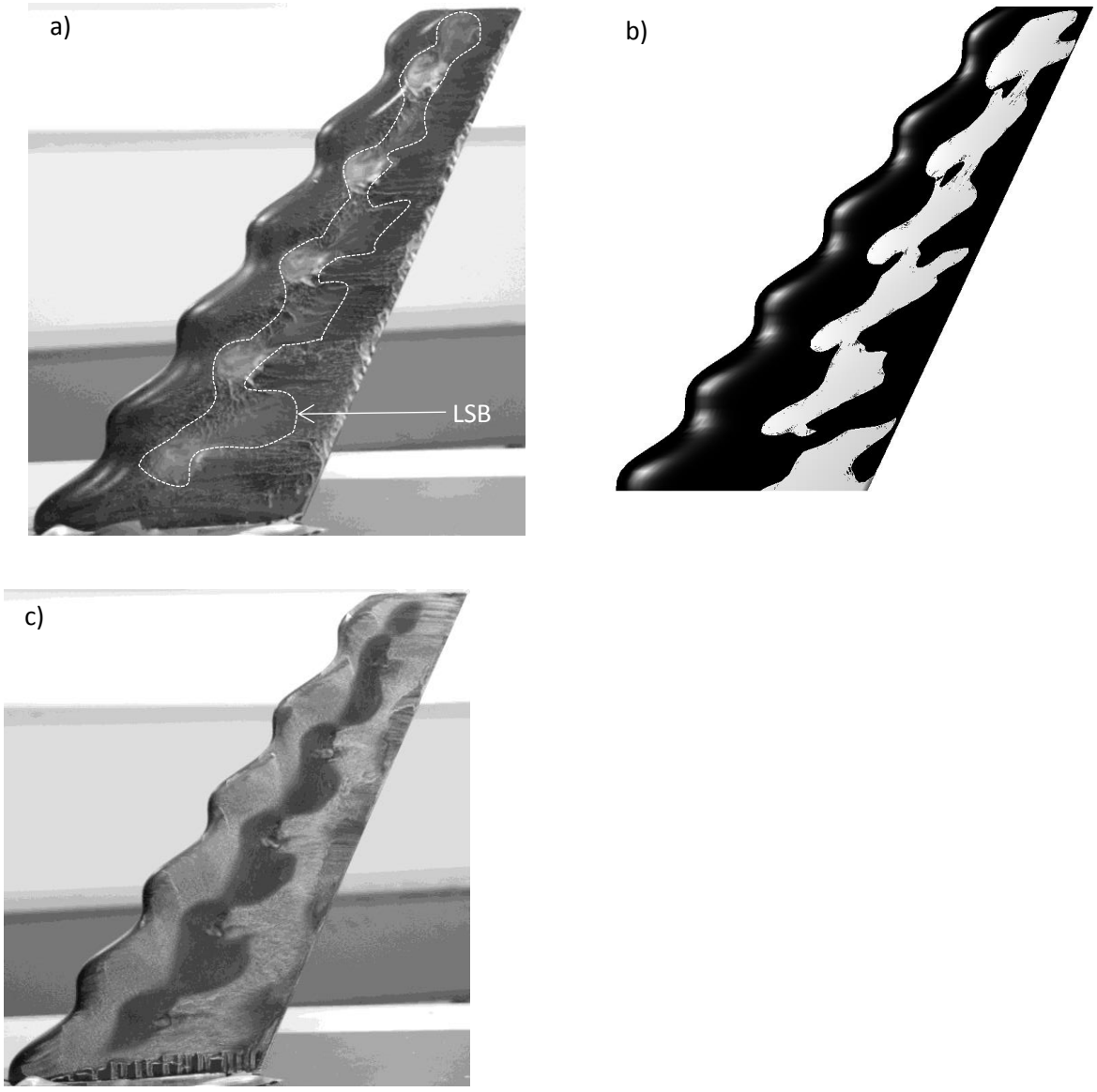

Figure 15: a), kerosene mix flow visualization, b), CFD result depicting regions of negative streamwise wall shear (white), and, c), ethanol mix flow visualization, of the tubercled wing's suction side at 0° AOA.

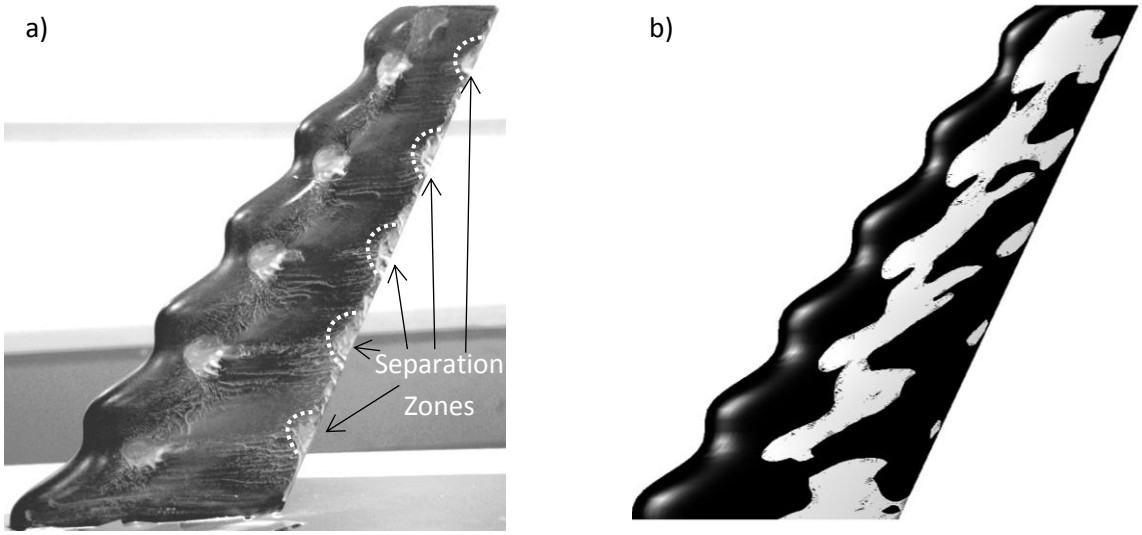

Figure 16: a), kerosene mix flow visualization, and, b), CFD result depicting regions of negative streamwise wall shear (white), of the tubercled wing's suction side at 3° AOA.

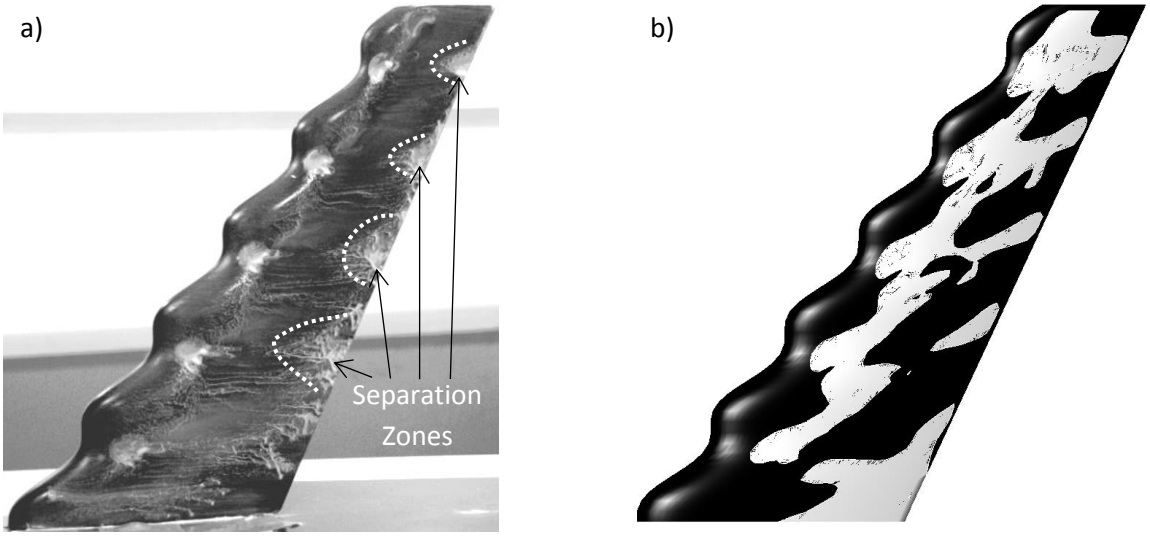

Figure 17: a), kerosene mix flow visualization, and, b), CFD result depicting regions of negative streamwise wall shear (white), of the tubercled wing's suction side at 6° AOA.

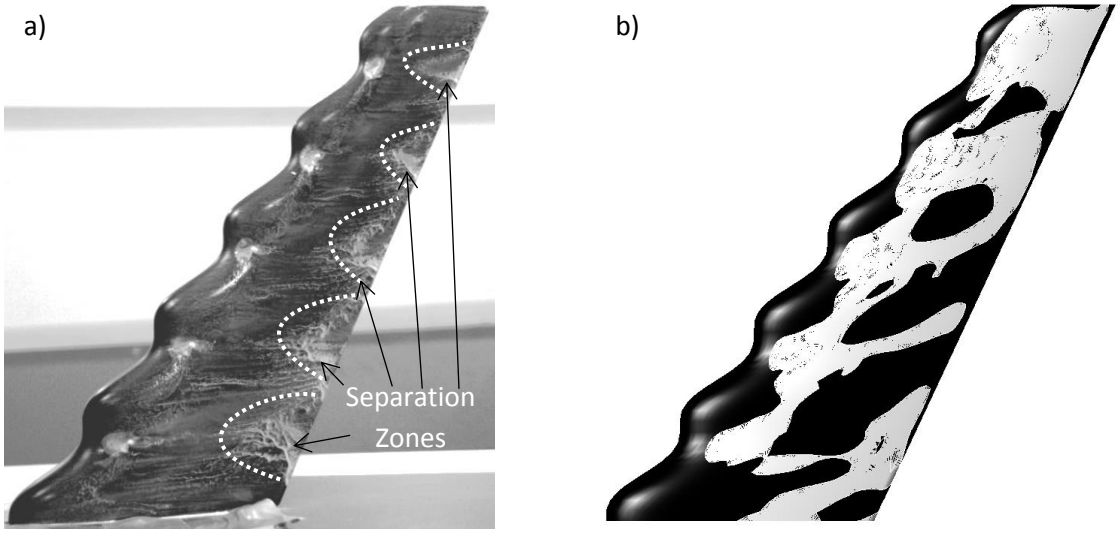

Figure 18: a), kerosene mix flow visualization, and, b), CFD result depicting regions of negative streamwise wall shear (white), of the tubercled wing's suction side at 9° AOA.

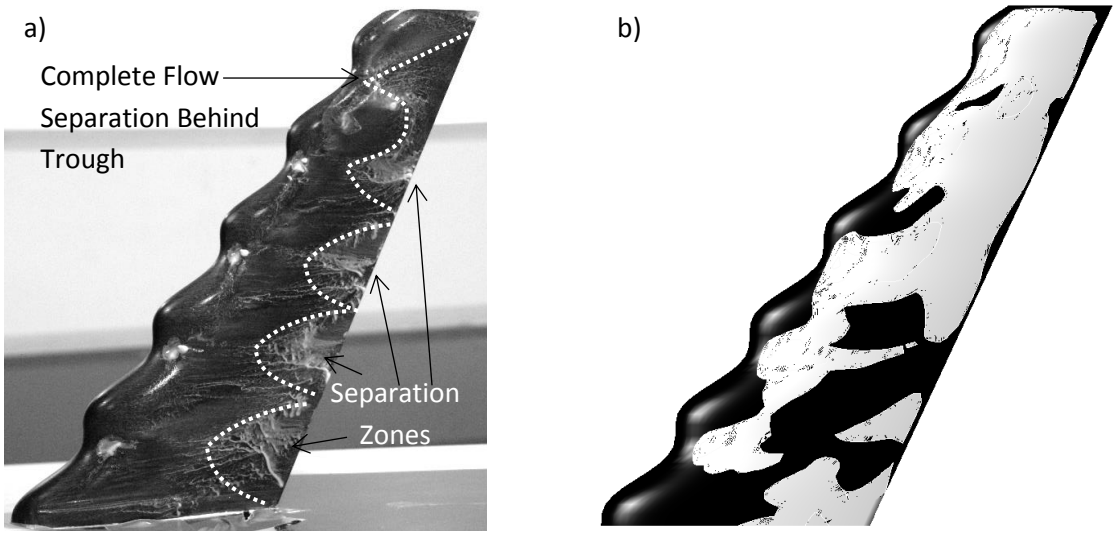

Figure 19: a), kerosene mix flow visualization, and, b), CFD result depicting regions of negative streamwise wall shear (white), of the tubercled wing's suction side at 12° AOA.

Table 3: The location of the Laminar Separation Bubble on the smooth and tubercled wing suction side as a percentage of the local chord.

Laminar Separation Bubble Location						
	Smooth Wing		**Tubercled Wing**			
			Trough		Peak	
Angle of Attack	Separation	Reattachment	Separation	Reattachment	Separation	Reattachment
0°	34%	66%	20%	47%	45%	68%
3°	31%	56%	14%	36%	25%	71%
6°	18%	48%	10%	28%	22%	64%
9°	15%	38%	8%	26%	11%	60%
12°	8%	30%	7%	12%	12%	58%

The Effect of Tubercles on Flow Separation:

As the wings were mounted vertically, it is relatively simple to determine the flow separation line; once the flow has separated, the kerosene mix will fall under the dominant force of gravity. For the smooth wing at 6° AOA, only a small amount of flow near the trailing edge has separated, as evidenced by the slight downturn of the kerosene mix presented in fig. 11. As was expected, as the AOA increases to 9° AOA, and subsequently to 12° AOA, the separation line moves towards the leading edge of the wing, as shown in figs. 12 and 13. At 12° AOA, approximately one fifth of the wing area has stalled. Coupling this stall pattern with the LSB formation, the stall type of the smooth wing is type (c) according to Polhamus, 1996).

The flow begins to significantly separate over the tubercled wing at a lower AOA than the smooth wing; 3° AOA compared with 6° AOA, respectively. The flow first separates behind the troughs of the tubercled wing, as seen in fig. 16 a) and b), and the area of flow separation increases in size with increasing AOA, as seen in figs. 17 to 19. There are two probable reasons why the flow separates behind the troughs at a lower geometric AOA than the peaks, and also the smooth wing. The first reason is that the vortices created by the tubercles induce a common upwash behind the troughs, thereby increasing their effective AOA and resulting in a lower geometric stall AOA. The common upwash also thickens the boundary layer behind the troughs, as presented in fig. 21, which makes it more prone to separate. The second reason is that because there is a greater adverse pressure gradient behind the troughs of the tubercles than there is behind the peaks, as presented in fig. 20 and detailed in the literature (van Nierop *et al.*, 2008; Hansen, 2012; Rostamzadeh *et al.*, 2014; Hansen *et al.*, 2016), the flow will separate behind the troughs at a lower geometric AOA than behind the peaks. Figures 20 and 21 show that the streamwise pressure gradients and the boundary layer developments are asymmetrical about the trough centrelines, which is likely caused by the sweep angle. The asymmetric streamwise pressure gradients are the likely cause of the asymmetric flow separation patterns, as shown in figs. 15 to 19, and the asymmetric boundary layer development.

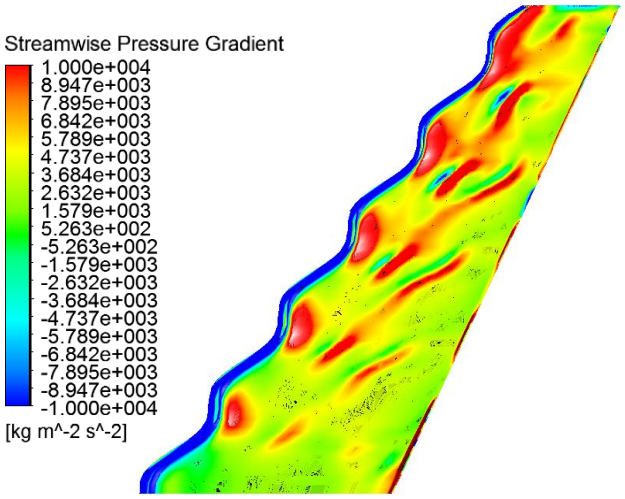

Figure 20: The streamwise pressure gradient over the tubercled wing's suction side at 6° AOA. Obtained from CFD study.

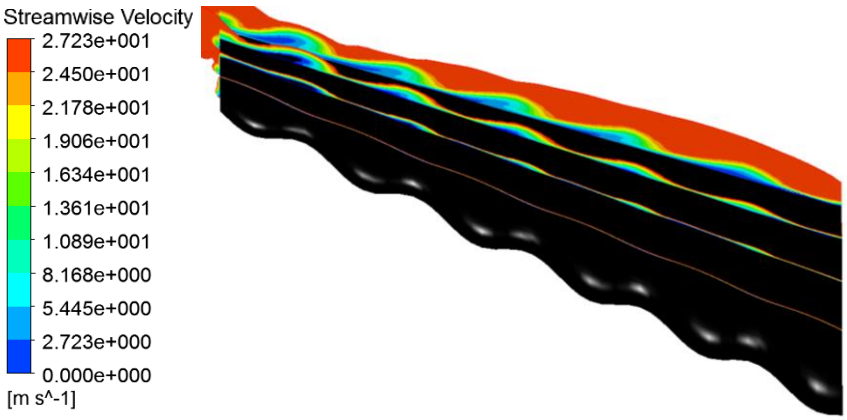

Figure 21: Perspective view of the computed streamwise velocity profiles over the tubercled wing indicating the boundary layer development over the suction side of the wing at 6° AOA. Quarter, half, three-quarter, and full chord planes shown. The boundary layer is typically thicker behind a trough than a peak.

The areas of separated flow, excluding the LSBs, over the smooth and tubercled wings at 3°, 6°, 9°, and 12° AOAs have been measured from the oil film flow visualization images presented above, and expressed in table 4 as a percentage of the total suction side area**.** At all AOAs considered, the flow separates to a greater extent over the tubercled wing than the smooth wing. As a result, the tubercled wing is expected to produce less lift, which agrees with the lift measurements by Bolzon *et al.* (2016, a) of these exact wings.

At 12° AOA, the flow phenomenon known as "compartmentalization" occurs over the tubercled wing. This flow phenomenon refers to when the separation zone behind each tubercle is isolated from the neighboring separation zones (Watts and Fish, 2001). From the oil film flow visualization, the flow behind the trough closest to the tubercled wingtip has completely separated, as annotated in fig. 19 a). Despite this, the flows behind each of the adjacent peaks are still attached, as shown in

fig. 19 a), and furthermore, the flows behind the neighboring troughs are still somewhat attached. Therefore, complete flow separation is confined to one region on the tubercled wing. A similar trend occurs at 9° and 12° AOAs in the CFD model, where the flows behind the outboard troughs are completely separated, however, the flows behind adjacent peaks and inboard troughs remain attached, as shown in figs. 18 b) and 19 b).

Table 4: Total area of separation over the suction side of the smooth and tubercled wings, expressed as a percentage of the suction side area.

Separated Area		
Angle of Attack	**Smooth Wing**	**Tubercled Wing**
3°	Negligible	4%
6°	8%	9%
9°	12%	14%
12°	20%	22%

The Location and Migration of the Tubercle Vortices:

Figure 22 shows the ethanol mix flow visualization results on the tubercled wing's suction side at 0°, 6°, and 12° AOAs. The 3° and 9° AOAs are not included for brevity as no new structures were visible at these AOAs. Circular structures appear behind the troughs of each tubercle, as shown in fig. 22. It is proposed that each of these circular structures corresponds to a vortex adjacent to a boundary layer detachment point as observed by Rostamzadeh *et al.* (2014) and Skillen *et al.* (2014). Each vortex is formed by the distortion of surface vortex lines by the pressure gradient behind each peak (Rostamzadeh *et al.*, 2014). The asymmetry in the sizes and orientations of these vortices is brought about by the different local sweep angles of the sides of each tubercle, as discussed below.

At 0° AOA, as shown in fig. 22 a), the vortices detach approximately midway between the leading edge and trailing edge. As the AOA increases, as presented in fig. 22 b) and c), the detachment points move towards the leading edge. At 12° AOA, no vortex detachment points are visible behind the trough closest to the wingtip, which also lies in the region of separated flow identified in fig. 19 a).

In fig. 22 d), the tubercle vortices can be seen more clearly. There are three troughs shown, and vortex detachment points can be seen behind each trough. Behind the bottom two troughs, there are pairs of vortex detachment points, and one vortex detachment point is significantly larger than the other. In addition, this larger vortex detachment point corresponds to the stronger vortex of the pair that arises from the wing sweep (Bolzon *et al.* 2016, b), which manifests itself in the different local sweep angles on either side of each tubercle.

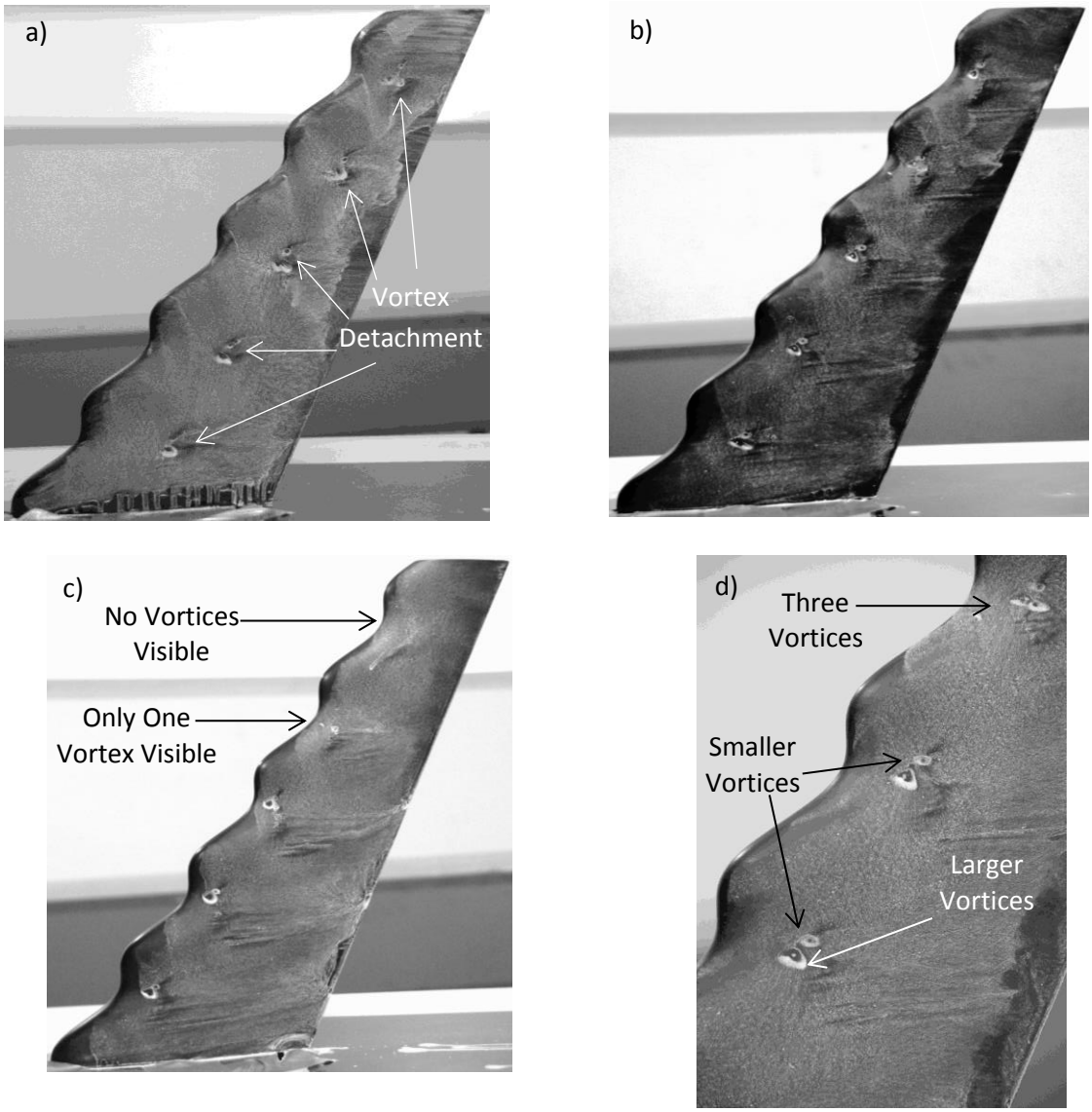

Figure 22: Ethanol mix flow visualization of the tubercled wing at, a), 0° AOA, b), 6° AOA, c), 12° AOA, and, d), a close-up at 6° AOA. Tubercle vortices visible behind the troughs.

The Flow Structure over a Tubercle:

Figure 23 shows, in detail, the kerosene mix oil film flow visualization over a tubercled wing at, a), 0° and, b), 12° AOAs. In addition, companion images from the CFD model depicting the wall shear stresses at 0° and 12° AOAs are presented in fig. 24 a) and b), respectively. Figure 25 shows the authors' interpretation of the surface flow topology that exists on the tubercled wing's suction surface over the range of AOAs described in this paper. The pattern consists of a series of *foci*, F, saddles, S, and bifurcation lines, BiL, connected by surface streamlines that resemble the surface streaklines (shear stress lines) in the images presented in this study. The *foci* correspond to the vortex detachment points described above. One obvious difference between the interpreted topology and the experimental and CFD surface patterns is the appearance of multiple roll-ups in the frozen surface flow patterns corresponding to *foci* F1 and F2, as labelled on fig. 23 a) and fig. 24 a), as indicated by the three vortex detachment points identified in fig. 22 d). Review of the video

recordings of the experiments confirms that the multiple roll-ups are probably the result of unsteadiness in the position of the focus. Multiple, closely-located roll-ups are also possible, although as a group (i.e. "in the large") these would form the same topology as shown here.

The pattern in fig. 25 is topologically similar to the flow pattern computed by Rostamzadeh et al. (2014) and Skillen *et al.* (2014), but with an asymmetry induced by the overall sweep of the wing and the difference in sweep between the inboard and outboard sides of each tubercle. The latter will have the effect of varying the turning and stretching of the wing boundary layer vortex lines, hence causing a difference in the strengths of positive-circulation and negative-circulation primary vortices, which are depicted in blue, that originate at F1 and F2. The larger appearance of the inboard vortex in each pair, as visible in the experimental results, and the anticlockwise rotation of each pair as a whole, are consistent with the difference in circulation between each primary vortex.

At the trailing edge of the wing, there appears to be a pair of secondary vortices, which are depicted in red in fig. 25, forming beneath the primary vortex pair. At low AOAs, this pattern is indistinct, appearing in some images and not others, probably due to the combination of the effects of gravity on the flowing kerosene mix and the weak circulation of these vortices. At larger AOAs, these structures are more clearly evident in triangular features adjacent to the trailing edge. Again, these features are generally indistinct, but their location and shape are consistent with the patterns computed by Rostamzadeh *et al.* (2014). Another consistent feature of these flow patterns is the presence of a "tail" (of kerosene mix) behind the trough downstream of each primary vortex pair, as identified in fig. 23 b). This corresponds to the region of reversed flow in the interpreted flow pattern. These tail regions are also visible to some extent in fig. 24 a) and b), as labelled.

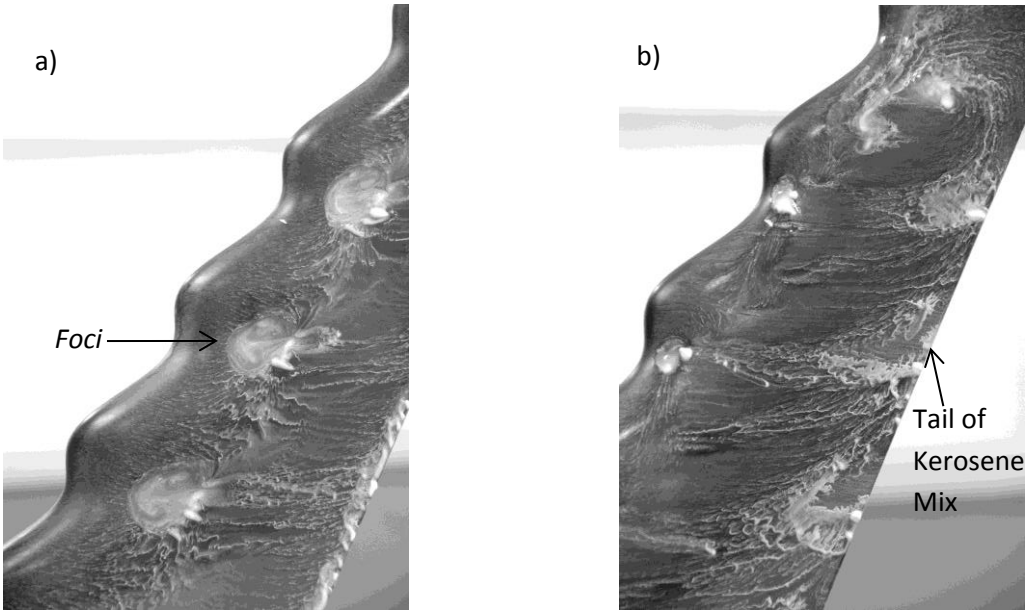

Figure 23: Kerosene mix flow visualization of the suction side, tubercled wing at, a), 0° AOA, and at, b), 12° AOA.Close-ups.

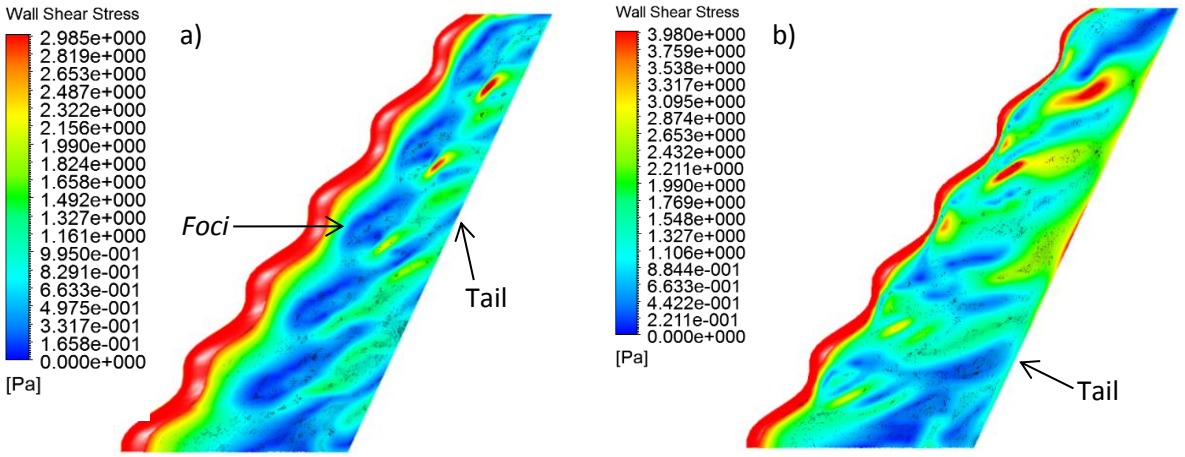

Figure 24: Wall shear stresses on the tubercled wing's suction surface at, a), 0° AOA, and at, b), 12° AOA.

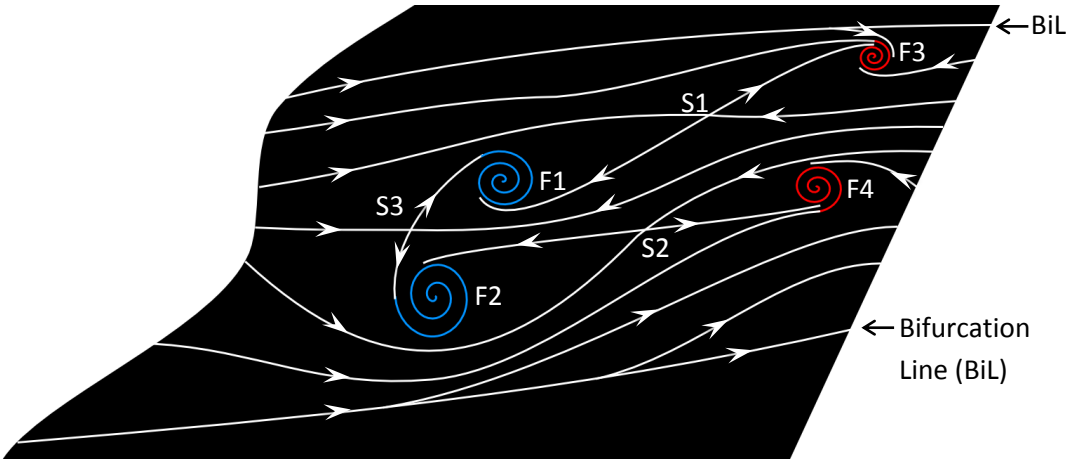

Figure 25: Interpreted flow topology over the suction surface of a swept tubercled wing. Primary vortex cores originate from blue *foci*, and secondary vortex cores originate from red *foci*.

The Effect of Tubercles on Wingtip Flow:

There is little difference in the wingtip flow visualization results between the two wings at the AOAs investigated. Therefore, only the results of the smooth and tubercled wings at 0°, 6°, and 9° AOAs are included, which are presented in figs. 26 to 31. In addition, companion images from the CFD model at 0° and 9° AOAs depicting wall shear stresses and vorticity are presented in figs. 32 to 35. The wings' suction sides are on the lower portions of the figures, while the pressure sides are on the upper portions of the figures.

Bolzon *et al.* (2016, b) found that there were large increases in the profile drag near the wingtips of the smooth and tubercled wings at all AOAs considered. They suggested that in a similar fashion to a finite cylinder (Rostamy *et al.*, 2013; Porteous *et al.*, 2014), the flow separates as it travels over the junction of the wing leading edge and the wingtip, which would then give rise to a greater wake deficit, and hence an increased pressure drag. This wingtip flow separation is evident in fig. 36, which depicts the streamlines over the tubercled wing at 0° AOA. Further evidence of this wingtip

flow separation can be seen in figs. 26 to 31 where there are white zones of accumulated ethanol mix near the leading edge.

For the smooth wing, a small circular formation appears in the separated zone indicating the presence of a vortex. This vortex has been labelled the “Leading Edge Vortex” in fig. 28. At 0° AOA, the circular region is located symmetrically about the centreline, but as the AOA increases, it starts to shift towards the pressure side. It should be noted that in all of the smooth wing’s tip figures, a distinct white line runs from the leading edge to the trailing edge. This line does not correspond to any particular flow feature, but to a superficial scratch.

The wingtip vortex rollup and the trailing edge vortex can also be seen in figs. 26 to 31, and have been labelled at 6° and 9° AOAs. At 6° AOA, little difference in either of these flow features exists between the two wings. Bolzon *et al.* (2016, b) found that tubercles did not affect the induced drag of this wing between 0° and 6°, which is consistent with these results. However, at 9° AOA, the wingtip vortex rollup of the smooth wing covers more of the wingtip area, qualitatively suggesting a stronger wingtip vortex, which indicates a greater induced drag. This agrees with Bolzon *et al.* (2016, b), where this smooth wing at 9° AOA produced 8% more induced drag than the tubercled wing.

The leading edge vortex and wingtip vortex rollup features identified in the tubercled wing’s oil film flow visualization are also evident in the CFD results, whereby at 9° AOA, the wall shear and vorticity color plots show signs of the leading edge vortex and of the wingtip vortex rollup along the chord. The surface streaklines of the oil film flow visualization and the color plots of the CFD model bear a strong similarity to the streamline patterns of Werlé shown in fig. 37, with the adjacent primary vortex pair being rotated within its velocity field.

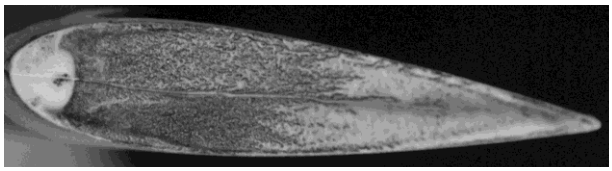

Figure 26: Smooth wing wingtip ethanol mix at 0° AOA, pressure and suction sides at top and bottom of the figure, respectively.

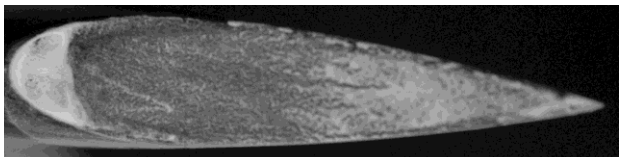

Figure 27: Tubercled wing wingtip ethanol mix at 0° AOA, pressure and suction sides at top and bottom of the figure, respectively.

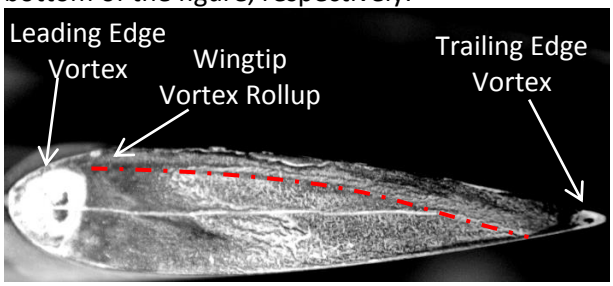

Figure 28: Smooth wing wingtip ethanol mix at 6° AOA, pressure and suction sides at top and bottom of the figure, respectively.

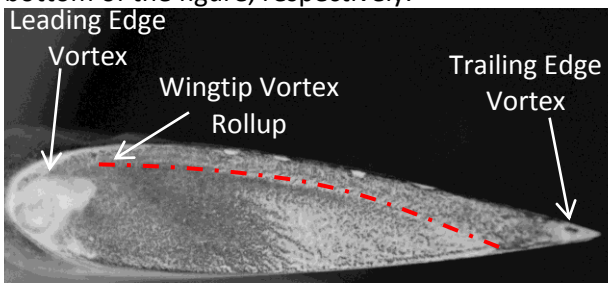

Figure 29: Tubercled wing wingtip ethanol mix at 6° AOA, pressure and suction sides at top and bottom of the figure, respectively.

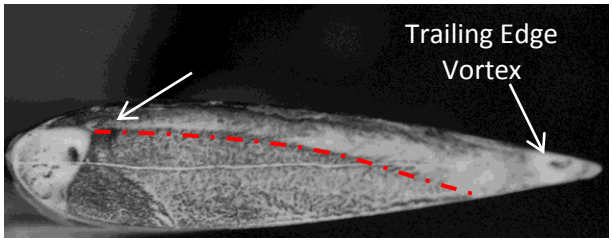

Figure 30: Smooth wing wingtip ethanol mix at 9° AOA, pressure and suction sides at top and bottom of the figure, respectively.

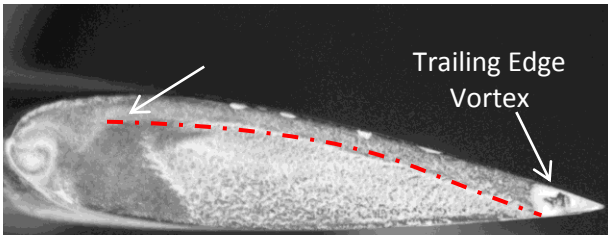

Figure 31: Tubercled wing wingtip ethanol mix at 9° AOA, pressure and suction sides at top and bottom of the figure, respectively.

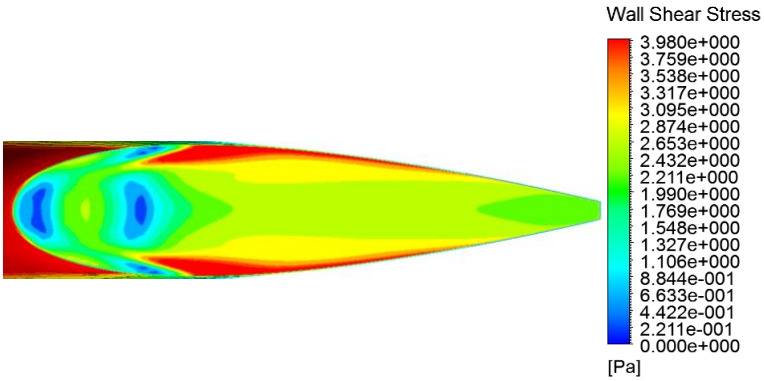

Figure 32: Tubercled wing wingtip wall shear at 0° AOA, pressure and suction sides at top and bottom of the figure, respectively.

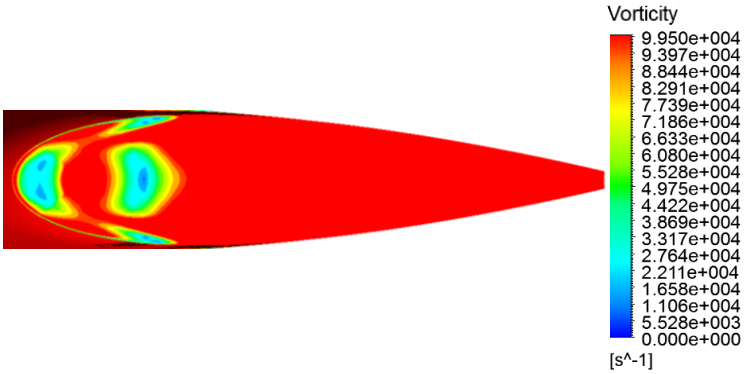

Figure 33: Tubercled wing wingtip vorticity at 0° AOA, pressure and suction sides at top and bottom of the figure, respectively.

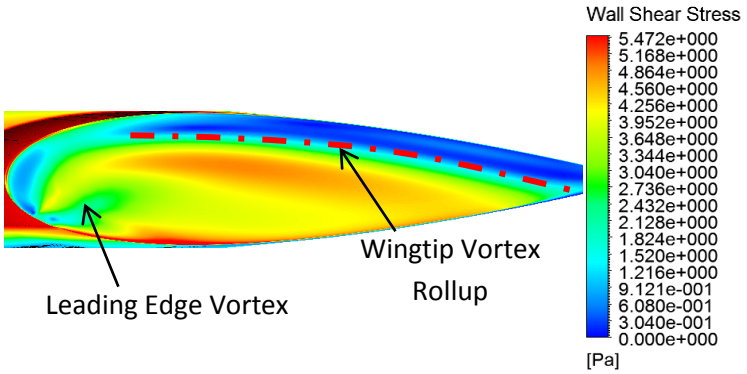

Figure 34: Tubercled wing wingtip wall shear at 9° AOA, pressure and suction sides at top and bottom of the figure, respectively.

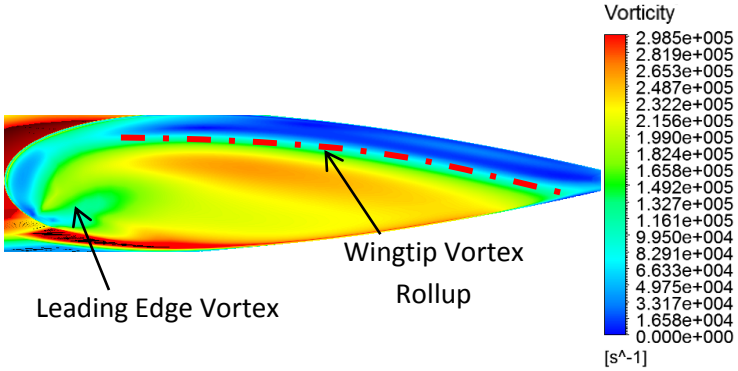

Figure 35: Tubercled wing wingtip vorticity at 9° AOA, pressure and suction sides at top and bottom of the figure, respectively.

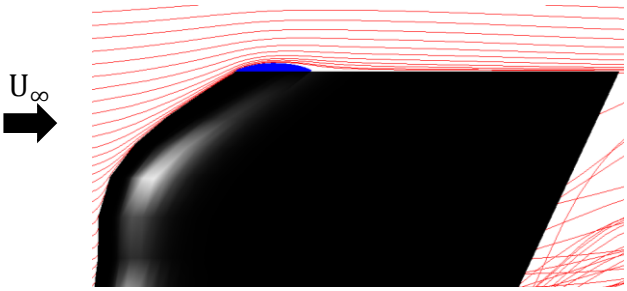

Figure 36: Streamlines over tubercled wing at 0° AOA. Flow separation over the wing leading edge and wingtip surface junction is indicated by the isolation of the blue streamlines from the red streamlines.

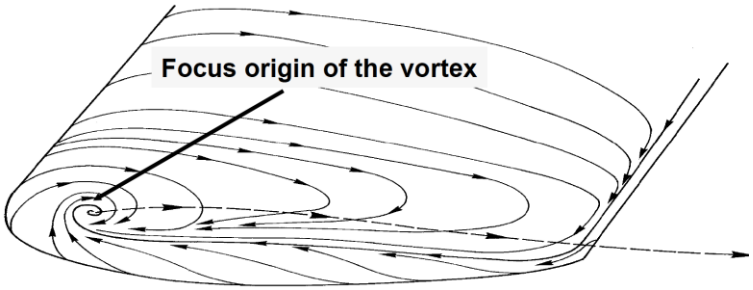

Figure 37: Streamlines on the surface of a wingtip by Werlé (Delery, 2016).

Conclusion:

An oil film flow visualization study was conducted on two NACA 0021 swept and tapered wings, one without tubercles and one with tubercles. The visualization was conducted at a mean aerodynamic chord Reynolds number of 225,000, which resulted in a Laminar Separation Bubble, LSB, forming on the suction side of each wing. A computational fluid dynamics (CFD) model of the tubercled wing was developed at the same mean aerodynamic chord Reynolds number. Both the oil film flow visualization study and the CFD modelling were conducted at 0°, 3°, 6°, 9°, and 12° angles of attack (AOAs).

The flow over the smooth wing, as expected, initially separated at the trailing edge, and the separation line progressed towards the leading edge with increasing AOA. The flow separation pattern on the tubercled wing, on the other hand, was more complicated; the flow behind the troughs tended to separate at a lower AOA than the flow over the smooth wing, however, the flow behind the peaks stayed attached to a higher AOA. This flow separation pattern is consistent with literature detailing unswept tubercled wings, however, this study showed that the wing sweep resulted in an asymmetrical separation pattern about the trough centreline. The flow over the tubercled wing typically separated to a greater degree than the flow over the smooth wing; by 2.5% on average. Furthermore, this study showed that tubercles do compartmentalize the flow, as, at 12° AOA, during the oil film flow visualization the flow behind one tubercle trough completely separated, however, the flow over the rest of the wing was relatively unaffected. Therefore, the stall was confined to one “pocket” and did not spread across the span, as was the case over the smooth wing. Similar displays of compartmentalization were observed in the CFD model. A future direction of investigation into tubercles that has arisen from the flow separation pattern observed, is to investigate if the amount of flow separation can be minimized by reducing the width of the troughs.

The LSB that formed over both the smooth and tubercled wings covered almost the entire span of the wings. The chordwise length of the LSB forming over the smooth wing was relatively uniform along the entire wingspan. Conversely, the LSB over the tubercled wing varied in chordwise length, typically decreasing behind the troughs and increasing behind the peaks. In addition, over the turbercled wing, the LSB formed asymmetrically about the trough centreline. The average chordwise length of the LSB at all AOAs considered over the smooth wing was 26.5% of the local chord, compared to 18.0% and 41.0% of the local chord when present behind the tubercle troughs and peaks, respectively. Additionally, the LSB was closer to the leading edge of the wing behind the troughs when compared with the peaks, which suggested an earlier transition to turbulence.

Therefore, a future investigation into tubercles could focus on manipulating the transition line through manufacturing tubercles in a shape other than one that follows a sine curve. The modulation of the LSB shape and size was consistent with results from studies investigating the effect of vortex generators on LSB formation.

The vortex detachment points associated with each tubercle were identified and found to form behind the troughs. One detachment point was typically larger than the other, which is likely to have been caused by the asymmetry in the strengths of the tubercle vortices. These detachment points progressed towards the tubercled leading edge with increasing AOA. A bifurcation line formed behind the peak of a tubercle and divided the flow downstream of each trough into two distinct sections. The flow in one section moved towards one of the vortices, while the flow in other section moved towards the other. The bifurcation line formed closer to the smaller, and expectedly weaker, vortex detachment point.

Flow visualization and CFD images on the end of the wingtip showed the wingtip vortex rollup. From 0° to 6° AOAs, there was little difference between the two rollup patterns of the two wings. At 9°, the wingtip vortex rollup of the smooth wing covered a greater area than the tubercled wingtip vortex rollup. This qualitatively suggested that the smooth wing had a greater induced drag than the tubercled wing, which was consistent with the quantitative findings of the previous study by the authors. The CFD model showed that the flow separated over the junction of the tubercled wing leading edge and the wingtip surface, before reattaching downstream.

Acknowledgements:

Research undertaken for this report has been assisted with a grant from the Sir Ross and Sir Keith Smith Fund (Smith Fund) (www.smithfund.org.au). The support is acknowledged and greatly appreciated.

The authors acknowledge the editorial assistance from Miss. Alison-Jane Hunter.

References:

Alam, M. and Sandham, N.D., "Direct Numerical Simulation of Short Laminar Separation Bubbles with Turbulent Reattachment", *Journal of Fluid Mechanics*, Vol. 403, pp., 223-250, 2000.

Bolzon, M.D., Kelso, R.M. and Arjomandi, M., "A Review of Tubercles and Their Applications", *The Journal of Aerospace Engineering*, 2015. doi: 10.1061/(ASCE)AS.1943-5525.0000491.

Bolzon, M.D., Kelso, R.M. and Arjomandi, M., "Force Measurements and Wake Surveys of a Swept Tubercled Wing", accepted for publication by *The Journal Aerospace Engineering*, 2016, a.

Bolzon, M.D., Kelso, R.M. and Arjomandi, M., "Formation of Vortices on a Tubercled Wing, and Their Effects on Drag", *Aerospace Science and Technology*, 2016, b. doi: 10.1016/j.ast.2016.06.025.

Counsil, J.N. and Goni Boulama, K.,"Validating The URANS Shear Stress Transport $\gamma - Re_\theta$ Model for Low-Reynolds-Number External Aerodynamics ", *International Journal for Numerical Methods in Fluids*, Vol., 69, pp.1411-1432, 2012.

Delery, J., "Topology of Some Remarkable Three-Dimensional Flows", ONERA. http://www.onera.fr/en/separation-in-threedimensional-flow-critical-points-separation-lines-and-vortices, accessed 13-04-2016.

Gaster, M., "The Structure and Behaviour of Laminar Separation Bubbles", *Aerodynamics Division N.P.L.*, Ministry of Technology, 1969.

Hansen, K.L., “Effect of Leading Edge Tubercles on Airfoil Performance”, Ph.D. Thesis, The University of Adelaide, S.A., Aus., February 2012.

Hansen, K.L, Kelso, R.M., and Dally, B.B., “Performance Variations of Leading-Edge Tubercles for Distinct Airfoil Profiles”, *AIAA Journal*, Vol. 49, No. 1, pp. 185-194, 2011, doi: 10.2514/1.J050631.

Hansen, K.L, Kelso, R.M., Choudhry, A., and Arjomandi, M., “Laminar Separation Bubble Effect on the Lift Curve Slope of an Airfoil”, *19th Australasian Fluid Mechanics Conference*, 8th-11th December 2014, Melbourne.

Hansen, K.L, Rostamzadeh, N., Kelso, R.M, and Dally, B.B., “Evolution of the Streamwise Vortices Generated Between Leading Edge Tubercles”, *Journal of Fluid Mechanics*, Vol., 788, pp.730-766, 2016.

Johari, H., Henoch, C., Custodio, D., and Levshin, A., “Effects of Leading-Edge Protuberances on Airfoil Performance”, *AIAA Journal*, Vol. 45, No. 11, pp. 2634-2642, 2007, doi:10.2514/1.28497.

Kerho, M., Hutcherson, S., Blackwelder, R.F. and Liebeck, R.H., “Vortex Generators Used to Control Laminar Separation Bubbles”, *Journal of Aircraft*, Vol. 30, No. 3, May-June, pp. 315-319, 1993.

Kerschgens, B., “Ähnlichkeitstheoretische Adaption eines Buckelwal-Flossenprofils für den Einsatz in kompressiblen Medien und anschließende Untersuchung der resultierenden Geometrie mittels CFD”, Study, Institut für Strahlantriebe und Turboarbeitsmaschinen, Aachen, 2008.

Menter, F.R., “Two-Equation Eddy-Viscosity Turbulence Models for Engineering Applications”, *AIAA Journal*, Vol. 32, No. 8, pp.1598-1605, 1994.

Merzkirch, W., “Flow Visualization”, *Academic Press*, 2nd Edition, Orlando, Florida, 1987, pp. 82-87.

Miklosovic, D. S., Murray, M. M., Howle, L. E. and Fish, F. E., “Leading-edge Tubercles Delay Stall on Humpback Whale (Megaptera Novaeangliae) Flippers”, *Physics of Fluids*, Vol. 16, No. 5, 2004, pp. L39-L42, doi:10.1063/1.1688341.

Nakayama, Y., Woods, W.A., and Clark D.G., “Visualized Flow: Fluid Motion in Basic and Engineering Situations Revealed by Flow Visualization”, *Pergamon Press*, United Kingdom, 1988, pp. 92-93.

Pedro, H.T. and Kobayashi, M.H., “Numerical Study of Stall Delay on Humpback Whale Flippers”, AIAA *Aerospace Sciences Meeting and Exhibit*, 7th-11th January 2008, Reno.

Polhamus, E.C., “A Survey of Reynolds Number and Wing Geometry Effects on Lift Characteristics in the Low Speed Stall Region”, *NASA Contractor Report 4745*, 1996.

Porteous, R., Moreau, D.J. and Doolan, C.J., “A Review of Flow-Induced Noise From Finite Wall-Mounted Cylinders”, *Journal of Fluids and Structure*, Vol. 51, pp. 240-254, 2014. doi: 10.1016/j.jfluidstructs.2014.08.012.

Roberts, W. B., “Calculation of Laminar Separation Bubbles and Their Effect on Airfoil Performance”, *AIAA Journal*, Vol. 18, No. 1, 1980. doi: 10.2514/3.50726

Rostamy, N., Sumner, D., Bergstrom, D.J. and Bugg, J.D., “Instantaneous Flow Field above the Free End of Finite-Height Cylinders and Prisms”, *International Journal of Heat and Fluid Flow*, Vol. 43, pp. 120-128, 2013. doi: 10.1016/j.ijheatfluidflow.203.04.005.

Rostamzadeh, N, Hansen, K.L., Kelso, R.M. and Dally, B.B., “The Formation Mechanism and Impact of Streamwise Vortices on NACA 0021 Airfoil’s Performance with Undulating Leading Edge Modification”, *Physics of Fluids*, Vol. 26, 2014, No. 107101, doi:10.1063/1.4896748

Seshagiri, A., Cooper, E. and Traub, L.W., “Effects of Vortex Generators on an Airfoil at Low Reyonlds Numbers”, *Journal of Aircraft*, Vol. 46, No. 1, pp. 116-122, Jan-Feb 2009. doi: 10.2514/1.36241.

Skillen, A., Revell, A., Pinelli, A. Piomelli, U., and Favier, J., “Flow Over a Wing with Leading-Edge Undulations”, *AIAA Journal*, Vol. 53, No. 2, 2014. doi:10.2514/1.J053142.

Stanway, M.J., “Hydrodynamic Effects of Leading-Edge Tubercles on Control Surfaces and in Flapping Foil Propulsion”, M.S. Thesis, Massachusetts Institute of Technology, MA, February 2008.

Stein, B. and Murray, M.M., “Stall Mechanism Analysis of Humpback Whale Flipper Models”, *Unmanned Untethered Submersible Technology (UUST)*, Autonomous Undersea Systems Inst., Lee, NH, 2005.

Van Nierop, E.A., Alben, S., and Brenner, M.P., “How Bumps on Whale Flippers Delay Stall: An Aerodynamic Model”, *Physical Review Letters*, Vol. 100, 2008. doi:10.1103/PhysRevLett.100.054502.

Watts, P. and Fish, F.E., “The Influence of Passive, Leading Edge Tubercles on Wing Performance”, *Unmanned Untethered Submersible Technology (UUST)*, Autonomous Undersea Systems Inst. , Lee, NH, Aug 2001.

Chapter 5

Optimising a Tubercled Wing Geometry

This chapter includes the following journal article:

Bolzon, M.D., Kelso, R.M. and Arjomandi, M., "Leading Edge Tubercles: A Parametric and Optimization Study", *submitted to Journal of Aerospace Information and Systems*, 2016.

The effects of tubercles on the swept wing's lift and drag coefficient and components of drag at pre-stall AOAs, have been found, thereby fulfilling the first two aims of this thesis. In addition, the effects of tubercles on the flow physics over a wing have been found, thereby elucidating reasons for the previously described tubercle effects. In accordance with the third aim of this thesis, this chapter describes an analysis of the effects of a tubercle's amplitude, wavelength, and phase on the lift coefficient, induced drag coefficient, and the lift-to-induced-drag ratio of an unswept wing at low AOAs. An unswept wing was chosen as the author had readily available experimental lift coefficient data for the semi-infinite and finite cases, which were required for the model and for validation, respectively. The model chosen for the parametric analysis, Prandtl's lifting-line theory, LLT, was satisfactory, given the flow conditions and computational requirements. A Genetic Algorithm, GA, was used to optimise the tubercle's amplitude, wavelength, phase, location, and number to produce the greatest lift-to-induced-drag ratio for the unswept wing.

The study concludes that the tubercle phase typically has the greatest effect on the wing's lift coefficient, induced drag coefficient, and lift-to-induced-drag ratio, whereas the wavelength tends to have the least. The tubercle configuration that produces the greatest lift-to-induced-drag ratio is one that essentially represented a notched wingtip.

From the results presented in this chapter, it is understood how a tubercle's geometry affects a wing's performance. Furthermore, by adhering to the trends described in this chapter, tubercles can now be designed to maximise a wing's lift coefficient or lift-to-induced-drag ratio, or minimise a wing's induced drag coefficient. The study described in this chapter showed that the tubercle

geometry does not affect the lift coefficient, induced drag coefficient, and lift-to-induced-drag ratio in the same fashion. Therefore, the relative effects of the tubercle geometric parameters on these wing performance parameters described in this chapter produce a framework for designing tubercles when optimising multiple wing performance parameters.

The final work described in this thesis completes the fulfilment of the third aim, whereby it is determined whether similar wing performance benefits to those observed throughout this thesis can be achieved with fewer tubercles. Once this is determined, accurate assessments of the benefits of tubercles for a given application can be made.

Statement of Authorship

Title of Paper	Leading Edge Tubercles: A Parametric and Optimization Study
Publication Status	☐ Published ☐ Accepted for Publication ☑ Submitted for Publication ☐ Unpublished and Unsubmitted work written in manuscript style
Publication Details	Bolzon, M.D., Kelso, R.M. and Arjomandi, M., "Leading Edge Tubercles: A Parametric and Optimization Study", *submitted to Journal of Aerospace Information and Systems*, 2016.

Principal Author

Name of Principal Author (Candidate)	Michael Bolzon		
Contribution to the Paper	Developed numerical model and optimisation code, processed data, wrote manuscript, and acted as corresponding author.		
Overall percentage (%)			
Certification:	This paper reports on original research I conducted during the period of my Higher Degree by Research candidature and is not subject to any obligations or contractual agreements with a third party that would constrain its inclusion in this thesis. I am the primary author of this paper.		
Signature		Date	

Co-Author Contributions

By signing the Statement of Authorship, each author certifies that:

i. the candidate's stated contribution to the publication is accurate (as detailed above);

ii. permission is granted for the candidate in include the publication in the thesis; and

iii. the sum of all co-author contributions is equal to 100% less the candidate's stated contribution.

Name of Co-Author	Richard Kelso		
Contribution to the Paper	Supervised numerical development, aided interpretation of results, and reviewed manuscript.		
Signature		Date	

Name of Co-Author	Maziar Arjomandi		
Contribution to the Paper	Supervised numerical development, aided interpretation of results, and reviewed manuscript.		
Signature		Date	

Leading Edge Tubercles: A Parametric and Optimization Study

Michael D. Bolzon[1], Richard M. Kelso[2], and Maziar Arjomandi[3]
The University of Adelaide, Adelaide, South Australia, Australia, 5005

Prandtl's lifting-line theory was implemented to determine the effects of a tubercle's amplitude and wavelength on the lift coefficient, the induced drag coefficient, and the lift-to-induced-drag ratio of an unswept NACA 0021 wing at an angle of attack of 3°, and at a Reynolds number of 120,000. In addition, a new tubercle design parameter was introduced and investigated; the point along a tubercle at which a wing terminates. This parameter is termed the phase of the tubercles. It was found that the phase of the tubercles has the greatest effect on the lift coefficient, the induced drag coefficient, and the lift-to-induced-drag ratio, while the wavelength has the least. The lift-to-induced-drag ratio is predicted to increase by as much as 6.8% for the considered tubercle geometries compared with the smooth wing. A genetic algorithm was employed to optimize the tubercle's amplitude, wavelength, phase, the location, and number of the tubercles along the wingspan in order to produce the greatest lift-to-induced-drag ratio. The highest lift-to-induced-drag ratios were achieved by halves of tubercles implemented near the wingtip, which essentially resulted in a notched wing configuration. This configuration of tubercles was predicted to increase the lift-to-induced-drag ratio by up to 4.3% over the smooth wing equivalent. The trends found at an angle of attack of 3° were also found to be applicable at lower angles of attack.

Nomenclature

A = tubercle amplitude

AR = wing aspect ratio

b = wingspan

[1] Ph.D. Candidate, The School of Mechanical Engineering, North Terrace, Adelaide, Australia, 5005, and AIAA student member.
[2] Associate Professor, The School of Mechanical Engineering, North Terrace, Adelaide, Australia, 5005.
[3] Associate Professor, The School of Mechanical Engineering, North Terrace, Adelaide, Australia, 5005.

c = chord

C_{D_I} = induced drag coefficient

$C_{L_{Wing}}$ = wing lift coefficient

$\bar{C}_n$ = a segment's mean geometric chord

C_{L_α} = segment's lift-curve slope

h_{max} = wing camber

n = segment

V = freestream velocity

X = coefficient

α = geometric angle of attack

α_0 = zero-lift angle of attack

Γ = circulation

Γ_i = ith segment circulation

Θ_i = ith segment angle

λ = tubercle wavelength

μ = grouping parameter

Φ = phase

I. Introduction

Tubercles on the leading edge of a lifting surface have received much attention recently as they can soften and delay stall [1,2], as well as increase a wing's efficiency at pre-stall angles of attack [3,4]. Tubercles can be found in the natural world, such as on Humpback whale pectoral flippers, and it is now known these tubercles are responsible, in part, for the Humpback whale's agility. Several studies have demonstrated that tubercles create pairs of counter-rotating, streamwise vortices [5-7]. The flow mechanisms that tubercles introduce are relatively complex, however, there is substantial evidence to support two mechanisms [8]. The first mechanism is that tubercles "compartmentalize" the flow thereby creating "pockets" of flow in the troughs. The result is that if the flow in one pocket separates, the flow in neighboring regions are not affected [9,10]. This allows the lifting surface to produce more lift during stall than a smooth leading edge wing. The second flow mechanism is that tubercles act in a similar

fashion to vortex generators, whereby in the regions of common downwash, higher momentum flow is mixed into the boundary layer, which delays separation [2,5,10].

The pre-stall regime is of high importance as many potential tubercle applications operate in this regime. One of the few studies investigating the pre-stall effects of tubercles on wing performance demonstrated that tubercles can increase the lift-to-drag ratio by up to 6% when tubercles were implemented on a swept wing [3,4]. This ratio depends on the lift and drag coefficients of the wing, and while tubercles reduced the lift coefficient of the swept wing considered, they reduced the drag coefficient to a greater extent. A subsequent study by Bolzon *et al.* [11] was performed on the same two wings that Bolzon *et al.* [3,4] investigated. This study showed that the total drag coefficient increased in the troughs and decreased over the peaks, thereby creating a modulation effect along the entire span of the wing.

A tubercle geometry is typically characterized by two main parameters; the amplitude and the wavelength, where the amplitude refers to the chordwise distance between a tubercle peak and trough, and the wavelength refers to the spanwise distance between two adjacent tubercle peaks or troughs, as shown in Fig. 1 a). However, there is a third parameter that has been previously overlooked; the point along a tubercle that a wing terminates, as shown in Fig. 1 b). This parameter will be termed the phase for the remainder of this study. If, for example, a wing terminates at a tubercle peak, then the phase of the tubercles is $6\pi/12$. The only parametric analyses of the effects of the tubercle geometry on wing performance conducted thus far, were limited to investigating the tubercle amplitude and wavelength [12-15]. In addition, due to the experimental nature of these investigations [12-15], relatively few geometries were considered. Furthermore, these studies largely focused on the stall regime of the wing [12-15], leaving the effects of a tubercle's geometry on wing performance in the pre-stall regime largely unconsidered. Therefore, it is currently difficult to design a tubercle geometry to fulfil wing performance requirements. This study, through the use of Prandtl's lifting-line theory, LLT, will parametrically analyze the effects of a tubercle's amplitude, wavelength, and phase on the wing's lift coefficient, induced drag coefficient, and the lift-to-induced-drag ratio.

Since the pioneering fluid mechanics study of tubercles by Watts and Fish [9], it has been largely assumed that tubercles refer to leading edge protuberance that extend along the entire span of a given lifting surface. To the authors' knowledge, only Yoon *et al.* [16] and Corsini *et al.* [17] have investigated the effects of tubercles spanning a fraction of the leading edge on wing performance. Yoon *et al.* [16] found that the effects of tubercles on the lift and

drag coefficients varied with the spanwise extent of tubercles along the leading edge. Tubercles on the outboard 20% of the wingspan conferred similar stall characteristics to a smooth wing. Tubercles on the outboard 40% or more of the wingspan softened the stall. Corsini *et al.* [17] found that tubercles located near the wingtip can positively affect the wing performance during stall. Neither study found any pre-stall improvements when tubercles are implemented. One limitation of these studies is that they did not consider the tubercles' locations. For example, it is not known whether tubercles located in the middle 20% of the span produce different effects on the wing performance to placement at the tip of the wing. If tubercles can be placed along a smaller, but strategically located, portion of the leading edge, manufacturing and retrofitting costs will probably decrease. In addition, more applications may utilize tubercles due to improved benefit versus cost. Therefore, a complete analysis of tubercles should include variations in the amplitude, wavelength, phase, the location of tubercles, and the number of tubercles. In this paper, optimization of these five parameters with respect to the lift-to-induced-drag ratio will be achieved through the use of a Genetic Algorithm, GA, combined with the LLT.

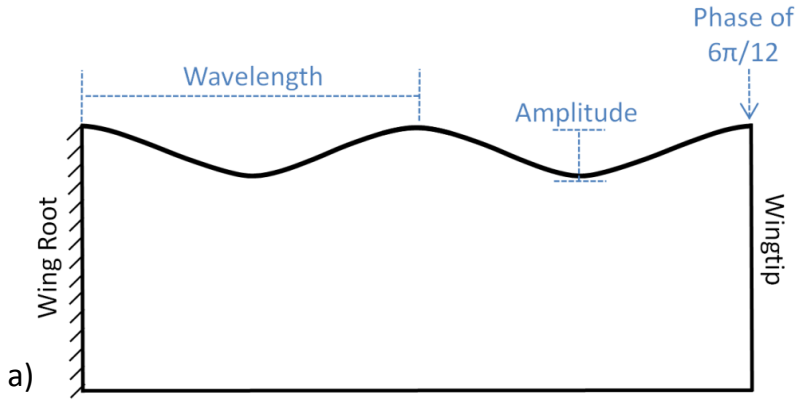

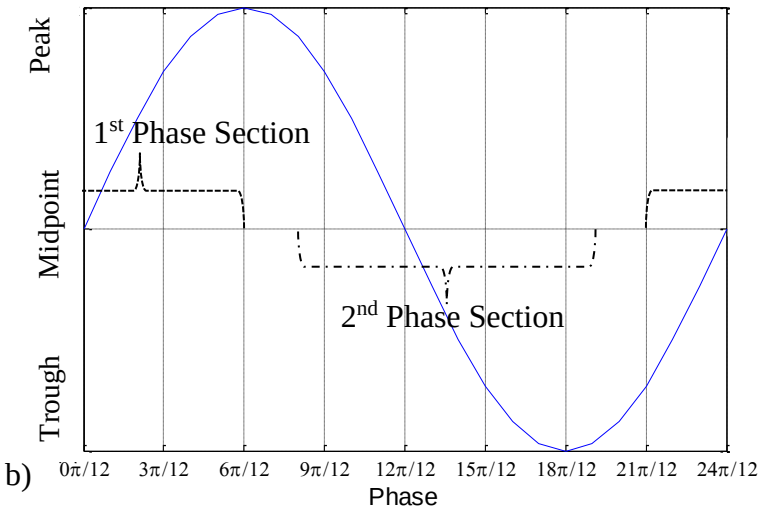

Fig. 1 The tubercled wing geometric parameters, a), and the point along the tubercle at which a wing will terminate given a specified phase, b).

II. Method

A. Lifting-Line Theory

The wing modelled was the same as that used in the experiments by Hansen [12]. This wing was an unswept, untapered NACA 0021 half-span wing profile. The half-span was 247.5mm, and the chord was 70mm, as presented in Fig. 2. For the simulation, only half of the wing was modelled as the smooth leading edge wing is symmetrical about the centreline. Tubercles were employed along the entire leading edge of the wing, and a parametric analysis of the tubercle amplitude, wavelength, and phase was performed using Prandtl's LLT. By knowing the wing planform shape, size, and the two-dimensional lift-curve slope, this theory allows, among other parameters, the calculation of the lift and the induced drag coefficients of a finite wing. A detailed explanation of the simulation process can be found in Houghton *et al.* [18]. A general outline of the process used is provided below.

Initially the wing is divided into N segments, as shown in Fig. 2. It should be noted that the segments depicted in Fig. 2 are for illustrative purposes. Typically, the wing segments become smaller towards the wingtip to better predict the faster changing circulation. Equations (1), (4), and (5) are used to find the circulation distribution, the lift and induced drag coefficients of the wing, respectively. Equations (2) and (3) show how to calculate the unknowns for Eqs. (1), (4), and (5). Equation (2) is known as the "Monoplane Equation". The X_n coefficients are found from

Eq. (2), the segment angle is depicted in Fig. 2, The zero-lift angle of attack is a function of the wing, the geometric angle of attack is a user-specified variable, and the segment's lift-curve slope is found from the two-dimensional lift characteristic.

$$\Gamma_i = 2bV\sum_{n=1}^{N} X_n \sin(n\theta_i) \tag{1}$$

$$\mu(\alpha_0 - \alpha) = \sum_{n=1}^{N} X_n \sin(n\theta_i)\left(1 + \frac{\mu n}{\sin\theta_i}\right) \tag{2}$$

$$\mu = \frac{\overline{C_n} C_{L_\alpha}}{4b} \tag{3}$$

$$C_{L_{Wing}} = \pi AR X_1 \tag{4}$$

$$C_{D_I} = \pi AR\sum_{n=1}^{N} nX_n^{\,2} \tag{5}$$

Despite being a relatively simple method for numerically determining the circulation distribution, the lift and the induced drag coefficients of a wing, the LLT is accurate for simple planform shapes, such as unswept wings [19]. Furthermore, this method is computationally inexpensive, which makes it ideal for a thorough parametric analysis. However, for more complex planform shapes, such as highly swept and tapered wings operating under compressible flow conditions, this theory becomes inadequate. This study investigated tubercles on an unswept, untwisted, and untapered wing at pre-stall angles of attack, therefore, Prandtl's LLT was suitable. The two-dimensional lift-curve slope was obtained from Hansen's experimental data [12], however, instead of using an average value for the entire data set, the lift-curve slope was calculated for each angle of attack. This method of calculating the lift-curve slope was chosen because it typically provides a more accurate lift coefficient prediction. The lift-curve slope was calculated using the central difference scheme. It should be noted that the LLT is an inviscid model and so flow separation cannot be predicted. Therefore, only pre-stall angles of attack, AOAs, are considered.

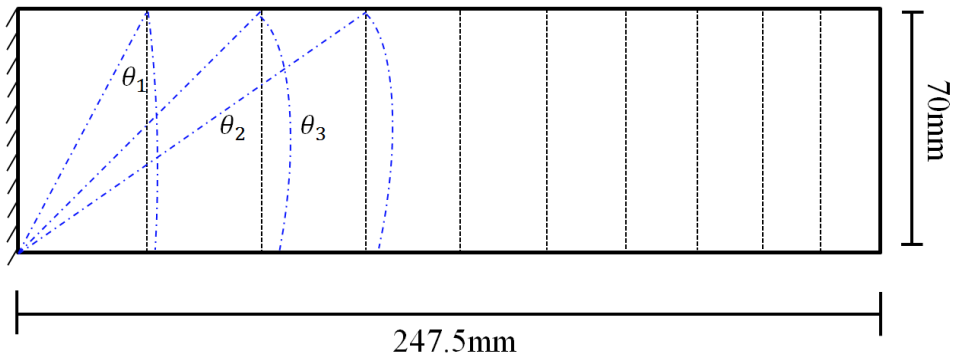

Fig. 2 Diagram of the half-span wing model illustrating a typical segmentation and the corresponding segment angle of the first three segments. Here the wing is divided into 10 segments.

The tubercles' amplitudes ranged from 0mm to 20mm. A maximum amplitude of 20mm was chosen as this corresponds to 29% of the wing chord, and as the LLT performs inadequately for swept wings, a larger amplitude would increase the local leading edge sweep, which would result in a larger inaccuracy. Therefore, 20mm was a satisfactory compromise. The wavelength ranged from 0mm to 495mm. As the wavelength increases past 247.5mm the wing begins to approximate a tapered wing. The phase ranged from 0 to 2π. The amplitude, wavelength, and phase were all incremented systematically through their respective ranges, and the amplitude, wavelength, and phase ranges were divided into 40, 33, and 25 equally-incremented points, respectively. Figure 3 shows a segment-independency study of a smooth wing and a tubercled wing with tubercles having an amplitude of 20mm a wavelength of 15.47mm, a phase of 0 π, and spanning the entire leading edge. It was found that 1000 segments or more results in the lift coefficient, induced drag coefficient, and the lift-to-induced-drag ratio converging for the smooth and tubercled wings. This tubercle geometry has the greatest gradient between the tubercle peak and trough out of all of the geometries tested in the Parametric Analysis section of this study. Therefore, the number of segments required to produce a segment-independent lift coefficient, induced drag coefficient, and a lift-to-induced-drag ratio for this geometry is expected to be suitable for the other tubercle geometries modelled. The model will be divided into 2000 segments for the remainder of this study because the GA optimization considers larger amplitude-to-wavelength ratio tubercles. The 2000 segments followed a cosine spacing distribution and became more densely populated near the wingtip.

The experiment by Hansen [12] was conducted at a freestream velocity of 25 m/s, giving a Reynolds number of approximately 120,000. This freestream velocity was used for the numerical simulations. The parametric analysis

and GA optimization were conducted at a 3° AOA, as this corresponds to a typical low angle of attack application, such as airplanes in cruise. Furthermore, as will be explained in the Model Validation section, 3° AOA was a suitable choice for this study.

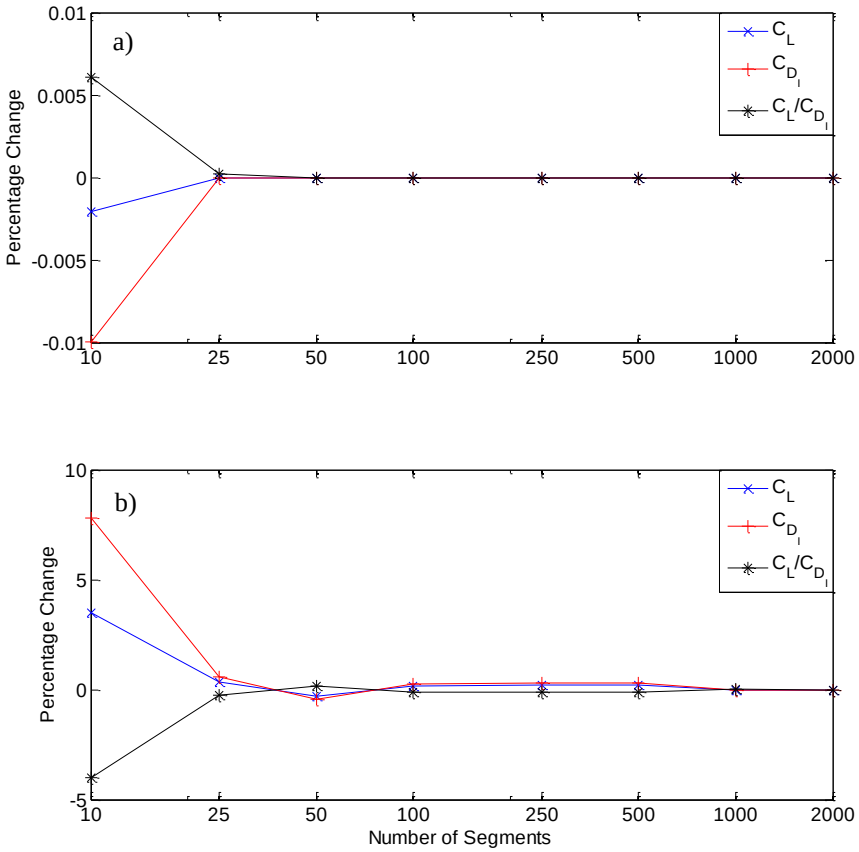

Fig. 3 Segment independency test for the smooth wing, a), and the tubercled wing, b), at a 3° angle of attack. The tubercle configuration is A20λ15.47Φ0π, with tubercles along the entire leading edge. The y-axis is expressed as a percentage change to the results of the 2000 segment models.

B. Genetic Algorithm Optimization

While the parametric analysis considered the effects on the wing performance of three tubercle variables; the amplitude, the wavelength, and the phase, the tubercle location and the number of tubercles, were not considered. Two problems arise by attempting to conduct a parametric analysis on the effects of five tubercle variables on a wing's lift coefficient, induced drag coefficient, and lift-to-induced-drag ratio. The first is that the analysis becomes much larger and is computationally more expensive. The second problem is that concisely representing, interpreting, and using the results is difficult, with many three-dimensional graphs required. Therefore, an optimization approach

is necessary. The optimization technique chosen was a GA. While other optimization techniques are available, the GA technique was chosen as it has the ability to produce a novel solution space while maintaining diversity among the specimens. In addition, the GA technique is suited to operating on several variables. The principle of a GA is that an initial sample space of specimens is randomly chosen. These specimens are assigned a "fitness" based on their ability to fulfil a given function. Next, a new sample space is produced based on the fitness of the previous "generation" sample space [20]. This process is continued until a certain criterion, or criteria, is met. While the basic principle of a GA is simple, there are many variations that can be implemented to produce a suitable algorithm. The range of options is not detailed here, but the options implemented are discussed below. If the reader is interested in the possible range of options of a GA, Whitley [20] provides an excellent introduction, and Holland [21] clearly presents the concept of GAs and their origins in nature.

Five tubercle parameters were optimized by the GA to give tubercle geometries that produce the highest wing lift-to-induced-drag ratio; the amplitude, the wavelength, the phase, the location of the tubercles, and the number of tubercles. The amplitude ranged from 0mm to 20mm, like in the Parametric Analysis section. Whereas, while in the parametric analysis the wavelength was allowed to range from 0mm to the entire span of the wing, 495mm, preliminary GA optimizations revealed that such a wide range resulted in the solution space converging on a wavelength comparable to the span of the wing, which resulted in a tapered wing planform. This solution space, arguably, is no longer in the tubercle family. To direct the solution space towards a planform that is arguably more like tubercles, the wavelength was limited to ½ of the span; 247.5mm. The phase of the tubercles was unbounded; 0π to 2π, and the tubercles could start anywhere along the span of the leading edge. There could be as few as 0 tubercles, or as many as the remainder of the span divided by the wavelength permitted. It should be noted that there could even be a fraction of a tubercle, for example 2.13 tubercles. While this allowance in the number of tubercles gives a more complete sample space, a problem arises; if the tubercles are allowed to terminate on a phase that is not $0\pi/12$ or $12\pi/12$, then a discontinuity in the wing chord forms, where the wing chord without tubercles is 70mm and the adjacent tubercle chord is not 70mm. To prevent this from occurring, a "failsafe" rule was implemented such that if the tubercles produced a discontinuity in the wing chord, the number of tubercles was set to 0, which resulted in a smooth wing. The risk of this failsafe is that the smooth wing configuration may permeate through the generations and potentially dominate the final solution space. To prevent this from occurring, the probability of a smooth wing configuration advancing to the next generation was set to a very small percentage, 0.001%. This then

resulted in the other non-smooth wings having a proportionally higher probability of advancing to the next generation. It should be noted that the tubercles could only exist in *one* continuous section of the wing and could not exist at two or more separate locations along the wingspan. The remainder of this section outlines the GA optimization process employed, which includes the initial sample space, the fitness function and probability assignment, and the development of the next generation. The general process is presented in Fig. 4. The preservation of diversity among the tubercled wing specimens was a key factor in developing the solution space and several efforts were made to do so.

1. Initial Sample Space

The five parameters that the GA optimized to produce the greatest lift-on-induced-drag ratio tubercle specimens can be thought of as five bits of information, where each bit corresponds to one of the parameters. A general rule of thumb of a GA optimization is to have a sample space that is at least 2^N samples in size, where N is the number of bits [20]. For this GA optimization, a sample space of 50 tubercled wings was chosen, which exceeds the 2^5 minimum recommendation. This sample space was chosen randomly. The lift coefficient, the induced drag coefficient, and the lift-to-induced-drag ratio were calculated for each specimen.

2. Fitness and Probability Assignment

The fitness of each specimen was calculated by dividing its lift-to-induced-drag ratio by the average lift-to-induced-drag ratio of the given generation. The probability of each specimen either proceeding to the next generation, which can also be thought of as breeding, was determined by dividing the fitness of each specimen by the total fitness of the given generation. The probabilities were then proportionally altered, as mentioned earlier, such that a smooth wing had virtually no chance of proceeding to the next round.

3. Development of the Next Generation

Typically in a GA, two specimens breed to produce a new specimen for the next generation. However, for this GA, a combination of sexual and asexual breeding was implemented, such that half of the new generation originated from one type and the other half from the other type of breeding. The sexual breeding preceded the asexual breeding, as presented in Fig. 4. This method was chosen due to the potential production of specimens that would activate the failsafe. This would then result in the given wing being assigned a 0 for the number of tubercles, i.e. becoming a smooth wing.

By allowing half of the new generation to form through asexual breeding, there was less chance of the smooth wing configuration dominating the GA optimization. For the sexual breeding, the "parents" were selected based on the specimens' probability values. Typically, the "offspring" is produced from two parents by aligning their bits and randomly choosing a point where any bits proceeding this point were inherited from one parent and any bits after this point were inherited from the other parent. However, to accelerate the evolutionary process and promote diversity, each bit was randomly selected from one of the two parents. The asexual breeding was relatively simple, where, based on probability, a specimen from the current generation was chosen and replicated in the new generation. However, to promote diversity, each specimen was only allowed to be selected once. In order to further promote diversity, the probability of each potential parent specimen was recalculated based on the original probability *and* the difference between a given specimen's parameters and all of the new generations' parameters. In order to recalculate the new probabilities, eq. 6 was used. The diversity of a given parameter was calculated by summing the differences between a given specimen's parameter and the offsprings' parameters. The diversity was then normalized to the sum of the potential parents' diversities for the given parameter.

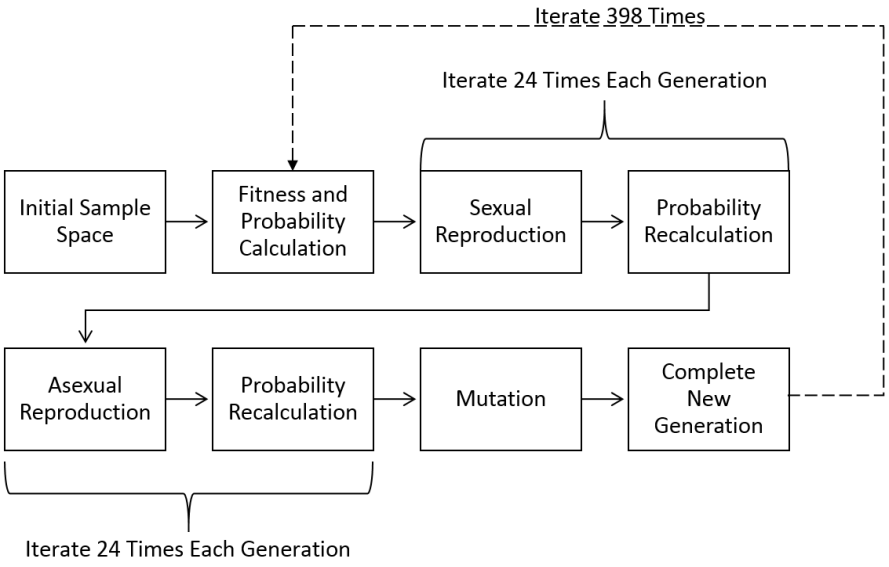

Fig. 4 Flowchart of the genetic algorithm optimization process.

The final operation employed to develop the next generation was mutation. Mutation was employed to increase the diversity of the specimens, as using a random mutation allows the potential for particular bit values that "died out" in previous generations to occur again. Mutation also allows for new bit values, that may have otherwise

remained unconsidered, to influence the evolutionary direction. Often the probability of a bit mutating is in the order of 1% [20], however, it was found that for this particular application, a probability of 10% produced a good trade-off between increasing the diversity of the specimens and maintaining a stable evolution. Furthermore, for mutation probabilities above 10%, more specimens had smooth leading edges as the failsafe was incurred more frequently. The mutation operation was implemented by randomly generating a number between 0 and 1 for each bit. If the number was less than 0.1, then the bit mutated. If the mutation took place, the new bit was recalculated in the same way as was initially done. The GA was iterated 398 times, which resulted in a total of 400 generations.

$$\begin{aligned} Probability = {} & 0.75\ x\ Probability + 0.05\ x\ Amplitude\ Diversity \\ & + 0.05\ x\ Wavelength\ Diversity + 0.05\ x\ Phase\ Diversity \\ & + 0.05\ x\ Tubercle\ Fraction\ Diversiy + 0.05\ x\ Location\ Diversity \end{aligned} \tag{6}$$

III. Lifting-Line Theory Model Validation

The wing planform for the simulation was chosen to match that of Hansen [12] as there are two-dimensional and three-dimensional experimental data on the lift coefficient of this particular smooth leading edge wing. The LLT requires a two-dimensional lift-curve slope input and it outputs a three-dimensional lift coefficient. Therefore, the lift-curve slope can be obtained from the two-dimensional experimental data [12], while a validation of the numerical simulation can be performed by using the three-dimensional experimental data [12]. Figure 5 shows the lift coefficient of the smooth wing calculated from the numerical simulation, the three-dimensional experimental data from Hansen [12], and the ideal lift-curve as calculated from Eq. (7), where α is in radians**.** Good agreement between all three results exists for angles of attack below 4° AOA, however, above 4° AOA a divergence of the Hansen [12] data occurs. The experiment by Hansen [12] was conducted in the transitional regime. The data presented shows an increase in the lift-curve slope, which can also be seen in Fig. 5 past 4° AOA, and it was deduced that this increase was due to the formation of a laminar separation bubble on the suction side of the wing [12]. This bubble effectively increased the camber of the wing, which resulted in a greater lift production [12,22]. Due to the relatively sparse lift coefficient data, the lift-curve slopes calculated from Hansen's experimental data [12] were not sufficient to allow the LLT to mimic this trend, therefore, deviation of the LLT lift coefficient from Hansen's data [12] at angles of attack greater than 4° AOA is expected. As there is good agreement between the

LLT lift coefficient results and Hansen's experimental data [12] below 4° AOA, this regime is optimal for the numerical simulation. It should also be noted that there is good agreement between the lift coefficients calculated by the LLT and the ideal lift coefficients for this NACA 0021 wing, as shown in Fig. 5.

Figure 6 shows the calculated induced drag coefficient from the LLT and a quadratic line-of-best-fit. In the pre-stall regime, the induced drag is proportional to the square of the angle of attack. Figure 6 shows that there is very good agreement between a quadratic line-of-best-fit and the induced drag coefficient. Therefore, the induced drag is proportional to the square of the angle of attack, as required. From Figs. 5 and 6, it is concluded that within the scope of this investigation, the LLT is applicable and the results obtained by its use are of value.

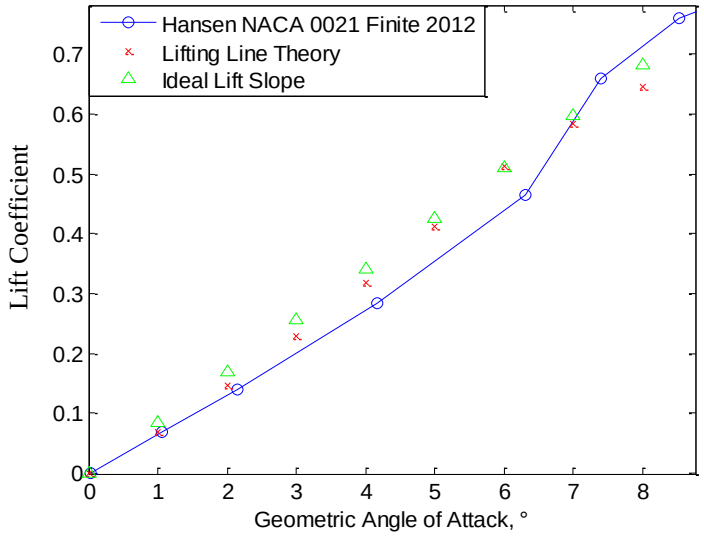

Fig. 5 Lift coefficient validation of the lifting-line theory with Hansen's experimental data [12], and the ideal lift slope of the smooth wing.

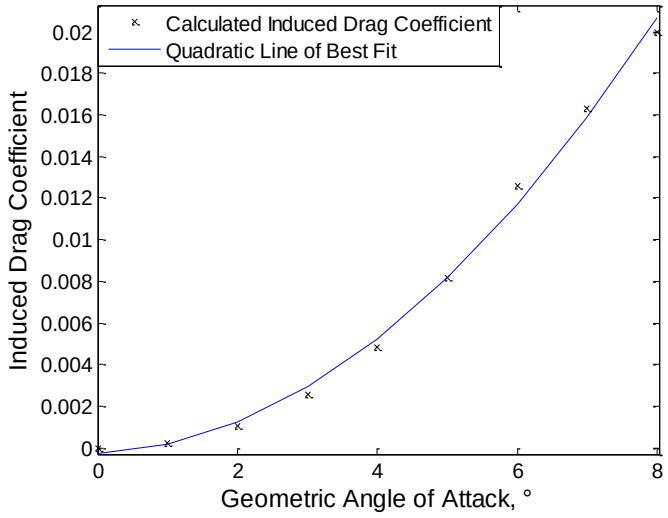

Fig. 6 Induced drag coefficient of the smooth wing as calculated by the lifting-line theory.

$$C_L = \frac{2\pi\left(\alpha + \frac{2h_{\max}}{c}\right)}{1 + \frac{2}{AR}} \tag{7}$$

IV. Results

A. Parametric Analysis

Perhaps, the most important effect of tubercles is their effect on the circulation distribution over a wing, as this distribution dictates the lift and induced drag coefficient productions. Figure 7 shows that for a smooth wing, the circulation distribution is, as expected, relatively uniform with a maximum at the wing root and a growing decrement towards the wingtip. It should be noted that the location along the wing, along the x-axis, has been normalized to the wingspan such that zero corresponds to the wing root and one to the wingtip. When tubercles are added to the leading edge of the wing, a constant modulation in the circulation along the wingspan occurs, before the decline at the wingtip. This modulation was also documented by Rostamzadeh *et al.* [23] who used a non-linear LLT. Two different tubercle configurations are depicted to demonstrate the effects of each parameter. The amplitude of the tubercle directly affects the amplitude of the circulation, where a greater tubercle amplitude results in a greater modulation amplitude. The wavelength of the tubercles affects the wavelength of the modulation. The phase of the

tubercles shifts the local maxima and minima of the circulation and lift distribution in the spanwise direction. This circulation modulation directly impacts the lift coefficient distribution over the wingspan, as shown in Fig. 8, where the same modulation occurs. The local maxima and minima along the wingspan in the circulation and lift coefficient distributions correspond to the tubercle peaks and troughs, respectively. The lift will also be higher over a peak due to the greater chord.

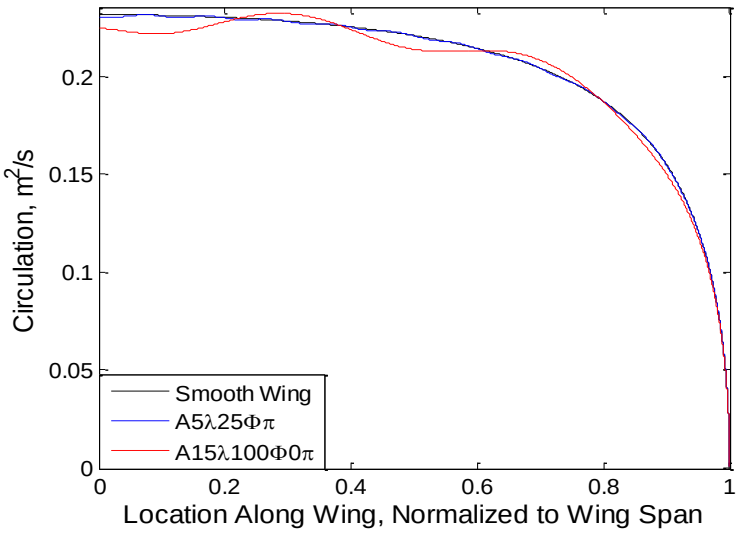

Fig. 7 The spanwise circulation distribution over the wing with a smooth leading edge, and two tubercled leading edge configurations; A5λ25Φπ and A15λ100Φ0π at a 3° angle of attack.

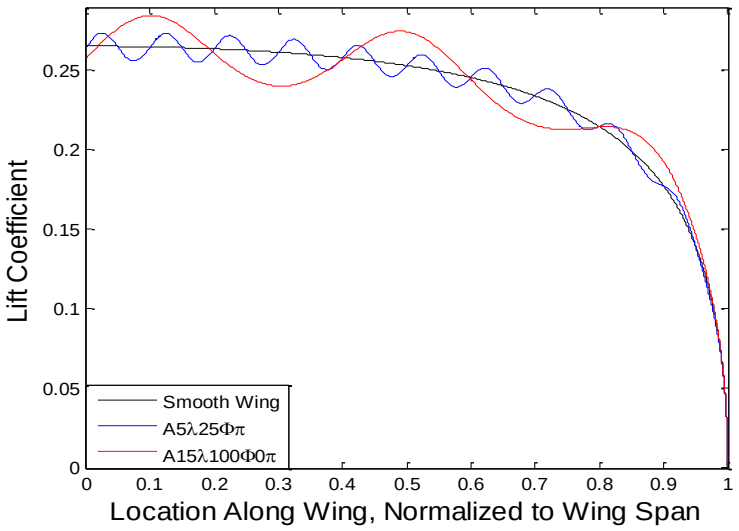

Fig. 8 The spanwise lift coefficient distribution over the wing with a smooth leading edge, and two tubercled leading edge configurations; A5λ25Φπ and A15λ100Φ0π at a 3° angle of attack.

Figures 9 to 11 show the effects of varying the tubercle amplitude, wavelength, and phase on the lift coefficient, induced drag coefficient, and the lift-to-induced-drag ratio. The phase can be determined from Fig. 1 b). It should be noted that for 3° AOA, the smooth wing has a lift coefficient of 0.2300, an induced drag coefficient of 0.0025, and a lift-to-induced-drag ratio of 91.77.

The most obvious result in Figs. 9 to 11 is that without accounting for the tubercle phase, there are no general effects of the amplitude and the wavelength on the lift or induced drag coefficients, or the lift-to-induced-drag ratio. For example, in Fig. 9, for a phase of 0π, increasing the amplitude and wavelength results in a reduced lift coefficient, however, if the phase is $7\pi/12$ then this relationship no longer holds true, and for a phase of $12/12\pi$, increasing the amplitude and wavelength results in a greater lift coefficient. Furthermore, in Fig. 9, for a phase of 0π, both the amplitude and wavelength of the tubercles impacts the lift coefficient, however, for a phase of $7\pi/12$, the lift coefficient is relatively insensitive to the wavelength. Similar conclusions are drawn from Figs. 10 and 11, which correspond to the induced drag coefficient and the lift-to-induced-drag ratio, respectively.

There are two distinct sections of the phase that determine the relationships between the tubercle parameters and the wing performance parameters, as presented in Figs. 9 to 11. The first section is a tubercle phase ranging from $21/12\pi$ to $6/12\pi$, and the second section is a tubercle phase from $8/12\pi$ to $19/12\pi$, as annotated in Fig. 1. In the first phase section, an increase in the amplitude results in both a decrease in the lift and induced drag coefficients, as shown in Figs. 9 and 10. The reduction in the induced drag coefficient is greater than the reduction in the lift coefficient, which results in an increase in the lift-to-induced-drag ratio, as seen in Fig. 11. Furthermore, Fig. 11 shows that in the first phase section, the lift-to-induced-drag ratio is almost always higher than in the second phase section, regardless of the tubercle amplitude and wavelength. The second phase section exhibits opposite trends to those identified in the first phase section.

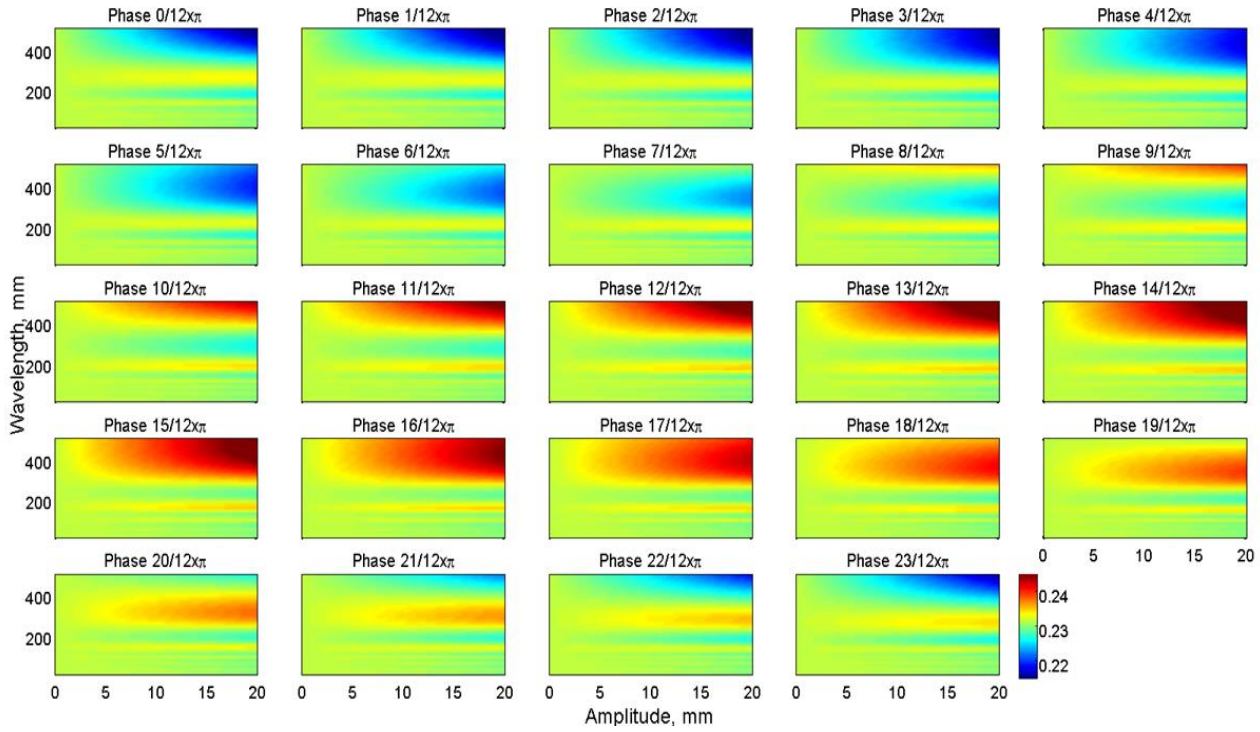

Fig. 9 The effects of the tubercle amplitude, wavelength, and phase on the lift coefficient. 3° angle of attack.

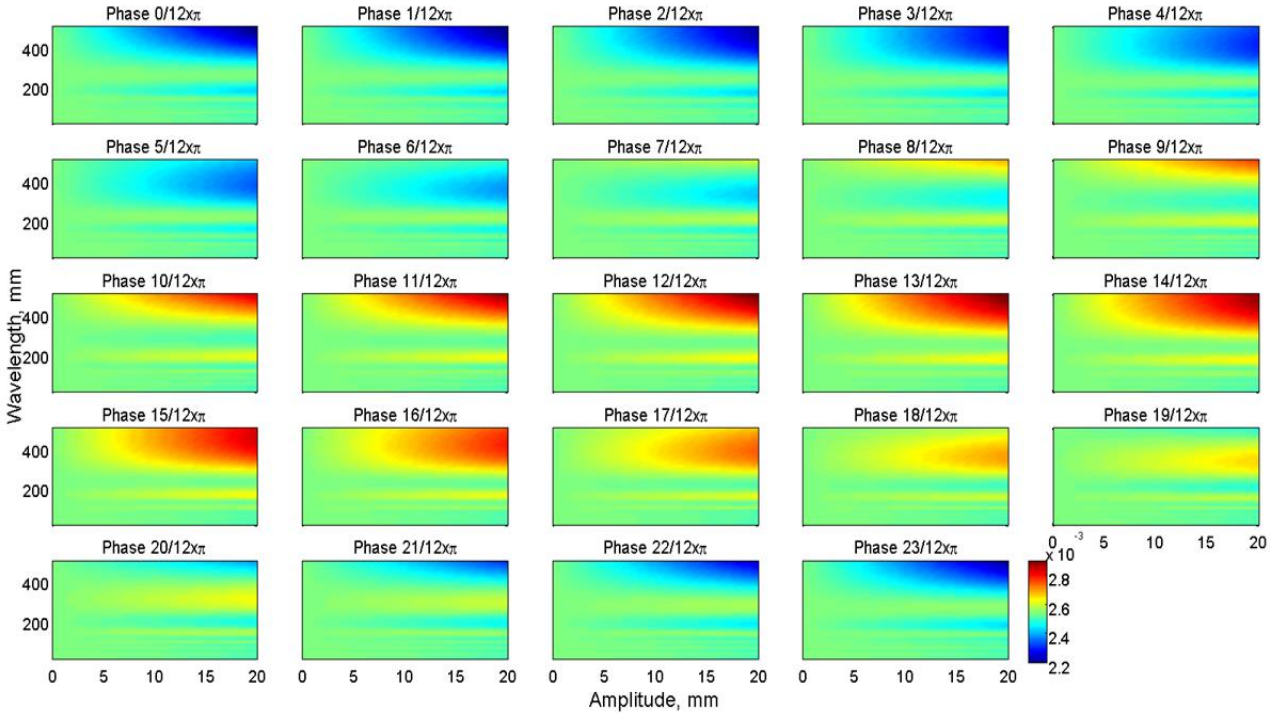

Fig. 10 The effects of the tubercle amplitude, wavelength, and phase on the induced drag coefficient. 3° angle of attack.

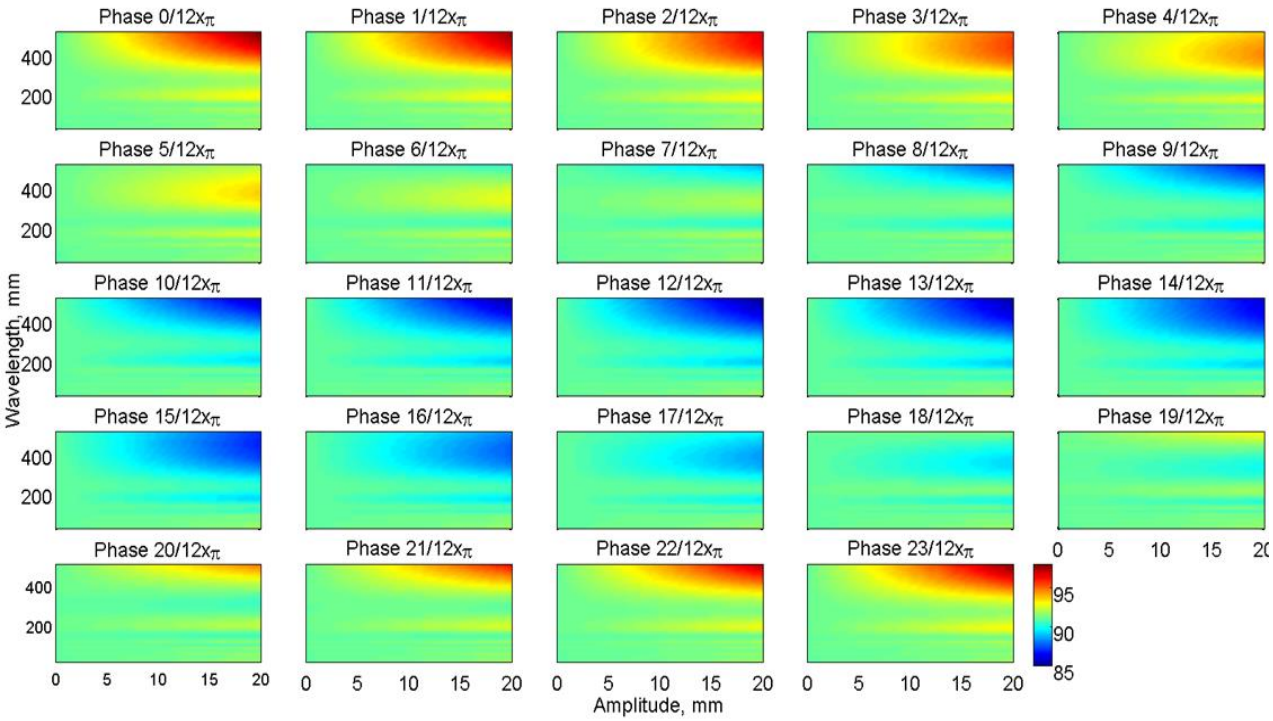

Fig. 11 The effects of the tubercle amplitude, wavelength, and phase on the lift-to-induced-drag ratio. 3° angle of attack.

From Fig. 11, the highest lift-to-induced-drag ratios occur at a tubercle phase ranging from 23/12π to 1/12π, and this is for a tubercle with an amplitude of 15mm to 20mm and a wavelength greater than 450mm. Some configurations reach a lift-to-induced-drag ratio over 98, which is over 6.7% greater than the smooth wing's lift-to-induced-drag ratio. However, for the same range of phases, this combination of amplitudes and wavelengths results in an approximate 6.5% lift coefficient reduction, as shown in Fig. 9. The tubercle configurations that yield the highest lift-to-induced-drag ratios are typically those with a relatively large amplitude, and a wavelength approximately twice the wingspan, which results in the wing becoming more like a gently tapered wing and less like a tubercled wing.

From Figs. 9 and 10, there are two phases where lift and induced drag coefficients are most insensitive to the tubercle wavelength; the first is 7/12π, and the second is 20/12π, and these are termed transition phases. These two transition phases correspond to a wing that terminates just after a tubercle peak or trough, respectively. On the other

hand, the lift and induced drag coefficients are most sensitive to the tubercle wavelength if the phase corresponds to the tubercle terminating midway between a tubercle peak and trough or midway between a trough and a peak.

Figure 12 shows the effects of increasing the tubercle wavelength on the circulation and lift coefficient distributions at one of the previously-identified wavelength-insensitive phases, 7/12π. The tubercles' amplitudes are the same; 10mm. The circulation distributions of both tubercle wings are very similar in shape and magnitude, as shown in Fig. 12 a), which results in the wings' lift coefficient distributions being very similar. The lift coefficients for these tubercled wings are 0.226 and 0.228 for wavelengths of 300mm and 450mm, respectively.

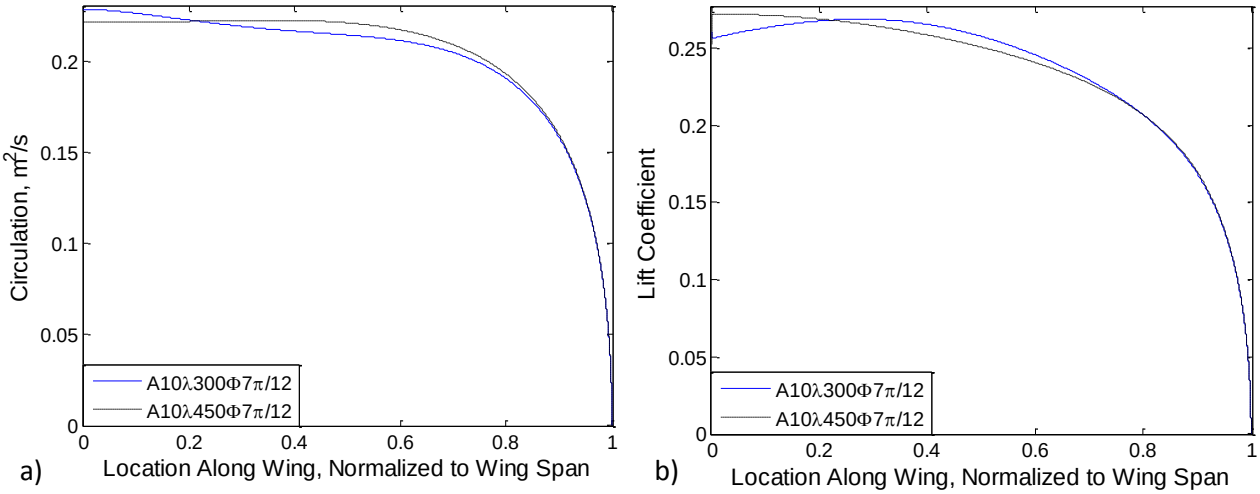

Fig. 12 The circulation, a), and the lift coefficient, b), spanwise distributions for two tubercle configurations; A10λ300Φ7/12π and A10λ450Φ7/12π at a 3° angle of attack.

B. General Trends of the Parametric Analysis

Phase-averaged color plots showing the effects of the tubercle amplitude and wavelength on the lift coefficient, the induced drag coefficient, and the lift-to-induced-drag ratio presented in Figs. 9 to 11 can be seen in Fig. 13. The colorbars on the right show that there is very little change in any of the wing performance parameters when changing the tubercle amplitude and wavelength. Therefore, without taking into account the phase of the tubercles, there is no significant relationship between the amplitude and wavelength of the tubercles and their effects on the lift and induced drag coefficients, and the lift-to-induced-drag ratio at 3°.

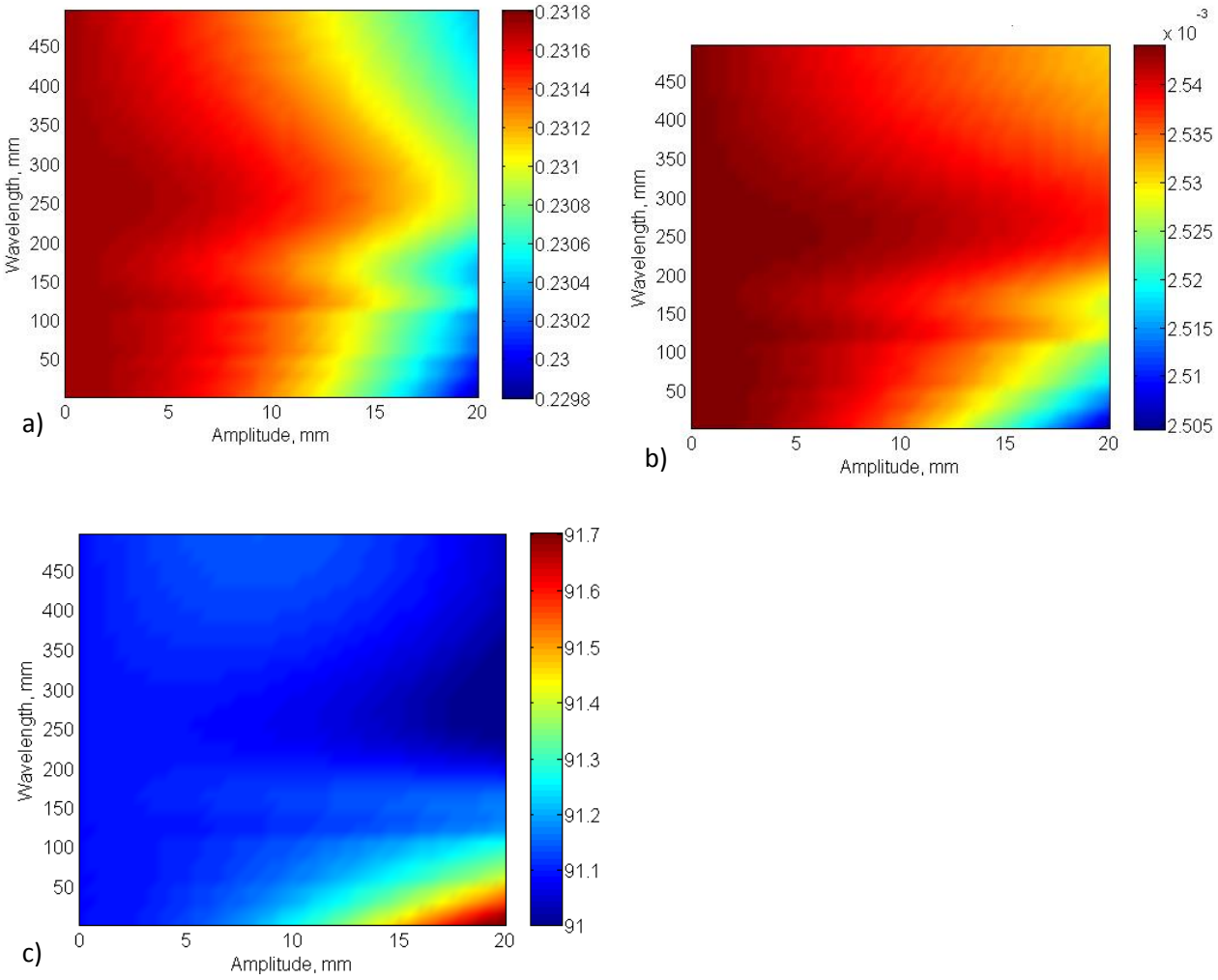

Fig. 13 The phased-averaged effects of the tubercle amplitude and wavelength on the lift coefficient, a), the induced drag coefficient, b), and the lift-to-induced-drag ratio, c). 3° angle of attack.

The data presented in Figs. 9, 10, and 11 have also been amplitude- and wavelength-averaged, and the results are presented in Figs. 14 and 15, respectively.

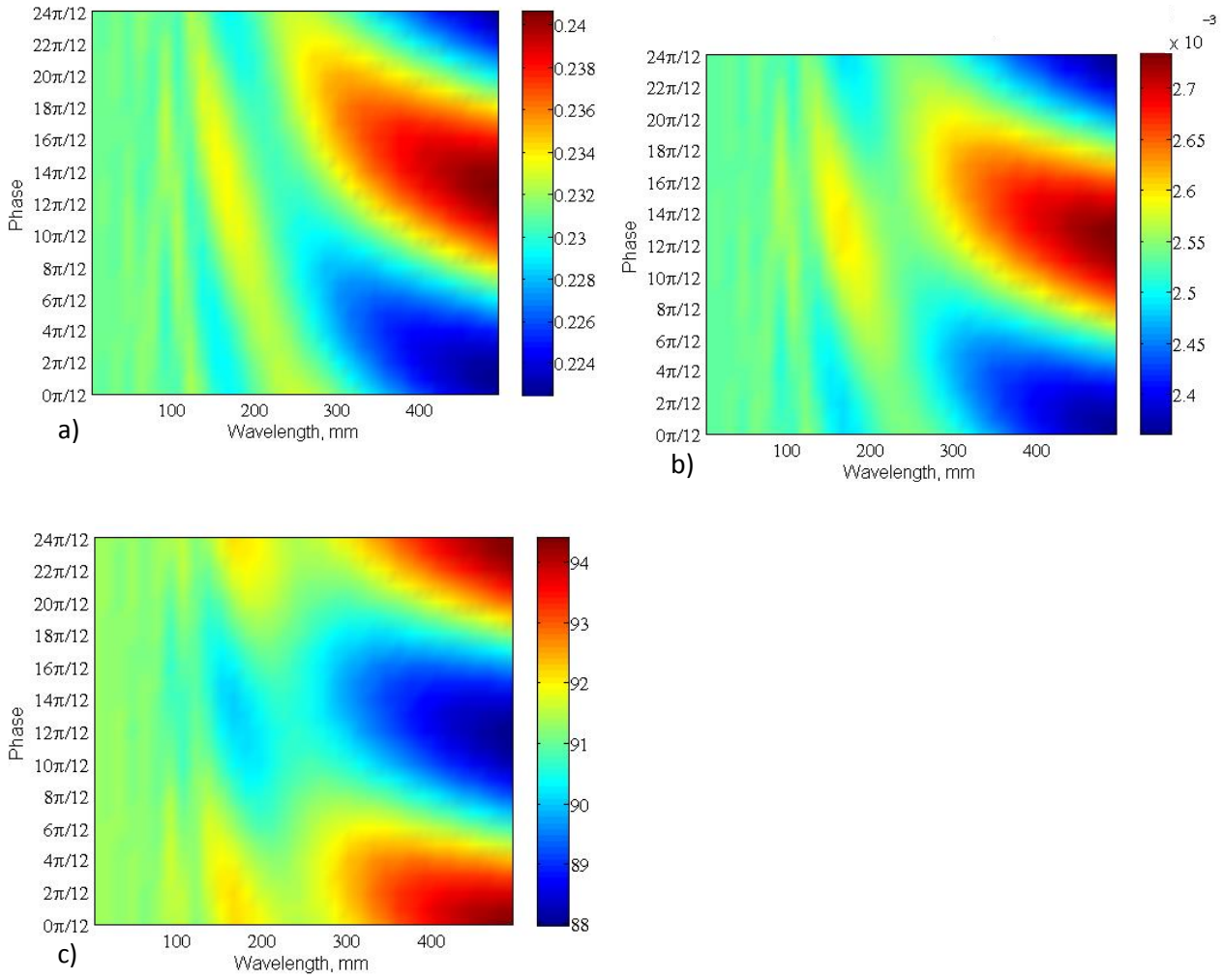

Fig. 14 The amplitude-averaged effects of the tubercle wavelength and phase on the lift coefficient, a), the induced drag coefficient, b), and the lift-to-induced-drag ratio, c). 3° angle of attack.

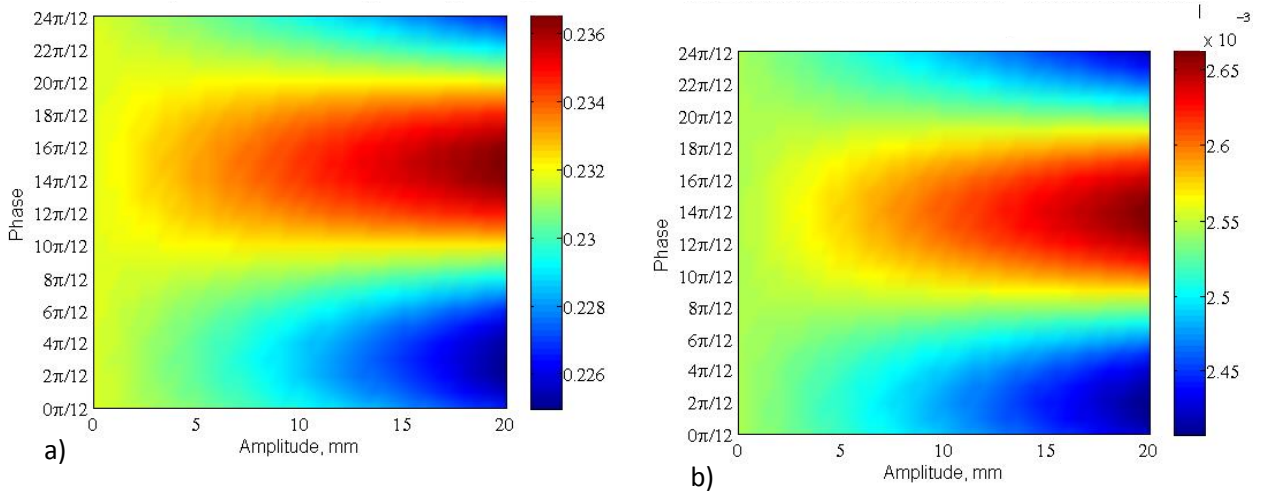

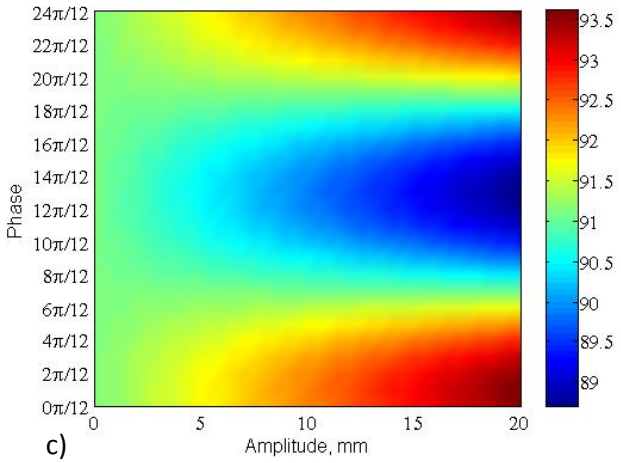

Fig. 15 The wavelength-averaged effects of the tubercle amplitude and phase on the lift coefficient, a), the induced drag coefficient, b), and the lift-to-induced-drag ratio, c). 3° angle of attack.

From Fig. 14, there is a definite trend between the phase and the wavelength on the lift and induced drag coefficients, and the lift-to-induced-drag ratio, which is independent from the tubercle amplitude. A phase of 12π/12 increases the lift and induced drag coefficients, and decreases the lift-to-induced-drag ratio, whereas the converse is true for a phase of 0π/12. A phase of 12π/12 corresponds to a physical geometry of the wing terminating midway between a peak and a trough, whereas a phase of 0π/12 corresponds to termination midway between a trough and a peak. Increasing the wavelength typically results in a greater change in the lift and induced drag coefficients, and the lift-to-induced-drag ratio. In addition, as determined previously, for certain phases, changing the wavelength has little effect on the lift coefficient, the induced drag coefficient, and the lift-to-induced-drag ratio, namely when the wing terminates just after a peak or trough, as shown in Fig. 14. Another interesting feature of Fig. 14 is that the wavelength-insensitive phases are not constant with the wavelength, as for a wavelength of approximately 300mm the insensitive phases are approximately 9π/12 and 21π/12, whereas for wavelength of 450mm the insensitive phases are 6π/12 and 18π/12.

Figure 15 shows that changing the phase of the tubercles tends to have the largest effect on the lift coefficient, the induced drag coefficient, and the lift-to-induced-drag ratio, which is also true in Fig. 14. In addition, while the phase has little impact on the lift and induced drag coefficients, and the lift-to-induced-drag ratio for small wavelengths, the phase still has significant effects on these parameters at small amplitudes, as shown in Fig. 15. This indicates that the wing performance is more sensitive to the amplitude of the tubercle than the wavelength.

C. Genetic Algorithm

Figure 16 shows the average lift coefficient, induced drag coefficient, and lift-to-induced-drag ratio of each generation. From these results, it is concluded that overall the GA was successful in increasing the lift-to-induced-drag ratio with successive generations, which was the goal. However, as expected, the average lift-to-induced-drag ratio did not increase monotonically with each new generation. For example, the average lift-to-induced-drag ratio global maximum occurred at generation 386, 93.6. After generation 386, the average lift-to-induced-drag ratio decreased slightly. As found in the Parametric Analysis section, of this study, the lift-to-induced-drag ratio tends to increase when both the lift and induced drag coefficients decrease. The GA reduced the average lift and induced drag coefficients as the generations progressed.

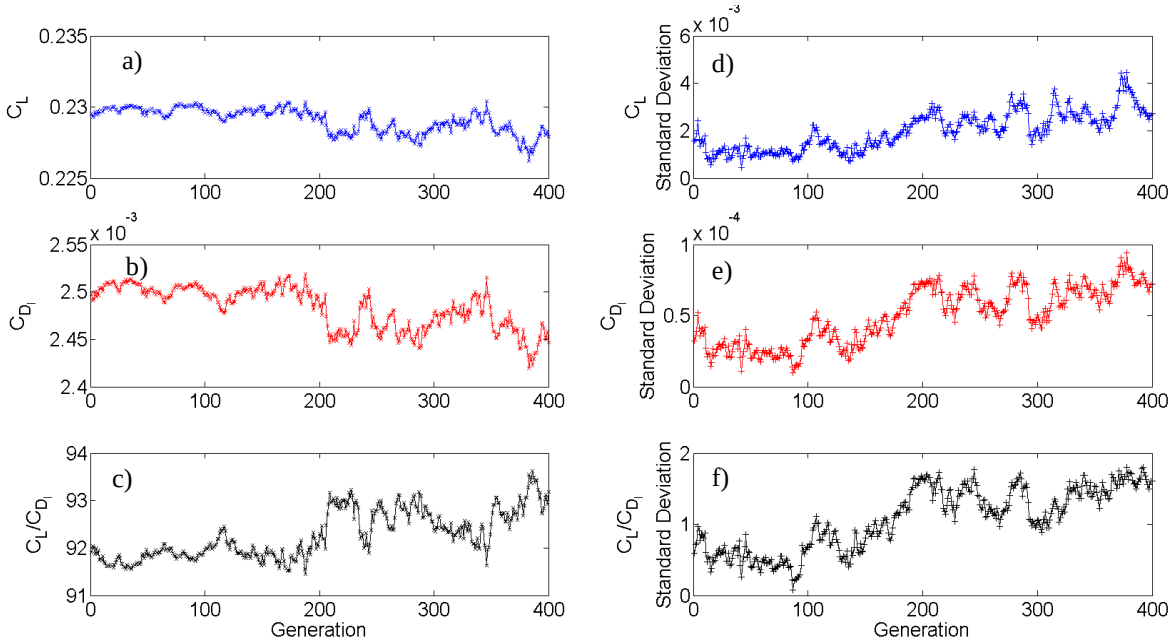

Fig. 16 The progressions of the average lift coefficient, a), induced drag coefficient, b), and the lift-to-induced drag ratio, c), of successive generations. The progressions of the standard deviations of the lift coefficient, d), induced drag coefficient, e), and the lift-to-induced-drag ratio, f), of successive generations. 3° angle of attack.

The standard deviations of the lift coefficient, the induced drag coefficient, and the lift-to-induced-drag ratio for each generation are also presented in Fig. 16. While diversity in the tubercle geometric parameters was sought from the GA, increases in the standard deviations of the lift coefficient, induced drag coefficient, and the lift-to-induced-drag ratio also occurred. The GA fulfilled the requirement of diversity while still achieving the goal of increasing the average lift-to-induced-drag ratio.

The GA typically increased both the maximum lift coefficient and the maximum lift-to-induced-drag ratio and reduced the minimum induced drag with increasing generations, as shown in Fig. 17. The maximum lift-to-induced-drag ratio found throughout the 400 generations was 95.7, and while 400 generations were produced, the tubercle geometry with this maximum lift-to-induced-drag ratio was produced as early as generation 210. From this generation onwards, the average lift-to-induced-drag ratio increased but the maximum lift-to-induced-drag ratio did not. It is concluded that for the given wing planform and the constraints applied to the tubercle geometric parameters, the maximum lift-to-induced-drag ratio that can be produced by any tubercle geometry is 95.7, which is 4.3% greater the smooth wing's lift-to-induced-drag ratio.

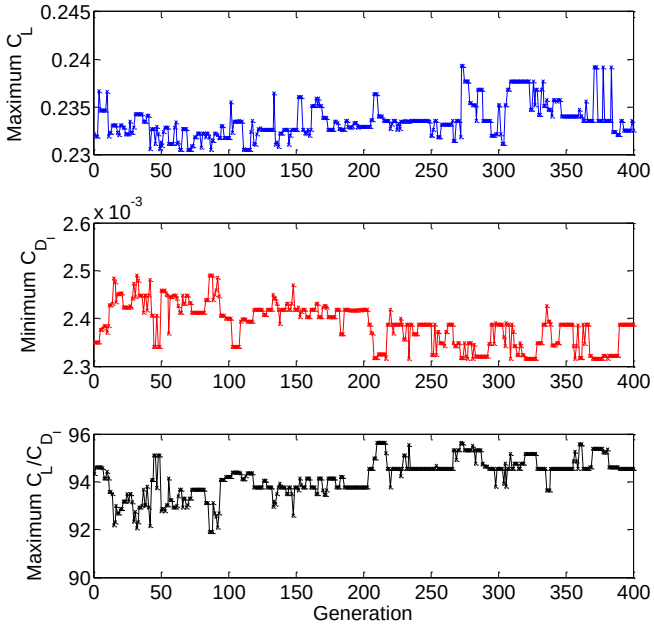

Fig. 17 The progressions of the maximum lift coefficient, a), minimum induced drag coefficient, b), and the maximum lift-to-induced-drag ratio, c), of successive generations. 3° angle of attack.

A potential flaw of a GA is that with each generation the specimens become more and more alike, becoming confined to one solution; "inbreeding". Figure 18 shows that the standard deviation of each tubercle parameter typically remained comparable to the first generation's standard deviations throughout the 400 generations. Therefore, the specimens' diversity was preserved with the progression of the generations. For some generations, the standard deviations of the tubercle amplitude, wavelength, phase, and the location of the tubercles reduced greatly, even reaching 0, which means that the given generation was completely homogenous with respect to that parameter,

however, the mutation operator allowed the specimens to again grow in diversity, which prevented consistent homogeneity between generations. Therefore, the mutation operator functioned as desired.

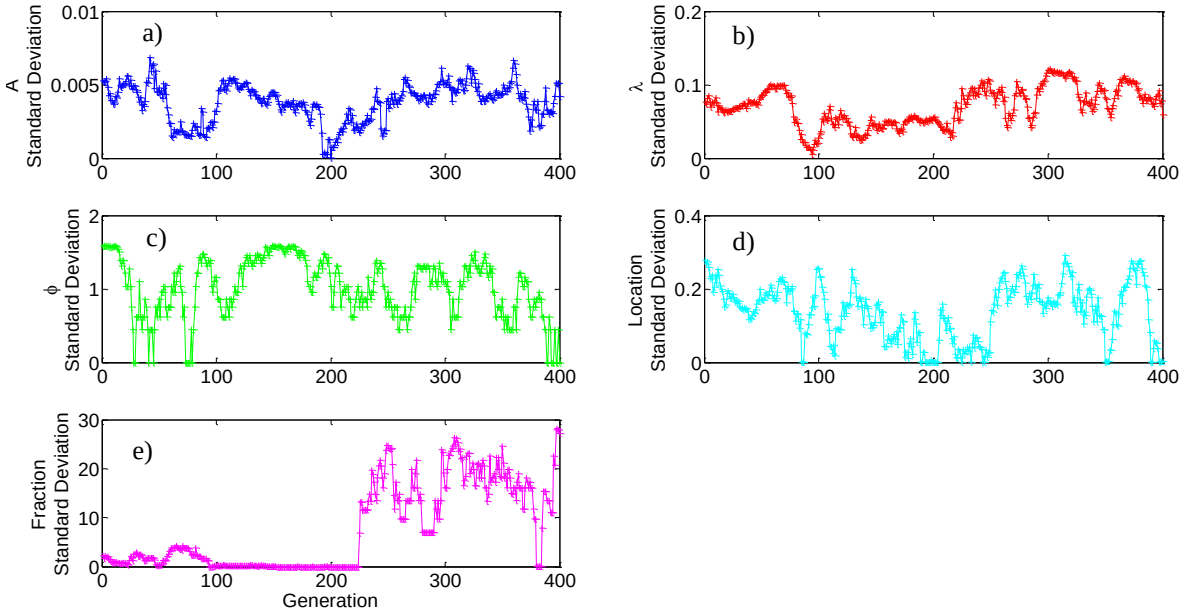

Fig. 18 The progressions of the standard deviation of the amplitude, a), the wavelength, b), the phase, c), the location of the tubercles, d), and the number of tubercles, e), of successive generations. 3° angle of attack.

The standard deviations of the tubercles' phase and location in the final generation are relatively low. The highest lift-to-induced-drag ratio in generation 400 is 94.54, however, 24 out of the 50 specimens have lift-to-induced-drag ratios of 94.5 or higher. Because of the lower diversity in this 400th generation, all 24 of these specimens are very similar in geometry; they have an amplitude of 20mm, the maximum permissible, a wavelength of 249mm, a phase of 12π/12, and the tubercles start from 65% of the span and extend to the wingtip. The resulting wing geometry can be seen in Fig. 19, which is essentially a notched wing. Looking solely at the 400th generation, it may seem that the specimens' parameters have converged, however, as has occurred in previous generations, a greater diversity is expected for future generations. There are several specimens throughout the 400 generations with lift-to-induced-drag ratios above 95.0, which are at least 3.5% greater than the smooth wing lift-to-induced-drag ratio. All of these specimens are similar in that they essentially represent notched wings, as depicted in Fig. 19, however, unlike the 400th generation where all of the tubercle parameters of the elite specimens are identical, the elite specimens throughout the GA optimization are more diverse, with slightly different amplitudes, wavelengths and starting locations. All of the tubercle configurations in the entire analysis surpassing a lift-to-induced-drag ratio

of 95.0 terminate approximately midway between a trough and a peak. The amplitude, wavelength, number of tubercles, and starting location range from 17.8mm to 20.0mm, 233.3mm to half the wingspan, 0.42 to 0.73 of a wavelength, and 27.25% of the span to 58.0% of the span, respectively. From these elite specimens, it can be concluded that while they all approximate a notched wing, the size of the notch can vary significantly. It is novel to note that from all of the specimens in all of the generations, there are only 78 specimens that have a lift-to-induced-drag ratio exceeding 95.0, and that the first five appear between generations 45 and 49, but then not until generation 210 does another appear.

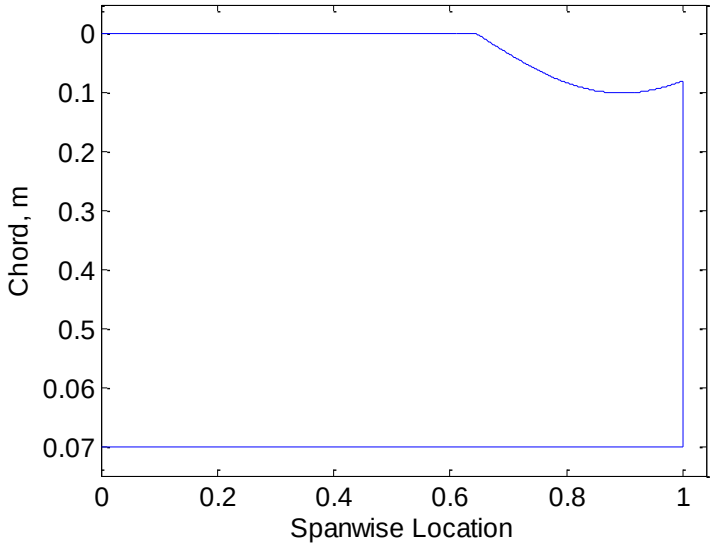

Fig. 19 The typical wing geometry of the elite tubercle configurations in the 400th generation. The x-axis has been normalized to the half wingspan, where 0 indicates the wing root and 1 indicates the wingtip. 3° angle of attack.

V. Discussion

The parametric analysis produced a framework for designing a tubercle's amplitude, wavelength, and phase to meet a given wing performance requirement at 3° AOA. The analysis showed that the phase has the greatest effect on the wing performance and the wavelength has the smallest effect. This is a pivotal result in the research into tubercles, as previous tubercle studies have not considered the effects of the tubercle phase on the wing performance, but this analysis demonstrates that the tubercle termination phase is in fact a crucial tubercle parameter. The results from the parametric analysis suggests that to produce the highest lift coefficient, the tubercle

amplitude should be upwards of 15mm (amplitude-to-chord ratios greater than 0.21), the wavelength should be greater than the half wingspan, and the wing should terminate approximately midway between a tubercle peak and a trough. To design a tubercled wing with the lowest induced drag coefficient or the highest lift-to-induced-drag ratio, the tubercle should, again, have an amplitude upwards of 15mm (amplitude-to-chord ratios greater than 0.21), and a wavelength greater than the half wingspan, however, the wing should terminate approximately midway between a tubercle trough and a peak. If an application requires both a high lift coefficient and a high lift-to-induced-drag ratio, then a trade-off between these two requirements must be made.

The conclusions drawn from the parametric analysis and the GA optimization arose from considering the wing at 3° AOA. Therefore, these conclusions, or other more appropriate conclusions, must be drawn for other angles of attack. Above 3° AOA, the flow in the tubercle troughs typically begin to separate [10,23], which alters the circulation, lift, and induced drag characteristics. The LLT employed is not capable of modelling the wing performance under such conditions. Therefore, above 3° AOA the conclusions drawn from this study are not wholly applicable. Below 3° AOA, the flow over a tubercled wing is typically completely attached [10,23], therefore, the LLT is capable of accurately modelling the wing performance, as presented in the Lifting-Line Theory Model Validation section. As the flow physics over the wing below 3° AOA are similar, the relative effects of the tubercle geometry on the wing lift coefficient, induced drag coefficient, and lift-to-induced-drag ratio for angles of attack below 3° AOA are expected to be the same. To demonstrate this, parametric analyses were performed again, but at 1° and 2° AOAs, and the same trends found at 3° occurred at these lower AOAs as well. As an example demonstrating this, the effects of an A10λ100Φ0π tubercled leading edge at 1°, 2°, and 3° AOAs on the lift coefficient, induced drag coefficient, and lift-to-induced-drag ratio are the same; this tubercle geometry reduces the smooth wing's lift coefficient by 0.65%, reduces the induced drag coefficient by 1.25%, and increases the lift-to-induced-drag ratio by 0.60%. In addition to these parametric analyses, GA optimizations have been conducted under the same conditions once again, but at 1° and 2° AOAs. The GA successfully optimized the lift-to-induced-drag ratio with respect to the tubercle amplitude, wavelength, phase, the location of the tubercles, and the number of tubercles at 1° and 2° AOAs. The elite tubercle configurations found at 1° and 2° AOAs conform to the same geometries found at 3° AOA; halves of tubercles near the wingtips, resulting in notched wings terminating approximately midway between at tubercle trough and a peak, with amplitudes ranging from 17.9mm to 20mm, and wavelengths equal to approximately 50% of the wingspan. At 1° AOA, the maximum increase in the lift-to-induced-

drag ratio compared with the smooth wing was 4.3%, which equals the maximum increase in the lift-to-induced-drag ratio found at 3° AOA. At 2° AOA, the maximum increase in the lift-to-induced-drag ratio compared with the smooth wing was 3.9%, which is slightly lower than the GA optimizations at 1° and 3°, however, this is due to the nature of the GA. Therefore, the conclusions drawn at 3° AOA are applicable to other angles of attack with similar flow physics; for this wing under the same conditions, from 0° to 3° AOAs, non-inclusive.

Other studies into the effects of the tubercle geometry on the wing performance have shown that the tubercle amplitude typically has a greater effect on the stalling characteristics than the wavelength [12,13,23]. Coupling those studies with this study, it is concluded that the tubercle amplitude has a greater effect on the wing performance than the wavelength regardless of the angle of attack.

The trend that tubercles modulate the spanwise lift coefficient distribution, producing local maxima and minima over the peaks and in the troughs, respectively, was also found by Rostamzadeh *et al.* [23].

VI. Conclusion

The effects of altering the tubercle amplitude, wavelength, and phase on a wing's lift coefficient, induced drag coefficient, and the lift-to-induced-drag ratio were investigated with Prandtl's Lifting-Line Theory. The phase of the tubercles refers to the point along a tubercle at which a wing terminates. A framework for designing tubercles based on the wing performance requirements was developed. The investigation considered a NACA 0021 wing at an angle of attack of 3° and a Reynolds number of 120,000. This model was also validated with experimental data. It was found that the tubercle phase has the greatest effect on these wing performance parameters, while the wavelength has the least. For some phases, the wavelength is almost ineffectual. The effects of the tubercle geometry on the wing performance parameters were categorized into two phase regions; between a phase of $8\pi/12$ and $19\pi/12$, the lift-to-induced-drag ratio of the tubercled wing typically exceeds that of the smooth wing, whereas the opposite occurs for a phase between $21\pi/12$ and $6\pi/12$. It was also found that the tubercle geometries that increase the lift-to-induced-drag ratio reduce the lift and induced drag coefficients, however, the increase in the lift-to-induced-drag ratio occurs because the relative decrease in the induced drag coefficient is greater than the relative decrease in the lift coefficient.

Without accounting for the phase of the tubercles, the amplitude and wavelength have little impact on the lift coefficient, induced drag coefficient, or the lift-to-induced-drag ratio, but when coupled with the phase, the effects of the amplitude and wavelength are more pronounced. Larger amplitudes and wavelengths have greater effects on the lift coefficient, induced drag coefficient, and the lift-to-induced-drag ratio. The lift-to-induced-drag ratio of a tubercled wing increases most at a phase of approximately $0\pi/12$, which corresponded to a wing terminating midway between a tubercle trough and peak. The lift and induced drag coefficients are greatest when the wing terminates midway between a tubercle peak and a trough, which corresponds to an approximate phase of $12\pi/12$. However at this phase, the lift-to-induced-drag ratio decreases.

A genetic algorithm was developed to maximize the lift-to-induced-drag ratio of a wing with respect to the tubercle geometry. The parameters optimized to produce tubercled wings with the greatest lift-to-induced-drag ratio by the genetic algorithm were the tubercle amplitude, wavelength, phase, the location of the tubercles along the wingspan, and the number of tubercles. At 3° angle of attack, the genetic algorithm showed that the highest lift-to-induced-drag ratios are achieved by tubercle configurations that are essentially notches near the wingtip. The lift-to-induced-drag ratio is relatively insensitive to the size of the notch. The genetic algorithm also demonstrated that the tubercle configurations that achieve a higher lift-to-induced-drag ratio reduce both the lift and induced drag coefficients.

The limitations of the conclusions found in this study for other angles of attack were considered. It was reasoned that above 3° angle of attack, where flow typically begins to separate in the troughs, the conclusions of this study are not wholly applicable. At 1° and 2° angles of attack, the same effects of the tubercle geometry on the wing performance, as at 3° angle of attack, were observed. Therefore, it is concluded that for angles of attack where the flow is completely attached over the tubercled wing, the effects of the tubercle geometry on the wing performance are consistent, and the trends found in this study at 3° angle of attack are applicable at these other angles of attack.

Future work on this topic includes assessing the effects of the tubercle geometry on the profile drag coefficient, and extending this analysis to swept wings.

Acknowledgments

Research undertaken for this report has been assisted with a grant from the Sir Ross and Sir Keith Smith Fund (Smith Fund) (www.smithfund.org.au). The support is acknowledged and greatly appreciated.

References

[1] Stein, B. and Murray, M. M., "Stall Mechanism Analysis of Humpback Whale Flipper Models", *Unmanned Untethered Submersible Technology (UUST), Autonomous Undersea Systems Inst*., Lee, NH, 2005.

[2] Miklosovic, D. S., Murray, M. M., Howle, L. E., and Fish, F. E., "Leading-edge Tubercles Delay Stall on Humpback Whale (Megaptera Novaeangliae) Flippers", *Physics of Fluids*, Vol. 16, No. 5, 2004, pp. 39-42. doi:10.1063/1.1688341

[3] Bolzon, M. D., Kelso, R. M., and Arjomandi, M., "Force Measurements and Wake Surveys of a Swept Tubercled Wing", *The Journal of Aerospace Engineering*, (in press), 2016, a, The University of Adelaide.

[4] Bolzon, M. D., Kelso, R. M., and Arjomandi, M., "The Effects of Tubercles on Swept Wing Performance at Low Angles of Attack", *19th Australasian Fluid Mechanics Conference (AFMC)*, Melbourne, Australia, 2014.

[5] Pedro, H. T., and Kobayashi, M. H., "Numerical Study of Stall Delay on Humpback Whale Flippers", *46th AIAA Aerospace Sciences Meeting and Exhibit*, 2008.

[6] Stanway, M. J., "Hydrodynamic Effects of Leading-Edge Tubercles on Control Surfaces and in Flapping Foil Propulsion", M.S. Dissertation, MIT, MA, 2008.

[7] Hansen, K. L., Rostamzadeh, N., Kelso, R.M., and Dally, B.B., "Evolution of the Streamwise Vortices Generated Between Leading Edge Tubercles", *Journal of Fluid Mechanics*, Vol. 788, 2016, pp.730-766. doi:10.1017/jfm.2015.611.

[8] Bolzon, M.D., Kelso, R.M., and Arjomandi, M., "Tubercles and Their Applications", *Journal of Aerospace Engineering*, Vol. 29, No. 1, 2015. doi:10.1061/(ASCE)AS.1943-5525.

[9] Watts, P., and Fish, F. E., "The Influence of Passive, Leading Edge Tubercles on Wing Performance", *Unmanned Untethered Submersible Technology (UUST*), Autonomous Undersea Systems Inst., Durham, New Hampshire, 2001.

[10] Bolzon, M. D., Kelso, R. M., and Arjomandi, M., "Tubercles: A Flow Visualisation Study", *Experimental Thermal and Fluid Science (submitted for publication)*, 2016, b, The University of Adelaide.

[11] Bolzon, M. D., Kelso, R. M., and Arjomandi, M., "The Formation of Vortices on a Wing with Leading Edge Tubercles, and Their Effects on the Components of Drag", *Aerospace Science and Technology)*, 2016, c. doi: 10.1016/j.ast.2016.06.025.

[12] Hansen, K. L., "Effect of Leading Edge Tubercles on Airfoil Performance", Ph.D. Dissertation, The University of Adelaide, 2012.

[13] Johari, H., Henoch, C., Custodio, D., and Levshin, A., "Effects of Leading-Edge Protuberances on Airfoil Performance", *AIAA Journal*, Vol. 45, No. 11, 2007, pp. 2634-2642.
doi:10.2514/1.28497.

[14] Hansen, K.L., Kelso, R.M., and Dally, B.B., "Performance Variations of Leading-Edge Tubercles for Distinct Airfoil Profiles", *AIAA Journal*, Vol. 49, No. 1, 2011, pp. 185-194.
doi:10.2514/1.J050631.

[15] Custodio, D., Henoch, C.W., and Johari, H., "Aerodynamic Characteristics of Finite Span Wings with Leading-Edge Protuberances", *AIAA Journal*, Vol. 53, No. 7, 2015, pp. 1878-1893.
doi:10.2514/1.J053568.

[16] Yoon, H.S., Hung, P.A., Jung, J.H., and Kim, M.C., "Effect of the Wavy Leading Edge on Hydrodynamic Characteristics for Flow Around Low Aspect Ratio Wing", *Computers & Fluids*, Vol. 49, 2011, pp. 276-289.

[17] Corsini, A., Belibra, G., and Sheard, A.G., "The Application of Sinusoidal Blade-Leading Edges in a Fan-Design Methodology to Improve Stall Resistance", *Journal of Power and Energy*, Vol. 228, No. 3, 2014, pp. 255-271. doi:10.1177/0957650913514229.

[18] Houghton, E. L., Carpenter, P. W., Collicott, S., and Valentine, D., *Aerodynamics for Engineering Students*, 6th ed., Butterworth-Heinemann, Massachusetts, 2012, pp. 306-313.

[19] Phillips, W.F., and Snyder, D.O., "Modern Adaptation of Prandtl's Classic Lifting-Line Theory", *Statistics and Computing*, Vol. 37, No. 4, 2000, pp. 662-670.

[20] Whitley, D., "A Genetic Algorithm Tutorial", *Statistics and Computing*, Vol. 4, 1994, pp 65-85.

[21] Holland, J.H., "Genetic Algorithms", *Scientific American*, July 1992.

[22] Hansen, K.L, Kelso, R.M., Choudhry, A., and Arjomandi, M., "Laminar Separation Bubble Effect on the Lift Curve Slope of an Airfoil", *19th Australasian Fluid Mechanics Conference (AFMC)*, Melbourne, Australia, 2014.

[23] Rostamzadeh, N., Kelso, R. M., Dally, B. B., and Hansen, K. L., "The Effects of Undulating Leading-Edge Modifications on NACA 0021 Airfoil Characteristics", *Physics of Fluids*, Vol. 25, No. 117101, 2013.
doi:10.1063/1.4828703.

Chapter 6

The Effects of a Single Tubercle Located at the Wingtip on a Swept Wing's Performance at Pre-Stall Angles of Attack

This chapter includes the following journal article:

Bolzon, M.D., Kelso, R.M. and Arjomandi, M., "Effects of a Single Tubercle Terminating at a Swept Wing's Tip on Wing Performance", *submitted to Experimental Thermal and Fluid Science*, 2016.

In previous chapters it was shown that tubercles implemented along the entire leading edge of a swept wing can reduce drag and increase its lift-to-drag ratio at pre-stall AOAs. Chapter 5 demonstrated that a single, relatively large, tubercle located at the wingtip can significantly affect the lift coefficient, induced drag coefficient, and lift-to-induced-drag ratio of an unswept wing. In an effort to reduce manufacturing costs of tubercled wings, and increase the number of applications that could potentially benefit from the implementation tubercles, this chapter aims at investigating the effects of a single, typically sized, tubercle terminating at a swept wing's tip on the wing performance at pre-stall AOAs. This final piece of work completes the fulfilment of the third and final aim of this thesis.

A wing and three interchangeable leading edges were manufactured; one smooth leading edge and two leading edges with a single tubercle terminating at the wingtip. The two tubercled leading edges had the same tubercle amplitude and wavelength, 10.5mm and 60mm, respectively, however, one had a phase of $\pi/2$, herein termed the "peak" configuration, and the other had a phase of $3\pi/2$, herein termed the "trough" configuration. Oil-film flow visualisation, force measurements, and wake surveys were conducted on these three wing configurations. These experimental methods were employed to produce similar types of data as detailed in Chapters 3 and 4.

This investigation demonstrated that neither tubercle configuration significantly affected the smooth wing's performance; changes in the lift coefficient, drag coefficient, and lift-to-drag ratio of 0.5-2% were observed at pre-stall AOAs. Both tubercle configurations had greater effects on the induced and profile drag coefficients, with 2% and 5% changes, respectively, typically observed.

From 6° to 12° AOAs, the tubercle configurations typically changed the wingtip vortex strength by 3%, and had opposite effects to each other. The trough configuration demonstrated the flow mechanism “compartmentalization”. Minor changes in the flow physics, which are consistent with observations reported in Chapter 4, were observed over the tubercled configurations.

The results from this final chapter show that a single, conventionally-sized tubercle located near the tip of a wing is less beneficial to wing performance than tubercles along the entire wing leading edge.

Statement of Authorship

Title of Paper	Effects of a Single Tubercle Terminating at a Swept Wing's Tip on Wing Performance
Publication Status	☐ Published ☐ Accepted for Publication ☑ Submitted for Publication ☐ Unpublished and Unsubmitted work written in manuscript style
Publication Details	Bolzon, M.D., Kelso, R.M. and Arjomandi, M., "Effects of a Single Tubercle Terminating at a Swept Wing's Tip on Wing Performance", *submitted to Experimental Thermal and Fluid Science*, 2016.

Principal Author

Name of Principal Author (Candidate)	Michael Bolzon		
Contribution to the Paper	Performed experiments, processed data, wrote manuscript, and acted as corresponding author.		
Overall percentage (%)			
Certification:	This paper reports on original research I conducted during the period of my Higher Degree by Research candidature and is not subject to any obligations or contractual agreements with a third party that would constrain its inclusion in this thesis. I am the primary author of this paper.		
Signature		Date	

Co-Author Contributions

By signing the Statement of Authorship, each author certifies that:

i. the candidate's stated contribution to the publication is accurate (as detailed above);

ii. permission is granted for the candidate in include the publication in the thesis; and

iii. the sum of all co-author contributions is equal to 100% less the candidate's stated contribution.

Name of Co-Author	Richard Kelso		
Contribution to the Paper	Supervised experimental development, aided interpretation of results, and reviewed manuscript.		
Signature		Date	

Name of Co-Author	Maziar Arjomandi		
Contribution to the Paper	Supervised experimental development, aided interpretation of results, and reviewed manuscript.		
Signature		Date	

Performance effects of a single tubercle terminating at a swept wing's tip

Michael D. Bolzon[1,†], Richard M. Kelso[1] and Maziar Arjomandi[1]

[1]School of Mechanical Engineering, The University of Adelaide, Adelaide, South Australia 5005, Australia

[†]Email address for corresponding author: michael.bolzon@adelaide.edu.au

This study investigates the effects of a single tubercle terminating at a swept wing's tip on its performance at pre-stall angles of attack (AOAs). Two tubercle geometries with amplitudes of 10.5 mm and wavelengths of 60 mm were investigated. One geometry had a phase of $\pi/2$, which was termed the "peak" configuration, while the other had a phase of $3\pi/2$, which was termed the "trough" configuration. Surface flow visualisation, force measurements, and wake surveys were conducted on the wing configurations at a 225,000 chord Reynolds number. The flow visualisation was conducted at 0°, 3°, 6°, 9°, and 12° AOAs, the wake surveys were conducted at 0°, 3°, 6°, and 9° AOAs, and the force measurements were conducted from -2° to 15° AOAs in 1° increments. The wings were NACA 0021 profiles, untapered, and swept at a 35° angle. Evidence of the flow mechanism "compartmentalization" was observed over the trough configuration at 12° AOA. At 1° and 2° AOAs, the tubercle configurations typically reduced the lift coefficient and lift-to-drag ratio by 3 %, but neither configuration greatly affected the drag coefficient. Neither tubercle configuration greatly affected the lift coefficient, drag coefficient, or lift-to-drag ratio from 3° to 15° AOAs, with typical changes of 1 % or 2 % observed. Both tubercle configurations typically changed the induced and profile drag coefficients by 2 % and 5 %, respectively, from 0° to 9° AOAs. From 6° to 9° AOAs, the $\pi/2$ and $3\pi/2$ tubercle configurations typically changed the wingtip vortex strength by 2.2 %, and had opposite effects from each other.

1. Introduction

Humpback whales can perform highly acrobatic manoeuvres such as somersaults; a feat that is unique among Baleen whales (Jurasz and Jurasz, 1979). Their unusual pectoral flipper design, which features leading edge protuberances, termed tubercles, is thought to be, in part, responsible for their agility (Fish and Battle, 1995).

Subsequent investigations into tubercles implemented on unswept lifting surfaces have revealed their ability to delay and soften stall (Miklosovic *et* al. 2004; Miklosovic, Murray & Howle, 2007). These abilities arise from the flow physics tubercles introduce; each tubercle produces a pair of streamwise, counter-rotating vortices (Pedro and Kobayashi, 2008; Hansen, 2012). These vortices begin developing from the lifting surface's leading edge (Rostamzadeh *et*

al., 2014), and mix higher momentum fluid into the boundary layer, thereby delaying stall (Miklosovic *et al.*, 2004; Pedro and Kobayashi, 2008). This boundary layer momentum exchange results in the flow behind the peaks separating at a higher angle of attack (AOA) than behind the troughs (Rostamzadeh *et al.*, 2014; Bolzon, Kelso & Arjomandi, 2016 d). In addition, tubercles "compartmentalize" the flow (Watts and Fish, 2001; Bolzon *et al.*, 2016 d), effectively segregating the flow into pockets and thereby isolating regions of separated flow from regions of attached flow. The stall and post-stall effects of tubercles decrease with increasing sweep angle (Murray *et al.*, 2005; Bolzon, Kelso & Arjomandi, 2014; Bolzon, Kelso & Arjomandi, 2016 e), which is probably due to the already delayed and softened stall pattern of a swept lifting surface (Bolzon, Kelso & Arjomandi, 2016 a).

At pre-stall AOAs, Bolzon *et al.* (2016, a) found that tubercles implemented along the entire leading edge of a swept and tapered NACA 0021 wing reduced the wing's lift coefficient (C_L) and total drag coefficient (C_D) by 4-6 % and 7-9.5 %, respectively, and increased the lift-to-drag ratio by 2-6 %. Tubercles also modulated the induced and profile drag coefficients (C_{D_I} and C_{D_P}), respectively, along the wingspan, with local maxima in the C_{D_I} and C_{D_P} occurring behind the peaks and troughs, respectively (Bolzon, Kelso & Arjomandi, 2016 b). Conversely, tubercles created local minima in the C_{D_I} and C_{D_P}behind the troughs and peaks, respectively (Bolzon *et al.*, 2016 b). In addition, at AOAs where the flow was largely attached over the swept wing tested, tubercles reduced the wing's overall C_{D_P}, but had little effect on the overall C_{D_I} (Bolzon *et al.*, 2016 b). At AOAs where the flow began to separate significantly, namely at 9° and 12° (Bolzon *et al.*, 2016 d), tubercles consistently increased the wing's overall C_{D_P}, whereas they had varied effects on the C_{D_I}, which arose from the location and size of the flow separation areas (Bolzon *et al.*, 2016 b).

Typically, tubercles are characterized by two parameters; their amplitude and their wavelength. However, a third parameter, termed the phase, must be detailed as well, as it impacts a wing's performance (Bolzon, Kelso & Arjomandi, 2016 c). The phase refers to the point along the tubercle at which a wing terminates. At low AOAs, the phase polarizes the effects of tubercles on the C_L, C_{D_I}, and the lift-to-induced-drag ratio (Bolzon *et al.*, 2016 c), whereby a tubercle terminating midway between a trough and a peak typically produces a wing with the lowest C_L and C_{D_I}, and the greatest lift-to-induced-drag ratio. Conversely, a tubercle terminating midway between a peak and a trough typically produces a wing with the greatest C_L and C_{D_I}, and the lowest lift-to-induced-drag ratio

Choosing to implement tubercles onto wings and lifting surfaces involves a compromise among manufacturing costs, cost savings during operation, and performance augmentation during operation. Typically, studies to date have investigated lifting surfaces with tubercles along the entire leading edge, but in recent years the effects of tubercles along a fraction of a lifting surface's leading edge on its performance have received increased attention; Murray, Gruber & Fredriksson (2011), Yoon *et al.* (2011), Corsini, Belibra & Sheard (2014), Bolzon *et al.* (2016, f), Shi *et al.* (2016, a), Shi *et al.* (2016, b), and Cai *et al.* (2016). All studies have found that implementing tubercles along a fraction of the leading edge can still affect the lifting surface's performance. Therefore, strategically implementing tubercles along a fraction of a wing's leading edge may be more

economical than implementing them along the entire leading edge. In addition, some applications may use other flow control and mechanical devices along portions of the leading edge, thereby limiting the regions where tubercles can be implemented. Thus, implementing tubercles along a fraction of a wing's leading edge may increase the applicability of tubercles.

An aim of this study is to investigate the effects of a single tubercle terminating at a wing's tip on a swept wing's C_L, C_D, C_{D_I}, C_{D_P}, and the lift-to-drag ratio at pre-stall AOAs. This AOA range was chosen as the extent to which tubercles along an entire leading edge affect a swept wing's performance is already known at these AOAs (Bolzon *et al.*, 2016 a; Bolzon *et al.*, 2016 b). In addition, this study aims to determine the effects of a single tubercle on the flow physics of a swept wing. To meet these aims, three experimental techniques were performed on one smooth leading edge configuration and two tubercled leading edge configurations. The first method used was a surface flow visualisation, which elucidated the flow physics. The second technique used force measurements, from which the C_L and C_D of the wings were determined. The third method used wake surveys, from which the C_{D_I}, C_{D_P}, C_D, and the vorticity fields were calculated.

2. Methods and uncertainties

2.1 *Wing models*

A swept NACA 0021 wing was chosen for this investigation as this profile was used during the experiments by Bolzon *et al.* (2016, a), which demonstrated tubercles' beneficial effects on a swept wing's performance at pre-stall AOAs. The wing was untapered, which was expected to increase the C_{D_I}, and hence highlight any effects of the tubercles on this component of drag.

One wing section and three interchangeable leading edges were 3D printed, and are shown in figure 1 (*a*). The assembled smooth wing configuration is shown in figure 1 (*b*). A male rail was incorporated onto the wing section and female rails into the leading edges to facilitate mating between these respective pieces. This allowed the leading edges simply to slide on and off the wing section. The interchangeable leading edge was used, as it reduced angular misalignment between the different wing configurations. This wing had a sweep angle of 35°, a span of 330 mm, and a chord of 130 mm, as labelled on figure 1 (*b*). The first leading edge was smooth, and was used as a benchmark for comparison. The second leading edge was smooth from the wing root to 82 % of the span, then featured one full tubercle from 82 % of the span to the wingtip, as labelled on figure 1 (*a*). This leading edge terminated midway between a tubercle peak and a trough, corresponding to a phase of $\pi/2$ (Bolzon *et al.*, 2016 c), and is hereafter termed the "peak" configuration. The third leading edge was exactly the same as the second leading edge, except the tubercle terminated midway between a trough and a peak, which corresponds to a phase of $3\pi/2$ (Bolzon *et al.*, 2016 c), and is hereafter termed the "trough" configuration. These two phases were chosen as they may have different effects on the wing performance (Bolzon *et al.*, 2016 c). The amplitude and wavelength of the tubercles were 10.5 mm and 60 mm, respectively, which Bolzon *et al.* (2016, a) found were able to reduce a

swept wing's C_D and increased its lift-to-drag ratio. The tubercle geometries were modelled by lofting sectional profiles at 5 mm intervals. The loft followed a sine curve.

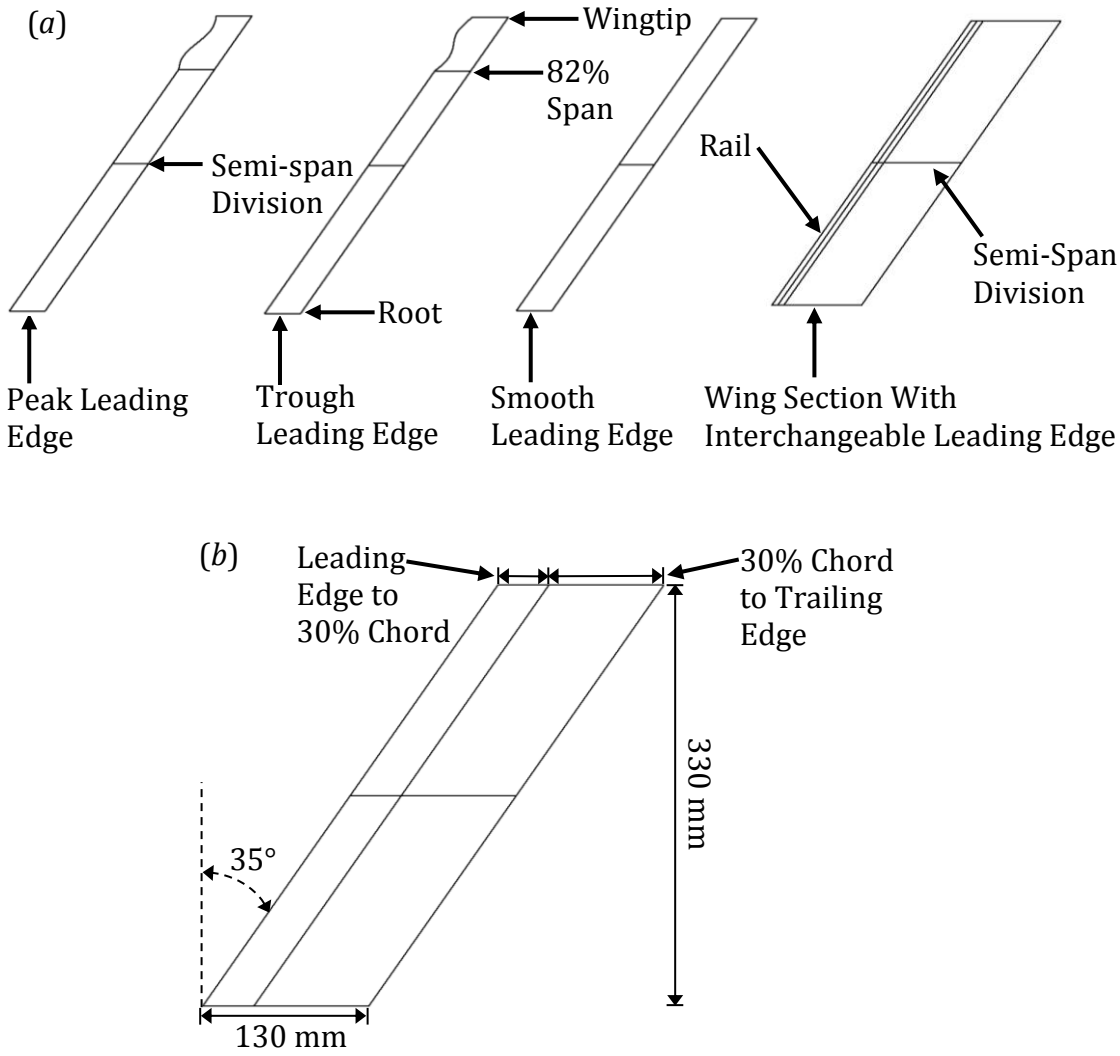

FIGURE 1. (a) Wing section and three leading edge sections modelled and manufactured, (b) assembled smooth wing configuration.

The wing section with the interchangeable leading edge was modelled from 30 % chord to the trailing edge, as labelled on figure 1 (a), while the interchangeable leading edges were modelled from the leading edge to 30 % chord, as labelled on figure. 1 (a). The tubercles were designed to preserve a constant thickness to chord ratio from the leading edge to 30 % chord, while the remainder of the wing preserved the profile of the smooth leading edge configuration. Due to the dimensional restrictions of the fabrication process, the wing section and leading edges were divided in the chordwise direction at the semi-span location. Therefore, a complete wing consisted of four pieces, as shown in figure 1 (b). The two wing sections were glued post-fabrication, and the

smooth leading edge from the wing root to the semi-span was then glued to the wing sections. The only piece that changed throughout the experiments was the wing leading edge from the semi-span to the wingtip. This piece featured the different tubercle geometries. To seal the interfaces between the four pieces, 40 micron thick aluminium foil tape was used. As will be shown in § 3, a Laminar Separation Bubble (LSB) formed over the suction side of each wing configuration at all AOAs investigated. All aluminium foil tape applied in the spanwise direction was either inside or aft of the LSB for all wing configurations and AOAs investigated. Therefore, it is concluded that the aluminium foil tape did not trip the boundary layer.

The 3D printer used to manufacture the wing models was a 3D Systems ProJet 3500 HDMax, and the resolution of the prints was 32 microns. The wing pieces were printed in VisiJet M3 X, which is a similar material to plastic Acrylonitrile Butadiene Styrene (ABS). The wings were painted with black acrylic paint to aid the surface flow visualisation. The wing pieces were incrementally sanded with wet sand paper from 80 grit to 1200 grit. Extrapolating from data presented by Mell (2010) and All Seals Inc (2016), the surface roughness was 3-4 microns.

2.2 Method of investigation

The surface flow visualisation, force measurements, and wake surveys were conducted in the "KC Wind Tunnel" at the University of Adelaide in the open-jet configuration. The working section measured 0.5m x 0.5m, and the turbulence intensity U_{rms}/U_{∞} was 0.6~0.8 %. The freestream velocity was 27.5 m/s for the entire study, which gave a chord Reynolds number of 225,000.

The wings were mounted on a JR3 load cell of 100 N capacity and the load cell was mounted on a Vertex rotary table. The rotary table was used to change the AOA. The experimental setup of the surface flow visualisation and the force measurements is shown in figure 2. The wake survey experimental setup was the same as presented in figure 2, with the exception of a 2-axis traverse and a probe located 440 mm (3.4 chord lengths) downstream of the wing root trailing edge, as shown in figure 3, to ensure complete wingtip rollup (Gerontakos and Lee, 2006). At 0° AOA, the lift and drag forces of the wings were aligned with the Z- and X-directions of the load cell, respectively. The angular misalignment was assumed to be small because of the manufacturing method. The wings were symmetrical, therefore at 0° AOA they would not produce lift, and the force in the Z-direction would read zero. Wake surveys were taken in the wingtip region to check the symmetry of the vorticity field at 0° AOA when aligning the wings for the surface flow visualisation, force measurements, and the wake surveys. It was found that this method of aligning the wings was satisfactory. A $\pm 0.017°$ angular uncertainty in the rotary table was estimated.

2.2.1. Surface flow visualisation

Surface flow visualisation was conducted on each of the three wing configurations to elucidate the effects of the tubercle configurations on flow features such as LSBs, flow separation regions, and vortex detachment points. The surface flow visualisation was conducted at 0°, 3°, 6°, 9°, and 12° AOAs. The film mixture consisted of 5 parts ethanol and 2 parts talcum powder, by weight.

As the film mixture dried, the white talcum powder became more visible. The amount of talcum powder visible was inversely proportional to the relative surface shear stress. Surface flow visualisation was only conducted on the suction side of these configurations, as the flow features of interest occur on this side of this airfoil profile (Hansen *et* al., 2014; Rostamzadeh *et al.*, 2014).

Due to the relatively fast drying time of the film mixture, a generous application was uniformly applied to the wing's suction side with a paintbrush. A Nikon D200 DSLR was used to photograph the surface flow visualisation. Matlab was used to convert the resulting images to grayscale, and to process the images further.

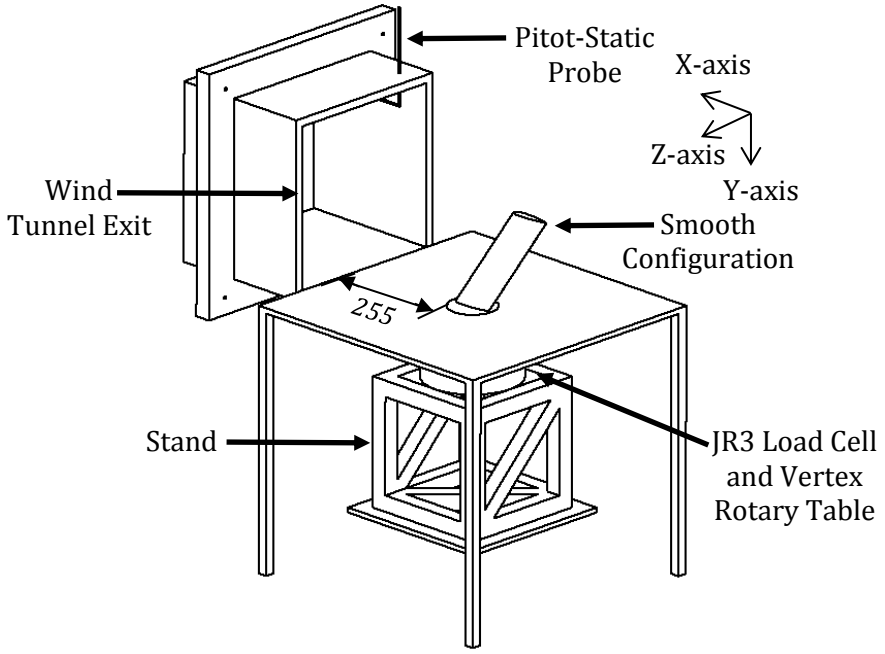

FIGURE 2. The surface flow visualisation and force measurement setup with the smooth configuration in place.

2.2.2. Force measurements

The forces were measured with the JR3 six-axis load cell for at least 10 seconds, at a 100 Hz sampling frequency, and the respective averages of these measurements are reported. This number of samples was chosen as it resulted in convergence. A factory supplied internal calibration matrix was used to decouple the force measurements during the experiment. From these measurements, the lift and drag forces were found through the coordinate transformation

$$\begin{bmatrix} L \\ D \end{bmatrix} = \begin{bmatrix} sin\alpha & cos\alpha \\ -cos\alpha & sin\alpha \end{bmatrix} \begin{bmatrix} F_x \\ F_z \end{bmatrix} \tag{2.1}$$

where L is the lift, D is the drag, α is the AOA in degrees, and F_x and F_z are the forces in the X- and Z- directions respectively. Each wing configuration underwent 3 runs from -2° to 15° AOAs in 1° increments, and the averages are reported.

From this setup, an uncertainty in the force measurements and an uncertainty in the wing alignment arose. The force measurements uncertainty was accounted for by calibrating the load cell with a number of forces, in the form of weights, across the expected force range. The weights were attached to the load cell and data were taken for at least 10 seconds at a 100 Hz sampling frequency. In the X-direction, the load cell had a 95 % confidence interval of $\pm$0.57 % for a force of 0.5 N and $\pm$0.15 % for a force of 8.4 N. In the Z-direction, the load cell had a 95 % confidence interval of $\pm$0.82 % for a force of 0.5 N and $\pm$0.30 % for a force of 1.3 N. A linear interpolation was used to determine the uncertainty of the force measurements between the calibration forces. The wing alignment uncertainty was the same as that detailed above in § 2.2.

The C_L and C_D were calculated from the lift and drag forces, the density of the air, the freestream velocity, and the wing's surface area. The density of the air was calculated from the temperature, barometric pressure, and humidity. The flow was considered incompressible. The temperature was measured by a TSI IFA300 Constant Temperature Anemometer module. The barometric pressure was measured by a Bosch BMP180 pressure module. The humidity was measured by a DHT22 module. The BMP180 and DHT22 modules were connected to an Arduino Uno R3, which was, in turn, connected to the data acquisition system. The freestream velocity was calculated from the dynamic pressure of the freestream flow and the density of the air. A Pitot-static probe was used to determine the dynamic pressure. A MKS Baratron and a Scanivalve DSA3217 pressure scanner were connected to the Pitot port and the static port, respectively. The 95% confidence intervals of the instruments list above are in table 1.

The uncertainties in the C_L and C_D were determined by using the method prescribed by Holman (1994) and Dieck (1992).

Instrument	95% Confidence Interval
IFA300	±0.1°C
BMP180	±4.0 pa
DHT22	±1.0 % relative humidity
Baratron	±0.5 pa (±0.1 % of the dynamic pressure)
Scanivalve	±3.0 pa (±0.6 % of the dynamic pressure)

TABLE 1. The 95 % confidence interval of various instruments used.

2.2.3. Wake surveys

The wake surveys were conducted at 0°, 3°, 6°, and 9° AOAs. The 9° AOA was the highest AOA surveyed due to the growing size of the wake, which exceeded the traverse limits. Three wake surveys were conducted for each wing configuration at each AOA and the averages are reported.

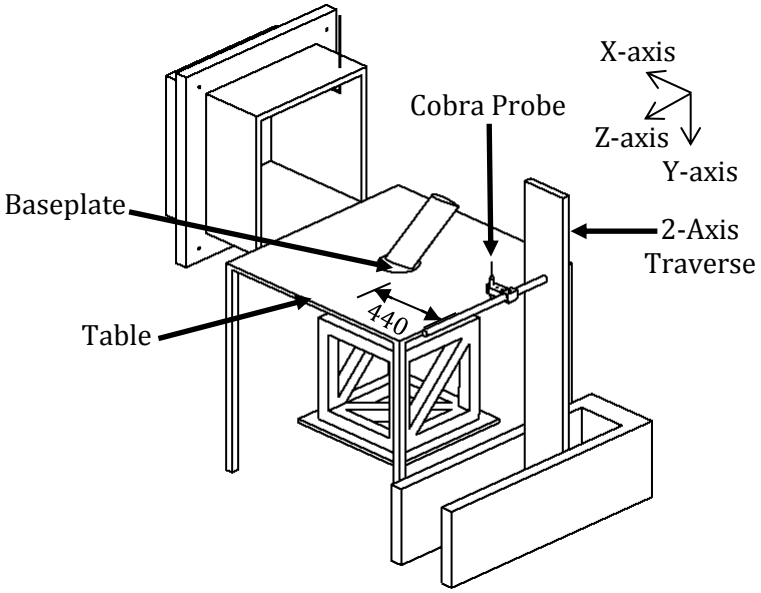

FIGURE 3. The wake survey setup with the smooth configuration in place.

The traverse moved a Turbulent Flow Instrumentation Pty Ltd, Cobra probe to the required location in the Y-Z plane, which is hereafter termed the "wake plane". A Cobra probe is a four-hole pressure probe from which three orthogonal velocities and the stagnation pressure can be calculated (Shepherd, 1981). The Cobra probe had a 3 x 3 mm triangular head and a sampling frequency of 600 Hz (TFI, 2011). The calibration curves for the Cobra probe were supplied by TFI Pty Ltd (TFI, 2011).

The induced drag was calculated from (Brune, 1994; Bolzon *et al.*, 2016 b)

$$D_I \approx \frac{1}{2}\rho_\infty \int\int_s (\psi\omega - \phi\sigma).dY.dZ, \tag{2.2}$$

where

$$\omega = \left(\frac{\partial w}{\partial y} - \frac{\partial v}{\partial z}\right) \tag{2.3}$$

$$\sigma = \frac{\partial v}{\partial y} + \frac{\partial w}{\partial z} \tag{2.4}$$

$$\frac{\partial^2 \psi}{\partial y^2} + \frac{\partial^2 \psi}{\partial z^2} = -\omega \tag{2.5}$$

$$\frac{\partial^2 \phi}{\partial y^2} + \frac{\partial^2 \phi}{\partial z^2} = \sigma. \tag{2.6}$$

The profile drag was calculated from

$$D_P = \int\int_S \left[P_{T_\infty} - P_T + \frac{\rho}{2}(U^* - u)(U^* + u - 2U_\infty)\right].dY.dZ, \tag{2.7}$$

where

$$U^* = \sqrt{u^2 + \left(\frac{2}{\rho}\right)(P_{T\infty} - P_T)} \tag{2.8}$$

$$u' = U^* - U_\infty. \tag{2.9}$$

The total drag was calculated from

$$D = D_I + D_P. \tag{2.10}$$

Equations (2.2) to (2.10) are derived by applying the conservation of momentum to a control volume in which the wing is contained (Brune, 1994; Kusunose, 1997). The integrals in equations (2.2) and (2.7) were applied to the wake plane. Quantities ω and σ, as expressed in equations (2.3) and (2.4), respectively, were calculated using the forward-difference scheme. Equations (2.5) and (2.6) were solved using the Gauss-Siedel iterative method and were considered solved when the root-mean-square of the difference between consecutive iterations was less than 10^{-7}, as detailed by Bolzon *et al.* (2016, a). Stream function and velocity potential ψ and ϕ were solved with the Dirichlet and Neumann boundary conditions of 0, respectively (Brune, 1994). Using these equations in an open-jet configuration is only applicable when the viscous wake does not extend to the tunnel jet's shear layer, and the flow only exits through the wake plane (Brune, 1994; Bolzon *et al.*, 2016 a). Prior to the wake surveys, the size and location of the wing configurations' wakes were investigated by traversing the Cobra probe in the wake plane of each wing configuration, in turn. Equations (2.2) to (2.10) were found to be applicable in this open-jet at all AOAs for all wing configurations, as the wakes were within the bounds of the tunnel jet shear layers. The boundary was chosen to be the interface between the potential core and the shear layer, as the boundary conditions were satisfied at this location. In addition, the interface between the viscous wake, where the measurements were required to be taken (Brune, 1994), and the potential flow, was chosen to be where the unsteadiness in the u, v, and w velocities decreased dramatically. The area surveyed was then defined by this interface, with a safety factor of 6 mm, 1 grid spacing, typically incorporated. The area surveyed increased with increasing AOA, but was kept constant for each wing configuration at a given AOA.

Boundary layers formed over the table, which introduced additional drag that did not arise from the wings, and as such was removed from the wake survey calculations. This was deemed acceptable as the drag arising from the flow over the baseplate was expected to be minimal, as the plate was made of polished stainless steel, and the drag incurred from the boundary layer over the table was not measured by the load cell. At 0° AOA, the boundary layer thickness at the wake plane was 24 mm, as determined from the wake survey measurements. This thickness was used in all of the calculations at all AOAs surveyed. The second integrands in equations (2.2) and (2.7) have been computed in the Z-direction to produce the spanwise induced drag coefficient, $C_{D_I}{}'$, and the spanwise profile drag coefficient, $C_{D_P}{}'$, which have been non-dimensionalised to the chord. The sum of these two coefficients gives the spanwise drag coefficient, $C_D{}'$.

From the Cobra probe measurements, the downstream total pressure, P_T, and downstream velocities u, v, and w were calculated. The 95 % confidence intervals of the u, v, and w velocities, calculated from the Cobra probe measurements, were ±0.45 m/s, ±0.31 m/s, and ±0.31 m/s, respectively. These values corresponded to ±1.6 % of the 27.5 m/s freestream velocity, and ±10 % for the typical v and w velocities throughout the surveys. The upstream total pressure, $P_{t\infty}$, was measured by the Baratron. The dynamic pressure, temperature, barometric pressure, and humidity were measured in the same fashion as during the force measurements. The upstream and downstream densities are denoted by ρ_∞ and ρ, respectively. The vorticity and cross-flow sources are denoted by ω and σ, respectively. The induced, profile, and total drags are denoted by D_I, D_P, and D, respectively.

Any potential inaccuracies due to flow quality issues were accounted for by surveying the same wake plane without any models present, and the drag calculated from this survey was subtracted from the drag of the wings (Brune, 1994).

A grid independency study on the C_D calculated from wake surveys of a smooth wing and a tubercled wing is detailed in Bolzon *et al.* (2016, a). These wings had the same spans and mean aerodynamic chords as the wing configurations in this study. Furthermore, the tubercles had the same amplitude and wavelength as the tubercle configurations in this study. This grid independency study considered 3, 5, and 6 mm spacings; 3 mm was the smallest spatial resolution due to experimental limitations. The study was performed in the wingtip region, as it was reasoned that the greatest spatial changes in the C_D occurred there. The C_D calculated from the 6 mm grid spacing wake survey measurements of both wings were within 7 % of the C_D calculated from the 3 mm grid spacing wake survey measurements. Furthermore, the C_D of the smooth and tubercled wings calculated from the 6 mm grid spacing wake survey measurements, from 0 to 12° AOAs, were typically consistent (within the uncertainty range) with the C_D determined from load cell measurements. Therefore, it was deemed that a 6 mm grid spacing was adequate for investigating the drag production of those wings (Bolzon *et al.*, 2016 a). As such, a 6 mm grid spacing was adopted for this study.

From the wake survey data, the circulations of the wingtip vortices can be calculated using either equation (2.11) or equation (2.12), however, equation (2.11) was used as it is typically more accurate (Hassan, Lau & Kelso, 2007), and

the results are reported. The circulations of the wingtip vortices were found in the same manner as was presented by Hassan *et al.* (2007), whereby a region of integration (ROI) was determined. To determine the ROI, the location of maximum vorticity in a given region was found, then if the vorticity of a neighbouring point was within a given vorticity threshold and distance from the location of maximum vorticity, this point would be added to the ROI. This process was continued until all neighbouring points were outside of the ROI requirements, and the ROI ceased growing. For the wingtip vortices, the vorticity threshold had a lower limit of +30 s^{-1} and an unbounded upper limit. The maximum distance was 30 mm at 3°, and 36 mm at 6° and 9° AOAs. The maximum distance was larger at 6° and 9° AOAs than at 3° AOA because of the larger wingtip vortex sizes at these AOAs. The vortices created by the tubercles were usually indistinct, therefore, their circulations were not calculated.

$$\Gamma_{vel} = \oint_c (vdy + wdz) \tag{2.11}$$

$$\Gamma_{vor} = \iint_s \omega \,.\, ds \tag{2.12}$$

3. Results

The surface flow visualisation at all AOAs, as presented in figures 4 to 8, shows that a long and uniform dark region appears at approximately the quarter-chord location over the suction side of the smooth configuration, and extends from the wing root to the wingtip, as annotated on figure 4 (*a*). Near the wingtip of the smooth configuration, the dark region extends slightly further towards the wing trailing edge, as labelled on figure 4 (*a*). This particular dark region is evidence of an LSB, where low shear stresses lead to a relatively long drying time (Hansen *et al.*, 2014; Bolzon *et al.*, 2016 d). Similar dark regions, representing LSBs, form at approximately the quarter-chord location over the suction sides of the peak and trough configurations for all AOAs presented; examples are annotated on figure 4 (*b,c*). It should be noted that for the majority of the surface flow visualisation presented, the LSB is relatively constant in chordwise length along the span, however, for some surface flow visualisation, there are discontinuities in the LSB's chordwise length at the interface of the two wing section pieces, as annotated on figure 4 (*b*). These discontinuities are not caused by manufacturing flaws because they are not consistently seen, and rare. Therefore, the authors conclude that they are random occurrences. In addition, the LSBs' chordwise lengths are modulated aft of the tubercle section for both configurations. From 0° to 9°, the LSBs over the tubercle configurations do not extend towards the trailing edge near the wingtip, unlike over the smooth configuration. The LSBs over all three configurations move towards the leading edge with increasing AOA.

Aft of the LSB, the film mixture over the smooth configuration, at 0° AOA, tends to dry uniformly along the span, except near the wingtip. As the AOA increases, most notably at 12° AOA, the film mixture typically dries more quickly near the wing root than the wingtip. At all AOAs, the film mixture dries

progressively more slowly from the LSB reattachment location towards the trailing edge, as annotated on figure 5 (*a*). At 0° and 3° AOAs, the tubercle configurations exhibit similar drying patterns to each other aft of the LSB; the film mixtures behind the tubercle peak and trough dry more slowly than behind the midway point between the tubercle peak and trough. At 6°, 9°, and 12° AOAs, the surface film mixture drying times, as annotated on figures 6 (*b,c*), 7 (*b,c*), and 8 (*b,c*), suggest that the boundary layers behind the troughs have significantly separated while the boundary layers behind the peaks have not (Johari *et al.*, 2007; Rostamzadeh *et al.*, 2014; Bolzon *et al.*, 2016 d). The drying pattern over the trough configuration at 12° AOA (figure 8 (*c*)) indicates flow "compartmentalization". In addition, at 12° AOA, the relative drying rates of the surface film mixture suggest that the shear stresses are lower near the tips of the tubercle configurations than occur in the smooth configuration.

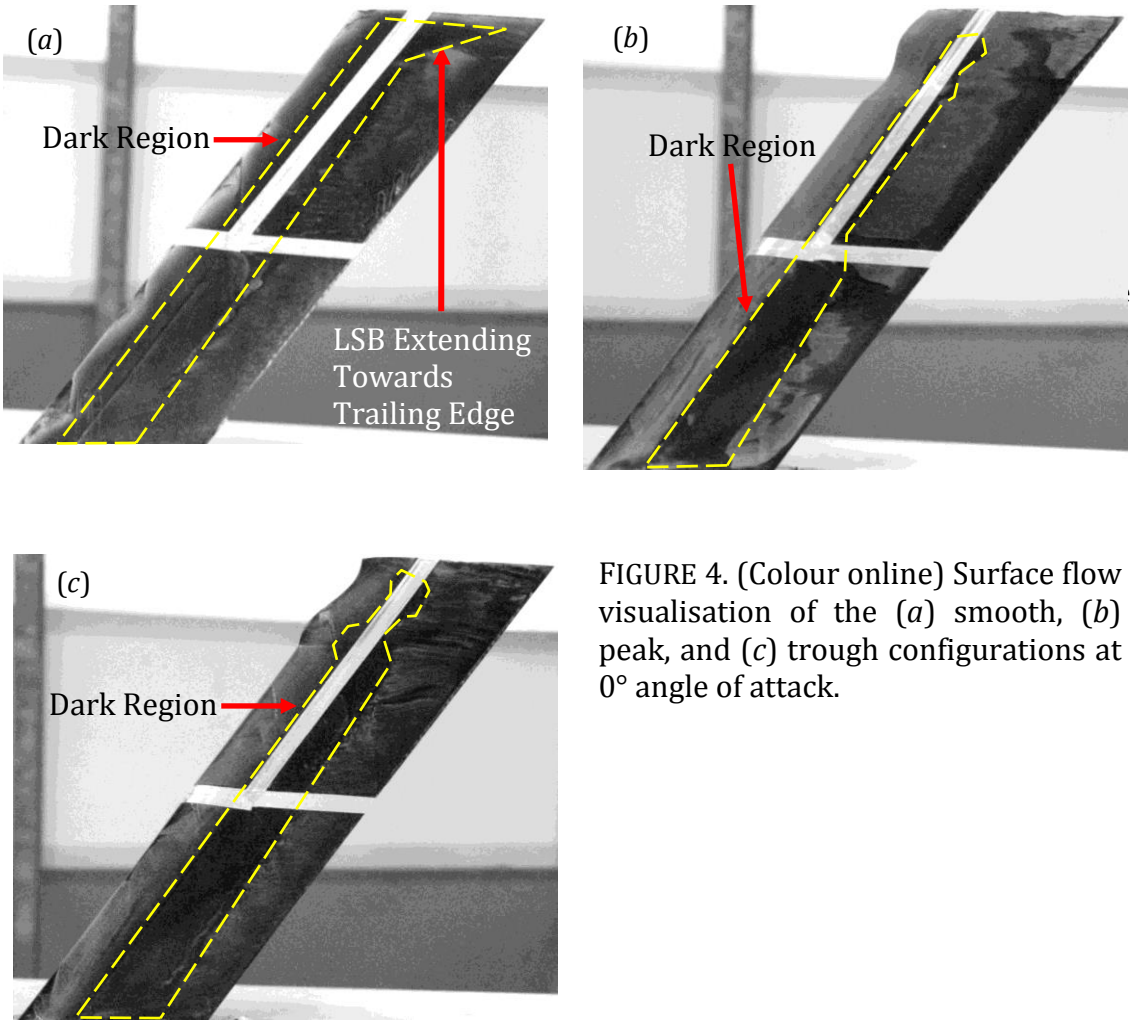

FIGURE 4. (Colour online) Surface flow visualisation of the (*a*) smooth, (*b*) peak, and (*c*) trough configurations at 0° angle of attack.

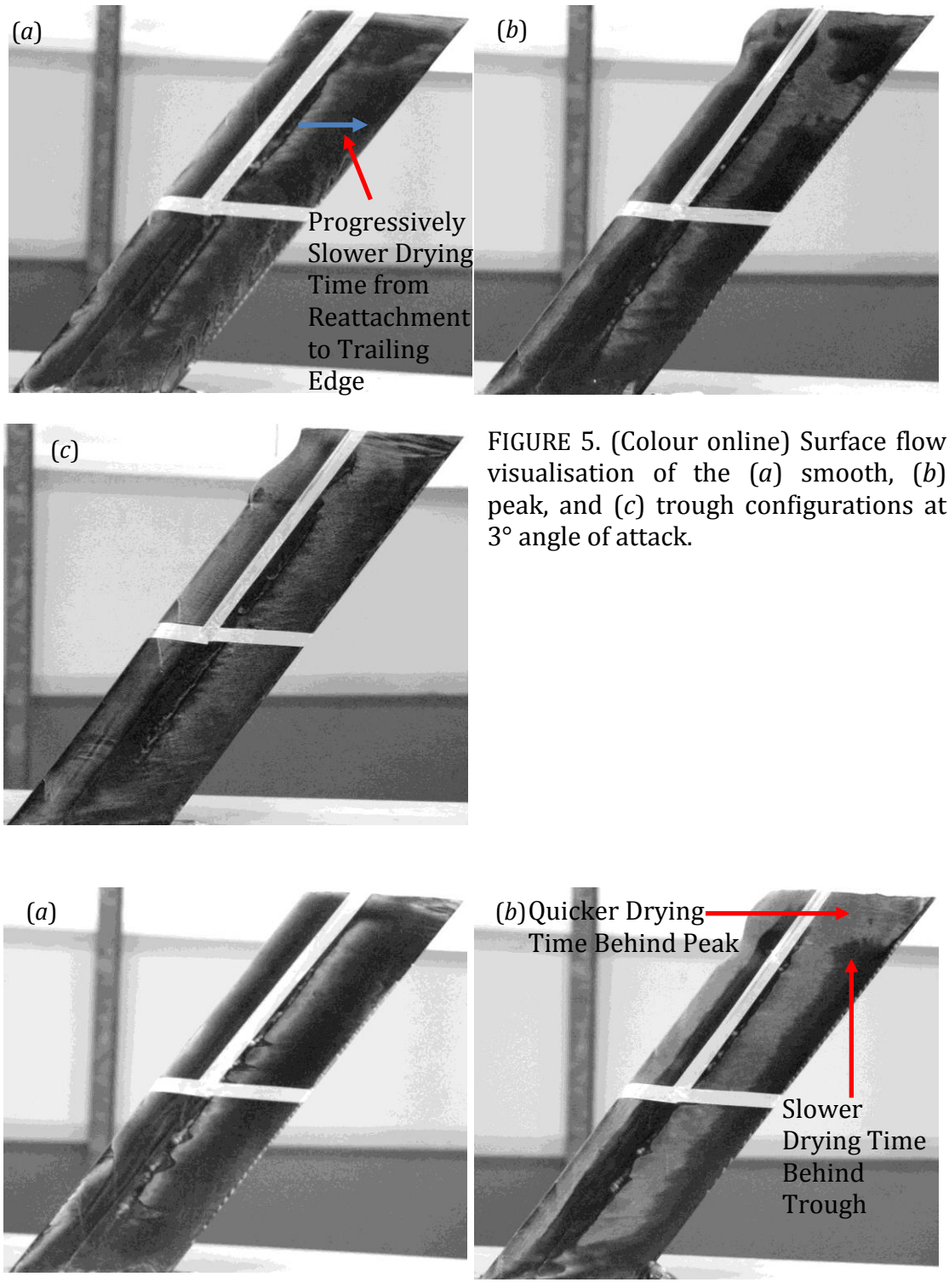

FIGURE 5. (Colour online) Surface flow visualisation of the (*a*) smooth, (*b*) peak, and (*c*) trough configurations at 3° angle of attack.

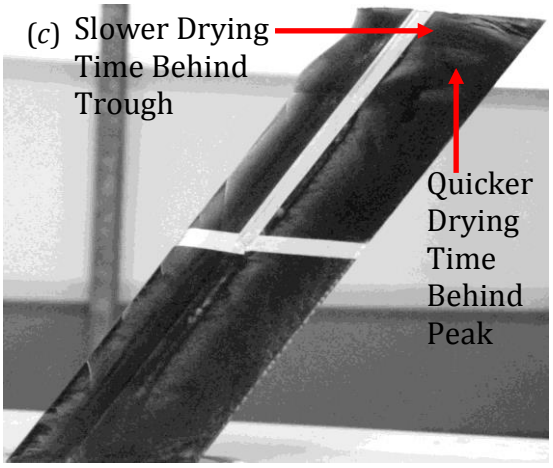

FIGURE 6. (Colour online) Surface flow visualisation of the (*a*) smooth, (*b*) peak, and (*c*) trough configurations at 6° angle of attack.

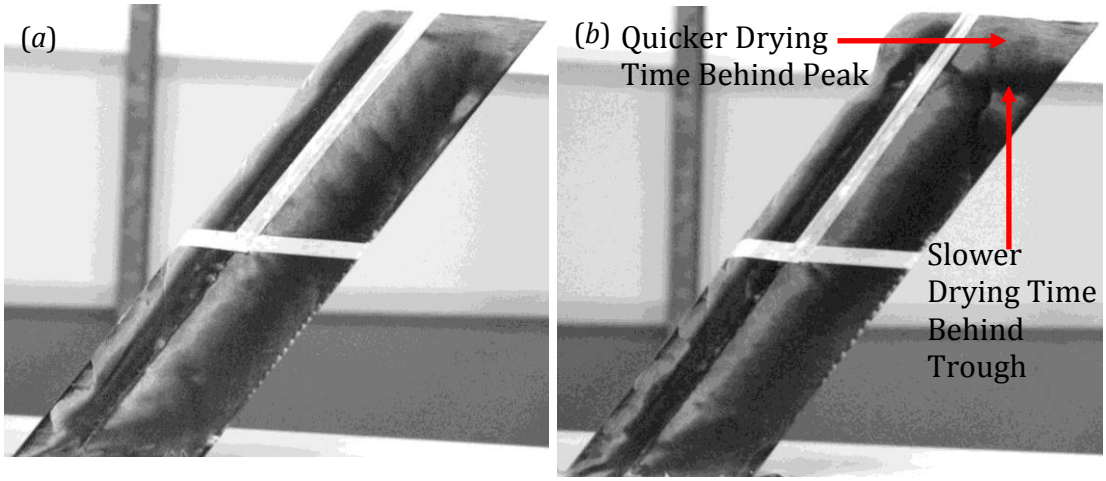

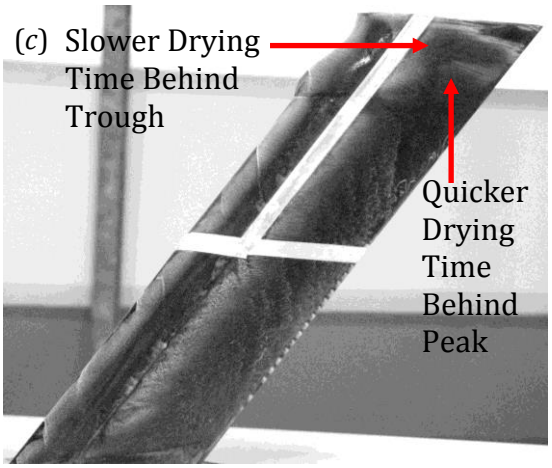

FIGURE 7. (Colour online) Surface flow visualisation of the (*a*) smooth, (*b*) peak, and (*c*) trough configurations at 9° angle of attack.

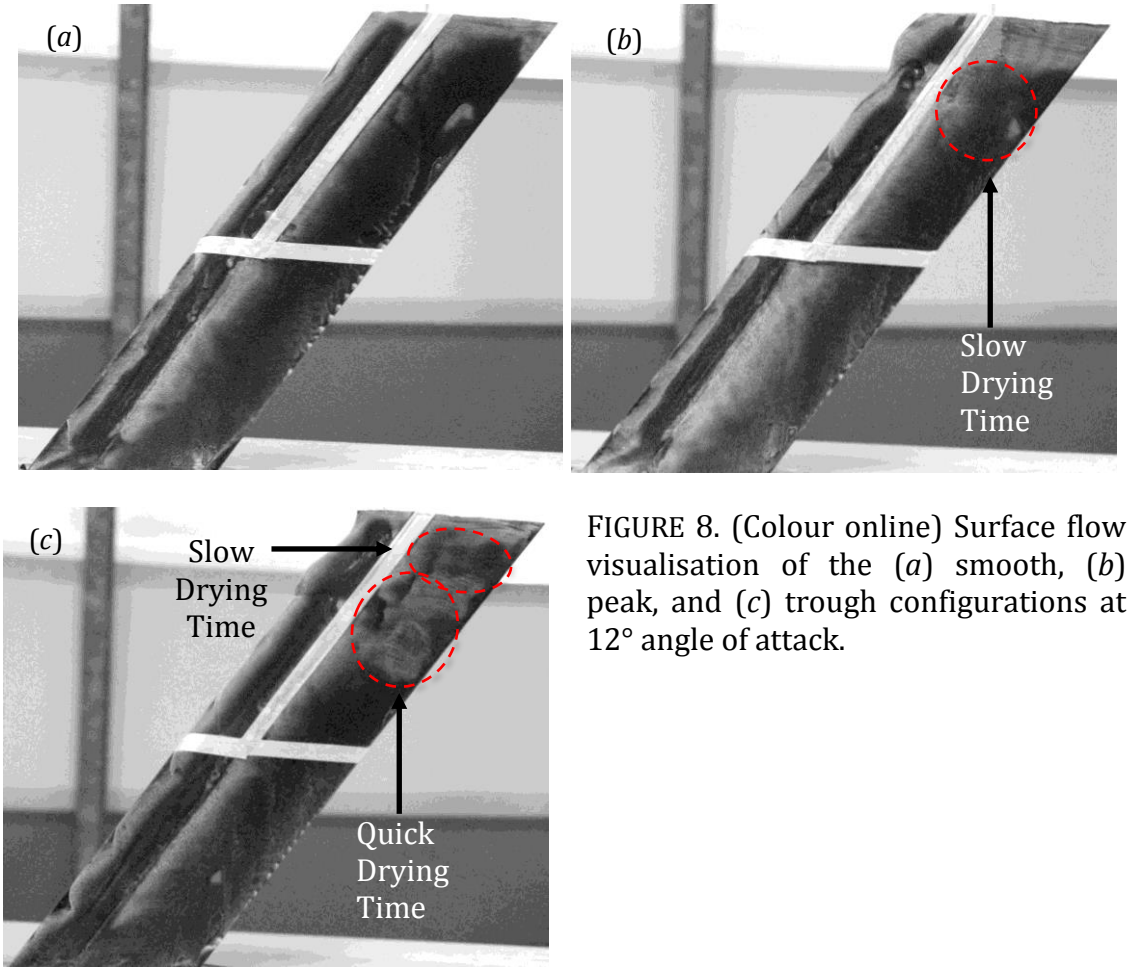

FIGURE 8. (Colour online) Surface flow visualisation of the (*a*) smooth, (*b*) peak, and (*c*) trough configurations at 12° angle of attack.

Vortex detachment points, that are similar to those found by Skillen *et al.* (2013) and Rostamzadeh *et al.* (2014), are visible on the peak and trough configurations at 3°, 9°, and 12° AOAs, and have been annotated on figures 9 to 11. A pattern that is consistent with an owl face of the first kind (Perry and Hornung, 1984) can typically be seen behind the troughs of both tubercle configurations for the AOAs presented, which is consistent with the findings of other studies (Rostamzadeh *et al.*, 2014; Hansen *et al.*, 2016). At 3° AOA, the vortex detachment points of both tubercle configurations occur at approximately 30 % of the chord from the leading edge. These vortex detachment points move towards the leading edge with increasing AOA.

The flow directions over the trough configurations at 9° and 12° AOAs are also discernible in figures 10 (*b*) and 11 *(b*). Downstream of the leading edge, the flow curves towards the vortex detachment points, which creates a bifurcation line, as annotated on figures 10 (*b*) and 11 (*b*). Due to the varying sweep of the leading edge, one vortex is expected to be weaker than the other (Bolzon *et al.*, 2016 b), as annotated on figures 10 (*b*) and 11 (*b*). The bifurcation lines lie closer to the expected weaker vortex.

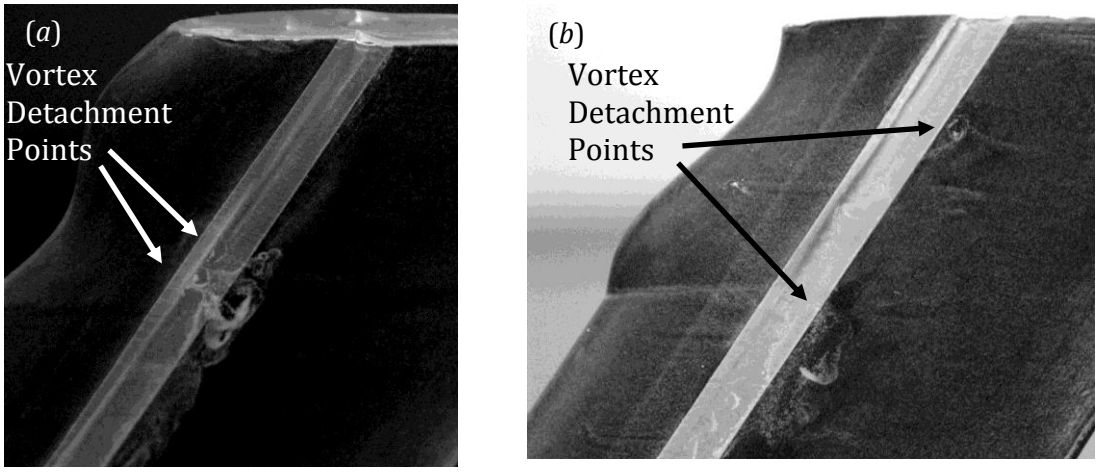

FIGURE 9. Surface flow visualisation of the (a) peak and (b) trough configurations at 3° angle of attack. Vortex detachment points shown.

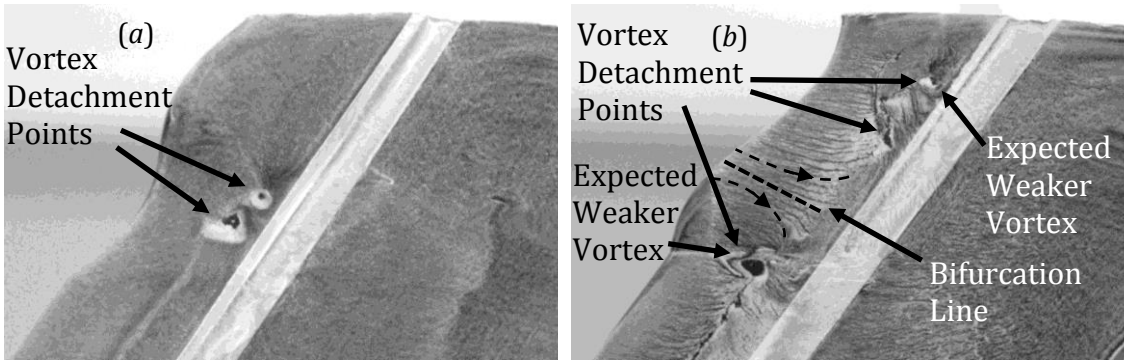

FIGURE 10. Surface flow visualisation of the (a) peak and (b) trough configurations at 9° angle of attack. Vortex detachment points shown.

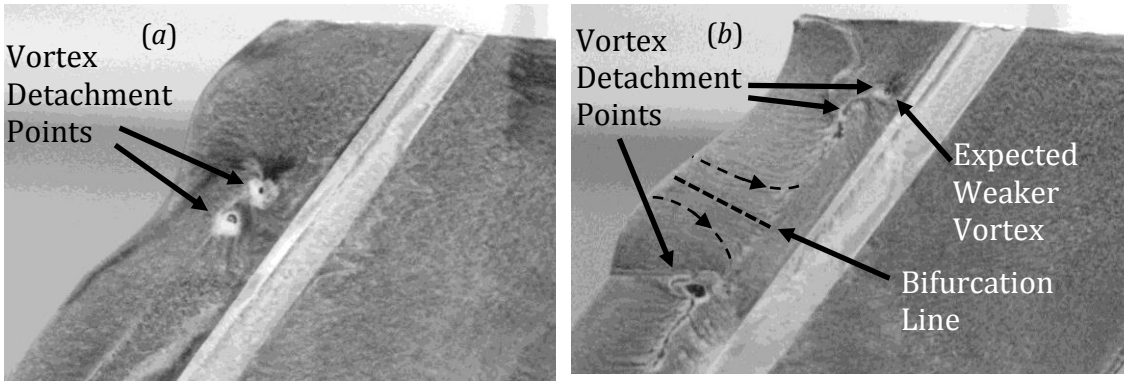

FIGURE 11. Surface flow visualisation of the (a) peak and (b) trough configurations at 12° angle of attack. Vortex detachment points shown.

Figure 12 shows the C_L and C_D of the smooth, peak, and trough wing configurations. The tubercle configurations have little effect on the C_L between -2° AOA and 15° AOA. From 13° AOA onwards, the lift-curve slopes of all three wings decrease, which indicates the onset of stall. From -2° to 11° AOA all three wings exhibit very similar C_D. The lift-to-drag ratios of all three wings are very similar for all AOAs considered, as shown in figure 13.

The lift-curve slopes of all the wing configurations have been calculated using the central-difference scheme, and are presented in figure 14. As expected from the data in figure 12, the lift-curve slopes of the three wings are nearly identical, with significant differences only appearing at 11°, 12°, and 14° AOAs onwards. However, these differences are typically within the experimental uncertainty and are therefore not conclusive. The greatest differences in the lift-curve slopes of the three wings occur from 14° AOA onwards, where the peak configuration has a lift-curve slope on average 13.2 % lower than the other two configurations, which suggests that the flow has separated to a greater extent over the peak configuration than the flow over the other two wing configurations. From 7° to 10° AOAs, the lift-curves slope of all three wing configurations increase. Similar trends in the lift-curve slope have been attributed to the formation of an LSB (Hansen, 2012; Rostamzadeh *et al.*, 2014; Bolzon *et al.*, 2016 a). A large LSB did form over each of the wing configurations, as detailed above, however, a single tubercle near the wingtip did not significantly alter the effect of the LSB on the lift-curve slope.

Figure 15 shows the changes in the C_L, C_D, and the lift-to-drag ratio of the peak configuration when compared with the smooth configuration, and are expressed as a percentage of the smooth configuration's respective parameter. The errorbars are included. Figure 16 is the same comparison, however, between the trough and smooth configurations. The peak configuration reduces the C_L and the lift-to-drag ratio at 1° AOA by approximately 5 %. From 3° to 7° AOAs, the peak configuration consistently reduces the C_L and C_D by approximately 1 %. From 8° AOA onwards, the peak configuration has little effect on the C_L and C_D. In addition, from 3° AOA onwards, the peak configuration has little effect on the lift-to-drag ratio, with changes in the order of 1 % typically observed.

The trough configuration reduces the C_L and lift-to-drag ratio at 1° AOA by approximately 3 %. From 2° to 6° AOAs, the trough configuration has little effect on any of the wing performance parameters. From 7° AOA onwards, the trough configuration typically increases the C_L and C_D by approximately 0.5 % and 1 %, respectively. As a result, the lift-to-drag ratio decreases by approximately 0.5 %.

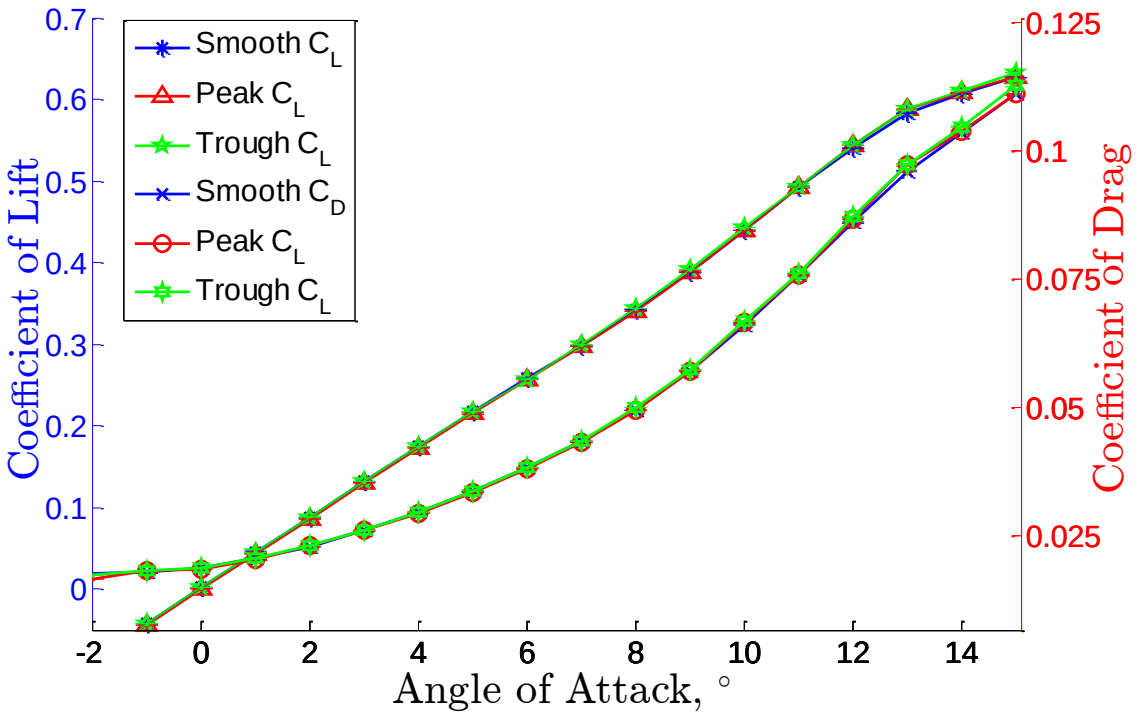

FIGURE 12. (Colour online) The lift and total drag coefficients of the smooth, peak, and trough configurations. Measurements are from the load cell.

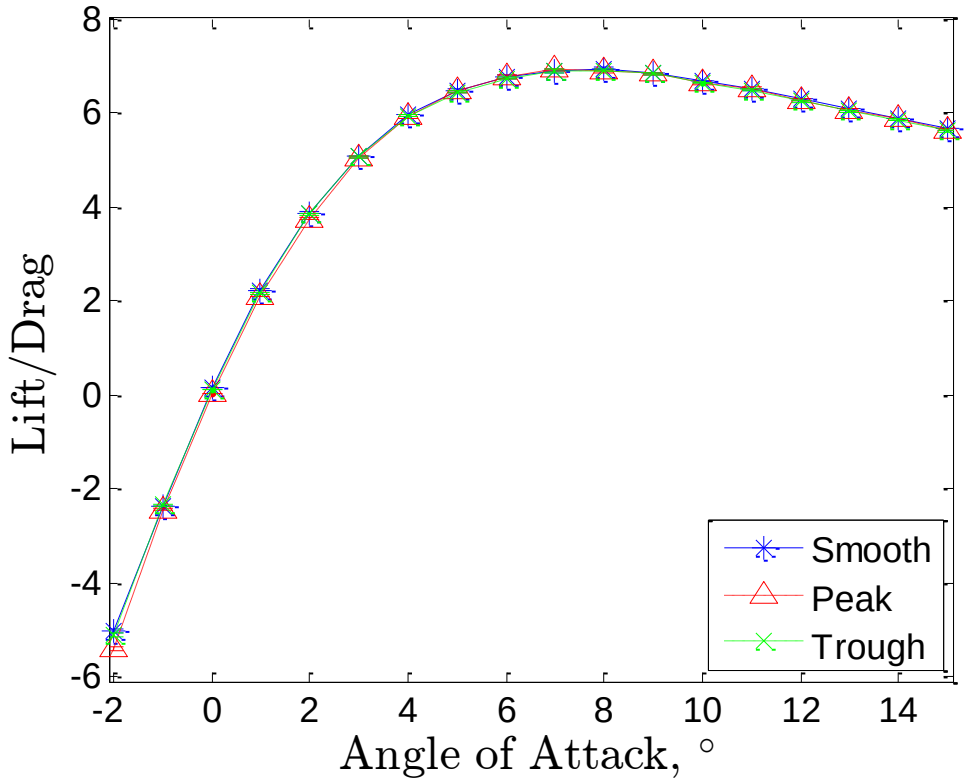

FIGURE 13. (Colour online) The lift-to-drag ratio of the smooth, peak, and trough configurations. Measurements are from the load cell.

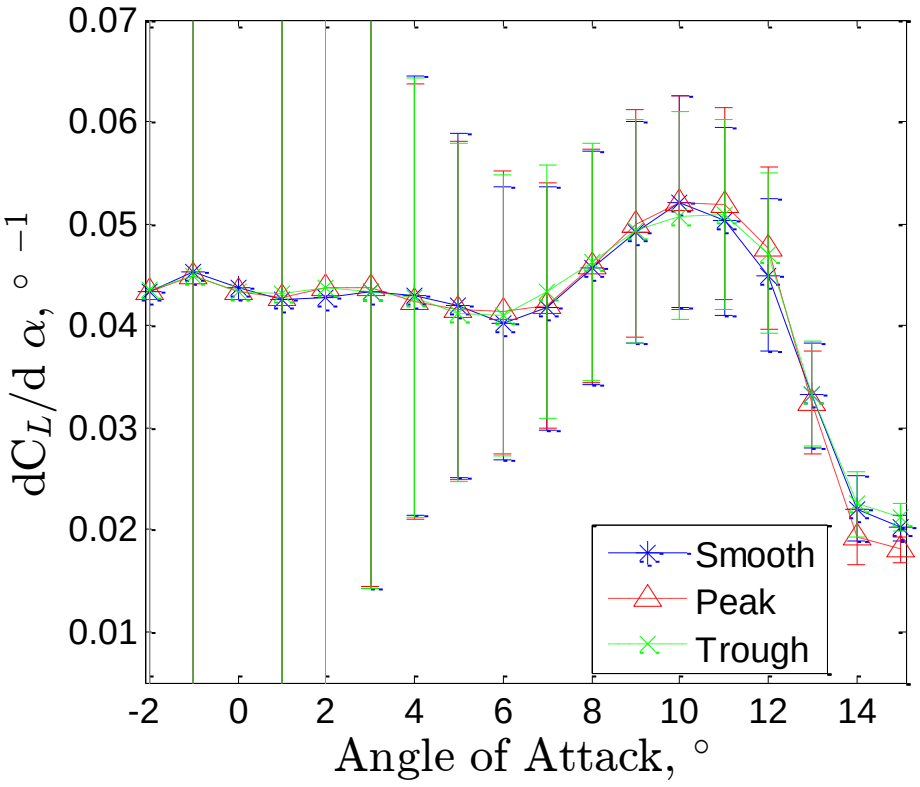

FIGURE 14. (Colour online) The lift-curve slope of the smooth, peak, and trough configurations. Measurements are from the load cell.

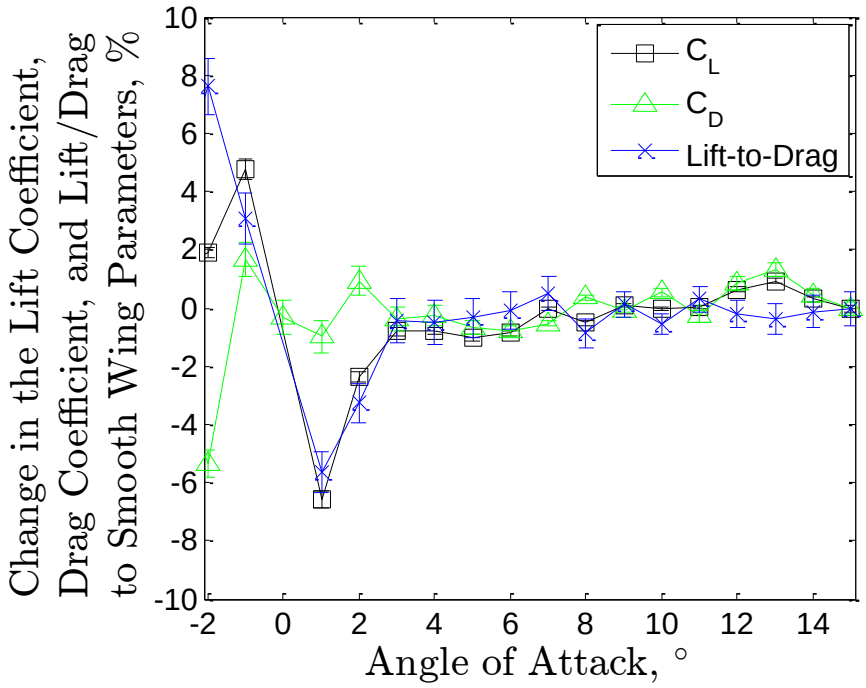

FIGURE 15. (Colour online) The change in the lift coefficient, the total drag coefficient, and the lift-to-drag ratio of the peak configuration, with respect to the smooth configuration's respective parameter. Expressed as a percentage of the smooth configuration's parameter. A positive value indicates an increase. Measurements are from the load cell and errorbars are included.

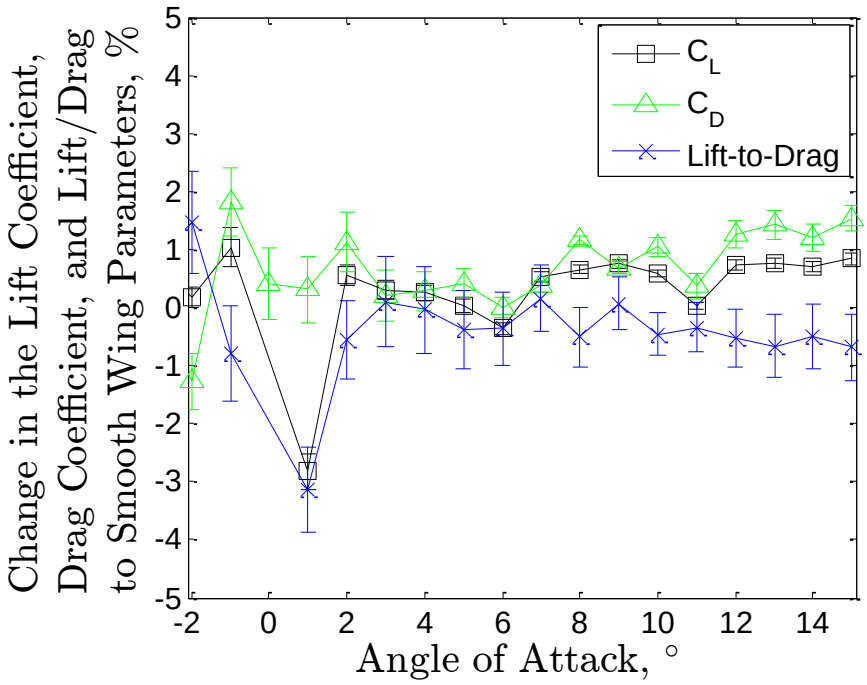

FIGURE 16. (Colour online) The change in the lift coefficient, the total drag coefficient, and the lift-to-drag ratio of the trough configuration, with respect to the smooth configuration's respective parameter. Expressed as a percentage of the smooth configuration's parameter. A positive value indicates an increase. Measurements are from the load cell and errorbars are included.

Figure 17 shows that the C_D of the three configurations obtained from the force measurements and wake surveys are in good agreement from 0° to 9° AOAs.

Figure 18 shows that at 0° AOA, the C_{D_P} of the three wings constitute the entirety of the C_D, whereas the C_{D_I} are approximately 0 (consistent with theory). As the AOA increases up to 9°, the C_{D_I} of the three configurations increase and become comparable to the C_{D_P}. The effects of the peak and trough configurations on the C_{D_I}, C_{D_P}, and C_D with respect to the smooth configuration's respective parameter are presented in figures 19 and 20. The errorbars are included. Figure 19 shows the changes as a magnitude, while figure 20 shows the changes as a percentage of the smooth configuration's respective parameter. Both of these figures show that, typically, both tubercle configurations have similar effects on the C_{D_I}, C_{D_P}, and C_D. In addition, as the AOA increases, both tubercle configurations typically have greater effects on the C_{D_I}, C_{D_P}, and C_D. Figures 19 and 20 show that both tubercle configurations affect the C_{D_P} more than the C_{D_I}. At 9° AOA, the greatest changes in the C_{D_P} of all the AOAs are seen, with the peak and trough configurations increasing it by 6.9 % and 11.4 %, respectively. From 0° to 6° AOAs, the peak and trough configurations change the C_{D_P} by 3.4 %, on average. At 0° AOA, while the peak and trough configurations increase the C_{D_I} by 30.3 % and 11.2 %, respectively, the magnitudes of these changes are minimal, and these percentage values arise primarily from error due to the near-zero C_{D_I} values at this AOA. Both tubercle configurations have minimal effects on the C_{D_I}

of the wing from 3° to 9° AOAs, with changes compared with the smooth wing's C_{D_I} in the range of -1.6 % to +3.7 % observed. Therefore, for this wing, any changes in the C_D are predominately caused by changes in the C_{D_P}.

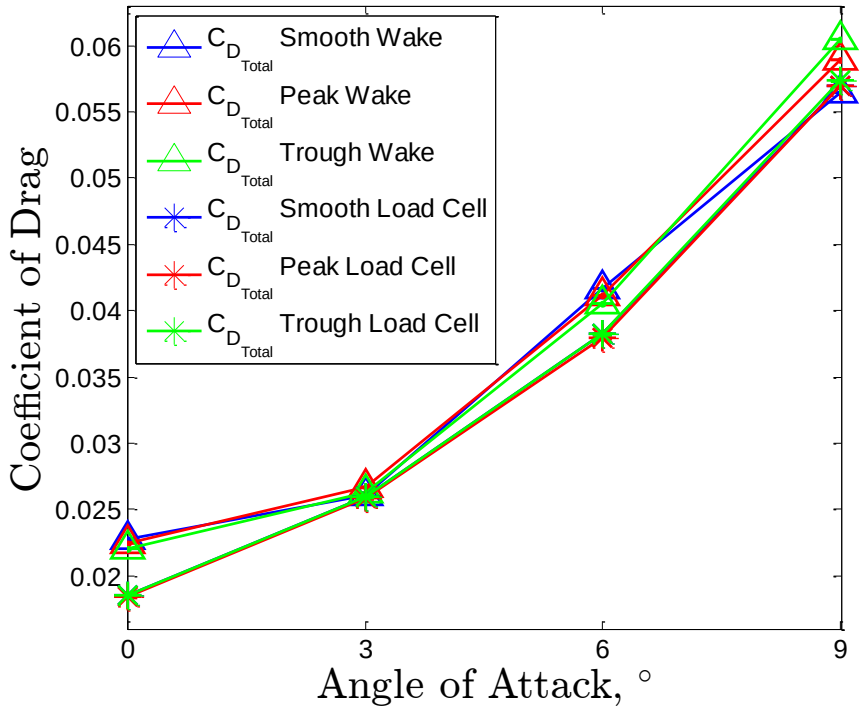

FIGURE 17. (Colour online) The total drag coefficients obtained from the force measurements and wake surveys.

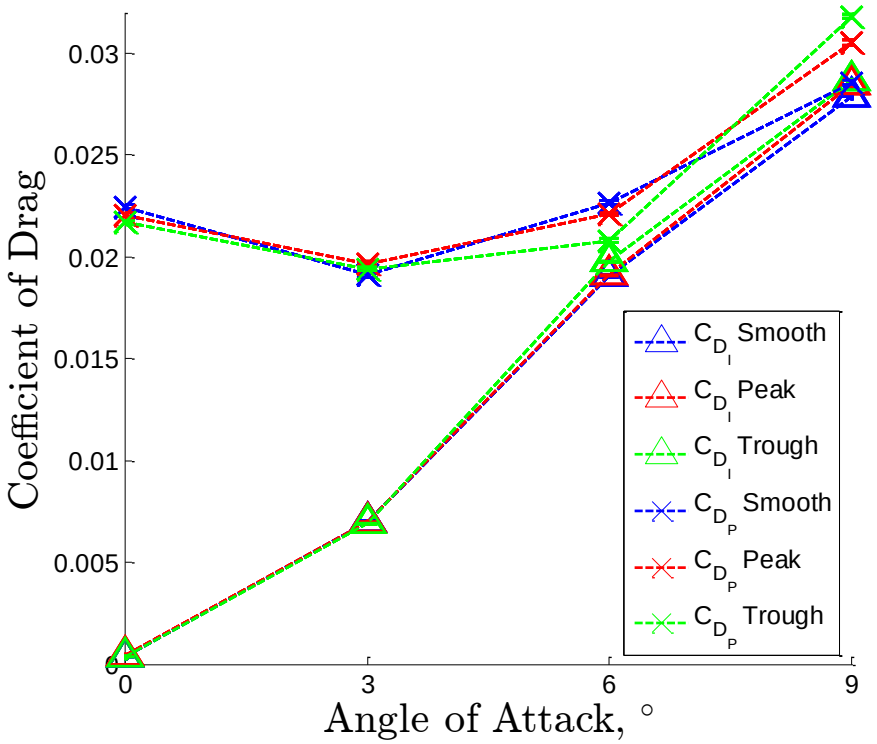

FIGURE 18. (Colour online) The induced and profile drag coefficients obtained from the wake surveys.

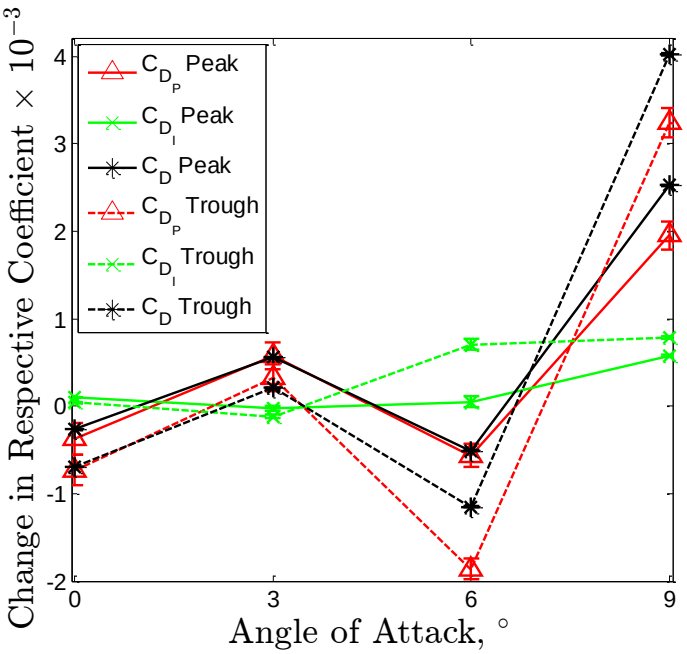

FIGURE 19. (Colour online) The change in the induced, profile, and total drag coefficients of the peak and trough configurations with respect to the smooth configuration's respective parameter. A positive value indicates an increase. Measurements are from the wake surveys and errorbars are included.

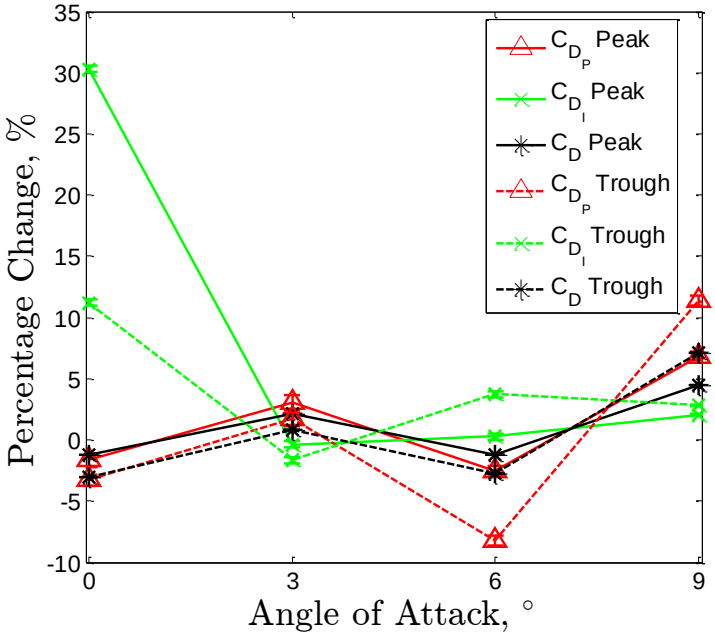

FIGURE 20. (Colour online) The relative change in the induced, profile, and total drag coefficients of the peak and trough configurations with respect to the smooth configuration's respective parameter. Values are expressed as a percentage of the smooth configuration's respective parameter, where a positive value indicates an increase. Measurements are from the wake surveys and errorbars are included.

Figures 21 to 24 show the distributions of the $C_{D_I}{}'$, $C_{D_P}{}'$, and C_D', as defined in §2.2.3, from 0° to 9° AOAs for all three wing configurations. Figure 21 (a) shows that at 0° AOA, the magnitudes of the $C_{D_I}{}'$ for all of the wing configurations are minimal, as expected. At 0° and 3° AOAs, inboard of the wingtip, the peak and the trough configurations each produce a local maximum and a local minimum in the $C_{D_P}{}'$ and the $C_D{}'$, as labelled on figures 21 and 22. The $C_{D_P}{}'$ local maxima and minima of both of the configurations occur approximately behind the troughs and peaks, respectively. However, due to vortex wandering, to determine the exact locations of these local maxima and minima and the reasons why they occur, these results must be analysed with the vorticity distributions, which is done below. The tubercle configurations also produce local maxima and minima in the $C_{D_I}{}'$ at 0° and 3° AOAs, however, the local maxima typically occur near the peaks, and local minima near the troughs. These trends are consistent with the literature (Bolzon *et al.*; 2016 a; Bolzon *et al.*, 2016 b). The exact locations of the $C_{D_I}{}'$ local maxima and minima are determined below, in a similar fashion as the $C_{D_P}{}'$ local maxima and minima. From 6° AOA onwards, the $C_{D_I}{}'$, $C_{D_P}{}'$, and $C_D{}'$ local maxima and minima are less noticeable, which is probably due to the flow separating behind the troughs of the tubercles, as detailed above. A discontinuity in the $C_{D_P}{}'$ typically occurs at the midspan of each wing configuration at all AOAs investigated, as labelled on figure 21 (b), which is caused by the interface (semi-span division) between the two wing sections (see figure 1).

At 0° AOA, the peak configuration reduces the $C_{D_P}{}'$ and $C_D{}'$ in the wingtip region, while the trough configuration increases the $C_{D_P}{}'$ and $C_D{}'$, when compared with the smooth configuration, as shown in figure 21 (b,c). This trend continues for the non-zero AOAs, however, the relative changes become less noticeable.

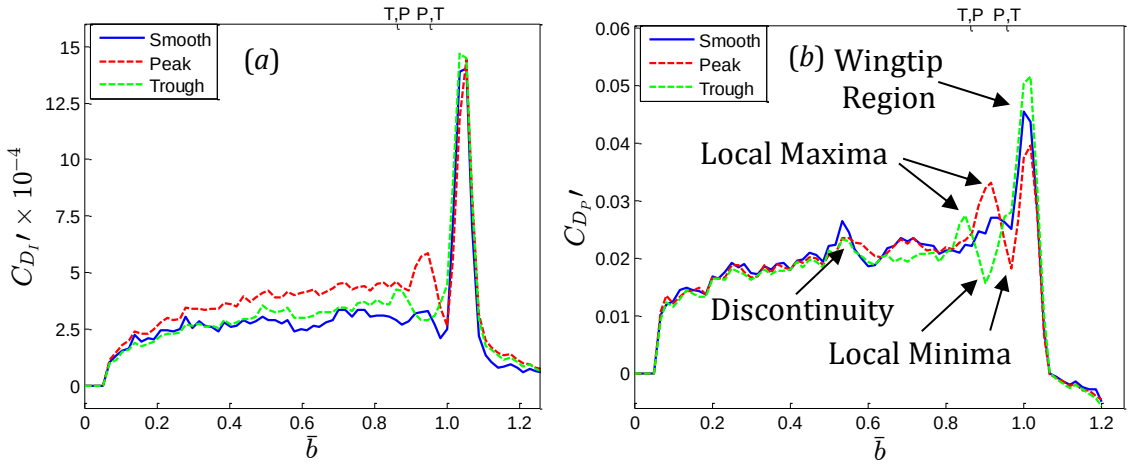

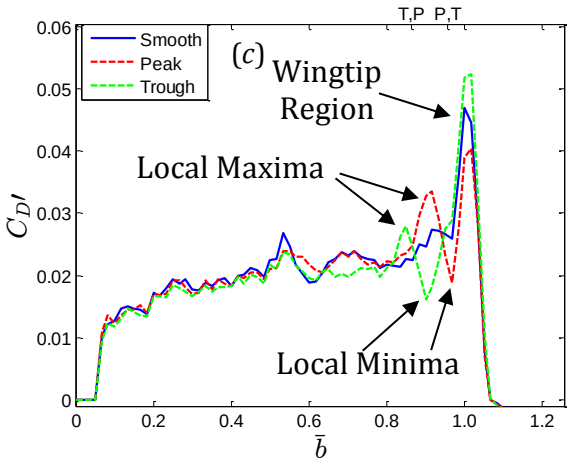

FIGURE 21. (Colour online) Distributions of the spanwise (*a*) induced, (*b*) profile, and (*c*) total drag coefficients of the smooth, peak, and trough configurations at 0° AOA. Measurements are from the wake surveys. Positions of troughs and peaks are shown on the top of each graph. The bottom horizontal axis has been normalized to the wingspan.

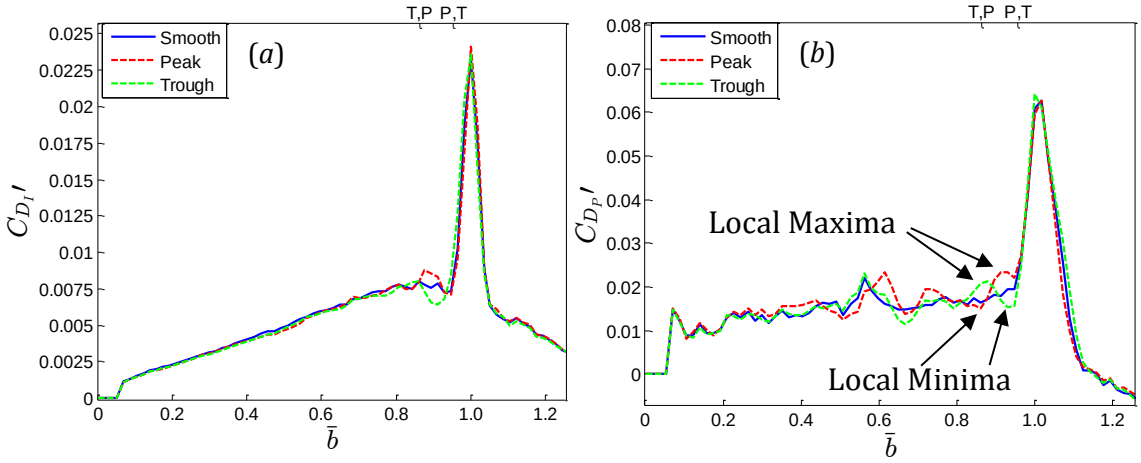

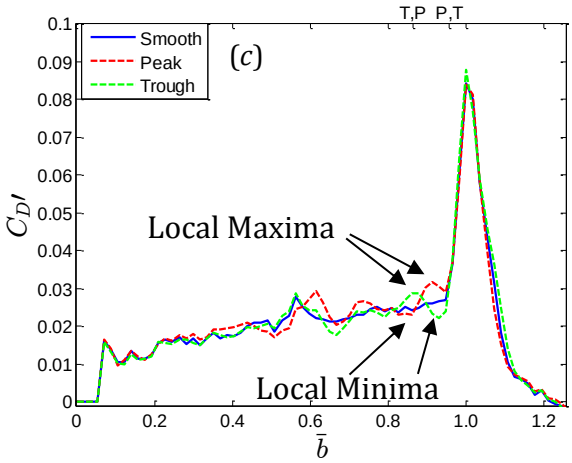

FIGURE 22. (Colour online) Distributions of the spanwise (*a*) induced, (*b*) profile, and (*c*) total drag coefficients of the smooth, peak, and trough configurations at 3° AOA. Measurements are from the wake surveys. Positions of troughs and peaks are shown on the top of each graph. The bottom horizontal axis has been normalized to the wingspan.

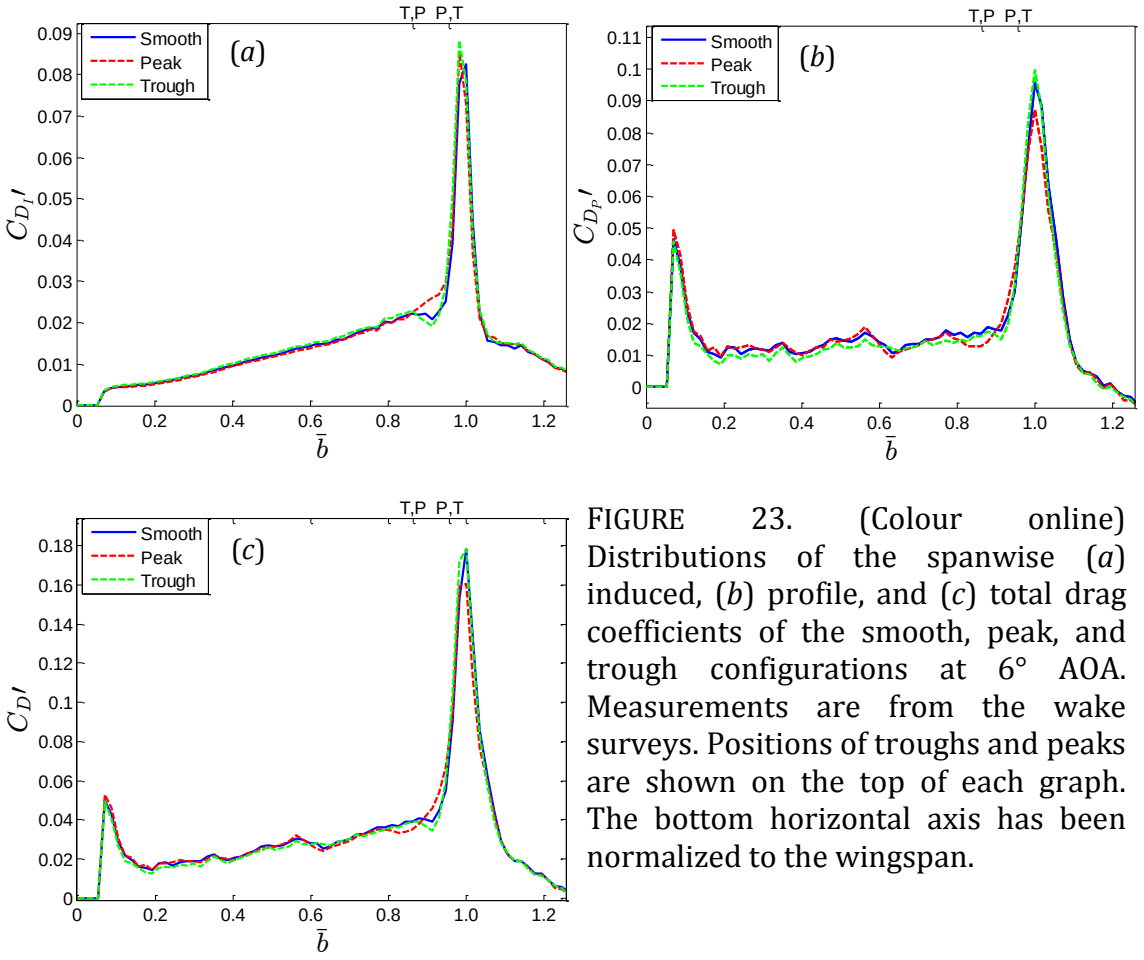

FIGURE 23. (Colour online) Distributions of the spanwise (*a*) induced, (*b*) profile, and (*c*) total drag coefficients of the smooth, peak, and trough configurations at 6° AOA. Measurements are from the wake surveys. Positions of troughs and peaks are shown on the top of each graph. The bottom horizontal axis has been normalized to the wingspan.

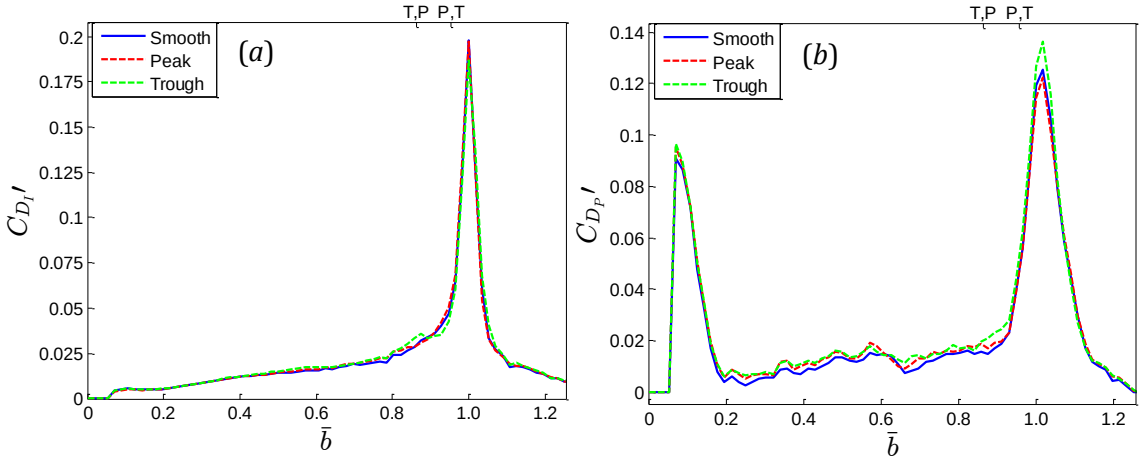

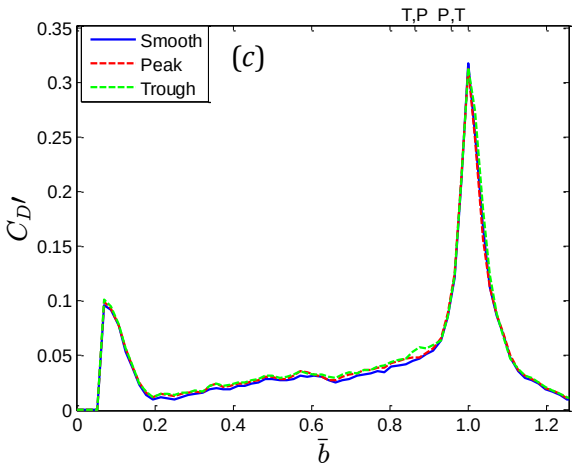

FIGURE 24. (Colour online) Distributions of the spanwise (a) induced, (b) profile, and (c) total drag coefficients of the smooth, peak, and trough configurations at 9° AOA. Measurements are from the wake surveys. Positions of troughs and peaks are shown on the top of each graph. The bottom horizontal axis has been normalized to the wingspan.

The C_{D_I}', C_{D_P}', and C_D' have been summated from the wing root to the wingtip, which has been designated the "span", and from the wingtip to the edge of the wake plane surveyed, which has been designated the "wingtip", for all wing configurations at all AOAs. The smooth configuration's span and wingtip values have been subtracted from the peak configuration's span and wingtip values, respectively, to give the differences. These differences have then been divided by the summated difference in the C_{D_I}', C_{D_P}', and C_D' from the wing root to the edge of the wake plane surveyed, and multiplied by 100 to give the percentage changes. These show the respective contributions of the span and the wingtip region to the overall changes in the C_{D_I}', C_{D_P}', and C_D'. The same has been done with the trough configuration's C_{D_I}', C_{D_P}', and C_D'. The results for the peak and trough configurations are presented in figure 25 (a,b), respectively. It should be noted that if, for example, the peak configuration reduces the overall C_{D_I}' compared with the smooth configuration, then the summation of the percentage changes in the C_{D_I}' over the span and the wingtip regions equals -100 %. Conversely, if, for example, the peak configuration increases the overall C_{D_I}' when compared with the smooth configuration, then the summation of the percentage changes in the C_{D_I}' over the span and the wingtip regions equals +100 %.

Figure 25 shows that for both tubercle configurations, similar changes to the overall C_{D_I}', C_{D_P}', and C_D' occur over the spans and in the wingtip regions.

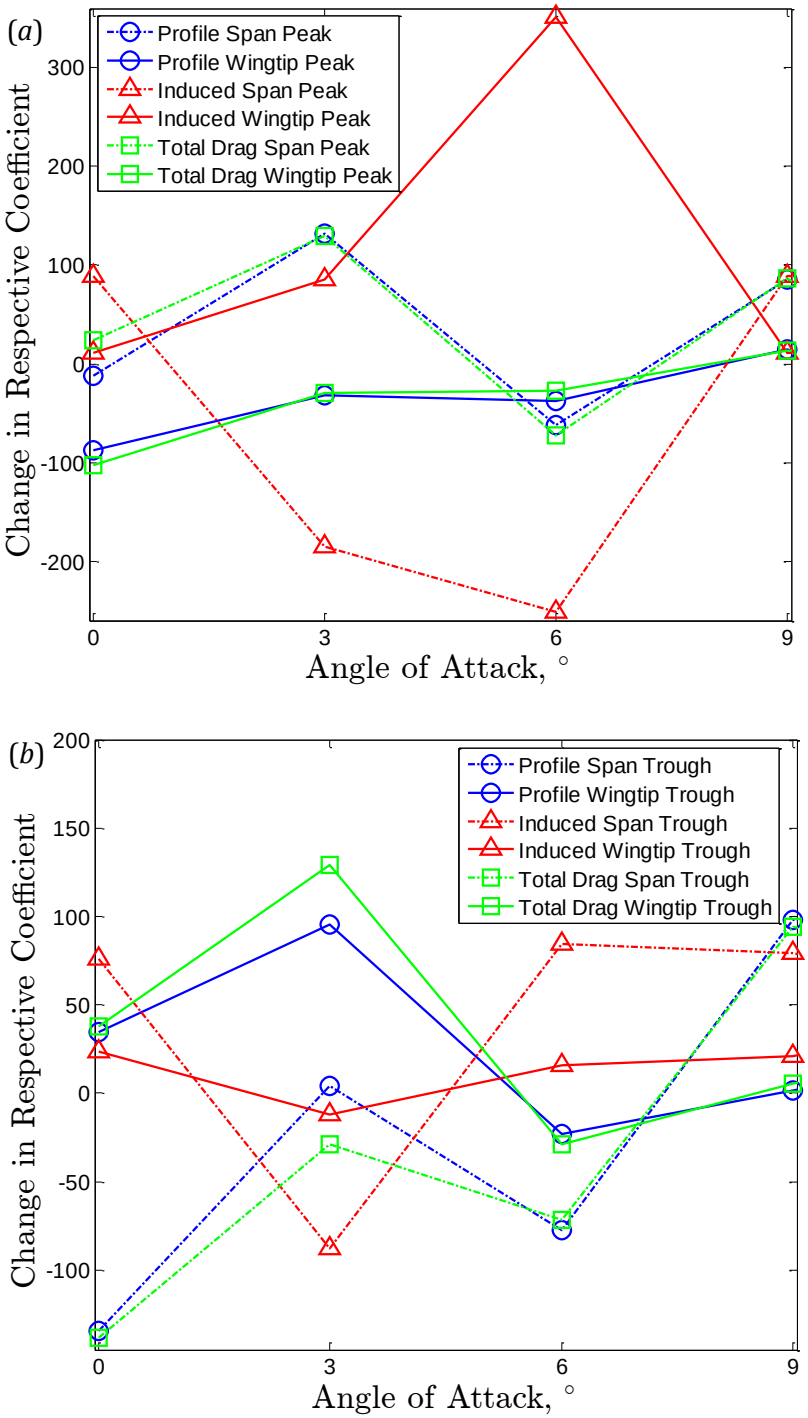

FIGURE 25. (Colour online) The relative changes in the spanwise induced, profile, and total drag coefficients in the span and wingtip regions of the (*a*) peak and (*b*) trough configurations with respect to the smooth configuration's respective parameter. Changes are expressed as a percentage of the overall change in each parameter with respect to the smooth configuration. Measurements are from the wake surveys.

The vorticity distributions of the three wing configurations at all AOAs are presented in figures 26 to 29. The circulations of the wingtip vortices of all wing configurations at non-zero degree AOAs are presented in figure 30. Figure 26

shows that there is no sign of a dominant wingtip vortex for any of the configurations at a 0° AOA, therefore, it is concluded that the wings were well aligned. Overall, neither tubercle configuration greatly alters the vorticity distribution of the smooth configuration, with similar maximum vorticity occurring in the wingtip region, and uniform vorticity spanning most of the wingspan. Typically, both of the tubercle configurations slightly affect the lower vorticity contours near the wingtip region at all AOAs; an example has been labelled on figure 28, where the smooth configuration produces two 150 s^{-1} contours; one around the dominant vortex at the wingtip and one adjacent to this region. The peak configuration only has one 150 s^{-1} contour, which is enlarged, as labelled on figure 28 (*b*). The trough configuration only has one 150 s^{-1} contour, as labelled on figure 28 (*c*), which is of similar size to the contour around the dominant vortex of the smooth configuration. As the AOA increases, the wingtip vortex, and the tubercle vortices in the case of the tubercle configurations, induce the large region of positive vorticity and skew it towards the bottom-right of the figures, as labelled on figure 29 (*b*). This trend agrees with the results presented in Bolzon *et al.* (2016, b), and with the results obtained by applying the "method of images" to these vortices.

There are negligible differences among the circulations of the wingtip vortices of the three wing configurations at 3° AOA. At 6° AOA, compared with the smooth configuration, the peak configuration increases the wingtip vortex's circulation by 3.3 %, while the trough configuration reduces it by 2.5 %. Both of these differences are greater than the uncertainty ranges. At 9°, the peak configuration has little effect on the wingtip vortex circulation compared with the smooth wing, whereas the trough configuration reduces it by 4.8 %, which is greater than the uncertainty range. The wingtip vortex circulations of all three configurations typically increase linearly with the AOA.

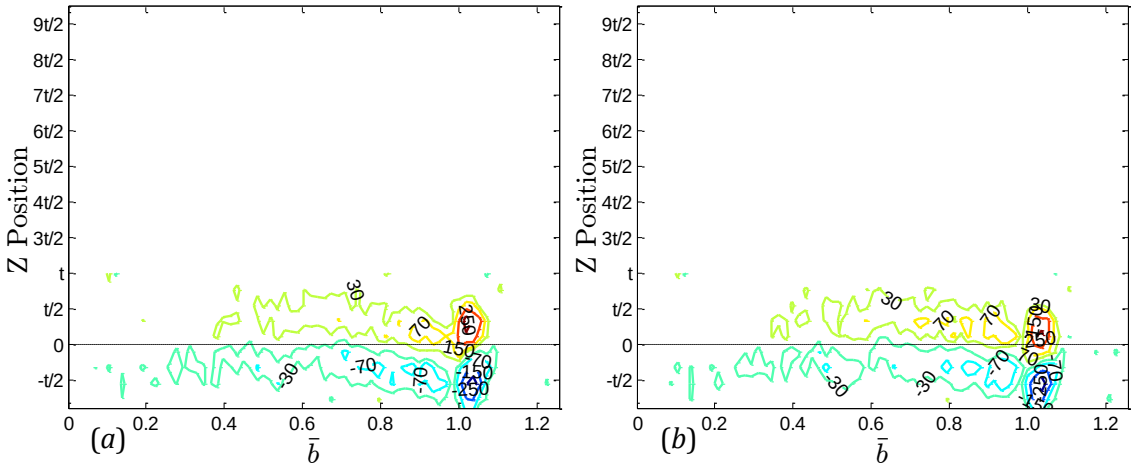

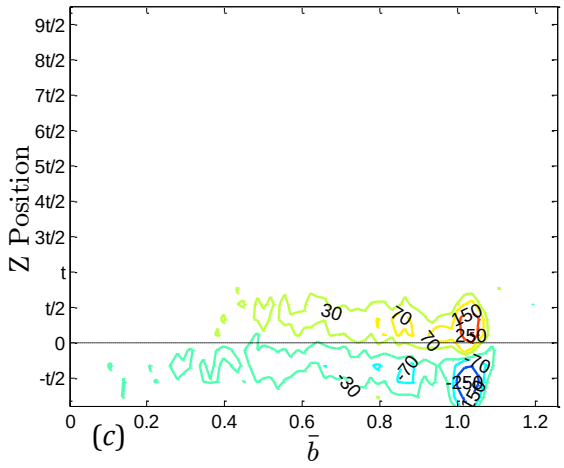

FIGURE 26. (Colour online) Vorticity distributions of the (*a*) smooth, (*b*) peak, and (*c*) trough configurations at 0° angle of attack. The horizontal axis has been normalized to the wingspan. The vertical axis has been normalized to the wing thickness. Measurements are from the wake surveys.

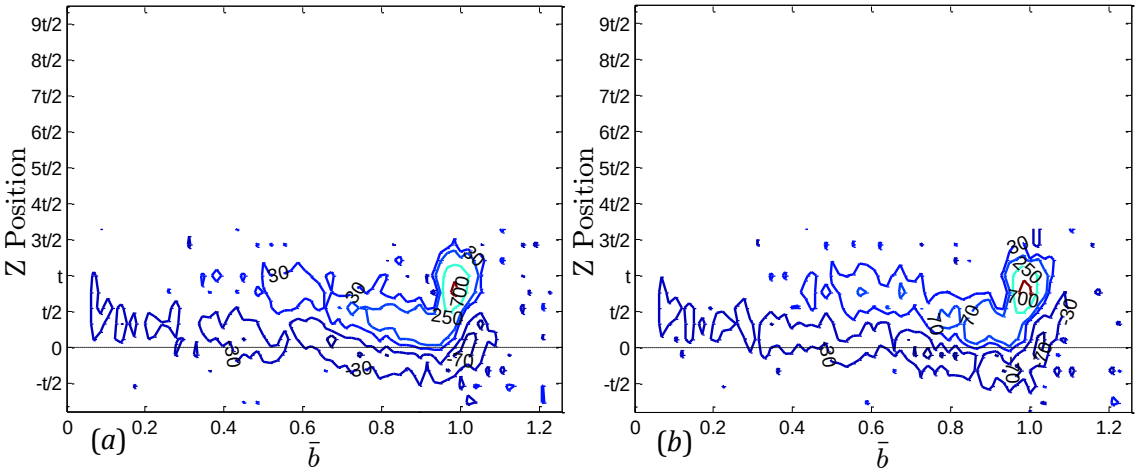

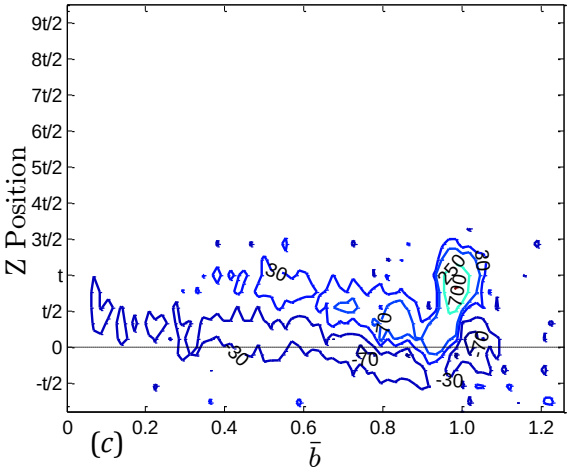

FIGURE 27. (Colour online) Vorticity distributions of the (*a*) smooth, (*b*) peak, and (*c*) trough configurations at 3° angle of attack. The horizontal axis has been normalized to the wingspan. The vertical axis has been normalized to the wing thickness. Measurements are from the wake surveys.

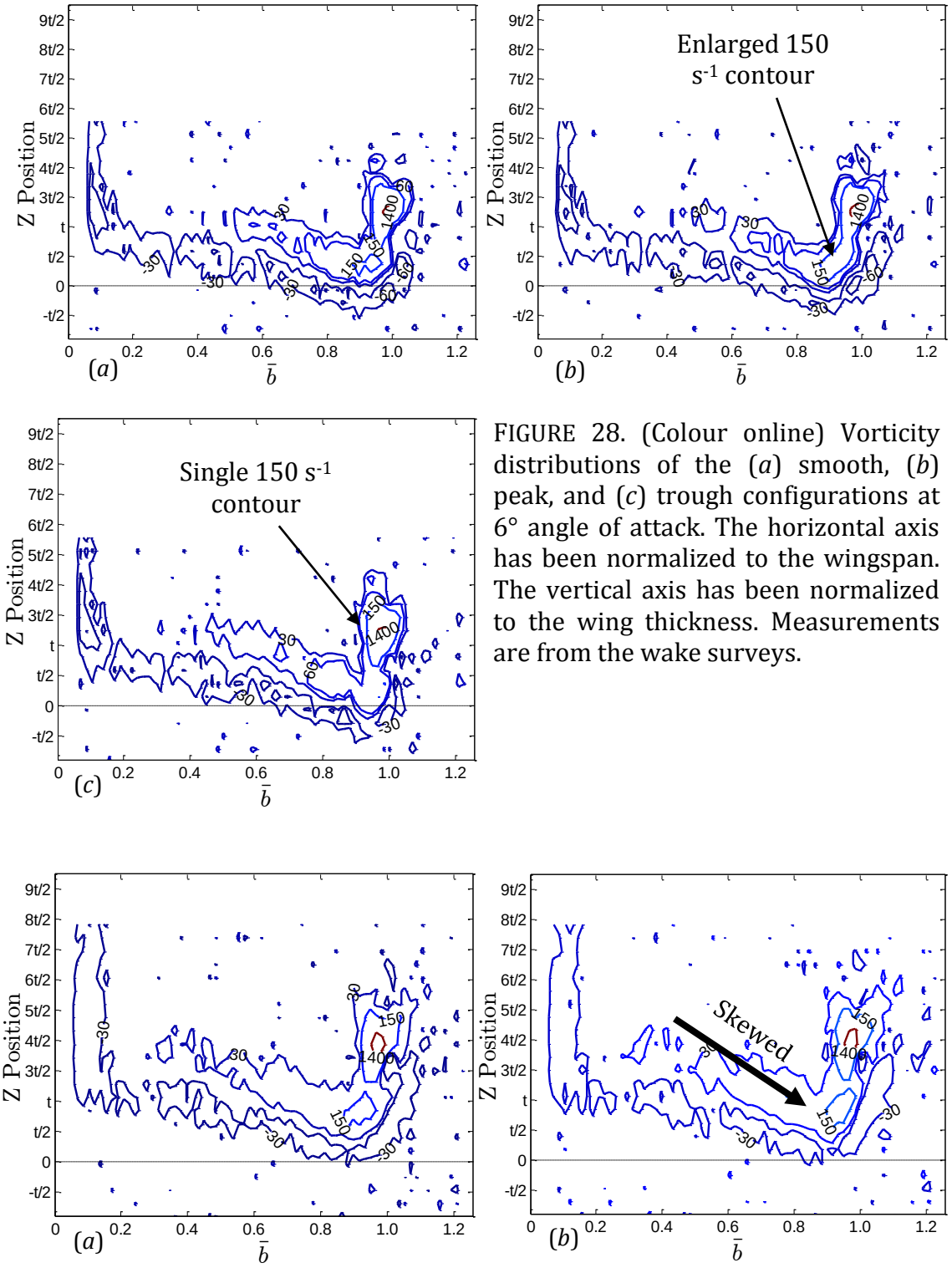

FIGURE 28. (Colour online) Vorticity distributions of the (*a*) smooth, (*b*) peak, and (*c*) trough configurations at 6° angle of attack. The horizontal axis has been normalized to the wingspan. The vertical axis has been normalized to the wing thickness. Measurements are from the wake surveys.

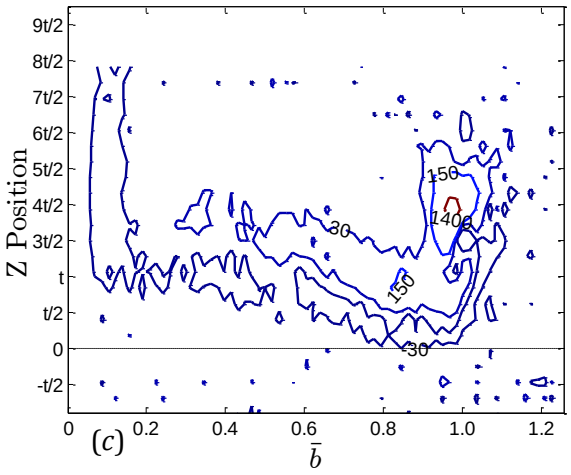

FIGURE 29. (Colour online) Vorticity distributions of the (*a*) smooth, (*b*) peak, and (*c*) trough configurations at 9° angle of attack. The horizontal axis has been normalized to the wingspan. The vertical axis has been normalized to the wing thickness. Measurements are from the wake surveys.

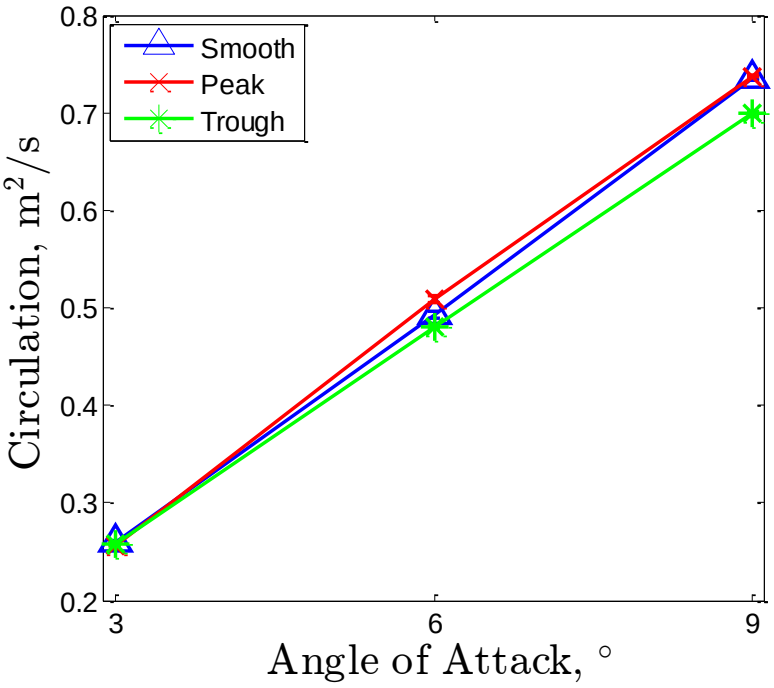

FIGURE 30. (Colour online) The wingtip vortex circulations of the smooth, peak, and trough configurations at non-zero degree angles of attack. Measurements are from the wake surveys. Errorbars are included.

4. Discussion

Overall, this study showed that a single tubercle of conventional sizing placed near the wingtip does not significantly affect a wing's C_L, C_D, or lift-to-drag ratio at the AOAs investigated. Furthermore, the tubercle configurations investigated typically change the C_{D_I}, C_{D_P}, and wingtip vortex strength by approximately 2 %, 5 %, and 2.2%, respectively. Therefore, more than one tubercle should be implemented on a wing's leading edge to achieve significant increases in wing performance at pre-stall AOAs.

A previous study by the authors (Bolzon *et al.*, 2016 b) showed that tubercles modulate the $C_{D_P}{}'$ into local maxima and minima behind the troughs and peaks, respectively. These effects are also shown in this study, however, it remains unclear why these effects occur at low AOAs; the modulations could be caused by a range of phenomena including the upwash and downwash occurring behind the troughs and peaks, respectively (Hansen *et al.*, 2016), the LSB modulation (Choudhry *et al.*, 2015), or flow patterns such as the owl-face separation. Therefore, further investigation is required. At higher AOAs, however, the upwash results in premature flow separation behind the troughs (Rostamzadeh *et al.*, 2014; Bolzon *et al.*, 2016 d), which adds to the already increased $C_{D_P}{}'$.

Similarly, a previous study by the authors (Bolzon *et al.*, 2016 b) showed that tubercles modulate the $C_{D_I}{}'$ into local maxima and minima behind the peaks and troughs, respectively. This study also shows that these local maxima and minima occur behind the peaks and troughs, respectively. The authors propose that the downwash behind the peaks (Hansen *et al.*, 2016) increases the $C_{D_I}{}'$ as it increases the downwash angle, which further tilts the local lift vector into the freestream direction. Conversely, the upwash behind the troughs (Hansen *et al.*, 2016) reduces the $C_{D_I}{}'$ as it reduces the downwash angle and thereby reduces the tilt of the local lift vector into the freestream direction.

Usually a stronger wingtip vortex is indicative of a greater C_{D_I}. However, it was found that the trough configuration slightly increases the C_{D_I}, but reduces the wingtip vortex strength. The authors suggest that, as the tubercle vortex closest to the trough configuration's wingtip is of opposite sign to the wingtip vortex, its breakdown weakens the wingtip vortex, however, its production increases the C_{D_I} overall.

Both tubercle configurations have similar effects on the C_{D_P}, however, these effects are not consistent from 0° to 9° AOAs, with decreases occurring at 0° and 6° AOAs, and increases occurring at 3° and 9° AOAs. At 0° AOA, both tubercle configurations reduce the $C_{D_P}{}'$ by keeping the flow attached over the wingtip and leading edge junction (Bolzon *et al.*, 2016 b; Bolzon *et al.*, 2016 c). At 3° AOA, the $C_{D_P}{}'$ of all wing configurations in the wingtip region are similar, but both tubercle configurations slightly increase the $C_{D_P}{}'$ over the span and, as a result, both tubercles increase the C_{D_P}. At 6° AOA, slight flow separation in the wingtip region of the smooth wing occurs, but both tubercle configurations reduce it to some extent, as evidenced by the surface film flow visualisation results. As a result, both tubercle configurations slightly reduce the C_{D_P}. At 9° AOA, the flow behind the tubercle troughs separate greatly, as evidenced by the surface film flow visualisation results and the $C_{D_P}{}'$ distributions, which increases the tubercle configurations' C_{D_P}.

The trends that tubercles create local maxima in the $C_{D_I}{}'$ and $C_{D_P}{}'$ behind the peaks and troughs, respectively, and create local minima in the $C_{D_I}{}'$ and $C_{D_P}{}'$ behind the troughs and peaks, respectively, provide a direction for a future investigation into tubercles; to determine the effects of the sharpness and the size of the tubercle peaks and troughs on the components of drag. By doing so, the greater component of drag, which depends on the application and flow conditions, may be further reduced while incurring a smaller drag penalty from the other component of drag.

At 3° AOA, the effects of the tubercle configurations on the wing C_L and C_{D_I} are minimal, which is consistent with the findings of the parametric study by Bolzon *et al.* (2016, c). That study also showed that larger tubercle amplitudes and wavelengths typically increase the effectiveness of tubercles on the C_L and C_{D_I}. Therefore, an investigation into the effects of larger tubercle geometries on wing performance is also required.

The finding that the peak configuration reduces the C_{D_P} in the wingtip region supports the findings presented in Bolzon *et al.* (2016, a), which showed that a swept tubercled wing, with a $\pi/2$ phase, can reduce the C_{D_P} in the wingtip region. This reduction is hypothesized to be caused by a smaller flow separation over the junction of the leading edge and the wingtip (Bolzon *et al.*, 2016 a).

5. Conclusion

A swept NACA 0021 wing, with three interchangeable leading edges, a smooth leading edge and two tubercled leading edges, were investigated experimentally in a wind tunnel. Both tubercle leading edges featured one entire tubercle, with an amplitude of 10.5 mm (0.081 amplitude-to-chord ratio) and a wavelength of 60 mm (0.46 wavelength-to-chord ratio), which terminated at the wingtip. One tubercle leading edge terminated midway between a tubercle peak and a trough, while the other terminated midway between a tubercle trough and peak. These two geometries were termed, the "peak" and "trough" configurations, respectively.

Surface film flow visualisation, force measurements, and wake surveys were conducted on these three wing configurations at pre-stall angles of attack. Neither tubercle configuration significantly affected the lift coefficient, the drag coefficient, or the lift-to-drag ratio compared with the smooth configuration.

The surface film flow visualisation showed that a Laminar Separation Bubble (LSB) formed over the suction side of all of the wing configurations. The LSB on the smooth configuration extended from the wing root to the wingtip with a uniform chordwise length. LSBs formed in a similar fashion over the peak and trough configurations, however, the LSBs' chordwise lengths were modulated aft of the tubercle sections. As the angle of attack increased, the LSB formed closer to the leading edge of all wing configurations. At 0° and 3° angles of attack, the three wing configurations had very similar flow visualisation results aft of the LSB, with the flow typically remaining attached. At 6°, 9°, and 12° angles of attack, the flow behind the peaks of both tubercle configurations remained attached, while the flow behind the troughs tended to separate, which is consistent with other studies.

The total drag coefficients of the three wing configurations obtained from the wake survey results were in good agreement with the total drag coefficients obtained from the force measurements. Both tubercle geometries modulated the spanwise induced and profile drag coefficients. Typically, local maxima in the spanwise induced and profile drag coefficients occurred behind the peaks and troughs, respectively. Conversely, local minima in the spanwise induced and profile drag coefficients occurred behind the troughs and peaks, respectively. At 0° and 6° angles of attack, the tubercle configurations reduced the profile drag coefficient by approximately 2.5 % and 5.3 %, respectively. At 3° and 9° angles of

attack, the tubercle configurations increased the profile drag coefficient by approximately 2.4 % and 9.1 %, respectively. Neither tubercle configuration significantly affected the induced drag coefficient at any non-zero angle of attack investigated. Therefore, the majority of the changes to the total drag coefficient by the tubercle configurations were caused by changes in the profile drag coefficient.

Neither tubercle configuration produced a significantly different (streamwise) vorticity distribution from that of the smooth configuration. The tubercle configurations typically had opposite effects on the smooth configuration's wingtip vortex strength. From 3° to 9° angles of attack, the peak configuration typically increased the wingtip vortex strength, whereas the trough configuration reduced it. Changes in the wingtip vortex strength were typically 2.2 %.

This study demonstrated that while a single tubercle terminating at the wingtip, with the geometries chosen, affects the flow physics over the wing, it does not significantly affect the wing performance at pre-stall angles of attack.

Acknowledgements

This study has been financially supported by the Sir Ross and Sir Keith Smith Fund. The authors greatly appreciate their support.

The authors acknowledge the assistance of Dr Peter Lanspeary and Mr Eyad Hassan in the vortex circulation calculations.

The authors acknowledge the editing assistance of Miss Alison-Jane Hunter.

REFERENCES

All Seals Inc 2016, February 19 Surface Finish Chart. Retrieved from http://www.allsealsinc.com/surface_finish_chart.pdf

Bolzon, M. D., Kelso, R. M. & Arjomandi, M. 2014 The Effects of Tubercles on Swept Wing Performance at Low Angles of Attack. In *19th Australasian Fluid Mechanics Conference, Melbourne, Australia*. Australasian Fluid Mechanics Society.

Bolzon, M. D., Kelso, R. M. & Arjomandi, M. 2016 a Force Measurements and Wake Surveys of a Swept Tubercled Wing. *The Journal of Aerospace Engineering* (in press).

Bolzon, M. D., Kelso, R. M. & Arjomandi, M. 2016 b Formation of Vortices on a Tubercled Wing, and Their Effects on Drag. *Aerospace Science and Technology*. doi: 10.1016/j.ast.2016.06.025.

Bolzon, M. D., Kelso R. M. & Arjomandi, M. 2016 c Parametric Study of the Effects of a Tubercle's Geometry on Wing Performance Through the Use of the Lifting-Line Theory. In *54th AIAA Aerospace Sciences Meeting, San Diego, California*.

Bolzon, M. D., Kelso, R. M. & Arjomandi, M. 2016 d Tubercles: A Flow Structure Study. *Submitted to Experimental Thermal Fluid Science*.

Bolzon, M. D., Kelso, R. M. & Arjomandi, M. 2016 e Tubercles and Their Applications. *The Journal of Aerospace Engineering*, **29**. doi: 10.1061/(ASCE)AS.1943-5525.0000491.

Bolzon, M. D., Kelso, R. M. & Arjomandi, M. 2016 f Leading Edge Tubercles: A Parametric and Optimization Study. *Submitted to Journal of Aerospace Information and Systems*.

Brune, G. W. 1994 Quantitative Low-Speed Wake Surveys. *Journal of Aircraft*, **31**, 249-255. doi:10.2514/3.46481.

Cai, C., Zuo, Z., Liu, S. & Wu, Y. 2016 Effect of a Single Leading-Edge Protuberance on NACA 63_4-021 Airfoil Performance. In *Proceedings of the International Symposium on Transport Phenomena and Dynamics of Rotating Machinery, Honolulu*. Lille University of Science and Technology.

Choudhry, A., Arjomandi, M. & Kelso, R. 2015 A Study of Long Separation Bubble on Thick Airfoils and its Consequent Effects. *International Journal of Heat and Fluid Flow*, **52**. doi: 10.1016/j.ijheatfluidflow.2014.12.001.

Corsini, A., Belibra, G. & Sheard, A. 2014 The Application of Sinusoidal Blade-Leading Edges in a Fan-Design Methodology to Improve Stall Resistance. *Journal of Power and Energy*, **228**, 255-271. doi: 10.1177/0957650913514229.

Dieck, R. H. 1992 *Measurement Uncertainty: Methods and Applications*. The Instrument Society of America.

Fish, F. M. & Battle, J. M. 1995 Hydrodynamic Design of the Humpback Whale Flipper. *Journal of Morphology*, **255**, 51-60. doi: 10.1002/jmor.1052250105.

Gerontakos, P. & Lee, T. 2006 Near-Field Tip Vortex Behind a Swept Wing Model. *Experiments in Fluids*, **40**, 141-155. doi: 10.1007/s00348-005-0056-y.

Hansen, K. L. 2012 Effect of Leading Edge Tubercles on Airfoil Performance. Ph.D. Dissertation, The University of Adelaide.

Hansen, K. L., Kelso, R. M., Choudhry, A. & Arjomandi, M. 2014 Laminar Separation Bubble Effect on the Lift Curve Slope of an Airfoil. In *19th Australasian Fluid Mechanics Conference, Melbourne, Australia*. Australasian Fluid Mechanics Society.

Hansen, K. L., Rostamzadeh, N., Kelso, R. M. & Dally, B. B. 2016 Evolution of the Streamwise Vortices Generated Between Leading Edge Tubercles. *Journal of Fluid Mechanics*, **788**, 730-766.

Hassan, E. R., Lau, T.C. & Kelso, R. M. 2007 Accuracy of Circulation Estimation Schemes Applied to Discretised Velocity Field Data. In *16th Australasian Fluid Mechanics Conference, Gold Coast, Australia*. Australasian Fluid Mechanics Society.

Holman, J. P. 1994 *Experimental Methods for Engineers*. McGraw-Hill.

Johari, H., Henoch, C., Custodio, D. & Levshin, A. 2007 Effects of Leading-Edge Protuberances on Airfoil Performance. *AIAA Journal*, **45**, 2643-2642.

Jurasz, C. M. & Jurasz, V. P. 1979 Feeding Modes of the Humpback Whale, Megaptera Novaeangliae, in Southeast Alaska. *The Scientific Reports of the Whales Research Institute*, **31**, 69-83.

Kusunose, K. 1997 Development of a Universal Wake Survey Data Analysis Code. *AIAA Inc.*, 2294, 617-626. doi: 10.2514/6.1997-2294.

Mell, B. 2010 Sandpaper Roughness Measurement Using 3D Profilometry. *Nanovea*.

Miklosovic, D. S., Murray, M. M. & Howle, L. E. 2007 Experimental Evaluation of Sinusoidal Leading Edges. *Journal of Aircraft*, **44**, 1404-1407. doi: 10.2514/1.30303.

Miklosovic, D. S., Murray, M. M., Howle, L. E. & Fish, F. E. 2004 Leading-edge Tubercles Delay Stall on Humpback Whale (Megaptera Novaeangliae) Flippers. *Physics of Fluids*, **16**, L39. doi:10.1063/1.1688341.

Murray, M., Gruber, T. & Fredriksson, D. 2011 Effect of Leading Edge Tubercles on Marine Tidal Turbine Blades. In *63rd Annual Meeting of the APS Division of Fluid Dynamics, Long Beach, CA.* American Physical Society.

Murray, M. M., Miklosovic, D. S., Fish, F. & Howle, L. 2005 Effects of Leading Edge Tubercles on a Representative Whale Flipper Model at Various Sweep Angles. In *Proceedings of the Twelfth International Symposium on Unmanned Untethered Submersible Technology UUST, Lee, NH*. Autonomous Undersea Systems Inst.

Pedro, H. T. & Kobayashi, M. H. 2008 Numerical Study of Stall Delay on Humpback Whale Flippers. In *46th AIAA Aerospace Sciences Meeting and Exhibit, Reno, Nevada.*

Perry, A. E. & Hornung, H. G. 1984 Some Aspects of Three-Dimensional Separation, Part II: Vortex Skeletons. *Z. Flugwiss. Weltraumforsch.* **8**, 155-160.

Rostamzadeh, N., Hansen, K. L., Kelso, R. M. & Dally, B. B. 2014 The Formation Mechanism and Impact of Streamwise Vortices on NACA 0021 Airfoil's Performance with Undulating Leading Edge Modification. *Physics of Fluids*, **26**, 107101. doi:10.1063/1.4896748.

Shepherd, I. C. 1981 A Four Hole Pressure Probe for Fluid Flow Measurements in Three Dimensions. *Journal of Fluids Engineering*, **103**, 590-594. doi: 10.1115/1.3241774.

Shi, W., Altar, M., Norman, R., Aktas, B. Turkmen, S. 2016 a Numerical optimization and Experimental Validation for a Tidal Turbine Blade with Leading-Edge Tubercles. *Renewable Energy*, **96**, 42-55. doi: 10.1016/j.renene.2016.04.064 0960-1481.

Shi, W., Rosli, R., Altar, M., Norman, R., Wang, D. & Tang, W. 2016 b Hydrodynamic Performance Evaluation of a Tidal Turbine with Leading-Edge Tubercles. *Ocean Engineering*, **117**, 246-253. doi: 10.1016/j.oceaneng.2016.03.044 0029-8018.

Skillen, A., Revell, A., Favier, J., Pinelli, A. & Piomelli, U. 2013 LES Study into the Flow Physics of an Undulating Leading-Edged Wing. In *ERCOFTAC International Symposium Unsteady Separation in Fluid-Structure Interaction, Mykonos, Greece*.

TFI 2011 Getting Started Series 100 Cobra Probe. *Turbulent Flow Instrumentation Pty. Ltd*.

Watts, P. & Fish, F.E. 2001 The Influence of Passive, Leading Edge Tubercles on Wing Performance. In *Proceedings of the Twelfth International Symposium on Unmanned Untethered Submersible Technology UUST, Lee, NH*. Autonomous Undersea Systems Inst.

Yoon, H. S., Hung, P. A., Jung, J. H. and Kim M. C. 2011 Effect of the Wavy Leading Edge on Hydrodynamic Characteristics for Flow Around Low Aspect Ratio Wing. *Computers & Fluids*, **49**, 276-289. doi:10.1016/j.compfluid.2011.06.010.

Chapter 7

Conclusions, Recommendations, and Future Work

This thesis investigated a flow control device known as tubercles. Tubercles are protuberances on the leading edge of airfoils and wings. From the literature review, three aims for this thesis were determined, which, along with the results, are detailed below. The overall achievements of this thesis are the finding that tubercles can improve a swept wing's performance at pre-stall AOAs thereby extending their industrial applicability. In addition, a framework and guidelines for designing tubercles to meet wing performance requirements at pre-stall AOAs have been developed and specified in section 7.4.

7.1 The Effects of Tubercles on Swept Wing Performance at Pre-stall Angles of Attack

The work detailed in this thesis demonstrated that at pre-stall AOAs, tubercles implemented along the entire leading edge of a swept wing can significantly reduce the lift and drag coefficients, and increase the lift-to-drag ratio. This is a major finding, as the vast majority of previous investigations on tubercles have focussed on their effects at stall and post-stall AOAs. Therefore, this finding extends the applicability of tubercles to pre-stall AOA applications. This finding was found by manufacturing two swept wings, one without tubercles and one with tubercles. The tubercles had an amplitude of 10.5mm (0.081 A/MAC) and a wavelength of 60mm (0.46 λ/MAC). Force measurements of the wings at pre-stall AOAs were conducted, from which the wings' lift coefficients, drag coefficients, and lift-to-drag ratios were calculated. The results of this investigation are detailed below.

Below 8° AOA, tubercles reduced the lift and total drag coefficients by 4 to 6% and 7 to 9.5%, respectively. This resulted in a 2 to 6% increase in the lift-to-drag ratio. In addition, both wings experienced increased lift-curve slopes from 6° AOA, which was due to laminar separation bubbles, LSBs, forming on their suction sides. However, the tubercled wing experienced a smaller augmented lift-curve slope, which was deduced to be caused by the interaction between the tubercle vortices and the LSB. Oil-film flow visualisation and CFD results demonstrated that, while the LSB over the smooth wing was relatively uniform in chordwise length from the wing root to the wingtip, the

tubercles modulated it, causing it to form closer to the leading edge behind the troughs and further from the leading edge behind the peaks. Above 8° AOA, the tubercles typically reduced the lift coefficient, increased the drag coefficient, and reduced the lift-to-drag ratio. These effects were caused by premature flow separation behind the troughs and in the wingtip region of the tubercled wing. This premature flow separation precedes the expected soft stall characteristics that tubercles produce.

As a side note, the finding that tubercles can increase wing performance at pre-stall AOAs also increases our understanding of the Humpback whale. The tubercles on their flippers may increase the flippers' performance during cruise, thereby aiding their well-known lengthy migrations, which are in the order of 10,000km (Department of the Environment, 2007).

7.2 The Effects of Tubercles on the Components of Drag at Pre-stall Angles of Attack, and Why They Affect the Components of Drag at Pre-stall Angles of Attack

Chapter 3 of this thesis showed that, at pre-stall AOAs, tubercles increase the profile drag coefficient (skin friction drag + pressure drag) and reduce the induced drag coefficient behind the troughs, with the opposite trends occurring behind the peaks. The induced drag coefficient decreases behind the troughs as the reduced bound vortex circulation combined with the induced velocity of the longitudinal vortices from the tubercles (see fig. 9), as found through Prandtl's lifting-line theory, LLT, reduces the tilting of the reduced lift vector into the freestream velocity direction. Conversely, behind the peaks, the increased circulation, as found through LLT, further tilts the augmented lift vector, as determined through the LLT, into the freestream velocity direction, thereby increasing the induced drag coefficient. Flow visualisation presented in Chapters 4 and 6 showed that the separation point of the LSB, which forms on the wings' suction surfaces, is shifted further upstream behind the troughs than behind the peaks. Furthermore, the LSB reattaches further upstream behind the troughs than the smooth wing, and the LSB reattaches further downstream behind the peaks than the smooth wing. The streamwise vortices that form behind the tubercles generate

downwash behind the peaks and upwash behind the troughs (Hansen *et al.*, 2016). The delay in the reattachment of the LSB behind the peaks may be the result of the downwash stabilising the separated layer and thereby suppressing the transition process by a process of strain. Conversely, the earlier reattachment of the LSB behind the troughs may be the result of the upwash destabilising the separated layer and thereby accelerating the transition process. The wake survey results indicate that reductions in the profile drag coefficient occurred behind the peaks, with smaller increases behind the troughs. However, reductions in the LSB length should cause a reduction in the drag coefficient (Choudhry *et al.*, 2015), and vice versa. Therefore, these contradictory observations suggest that more complex mechanisms, such as the observed owl-face separation pattern, may be impacting the profile drag coefficient. Therefore, further research is required to elucidate these effects.

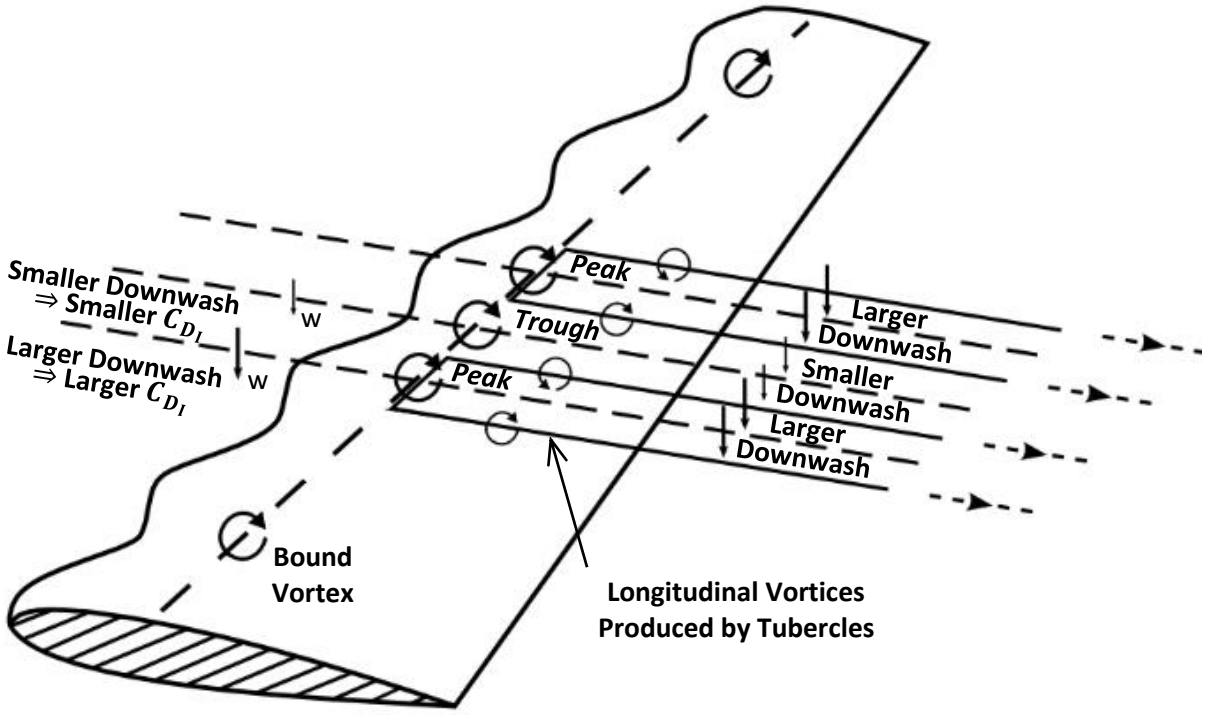

Figure 9: The vortex production, and relative upwash and downwash, over a tubercled wing.

By knowing the effects of tubercles on the components of drag, now tubercles can be designed to reduce the total drag coefficient, given the flow conditions. These effects of tubercles on the components of drag at pre-stall AOAs were found by performing wake surveys on the wings as discussed in section 7.1. The induced and profile drag coefficients were calculated from these surveys. The wake survey results were in good agreement with the force measurements, with the total drag coefficients aligning. The results found from these wake surveys are described below.

The wake surveys showed that the majority of the drag reduction caused by the tubercles on this wing below 8° AOA resulted from a reduced profile drag coefficient along the span of the wing; reductions in the order of 20% occurred. These reductions occurred, firstly, because there were more peaks than troughs on the tubercled wing, and secondly, because the reductions in the profile drag coefficient behind the peaks were greater than the augmentations behind the troughs. It is unknown why the profile drag coefficient was affected to a greater extent behind the peaks than the troughs, and as discussed above, the reasons are complex, and warrant further investigation.

Tubercles had an insignificant effect on the induced drag coefficient. Above 8°, premature flow separation near the tubercled wingtip typically resulted in a 9.2% increase in the total drag coefficient, a 72.6% increase in the profile drag coefficient, but an 8.1% reduction in the induced drag coefficient. The dramatic increase in the profile drag coefficient arose from the flow separating behind the troughs to a greater extent than the flow over the smooth wing, as shown in the flow visualisation results. While compartmentalization occurred, the adverse pressure gradient behind each trough caused the flow to eventually separate in each “compartment”. It is expected that there would be another transition AOA, above 8°, where the extents of flow separation over the smooth and tubercled wings would be approximately equal. Due to compartmentalization, as shown by the flow visualisation and CFD results, and the weaker adverse pressure gradients shown by the CFD results, the flow would remain largely attached behind the peaks above this AOA, which would result in the tubercled wing reducing the profile drag coefficient. The reduction in the induced drag

coefficient above 8° AOA follows from the above explanation, where the flow separation behind the troughs reduced the circulation and lift production.

At 3° AOA, the oil-film flow visualisation and CFD results showed that the flow behind the troughs of the tubercled wing began to separate, and the amount of separation increased with increasing AOA. This was reflected in the wake survey results, where the local maxima in the profile drag coefficients along the span became increasingly indistinct with increasing AOA.

In addition, while an unswept tubercle produces a pair of streamwise, counter-rotating vortices of equal strength (Hansen *et al.*, 2011), the wake surveys showed that sweeping a tubercled wing results in one vortex becoming stronger than the other; in this particular case, one tubercle vortex was at least 4 times the strength of its paired vortex. When the flow over the wing near the tip is largely attached, for this wing at 3° and 6° AOAs, tubercles do not significantly affect the strength of the wingtip vortex. However, when the flow near the wingtip significantly separates, for this wing at 9° and 12° AOAs, tubercles reduce the wingtip vortex strength, and for this wing, reductions in the order of 10% were observed.

7.3 The Effects of a Tubercle's Geometry on Wing Performance at Pre-stall Angles of Attack

Finally, this thesis describes the effects of a tubercle's geometry on the wing performance at pre-stall AOAs. As a result, a framework to design tubercles in order to fulfil a desired wing performance at pre-stall AOAs has been developed. This framework was developed through the results of a parametric analysis, a Genetic Algorithm, GA, optimisation, and a final experiment. The details and results of these works are discussed below.

The parametric analysis used LLT and investigated the effects of the tubercle amplitude, wavelength, and phase on an unswept wing's lift coefficient, induced drag coefficient, and lift-to-induced-drag ratio. The phase of the tubercles is a parameter that was introduced in this thesis to describe the

point along a tubercle at which a wing terminates. An unswept wing was chosen as the LLT required a 2D lift-curve input and a 3D lift-curve for validation, and the author only had access to one wing data set detailing these two lift-curves (Hansen, 2012). Previous researchers have found that the tubercle amplitude has much greater effects on wing performance than the wavelength (Johari, 2007; Hansen *et al.*, 2011; Hansen, 2012), with the wavelength having negligible effects in some cases. The results from the parametric analysis were consistent with this finding, however, in general the phase of the tubercles had the greatest effect on the wing's lift coefficient, induced drag coefficient, and lift-to-induced-drag ratio. The effects of the phase on these wing performance parameters were polarised, whereby depending on the phase, tubercles would either improve or degrade these performance parameters. A GA was developed and used to optimise a tubercle's amplitude, wavelength, phase, location, and the number of tubercles to produce the greatest lift-to-induced-drag ratios. The tubercle configuration with the highest lift-to-induced-drag ratio was found to be one that essentially results in a notched leading edge near the wingtip. This reduces the circulation and the spanwise circulation gradient near the wingtip, which results in an increased lift-to-induced-drag ratio. From the parametric analysis and GA, when a tubercle geometry reduces the induced drag coefficient, it also reduces the lift coefficient. A similar trend occurs when the tubercle geometry increases the induced drag coefficient. However, as tubercles affect both the circulation **and** lift coefficient, the tubercle geometry typically affects the induced drag coefficient to a greater extent than the lift coefficient. Therefore, the tubercle geometries that produce augmented lift-to-induced-drag ratios reduce both the lift and induced drag coefficients. From these investigations, in extreme cases, lift coefficient augmentations of up to 9% were observed. However, for more conventionally sized tubercle geometries, such as tubercles with 10mm amplitudes (0.14 A/MAC) and 50mm wavelengths (0.71 λ/MAC), changes in the lift coefficient of 1-2% were typical. The greatest increases in the lift-to-induced-drag ratio observed were approximately 5%.

The final set of experiments conducted was aimed at determining if significant improvements in the wing performance could be achieved with a single tubercle at the wingtip. Three wing configurations

were investigated; one smooth leading edge configuration, and two tubercled leading edge configurations. Both tubercle configurations featured a single full tubercle terminating at the wingtip. These tubercles had 10.5mm amplitudes (0.081 A/MAC) and 60mm wavelengths (0.46 λ/MAC), however, they had opposite phases to each other. Oil-film flow visualisation, force measurements, and wake surveys were conducted on these wing configurations. The effects of the tubercle configurations on the lift coefficient, drag coefficient, and lift-to-drag ratio at pre-stall AOAs were minimal, with changes of 1% to 2% typically observed. The tubercle configurations had slightly greater effects on the induced and profile drag coefficients, with typical changes of 2% and 5% observed, respectively. Whether the tubercle configurations increased or decreased the induced and profile drag coefficients was dependent on the AOA. From 6° to 12° AOA, the tubercle configurations typically changed the wingtip vortex strength by 3%, and typically had opposite effects from each other. The effects of the tubercle configurations on the lift and induced drag coefficients were in agreement with the parametric analysis results, which predicted negligible change in the lift and induced drag coefficients for tubercled wings terminating midway between a peak and trough, or midway between a trough and peak.

Combining the results of the parametric analysis, GA, and experiments, it is concluded that a single tubercle of conventional sizing typically cannot produce general wing performance improvements at pre-stall AOAs of similar magnitudes to tubercles implemented along the entire leading edge; performance improvements in the order of 5 to 10% when tubercles are implemented along the entire leading edge compared to 1 to 2% when tubercles are implemented only at the tip. In the extreme case, where the amplitude and wavelength are comparable with the wing chord and span, respectively, then similar improvements in the general wing performance can be produced by a single tubercle at the wingtip compared to tubercles along the entire leading edge.

7.4 Tubercle Recommendations

The following are general tubercle design recommendations based on either increasing a swept wing's lift coefficient, or reducing its drag coefficient at pre-stall AOAs.

1) As a general rule, larger amplitude and wavelength tubercles have greater effects.

2) To increase a wing's lift coefficient, a single peak located near the wing's tip should be implemented.

3) To reduce a wing's drag coefficient, tubercles should typically be implemented along the entire leading edge. Implementing tubercles along a portion of the leading edge will typically result in a smaller drag coefficient reduction.

4) If the wing's profile drag coefficient is greater than its induced drag coefficient, then implementing more peaks than troughs will result in a greater total drag coefficient reduction.

5) If the wing's induced drag coefficient is greater than its profile drag coefficient, then implementing more troughs than peaks will result in a greater total drag coefficient reduction.

6) A single tubercle trough located at the wingtip will achieve the greatest induced drag coefficient reduction, as both the circulation and circulation gradient will be reduced.

7.5 Future Work

7.5.1 Reynolds Number

The beneficial effects of tubercles on the wing performance detailed in this thesis were found in the transitional flow regime, which resulted in an LSB forming over both the smooth and tubercled wings. It is unclear whether the augmented wing performance was solely a function of the presence of tubercles, or the interaction between the tubercles and the LSB. If the augmented wing performance arises from the interaction, then this augmentation is not expected to occur in fully-

turbulent flow regimes, where LSBs are not present. As the Reynolds number increases, the effects of tubercles at stall and post-stall AOAs become smaller (Custodio *et al.*, 2015; Rostamzadeh *et al.*, 2016). However, the influence of the Reynolds number on the tubercle mechanism at pre-stall AOAs is still unknown. Furthermore, is also unknown if interactions between tubercles and higher Reynolds number flow phenomena produce different effects on wing performance. Therefore, determining the effects of tubercles on wing performance in a fully turbulent flow regime at pre-stall AOAs will allow more accurate assessments of their applicability to higher Reynolds number flows.

Furthermore, the profile drag coefficient reductions typically become smaller as the AOA increases, as the flow behind the tubercle troughs separate to a greater extent. However, at higher Reynolds number, the flow behind the troughs is expected to stay attached to a higher AOA, which could result in a greater profile drag coefficient reduction. Therefore, there is reason to believe that tubercles may have greater benefits in higher Reynolds number flows.

7.5.2 Profile Drag at Pre-Stall Angles of Attack

The parametric study carried out in this thesis considered the effects of tubercles on the lift and induced drag coefficients at pre-stall AOAs. The final part in the parametric analysis is to consider the effect of tubercles on the profile drag at pre-stall AOAs. Once this has been determined, the tubercle geometry can be accurately designed, computationally, to fulfil wing performance requirements at pre-stall AOAs.

7.5.3 Tubercle Shape

Tubercles are typically modelled as a sinusoidal wave along the entire leading edge (Johari *et al.*, 2007; Hansen, 2012; Rostamzadeh *et al.*, 2013). The A/λ ratio of a tubercle affects the strength of

the vortex created (Hemsch and Luckring, 1990; Hansen *et al.*, 2011; Wei *et al.*, 2015), where a greater A/λ angle results in stronger vortices due to the greater local leading edge sweep angle, and as such become more effective at delaying flow separation. Increasing the sharpness of the pattern, such as approximating tubercles as triangular shapes, may also affect the magnitude of a tubercle's effect on wing performance at pre-stall AOAs.

In addition to increasing the overall sharpness of the sinusoidal wave, decreasing the radius of curvature in certain regions may produce greater benefits to wing performance. For example, it was found that tubercles tend to reduce the profile drag coefficient behind the peaks, while reducing the induced drag coefficient behind the troughs. Decreasing the radius of the peak, may cause one of these components of drag to further decrease, which could maximise the total drag coefficient reduction. However, it would be a restrictive tubercle design technique, as the dominant component of drag changes with operating conditions.

Finally, tubercles that differ from the typical sinusoidal wave are likely to produce different effects on wing performance (Moore *et al.*, 2016). By investigating different protuberance designs, it is possible that the known effects of tubercles on wing performance may be augmented, or even new effects discovered.

References

Choudhry, A., Arjomandi, M., and Kelso, R., "A Study of Long Separation Bubble on Thick Airfoils and its Consequent Effects", *International Journal of Heat and Fluid Flow*, Vol. 52, 2015. doi: 10.1016/j.ijheatfluidlfow.2014.12.001.

Custodio, D., Henoch, C.W., and Johari, H., "Aerodynamic Characteristics of Finite Span Wings with Leading-Edge Protuberances", *American Institute of Aeronautics and Astronautics* (AIAA) Journal, Vol. 53, No. 7, 2015. doi: 10.2514/1.J053568.

Department of the Environment, "The Humpback Whales of Eastern Australia", Australia Government, 2007. Accessed: 20th May 2016, https://www.environment.gov.au/resource/humpback-whales-eastern-australia.

Hansen, K.L., "Effect of Leading Edge Tubercles on Airfoil Performance", *Ph.D. Thesis Univ. of Adelaide*, Adelaide, Australia, 2012.

Hansen, K.L., Kelso, R.M., and Dally, B.B., "Performance Variations of Leading-Edge Tubercles for Distinct Airfoil Profiles", *American Institute of Aeronautics and Astronautics* (AIAA) Journal, Vol. 49, No. 1, 2011. doi: 10.2514/1.J050631.

Hansen, K.L., Rostamzadeh, N., Kelso, R.M., and Dally, B.B., "Evolution of the Streamwise Vortices Generated Between Leading Edge Tubercles", *Journal of Fluid Mechanics*, Vol. 788, pp. 730-766, 2016. doi: 10.1017/jfm.2015.611.

Hemsch, M.J., and Luckring, J.M., "Connection Between Leading-Edge Sweep, Vortex Lift, and Vortex Strength for Delta Wings", *AIAA Journal Engineering Notes*, Vol. 27, No. 5, 1990.

Johari, H., Henoch, C., Custodio, D., and Levshin, A., "Effects of Leading-Edge Protuberances on Airfoil Performance", *AIAA Journal*, Vol. 49, No. 1, pp. 185-194, 2007. doi: 10.2514/1.J050631.

Moore, K.R. and Ning, A., "Aerodynamic Performance Characterization of Leading Edge Protrusions on Small Propellers", *AIAA SciTech*, 4th-8th January 2016, San Diego.

Rostamzadeh, N., Kelso, R.M., and Dally, B.B., "A Numerical Investigation into the Effects of Reynolds Number on the Flow Mechanism Induced by a Tubercled Leading Edge", *Theoretical Computational Fluid Dynamics*, 2016. doi: 10.1007/s00162-016-0393-x.

Rostamzadeh, N., Kelso, R.M., Dally, B.B., and Hansen, K.L., "The Effect of Undulating Leading-Edge Modifications on NACA 0021 Airfoil Characteristics", *Physics of Fluids*, Vol. 25, No. 11, 2013.

Wei, Z., New, T.H., and Cui, Y.D., "An Experimental Study on Flow Separation Control of Hydrofoils with Leading-Edge Tubercles at Low Reynolds Number", *Ocean Engineering*, Vol. 108, pp. 336-349, 2015. doi: 10.1016/j.oceaneng.2015.08.004 0028-8018.